2012-10-23

Understanding the Interior Characteristics of a Deep Cavity Cavitand and Its Role in Modulating Photophysical Processes of Organic Molecules

Mintu Porel
University of Miami, m.porel@umiami.edu

UNIVERSITY OF MIAMI

UNDERSTANDING THE INTERIOR CHARACTERISTICS OF A DEEP CAVITY CAVITAND AND ITS ROLE IN MODULATING PHOTOPHYSICAL PROCESSES OF ORGANIC MOLECULES

By

Mintu Porel

A DISSERTATION

Submitted to the Faculty
of the University of Miami
in partial fulfillment of the requirements for
the degree of Doctor of Philosophy

Coral Gables, Florida

December 2012

UNIVERSITY OF MIAMI

A dissertation submitted in partial fulfillment of
the requirements for the degree of
Doctor of Philosophy

UNDERSTANDING THE INTERIOR CHARACTERISTICS OF A DEEP CAVITY CAVITAND AND ITS ROLE IN MODULATING PHOTOPHYSICAL PROCESSES OF ORGANIC MOLECULES

Mintu Porel

Approved:

_____ Vaidhyanathan Ramamurthy, Ph.D. Professor of Chemistry	_____ M. Brian Blake, Ph.D. Dean of the Graduate School
_____ Burjor Captain, Ph.D. Assistant professor of Chemistry	_____ Rajeev Prabhakar, Ph.D. Assistant professor of Chemistry
_____ Sivaguru Jayaraman, Ph.D. Associate professor of Chemistry North Dakota State University	

POREL, MINTU (Ph.D., Chemistry)

Understanding the Interior Characteristics of a Deep Cavity Cavitand and Its Role in Modulating Photophysical Processes of Organic Molecules. (December 2012)

Abstract of a dissertation at the University of Miami.

Dissertation supervised by Professor Vaidhyanathan Ramamurthy.
No. of pages in text. (328)

The central tenet of this thesis is to explore the use of a deep cavity cavitand known by the trivial name 'octa acid' as a reaction cavity for manipulating photochemical and photophysical properties of organic molecules. The micropolarity of the interior of the cavitand was monitored by recording the fluorescence of different polarity probes. They all indicated that the interior of octa acid capsuleplex (2:1, host/guest complex) is nonpolar and does not contain water molecules despite the complex being present in water. Photophysical and NMR experiments suggested that the structure of the host/guest complex depends on the size and hydrophobicity of the guest molecule. We also probed the dynamics of guest molecules included within octa acid with the help of ^{1}H NMR and EPR techniques.

We have studied the photoinduced electron transfer from the donor incarcerated within octa acid nanocapsule to the acceptor free in solution. Comparison to the electron transfer in free solution showed significantly accelerated dynamics and essentially no solvent relaxation when the donor was encapsulated into the host molecule. In that context we were able to bind a dye molecule encapsulated within OA capsule to the semiconductor (TiO_2) and hence monitor electron transfer from the dye to the

semiconductor. The molecular communication between two molecules, one confined and excited (triplet or singlet) and one free and paramagnetic was studied through quenching of fluorescence and/or phosphorescence by nitroxides as paramagnetic radical species. Results presented in this thesis highlight the role of the lifetime of the encounter complex in electron-electron spin communication when the direct orbital overlap between the two molecules was prevented by the intermediary wall. In a separate work, we have shown that the high-energy axial conformer of propyloxy-substituted piperidine gets stabilized within octa acid capsule, which highlights the value of confined spaces in physical organic chemistry.

This work also spans disciplines to understand the complexation patterns between nitroxides and cucurbiturils. One of the key findings of this work was that a selective triangular geometry of the supramolecular aggregate ([nitroxide@cucurbit[8]urils]$_3$) leaded to spin exchange between the three radical centers. The use of supramolecular architectures to control the spatially dependent spin exchange between two/three covalently linked radical centers (biradicals/triradical respectively) has been explored.

This thesis is dedicated to my parents
for their love, endless support
and encouragement

"Even if you're on the right track, you'll get run over if you just sit there."

Will Rogers

ACKNOWLEDGEMENTS

This thesis is the end of my journey in obtaining my Ph.D. At the end of my thesis, it is my great pleasure to express my thanks to my teachers, family, friends, and colleagues who made this thesis possible with their continuous support and encouragement and made it an unforgettable experience for me.

This thesis would not have been possible without the help, support and patience of my supervisor, Prof. Vaidhyanathan Ramamurthy, not to mention his advice and unsurpassed knowledge of physical organic chemistry. As a research advisor, Prof. Ramamurthy has always motivated me to perform to the best of my capability, and given me great freedom to pursue independent work. He patiently provided me the vision, encouragement and advice necessary for me to continue the doctoral program and complete my dissertation. I feel very fortunate to have had my doctoral training under the supervision of Prof. Ramamurthy and will be indebted for the time he has spent mentoring me. The way he does science will always inspire me and I can only say a proper thanks to him through my future work.

Secondly, I would like to thank Prof. Nicholas Turro and Dr. Steffen Jockusch from Columbia University for giving me the opportunity to carry on various EPR studies and laser experiments. I had many enlightening scientific discussions with Prof. Turro and Dr. Jockusch regarding our collaborative projects and I am grateful to them in every possible way.

A lion part of the works described in this thesis has been conducted in collaboration with different research groups. I take this opportunity to thank Prof. Maria Francesca Ottavini from University of Urbino, Italy; Prof. Elena Galoppini from Rutgers

University, United States; Prof. Clemens Burda from Case Western Reserve University, United States; Prof. José P. Da Silva from Universidade do Algarve, Portugal, and Prof. S Raghothama from Indian Institute of Science, India. Special thanks to my committee, Dr. Burjor Captain, Dr. Rajeev Prabhakar and Dr. Sivaguru Jayaraman for their support, guidance and helpful suggestions.

I would like to thank all the current and former members of our lab, and other labs where I worked in last five years: Dr. Nithyanandhan Jayaraj, Shipra Gupta, Shampa Rani Samanta, Revathy Kulasekharan, Rajib Choudhury, Elamparuthi Ramasamy, Barnali Mondal, Pradeep kumar Jagadesan, Dr. Murthy V. S. N. Maddipatla, Dr. Arunkuamr Sundaresan, Dr. Anand Parthasarathy, Dr. S. Annalakshmi, Dr. Bala Krishna Bhogala, Dr. Yaopeng Zhao, Dr. Raja Kaliappan, Dr. Lakshmi Sireesha Kaanumalle from our lab and Dr. Marina Fattig, Agnishikha (Rutgers University), Chi-Hung Chuang, Tennyson Doane (Case Western Reserve University). I am extremely grateful to Dr. Jayaraj for his scientific advice and knowledge and many insightful discussions and suggestions. He was my primary resource for getting my science questions answered and was instrumental in helping me all possible ways.

My most heartfelt thanks must go to my family and friends. The two most important persons that I must thank foremost: my mom and dad. My hard-working parents have sacrificed their lives for myself and provided unconditional love and care. Thank is not a big enough word to appreciate their support. It could have never been possible for me to continue my graduate studies without their continuous support and love. I owe everything to them and wish I could show just how much I love and

appreciate them. Special thanks go to my sister, Swagata and youngest maternal uncle who have been a source of laughter and in-depth support for me.

My husband, Sushabhan Sadhukhan, has been the inspiration and driving force which allowed me to finish this journey. He has helped me in every possible way and I would not have made it this far without him. I know I always have him to count on when times are rough and he continuously provided the encouragement and advice necessary for me at every stage to override every hurdle that came in the way. I would also like to thank all my friends in US, India and other parts of the World for their thoughtful supports.

I take this opportunity to sincerely acknowledge Department of Chemistry, University of Miami for providing me the opportunity to continue the Doctoral program and all instrumental assistance.

TABLE OF CONTENTS

LIST OF FIGURES

LIST OF SCHEMES

LIST OF TABLES

CHAPTER 1

Introduction:
Background and Significance

1.1 What is supramolecular chemistry?

Supramolecular chemistry has been described as "*chemistry beyond the molecule*", whereby a 'supermolecule' is a species that is held together by non-covalent interactions between two or more covalent molecules or ions. Supramolecular chemistry deals with the formation of superstructures through the design and utilization of non-covalent interactions, using small molecular building blocks.[1,2] It is a multidisciplinary research field which impinges on various other disciplines, such as the traditional areas of organic and inorganic chemistry, physics, biology and materials science.[1,3]

Supramolecular chemistry can be divided into two broad categories; *guest-host chemistry* and *self-assembly*. The driving force behind the two different supramolecular systems is the molecular size and shape. If one molecule is significantly larger than another and can wrap around it then the former is termed as 'host' and the smaller molecule is its 'guest', which becomes enveloped by the host. Donald Cram defined the hosts and guests as: "*The host component is defined as an organic molecule or ion whose binding sites converge in the complex. The guest component is any molecule or ion whose binding sites diverge in the complex*."[4] The host-guest complex is often represented as guest@host where the "@" symbol indicates a non-covalent complex between a guest and a host. Host-guest complexes are common in biological systems, such as enzymes and their substrates, where enzymes are the host and the substrates act as guest. In terms of coordination chemistry, metal-ligand complexes can be thought of as host-guest species, where large (often macrocyclic) ligands act as hosts for metal cations.

On the other hand, where there is no significant difference in size and no species is acting as a host for another, the non-covalent joining of two or more species is called

self-assembly. Self-assembly is equilibrium between two or more molecular components to produce an aggregate with a defined structure. This type of supramolecular structure is also present in nature, for example, deoxyribonucleic acid (DNA) is made up from two strands which self-assemble via hydrogen bonds and aromatic stacking interactions to form the double helical structure.

1.2 Supramolecular chemistry: guest@host complexation

For a stable guest@host complexation to occur the host molecule must contain the appropriate binding sites for the guest molecule to bind to. For example, if the host has many hydrogen bond donor sites then the guest must ideally contain a number of hydrogen bond acceptor sites, which are positioned in such a way that it is feasible for multiple interactions between host and guest to occur. In this thesis we focus on the water soluble hosts for our studies. The advantage of the water soluble hosts is that we can avoid using the hazardous organic solvents to carry out organic reactions.

There are various types of water soluble hosts that are different both in structure and physical properties.[5,6] A micelle is an assembly of small molecules, held together by non-covalent interaction that can completely surround a small guest molecule. Some commonly used micelles are sodium dodecyl sulfate (SDS), hexadecyl trimethyl ammonium chloride (HDTCl). There also some host molecules which process a structurally intrinsic permanent cavity that can contain a guest molecule by partially surrounding it. These kinds of hosts are termed as ‘cavitand’. Cyclodextrins (CDs), cucurbiturils (CBs) fall into this category. A capsule is formed when two cavitands come together and form an assembly through non-covalent interactions to completely surround a guest molecule. Octa acid (OA) and CDs are known to form capsules. A last category is

termed as carcerand and hemicarcerand which are molecules possessing a structurally intrinsic permanent cavity that can completely surround (thereby incarcerate) a guest molecule. The cavity may have portals through which guest molecules may enter and exit. If the guest is unable to exit or enter through the portals during the photochemical process the host is considered a carcerand. If the guest is able to exit or enter through the portals the host is considered a hemicarcerand. Cram's carcerand, supercages in faujasite (FAU) and pentasil (MFI) zeolites are good examples of carcerand and hemicarcerand.

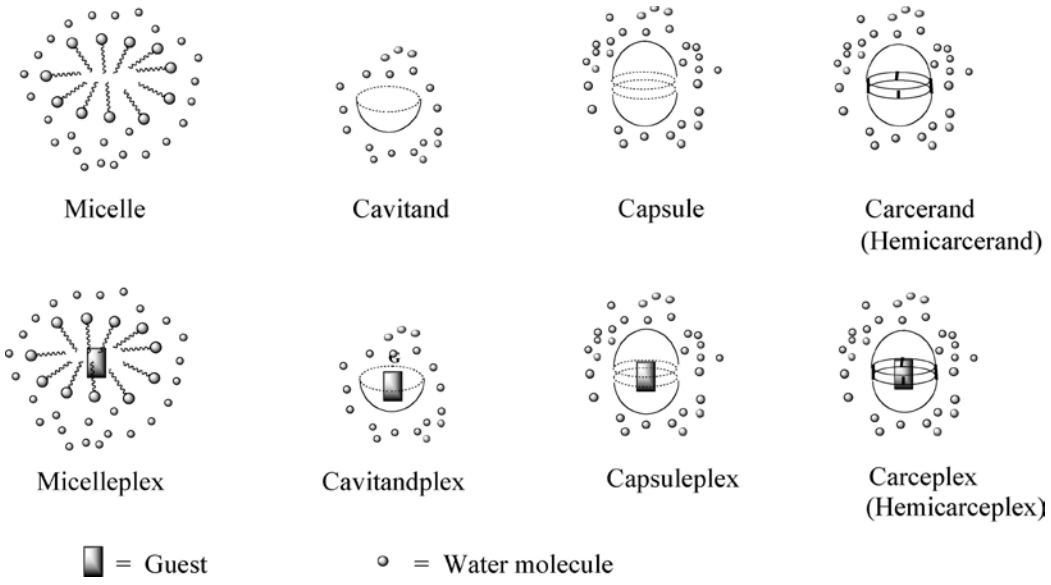

Figure 1.1 Definition of various possible host and host/guest complexes and their schematic representations

In **Fig 1.1**, schematic representations of various commonly used hosts, e.g., micelle, cavitand, capsule, and carcerand, and their corresponding host/guest complexes are presented. It should be noted that, of the various hosts presented, both micelle and capsule are made up of more than one molecule and thus could be dynamic in character,

i.e., the structure could be time dependent. It is important to recognize that carcerand (originally synthesized by Cram), in which the two cavitands that make up the capsule are covalently linked, has a time-independent structure.[7,8] The structure that is relevant to this presentation is the capsuleplex that has a close similarity to carceplex. An important difference between the two is that in the former the guest is held within the capsule through weak interactions, while in the latter it is incarcerated through covalent linkages.

1.3 Water soluble host

Why it is important to conduct organic reactions in water? Using non-toxic and environmental friendly chemicals is one of the main principles of 'green chemistry'. Organic solvents are hazardous, toxic and not eco benign. Thus extensive research is being carried out to identify nontoxic media to conduct important organic reactions. Water is the best solvent for accomplishing this goal. But the problem is organic molecules are not soluble in water. What is the solution then? Synthesizing water soluble organic hosts and exploring organic reactions using the supramolecular strategy brought a big solution.

The development of water soluble host systems has become a challenge for researchers working in the field of molecular recognition. One of the most primitive accounts of molecular recognition in water involved the formation of a non-stoichiometric complex between deoxycholic acid and hydrolyzed fatty acids.[9] This was the first historical note that used the terms "host" and "guest" to describe their roles in chemical complexation. Thereafter a series of synthetic, macrocyclic receptors with stoichiometric complexation properties have been added to the arsenal of supramolecular

hosts such as Pedersen's crown ethers,[10,11] cyclodextrins,[12] cyclophanes,[13] calix[*n*]arenes[14] and the glycoluril-derived cucurbiturils (**Fig 1.2**).[15]

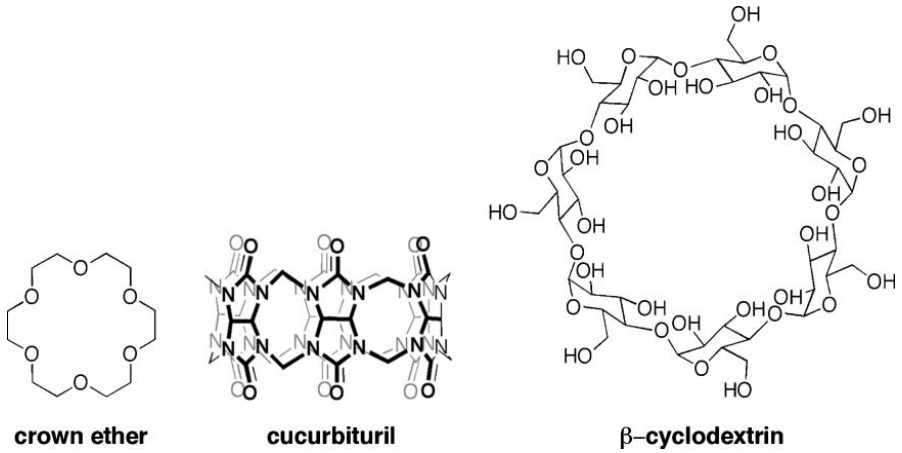

Figure 1.2 Structures of three water-soluble macrocyclic hosts

1.3.1 Water soluble cavitands

The resorcin[*n*]arene based cavitands show the similar behavior to the hosts described above. The initial structures were quite flexible and thus were unable to form a strong complex. In order to synthesis hosts with less flexible cavities, the bowl-shaped resorcin[4]arenes were rigidified by reaction with four equivalents of bromochloromethane (**Fig 1.3(i)**).[16] The hydroxyl groups on the rim were bridged with a methylene spacer. Further modifications were carried out on either the pendant alkyl groups on the lower rim or by additional substitutions to the upper rim (**Fig 1.3(ii)** and **1.3(iii)**)[17,18] Inspired from the above resorcinarenes, researchers further synthesized a list of water soluble cavitands introducing a hydrophilic group on the top rim (see some example in **Fig 1.4**).[19-28] To incarcerate a variety of guest molecule there was a need for

larger cavity. To accomplish this resorcin[4]arene was condensed with electron-poor aromatic rings to give "deep cavitands", as shown in **Fig 1.5** and **Fig 1.6**.[29-35]

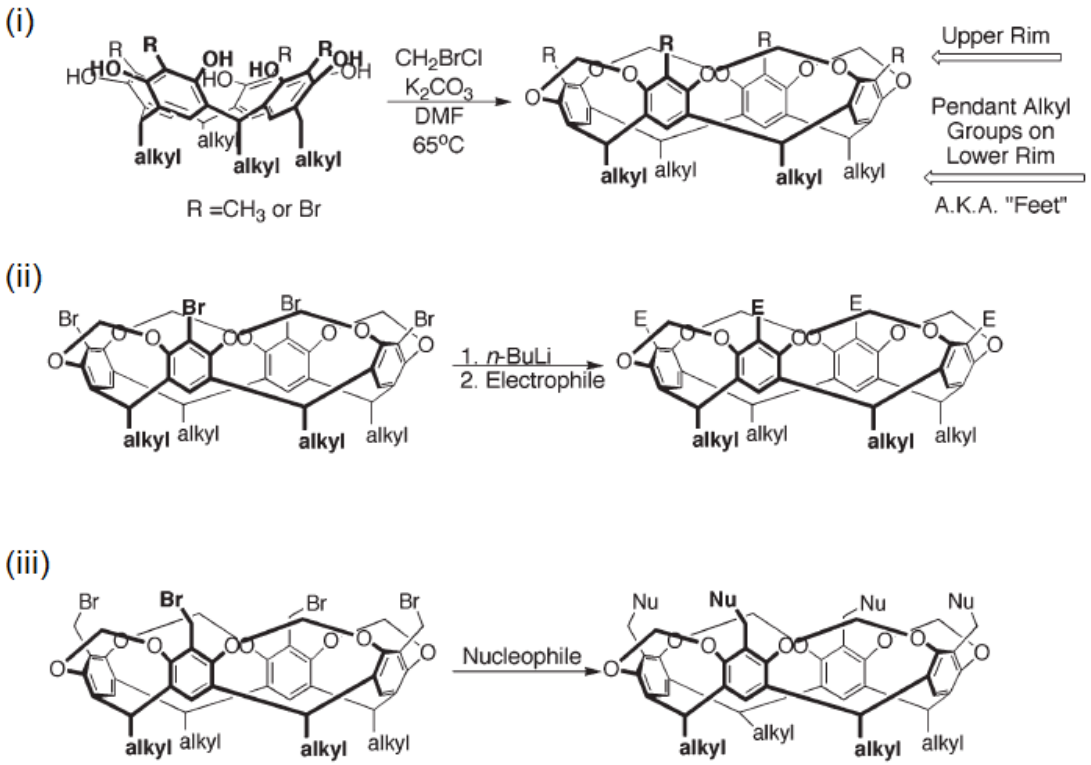

Figure 1.3 Synthesis of resorcin[4]arenes bearing (i) a variety of pendant R groups such as (ii) Electrophile and (iii) Nucleophile

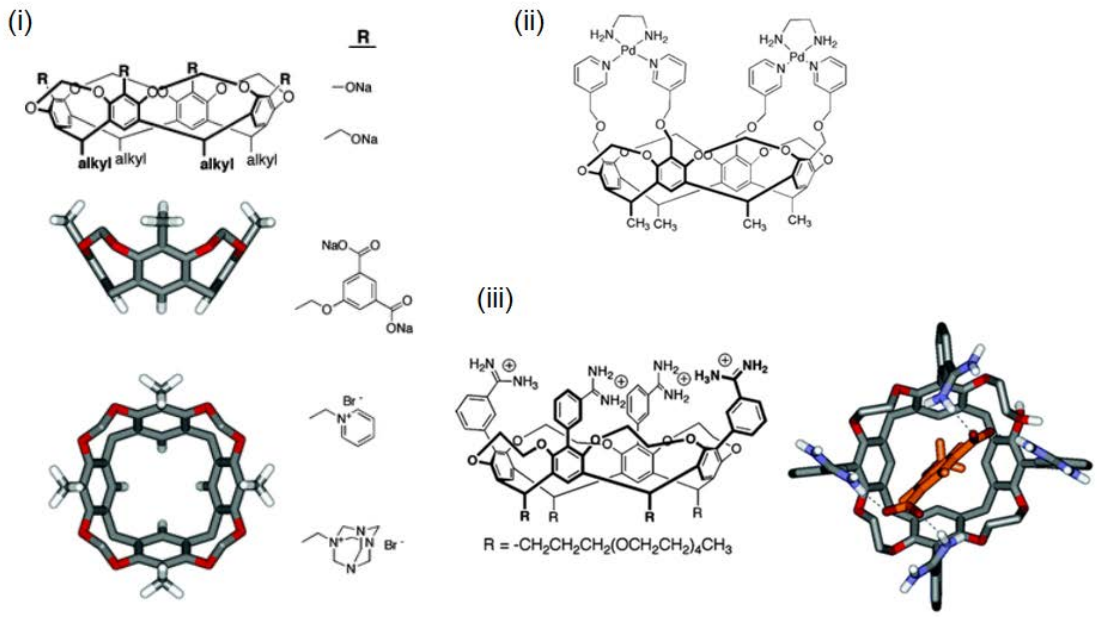

Figure 1.4 (i) Left column: depiction of general methylene-bridged resorcin[4]arene cavitands where R = methyl (some protons and the pendant alkyl feet have been omitted for clarity); Right columns: Solubilizing groups appended to the upper rim of simple cavitands and examples of a suitable guest, (ii) Structure of Pd(II)-pyridine complexed cavitand and (iii) Left: Structure of Diederich's ethylene bridged cavitand bearing PEG groups on the lower rim; Right: top view of energy-minimized model of cavitand methoxyisophthalate complex showing hydrogen bonds between host and guest (dashed lines, some protons and the pendant chains have been omitted for clarity).

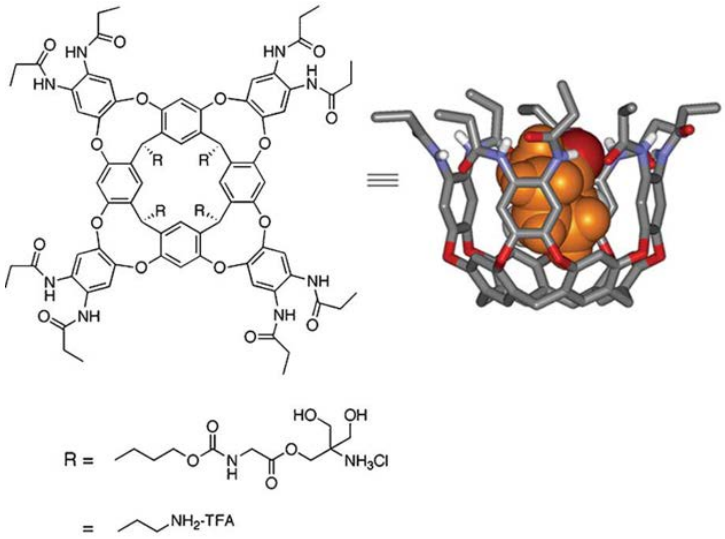

Figure 1.5 Structure of water-soluble, octa amide cavitands with its energy-minimized structure

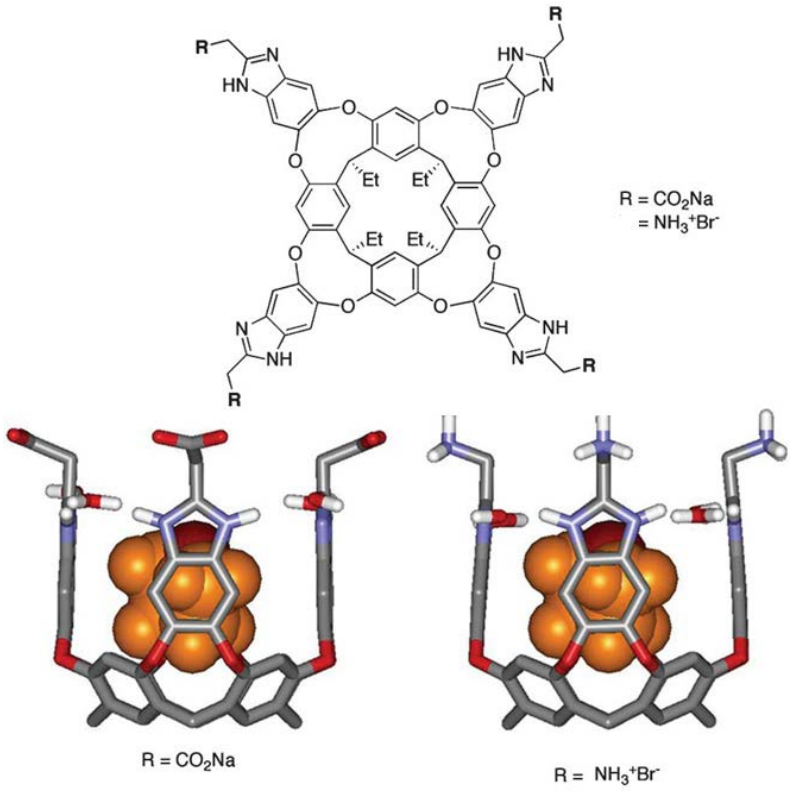

Figure 1.6 Structure of deep, tetraanionic cavitands binding one molecule of THF.

1.3.2 Water soluble capsules

The formation of molecular capsules in organic solvents depends on the properly oriented hydrogen bonding functionalities to bring two (or more) species together in solution.[36] Unfortunately, in aqueous medium, water forms hydrogen bond with these recognition sites and thus does not drive multi-component assemblies. Due to this limitation there are fewer examples of water-soluble molecular capsules in the literature.

Capsules assembled through non-covalent interactions: The Reinhoudt group reported the preparation of the derivatives of calix[4]arenes with either amidinium, sulfonate or

carboxylate groups on their upper rims (see **Fig 1.7**).[37] A similar result was obtained by Schrader and co-workers with ammonium and phosphonate substituted calix[4]- and calix[6]arenes.[37-39]

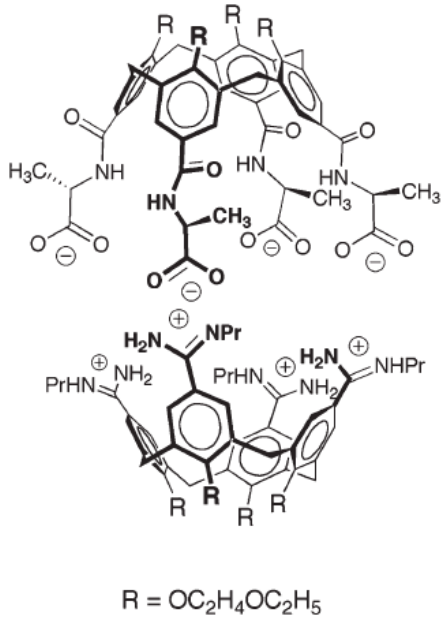

Figure 1.7 Structure of a water-soluble dimeric capsule assembled through electrostatic interactions.

Another example of molecular capsule, formed from two deep, water-soluble cavitands was assembled *via* the hydrophobic effect.[40] The eight carboxylate groups on the top and bottom rims of that host afforded its solubility in water (**Fig 1.8**).

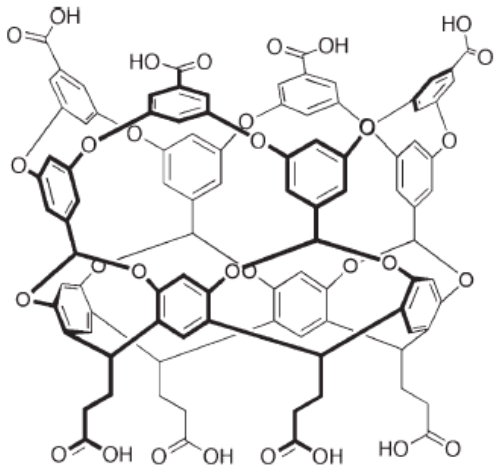

Figure 1.8 Structure of cavitand monomer which dimerizes via the hydrophobic effect

Cage complexes: hemicarcerands: Hemicarcerands are cage-like structures assembled from two rigid bowl-shaped units, most often resorcin[3]- or resorcin[4]arenes.[41] These bridges can range from rigid aromatics to flexible alkyl chains. While these structures are assembled through covalent bonds, the flexible bridges create portals to allow small guests to move in and out of the cavity. The water-soluble hemicarcerand was first reported in 1997 which was used in an efficient drug delivery system (**Fig 1.9(i)**).[42] A closely related derivative with only three bridging aromatic groups was synthesized and studied by Deshayes and co-workers (**Fig 1.9(ii)**).[43]

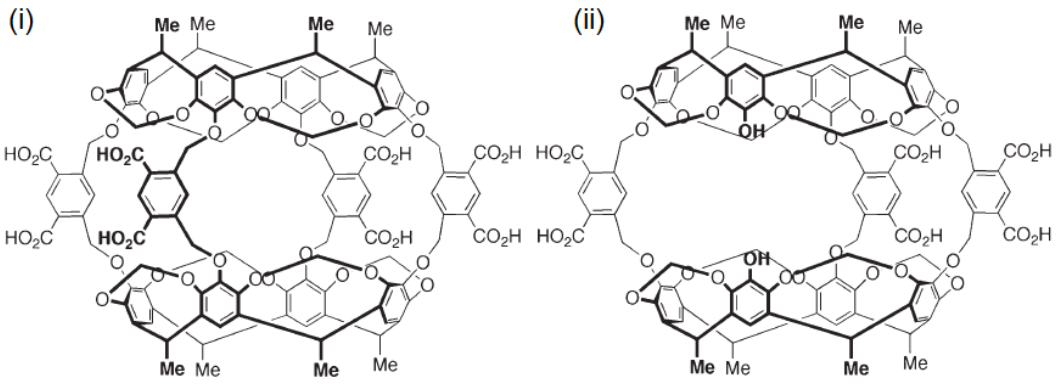

Figure 1.9 Two examples (**i** and **ii**) of hemicarcerands

Recently Gibb *et al* synthesized a deep cavity cavitand known by its trivial name octa acid (OA).[40] OA is a resorcinarene based synthetic cavitand. Two more layers of aromatic rings were introduced one on top of each other on the 1st row to make the cavity deeper and structure more rigid. It is comprised of eight carboxy acid groups on the top and bottom rim which make it soluble in water under slightly alkaline conditions (pH≈ 9). **Fig 1.10(i)** provides the structure and dimensions of cavitand OA. It has a narrow lower rim (bottom) and a wider upper rim (top). The upper rim acts as portal for the incoming guest while lower rim is narrow enough not to let the encapsulated molecules to pass through. CPK Model has shown that a molecule as small as oxygen cannot penetrate the tapered, lower rim of the host (**Fig 1.10(ii)**).

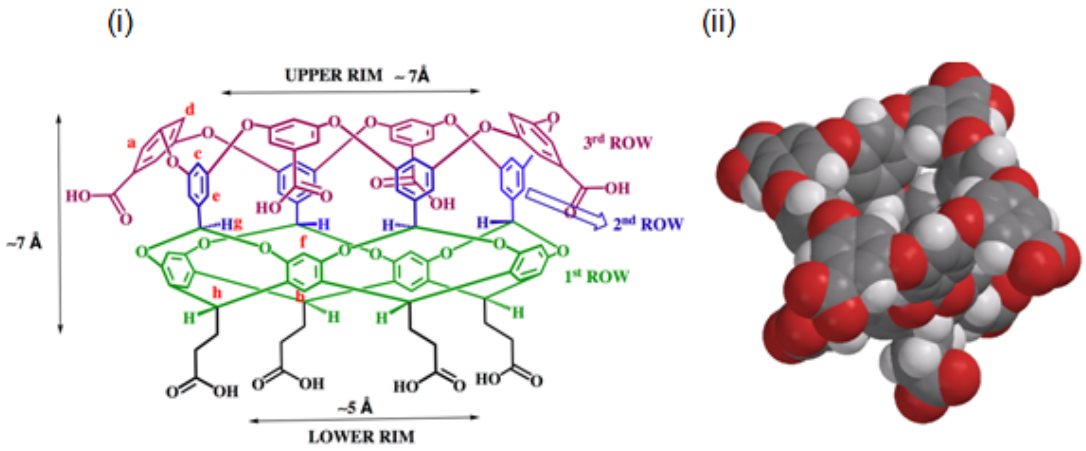

Figure 1.10 (i) Structure and dimensions and (ii) space filling model of cavitand octa acid (OA).

There are six distinct aromatic hydrogen atoms (marked by '**a-f**') on the host. At lower concentrations of the host (1 mM) the aromatic host regions shows six distinct signals indicating the host exists as a well-defined species. The remarkable observation is that it formed a capsular complex with two hosts self-assembling by encapsulating the guest molecule in aqueous medium (**Figure 1.11**). The formation of capsular complex of OA is driven mainly by hydrophobic effect.

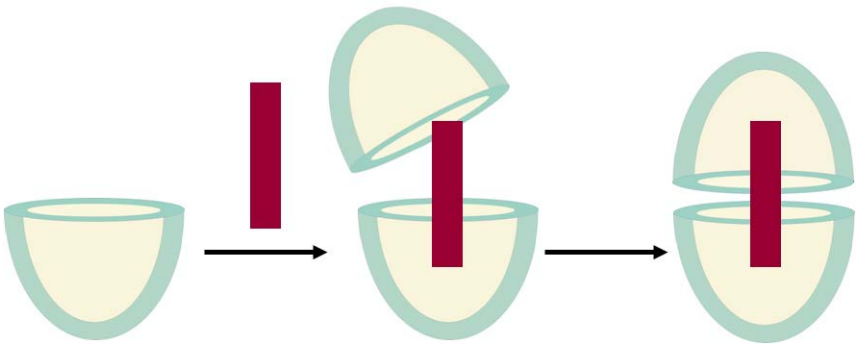

Figure 1.11 Pictorial representation of formation of capsular assembly.

1.4 Weak interactions and host-guest chemistry

Non-covalent interactions are much weaker than their covalent counterparts and a strong binding is only observed while multiple interactions cooperate. Consequently, most supramolecular complexes are reversibly formed and are prone to dynamic processes. This is a prerequisite for the self-assembly[44] of defined aggregates that occurs under thermodynamic control. Due to the reversibility of non-covalent bond formation many supramolecular aggregates should be considered as highly dynamic units.

Unlike in molecular chemistry, which is predominantly based upon the covalent bonding of atoms, supramolecular chemistry is based upon intermolecular interactions, such as metal coordination, electrostatic interactions, hydrogen bonding, π-π interactions, cation-π interactions, CH-π interactions, dispersion interactions and hydrophobic or solvophobic effects (**Figure 1.12**). Those non-covalent interactions are considered to be much weaker than the covalent interactions (ca. 150-450 kJ/mol for single bonds). Non-covalent bond energies range from 2 kJ/mol for dispersion interactions to 300 kJ /mol for 'ion-ion' interactions. But when the non-covalent interactions act together, they can stabilize a supramolecular system. The reversible weak interactions also make it easier to manipulate the supramolecular system while avoiding the complexity of synthesis. The typical energy associated with different non-covalent interactions in supramolecular systems[45] is listed in **Table 1.1**.

Table 1.1 Different non-covalent interactions[45]

Interaction	Strength (KJ/mol)	Example
Ion-ion	200-300	Tetrabutylammonium chloride
Ion-dipole	50-200	Sodium [15]crown-5
Dipole-dipole	5-50	Acetone
Hydrogen bonding	4-120	HF complexes (60-120 KJ/mol);C–H…acceptor or donor–H…π (4-12 KJ/mol)
Cation-π	5-80	K^+ in benzene
π-π	0-50	Benzene and graphite
van der Waals	< 5 but variable depending on surface area	Argon; packing in molecular crystals
Hydrophobic	Related to solvent-solvent interaction energy	Cyclodextrin inclusion compounds

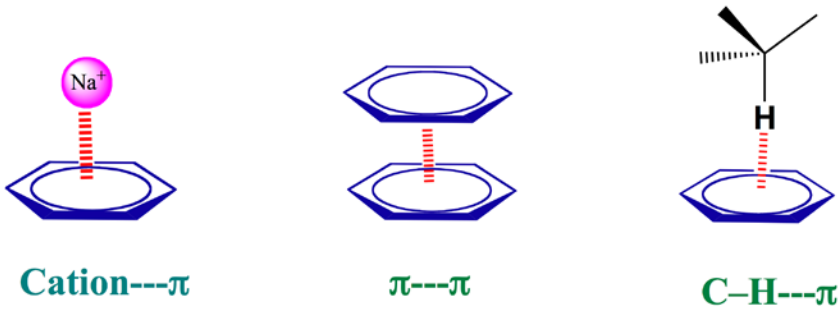

Figure 1.12 Different types of weak interactions in supramolecular chemistry.

1.5 Importance of supramolecular chemistry

Supramolecular hosts have been shown to possess a variety of potential applications, some of which are discussed below. Applications include catalysis and

inhibition of reactions, molecular sensors, molecular switches and machines, drug delivery systems and controlled release of drugs, conducting organic reaction in an environmental friendly media.

1.5.1 Catalysis

Catalysis is divided into homogeneous catalysis, heterogeneous catalysis and biocatalysis. In parallel to these well-developed fields in the past few decades, the area of supramolecular chemistry has emerged into them. Compared with these individual disciplines, the science at the interface between catalysis and supramolecular chemistry, supramolecular catalysis, has received relatively little attention.[46] Supramolecular chemistry is mainly based on the non-covalent interactions as described earlier and a major application of this discipline has been the design and understanding various catalytic processes. Non-covalent interactions play a key role in catalysis through stabilizing the transition states of reaction. Encapsulation systems such as micelles and dendrimers are also used in catalysis to create microenvironments suitable for reactions to progress.

A lot of effort has been put in creating systems in which a host molecule is connected to a binding site, with the aim of mimicking enzyme catalysis, generally involving typical reactions that are carried out by enzymes. This approach has resulted in several useful cage-driven reactions that display enhanced selectivity.[47] For example, the special micro-environment in the cage-like host molecules reported by Pluth *et al.*, formed by a metal-ligand assembly, dramatically increases the acid-catalysed hydrolysis reaction of ortho esters, even in a basic reaction medium.[48]

1.5.2 Drug delivery Supramolecular chemistry has also made considerable contributions in the pharmaceutical research by understanding the interactions of a drug binding site as well as the efficient release of the drug. The drug delivery mechanism has also made critical advances as a result of supramolecular chemistry providing encapsulation and targeted release mechanisms.[49] In the last decade, cucurbit[n]uril and cucurbit[n]uril-based supramolecular structures, in particular, have emerged as promising systems for drug delivery.[50] For example, Nau and coworkers[51] have shown the incarceration of drug thiabendazole to CB7. The complexation was reported to catalyze the formation of the active form of the drug (the sulfenamide form) and enhancing the stability of the active form. The limitations to the use of thiabendazole as a drug is its slow conversion to the active cyclic sulfenamide form, while at the same time the active form of the drug is unstable and readily undergoes dimerization and decomposition in acidic environments. As this drug is used to reduce gastric acid production in the stomach, stability in an acidic environment is compulsory for its effectiveness. Nau and coworkers have found that the half-life of the formation of the active form of the drug decreased from 5 min without CB7 to 20 sec in the presence of CB7. Meanwhile, the active form of the drug had a half-life of 60 min at pH 2.9 in the absence of CB7, which increased to three weeks in the presence of CB7. The driving force of this stabilization is a complexation-induced pKa shift, as complexation of a guest inside CB7 stabilizes the protonated form of the guest.

1.5.3 Molecular Switches

Molecular switches are molecular or supramolecular systems that are able to modulate an output signal in response to an external stimulus such as pH, electrochemical

potential, temperature, or solvent polarity. For example, Becuwe et al.[52] have shown a pH dependent molecular switch based on pyridin-4-yl indolizin β-cyclodextrin **1** (**Fig 1.3 (i)**) in water. The reversibility of fluorescent emission was attributed to a molecular motion of enclosed fluorescent moiety to inside/outside location (**Fig 1.3 (ii)**). In their work, they have synthesized pyridin-4-yl indolizin β-cyclodextrin and demonstrated a pH-driven fluorescent molecular switch in water based on a β-cyclodextrin core. The protonation of the free nitrogen localized on the pyridyl group seems to be an efficient straightforward way to modulate the conformation and the fluorescent properties of sensor **1**.

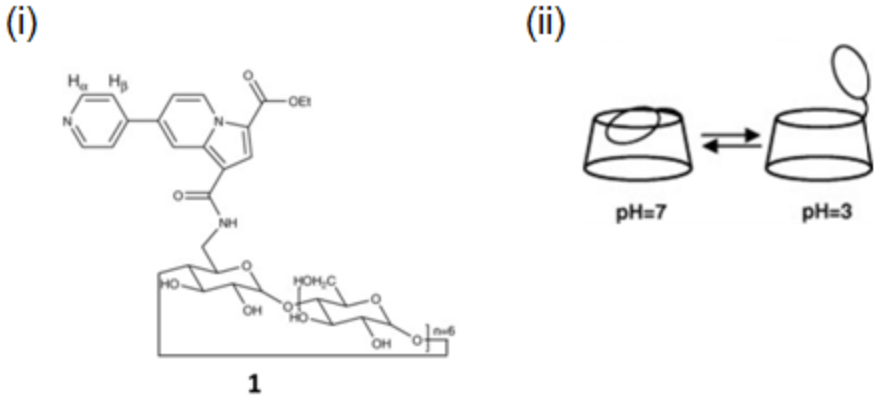

Figure 1.3 (i) Structures of pyridin-4-yl indolizin. β-cyclodextrin **1**. (ii) Structure of 1 at pH 3 and pH 7.[52]

1.5.4 Resolution of enantiomers by functionalized crown ether

Seminal work by Pedersen on crown ethers paved way for emergence of new field of host-guest chemistry and researchers started exploring host-guest chemistry to make stable 'host-guest' systems. Cram and coworkers synthesized crown ether derivatives with one or more 1,1'-binaphthyl units into crown ethers for incarcerating chiral amines such as 1-phenylethyl ammonium salts enantioselectively[53] (**Figure 1.14)**. The designed crown ether derivative upheld the (*S*)-1-phenylethyl derivative to form stable diasteromer

as suugested by CPK models. Thus they were able to accomplish a 'supramolecular resolution' of enantiomers.

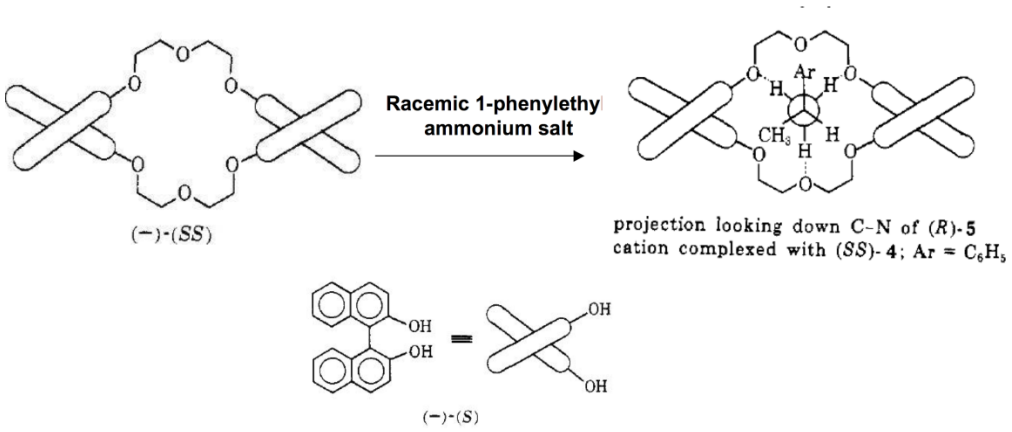

Figure 1.14 Resolution of enantiomers by a crown ether derivative.[53]

1.6 Electron transfer process in supramolecular assemblies

Electron transfer occurs when an electron moves from an atom or a chemical species (e.g. molecules) to another. Electron transfer is a redox process where the oxidation states of reaction partners, electron donor and electron acceptor, change. Photoinduced electron transfer is an electron transfer which occurs when certain photoactive materials interact with light and thus one electron goes from its ground state to excited state (**Fig 1.14 (i)**). There are two possibilities: The excited molecule can function as (i) electron donor or (ii) electron acceptor. **Fig 1.14 (ii)** shows the electron transfer from an excited donor molecule to an acceptor. In the other case an excited chromophore can accept an electron in the half field ground state orbital from a donor **Fig 1.14 (iii)**). Thus an excited molecule has the ability to act as an oxidant or reductant.[54]

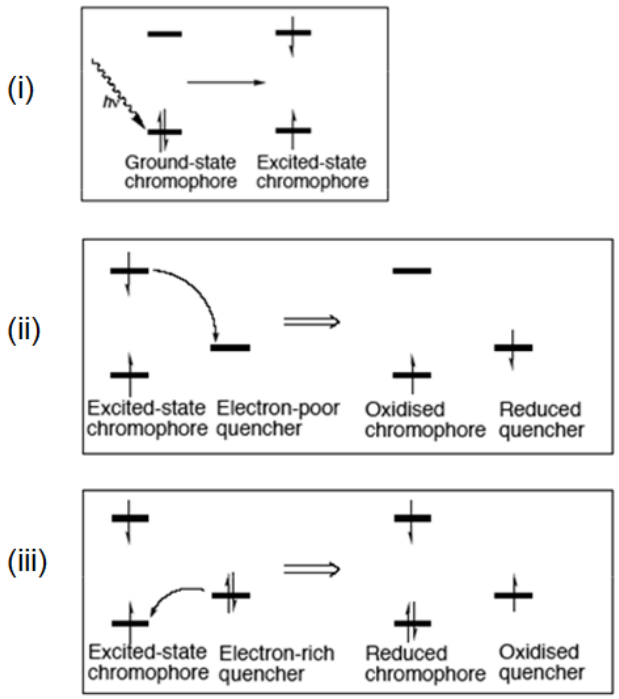

Figure 1.15 Electron transfer mechanism of a chromophore excited state

The importance and complexity of electron-transfer reactions in nature have prompted researchers to study the fundamental chemistry of these processes in simplified model systems. A major part of this effort has been devoted to the study of photoinduced electron transfer as a means of capturing and storing energy. A vital part of this research is the design of complex molecular systems which are comprised of electron donors and acceptors that mimic the charge separation function of photosynthetic proteins. These complex molecules are usually referred to as supramolecular systems. In this context, supramolecular systems have been developed to mimic the stepwise nature of photosynthetic charge separation. For example, Sessler et al.[55,56] have designed an interesting set of supramolecular donor-acceptor molecules to mimic the multichromophoric electron-transfer events of photosynthesis, (**Fig 1.16**). Substitution of

a porphyrin macrocycle with quinone resulted in a positive shift of the potential for porphyrin oxidation, while the quinone dianion gave a negative shift in the potential for porphyrin reduction.

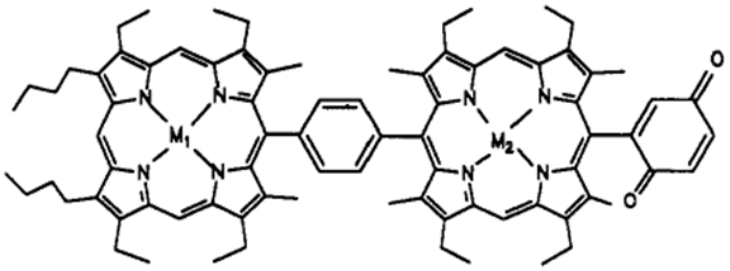

Figure 1.16 Structure of the supramolecular electron transfer system

Hence designing of supramolecular systems for charge separation would be able to deal with the problem of interfacing these systems to other chemical reactions. The stored oxidizing and reducing potential produced in these systems can be used to explore other chemistry in organized systems.[57]

1.7 Spin-spin interaction

Polyradicals (di-, tri- tetra- etc) are the compounds of critical importance, due to their paramagnetic nature, as well as their use as potential probes and sensors in many physical, chemical, or biological processes, or in labeling of nanoparticles, polymers, etc.[58-61] Organic materials based on stable polyradicals exhibit many interesting features, like ferro- or ferric magnetism, molecular magnets or wires, switches, and other metallic properties. The basis for bulk and molecular magnetic properties is the electron spin-spin interaction between unpaired electrons localized on different centers. The distances between spin centers in a polyradical system greatly affect the shape of Electron

paramagnetic resonance (EPR) spectra because an exchange interaction appears between two or more vicinal spins.[58,59] An EPR spectrum is usually characterized by the hyperfine coupling constants A_N, the *g* value, and the exchange interaction *J*.[58,59] If the distance between two spins is large, the EPR spectra of the system looks like two superimposed EPR spectrum, if the distance is short enough that the two unpaired electrons start to 'feel' each other (because they act as a small magnets), the corresponding spectra have a complicated shape, with supplementary lines *between* and *outside* the normal spectra lines. In the last case, if the distance is very short, a strong interaction appears between the two unpaired electrons, and in the EPR spectra characteristic supplementary lines appears in the middle of the normal ones.[58,59]

We will describe the spin-spin exchange interaction with diradical system as it is the simplest of all. The exchange interaction between two electrons 1 and 2 is demonstrated by the isotropic Heisenberg Hamiltonian $H = -2JS_1S_2$ where the eigen functions are the singlet and triplet functions and the eigenvalues are separated by $2J$ as shown below

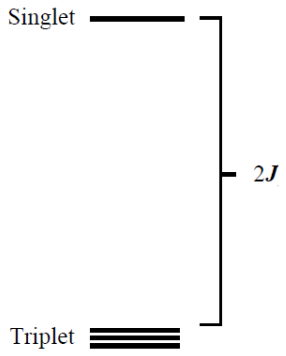

The spin Hamiltonian for a biradical can be described by the following equation[62,63]

$$H = g\beta_e B(S_z^{(1)} + S_z^{(2)}) + a(S_z^{(1)} \cdot I_z^{(1)} + S_z^{(2)} \cdot I_z^{(2)}) + J(S_z^{(1)} . S_z^{(2)})$$

where the first component is the Zeeman coupling between the unpaired electron spin and the magnetic field, the second component is the hyperfine coupling between the electron

spin and the nitrogen nuclear spin (I = 1 for a nitroxide-^{14}N radical; a is the hyperfine coupling constant between the electron spin and the nuclear spin), and the third component is the exchange coupling between the two electron spins (J is the exchange coupling constant). For the nitroxide biradical, two limiting cases are possible: (i) $a > J$, where each nitroxide separately contributes to the EPR signal which is therefore constituted of three lines (number of lines = $2I + 1$) corresponding to the nuclear configurations $I^{(1)} = I^{(2)} = -1, 0, +1$ with relative intensities of 1:1:1; (ii) $J > a$, that is, each electron interacts equally with the two nitrogen nuclei; in this latter case the spectrum consists of five lines with relative intensities 1:2:3:2:1, as schematically represented in **Fig 1.17 (i)**. Analogously, the trinitroxides present the same pattern in terms of number and position of lines. However, in these cases we are potentially dealing with three different J values, J_{12}, J_{23}, and J_{13}, corresponding to three different spin–spin interactions between the three nitroxides of the molecule. In the absence of spin–spin interactions, i.e., $J_{12} = J_{23} = J_{13} = 0$, the resulting spectrum is the typical three-line spectrum, whereas for $J_{12} \sim J_{23} \sim J_{13} > a$ a seven-line spectrum is expected with relative intensities of 1:3:6:7:6:3:1 (shown schematically in **Fig 1.17 (ii)**). Similarly, for the tetranitroxides shown schematically in **Fig 1.17 (iii)**, is composed of two configurations, one with $J = 0$ and the other with all $J > a$. For the latter, nine lines with relative intensities of 1:4:10:16:19:16:10:4:1 are expected.

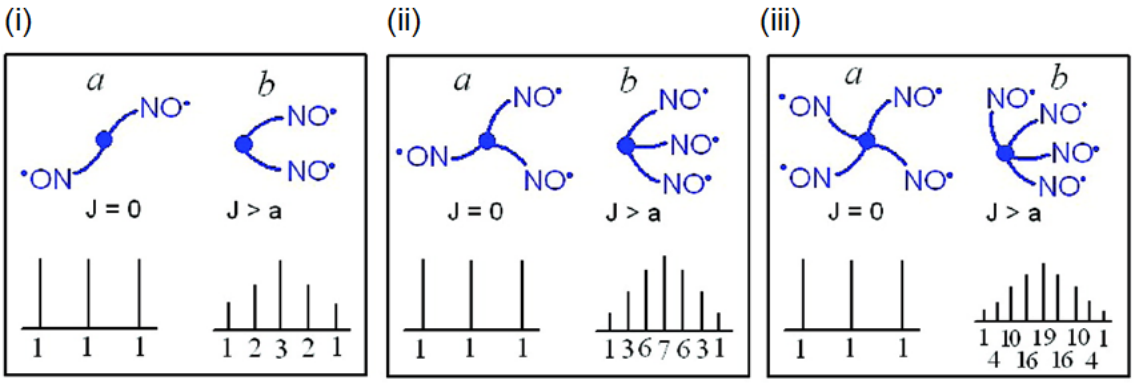

Figure 1.17 Schematic representation of slow exchange between two conformations (a, "far" conformation, with residence time τ_a; b, "close" conformation, with residence time τ_b) providing a two-component spectrum: (i) binitroxide; (ii) trinitroxide; (iii) tetranitroxide.

1.8 Aim and scope of this thesis

The main emphasis of this thesis is a detailed photophysical study on the complexation chemistry of a water soluble organic host, octa acid (OA). In **Chapter 2** we will discuss different analytical tools that we have used to characterize the host@guest complexes and study their photophysical behavior. One of our major goals was to explore this host as a photochemical reaction cavity for manipulating photochemical and photophysical properties of organic molecules in water. A detailed understanding of the internal characteristics of the OA cavity was needed to rationalize the selectivity within the cavity. This urge prompted us to study its molecular features such as micropolarity inside OA cavity which is detailed in **Chapter 3**.

In **Chapter 4**, we investigated the nature of supramolecular complexes formed by OA using 2-alkoxy naphthalene derivatives of different chain length and 2-naphthoic acid as guest. Studies on anthracene and naphthalene complexes with OA provided more in depth information about the mode of complexation. We further studied the dynamics of

the guest in the host-guest complex on the excited-state timescale. Using EPR spectroscopy on a series of paramagnetic guest molecules we monitored the rotation of the guest in nanosecond timescale (EPR time scale) within OA capsule.

After investigating the physical characteristics of the host system, we further extended our studies to explore the chemical processes which would be influenced by the host cavity. In that context we first studied the mechanism of electron transfer in supramolecular system. We developed a supramolecular system with the hydrophobic guest (4,4' dimethyl stilbene, donor) present within the capsule and the hydrophilic molecule (acceptor, cationic) interacting with the negatively charged exterior of OA (detailed in **Chapter 5**). Nanosecond flash photolysis enabled us to capture the transient intermediate species in the electron transfer process.

Despite elucidating a number of key features regarding photoinduced electron transfer in supramolecular assembly in **Chapter 5**, nanosecond flash photolysis did not allow us to study the electron transfer rates that occur in picosecond time scale or faster. In that case femtosecond pump-probe spectroscopy was useful to monitor the forward and back electron transfer rates in the supramolecular system (**Chapter 6**). In this chapter we also showed the adsorption of OA complex on TiO_2 surface and thus electron transfer from an encapsulated donor to TiO_2 semiconductor.

We also explored the feasibility of the nuclear spin-electron spin communication between an incarcerated excited diamagnetic guest molecule within OA capsule and a free paramagnetic nitroxide in water even without direct overlap of their orbitals (**Chapter 7**). Using time resolved EPR spectroscopy we showed the feasibility of

electron spin polarization transfer from a spin polarized triplet of a guest, encapsulated within OA capsule, to nitroxide in water.

In **Chapter 8**, we have demonstrated the possibility of trapping a high-energy conformer of a piperidine derivative within a supramolecular assembly in aqueous solution.

In addition to OA host system, we further the studied the complexeation pattern of the paramagnetic guest molecules (nitroxide derivatives) with the water soluble cucurbituril (CB) host system. We focused on the two widely used CB derivatives, CB7 and CB8 for complexation study (**Chapter 9**).

Finally in **Chapter 10**, we established that spin-spin communication in the diradical and polyradical system can be controlled by supramolecular effect. In this context we compared the efficiency of different host systems such as CB8, CB7, β-cyclodextrin (β-CD), γ-cyclodextrin (γ-CD), calixarene[8]octa sulfonic acid (CA8) and sodium dodecyl sulfate (SDS) micelle.

CHAPTER 2

Experimental Tools Used in This Thesis

In this thesis we have studied the formation and characterization of a number of host/guest complexes and their photophysical behavior. To accomplish with that we used a variety of analytical techniques such as nuclear magnetic resonance (NMR) spectroscopy, UV-visible (UV-Vis) spectroscopy, emission spectroscopy, nanosecond flash photolysis and femtosecond pump-probe spectroscopy, mass spectroscopy, fourier transformed attenuated total reflectance infrared (FT-ATR-IR) spectroscopy and electron paramagnetic resonance (EPR) spectroscopy. In this chapter we will discuss a brief description of these characterization techniques.

2.1 NMR spectroscopy

NMR spectroscopy is one of the most important characterization tools in studying supramolecular systems. Both 1D and 2D NMR experiments were found to be very useful to provide information regarding the host/guest interaction and orientation of the guest within the host. The different NMR experiments that have been used in the work presented in this thesis are enlisted below:

2.1.1 ^{1}H NMR spectroscopy

An upfield shift of the guest proton signals in the ^{1}H NMR spectra caused by the magnetic shielding provided by the aromatic walls of the host interior served as an experimental test for inclusion of a guest within the host cavity.[64-66] For example, the chemical shift (δ) of $-CH_3$ group of 2-acetyl antracene was 2.5 ppm and -0.5 ppm in absence and presence of a host, octa acid respectively.[5] This experiment revealed whether the guest was encapsulated by the host or not. Depending on the supramolecular system, the magnitude of the chemical shift of the guest protons observed varied. For example the

upfield shift of the guest protons in presence of a host octa acid (**Chapter 3**) and another host cucurbituril (**Chapter 9**) were different.

2.1.2 Pulse gradient spin-echo diffusion spectroscopy (PGSE DOSY)

We performed the pulse gradient spin−echo diffusion NMR experiments to obtain the diffusion constants for the host@guest complexes. The diffusion constant (D) was calculated using the following equation:

$$D = kT/6\ \pi\eta R_h$$

R_h is the hydrodynamic radius of the sphere (the host-guest complex is considered as a sphere), k is the Boltzmann constant, T is the temperature in kelvin, and η is the solvent viscosity. From the equation it is clear that diffusion constant of the supramolecular complex depends on its hydrodynamic radius. With this information we were able to distinguish the formation of cavitandplex or capsulplex as capsuleplex would be larger in size than the cavitandplex formed by the same host.

2.1.3 Two-dimensional correlation spectroscopy (2D COSY)

Two-dimensional correlation spectroscopy (2D COSY) shows the correlation between two hydrogen of the adjacent carbon atom and allows us to conclude the connectivity of a molecule by determining which protons is spin-spin coupled. 2D COSY spectra of the complexes also helped us to assign the ^{1}H NMR signals of the host and the guest in the complex ^{1}H NMR spectra.

2.1.4 Double quantum filtered correlation spectroscopy (2D DQF COSY)

We also performed 2D DQF COSY in addition to 2D COSY to get more inside the host/guest complex. Strong cross peaks between diaxial- and geminal-hydrogens and weak or negligible cross peaks between axial-equatorial hydrogens are expected in 2D

DQF-COSY spectra. In **Chapter 8**, we distinguished the two conformers (axial-equatorial) of a piperidine derivative within the host capsule by 2D DQF COSY inside the host.

2.1.5 Two-dimensional nuclear overhauser spectroscopy (2D NOESY)

2D NOESY shows the correlation among the protons that are spatially close rather than those that are through-bond coupled to each other. The NOE interaction between the guest and host protons helped us to confirm the complex formation between the guest and host. It also allowed us to investigate the guest orientation within the host capsule.

2.1.6 Rotating-frame nuclear Overhauser effect correlation spectroscopy (2D ROESY)

The exchange peaks (via exchange spectroscopy (EXSY)) and through space interacting peaks (via NOESY) can be easily distinguished in the ROESY spectrum. Importantly, the EXSY cross-peaks have the same sign as the diagonal whereas the NOESY cross-peaks have the opposite signs as the diagonal ones.[67-69] Therefore this NMR experiment was used to identify the exchange between the two conformer of a guest inside the host capsule in the NMR time range (**Chapter 8**).

2.2 UV-vis spectroscopy

The sensitivity of UV-vis spectroscopy is greater than that of NMR. Sample concentrations for UV-visible experiments are typically in the order of 10^{-4} to 10^{-5} M, depending on the extinction coefficient of the compounds under study. UV-vis spectroscopy generally cannot provide as much information about the location of the

host-guest binding as NMR spectroscopy can but the former was very useful to characterize the photophysical behavior of the host@guest complex. The minimum requirement to use UV-vis spectroscopy in our study was that at least one of the samples needs to show absorption in the UV-visible region (between approximately 200 and 800 nm). We conducted UV-vis experiment prior to each emission study on supramolecular complex to select the excitation wavelength for the emission experiments.

2.3 Emission spectroscopy

Emission spectroscopic experiments have been extensively used in the works that have been reported in this thesis. The sensitivity of emission spectroscopy is even more than that of the UV-vis spectroscopy. The encapsulation of a guest in a host can affect its emission (fluorescence and phosphorescence) properties, such as change in wavelength (red shift or blue shift) and change in the intensity of emission spectra, which were utilized as an indication of complexation. In addition to that, we were able to monitor whether there were one or two guests inside host capsule from the monomer and excimer emission of the guest in complex (**Chapter 4**). Steady state emission experiments were used to explore the photophysical behavior of the host/guest complex. We used time resolved emission experiment to obtain the life time of the chromophore in the singlet or triplet excited state.

2.4 Nanosecond flash photolysis and femtosecond pump-probe spectroscopy

These two techniques provide the spectra of the transient spices generated in a chemical process in excited state such as electron transfer process. The transient spectra are composed of three contributions: (i) transient absorption of the excited state species generated, (ii) laser induced fluorescence from the singlet excited state and (iii) ground

state absorption bleaching, due to the transient depopulation of the ground state. We were able to capture the transient intermediates generated in the electron transfer process in the supramolecular assembly. Kinetic study was useful to measure their lifetime in nanosecond timescale (by nanosecond flash photolysis) and also in femtosecond time scale (femtosecond pump-probe).

2.4.1 Nanosecond flash photolysis

Laser flash photolysis experiments employed the pulses from a Lambda Physik Lextra 50 excimer laser (308 nm, pulse width 15 ns) and a home built system.[70] (**Chapter 5)**

All the flash photolysis experiments were performed in Prof. NicholasTurro's lab (Columbia University, New York) and the transient absorption spectra were recorded by Dr. Steffen Jockusch. I heartily thank Prof. Turro and Dr. Jockusch for their continuous help and support.

2.4.2 Femtosecond pump-probe spectroscopy

Femtosecond transient absorption measurements were conducted using a Clark MXR 2001 femtosecond laser system producing 780 nm, 150 fs pulses from a regenerative amplifier.[71-73] The laser pulse train was split to generate a white light continuum probe pulse in a sapphire crystal and a 390 nm pump pulse using second harmonic generation. The excitation power of ~ 5 mJ / cm^2 per pulse fluence was controlled carefully. All femtosecond laser experiments were carried out in a 2 mm quartz cuvette at room temperature. The instrumental time resolution was determined to ~150 fs via a pump-probe cross-correlation analysis (**Chapter 6**).

The femtosecond pump-probe experiments were carried out in Prof. Clemens Burda's lab (Case Western Reserve University, Ohio) and the transient absorption spectra were recorded by Chi-hung Chuang. I am very much thankful to Prof. Burda and Chi-Hung for their help.

2.5 FT-ATR-IR spectroscopy

Infrared spectroscopy is a reliable and well recognized method to characterize, identify and also quantify the chemical substances. IR spectroscopy is an important analytical technique to obtain spectra from a very wide range of solids, liquids and gases. An attenuated total reflection (ATR) technique measures the changes that occur in a totally internally reflected infrared beam when the beam comes into contact with a sample (**Figure 2.1**). An infrared beam is absorbed onto an optically dense crystal with a high refractive index at a certain angle. The internal reflectance creates an evanescent wave that extends beyond the surface of the crystal into the sample held in contact with the crystal. This evanescent wave protrudes only a few microns (0.5 μ - 5 μ) beyond the crystal surface and into the sample. Thus, there must be good contact between the sample and the crystal surface. The evanescent wave will be attenuated in the regions of the infrared spectrum where the sample absorbs energy. The attenuated energy from each evanescent wave is passed back to the IR beam, which then exits the opposite end of the crystal and is passed to the detector in the IR spectrometer. The system then generates an infrared spectrum.

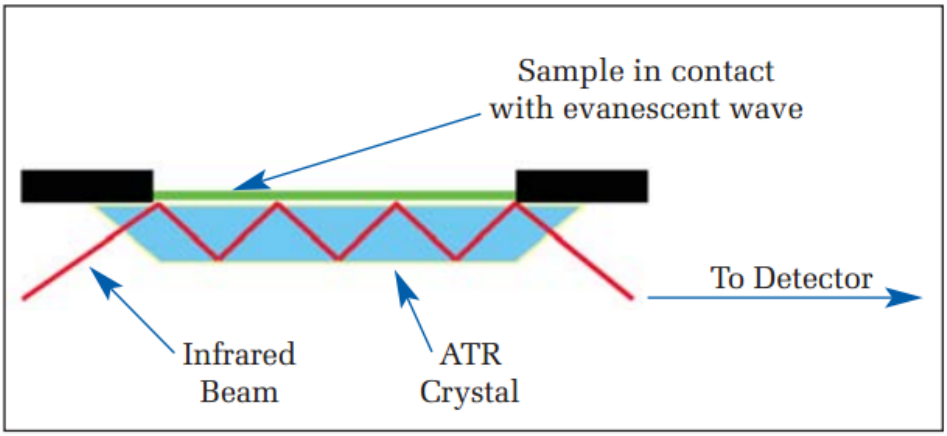

Figure 2.1 Schematic representation of a multiple reflection ATR system

FT-ATR-IR was very useful in our works to characterize the metal oxide films (TiO_2 and ZrO_2) coated with supramolecular assembly (**Chapter 6**). All FT-ATR-IR spectra for supramolecular assembly on TiO_2/ZrO_2 films were recorded on a Thermo Scientific, Nicolet 6700Ft-IR. The films were dried by heating in the oven to 110 ^oC for 30 min before all measurements.

The FT-ATR-IR experiments were carried out in Prof. Elena Galoppini's lab (Rutgers University, New Jersey) and the FT-ATR-IR spectra were recorded by Dr. Marina Freitag and Agnieszka Klimczak.

2.6 EPR spectroscopy

Electron paramagnetic resonance (EPR) or electron spin resonance (ESR) spectroscopy is a technique for studying materials with unpaired electrons. The basic concept of EPR is analogous to that of NMR, but it is electron spin that is excited instead of the spin of atomic nuclei.

In addition to diamagnetic guest molecules we also used a number of paramagnetic guest molecules in this work. As ^1H NMR signal of those guests became

broaden due to the presence of radical, we used EPR spectroscopy to identify the different features in those systems. EPR spectra were recorded at room temperature in Bruker EMX spectrometer at 9.5 GHz (X band) employing 100 KHz of field modulation frequency. Spectrometer setting: Power, 1.997 mW; amplitude modulation, 0.50 G; time constant, 163.84 ms; conversion time, 163.84 ms. Samples were loaded to quartz (CFQ) EPR tubes from Wilmad LabGlass (2 mm OD, 0.5 mm wall thickness, 10 cm height) for the EPR experiments. The experimental spectra were simulated to obtain the informative parameters in the working systems.

2.6.1 EPR Simulations

The EPR spectra were computed by using the program Simfonia by Bruker. The EPR signals were computed by the well-established procedure of Budil and Freed.[74] The main input parameters were as follows: (a) the g_{ii} components (for the coupling between the electron spin and the magnetic field) were the ones used for the nitroxide (g_{xx}=2.009, g_{yy}=2.006, g_{zz}=2.0025),[75] and were considered constant for all samples; (b) The A_{ii} principal values of the **A** tensor for the coupling between electron and nuclear spin ($<A_N>=(A_{xx}+A_{yy}+A_{zz})/3$). An increase in the environmental polarity of the NO group provokes an increase in the **A** tensor components owing to the increased electron spin density on the nitrogen nucleus. (c) The perpendicular component of the correlation time for rotational diffusion (τ_{perp}). Brownian motion was assumed in the calculation, for which the diffusion component is $D_{perp} = 1/(6\tau_{perp})$.

g-factor

In the absence of nuclear hyperfine interaction the nuclei involved have no nuclear spin, and therefore, there will be no nuclear Zeeman term or nuclear electric quadrupole term.

In that condition, magnetic field B and frequency, ν are related by

$$h\nu = g\mu B B$$

where h is the Planck constant, μB is the Bohr magneton $eh/(4\pi m e)$, and the dimensionless scalar g is called g-factor.

g-matrix

When the paramagnetic species exhibits anisotropy, the spatial dependency of the g-factor is represented by a 3×3 matrix g. The matrix representation is referred to as g-matrix. In a general coordinate system, such as (x, y, z), the components are designated as g_{xx}, g_{xy}, ..., etc. In cases where a principal axis system are assigned, in which the off-diagonal terms are zero, the three principal values of the g-matrix would be expressed by g with a single subscript identical to the principal axis designation adopted for the g-matrix g_{xx}, g_{yy}, g_{zz} for the principal axes (x, y and z).

Hyperfine coupling constant

The interaction energy between the electron spin and a magnetic nucleus is characterized by the hyperfine coupling constant A. It is known that the ^{14}N isotropic hyperfine splitting constant, A_N, EPR spectrum of nitroxide free radicals is sensitive to the polarity of the solvent in which they are dissolved. In terms of valence bond theory two canonical structures (**I** and **II**, **Fig 2.2**) can be drawn for the nitroxide functional group.

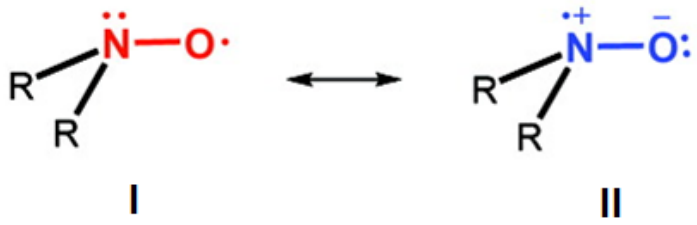

Figure 2.2 Two canonical structures of nitroxide

More polar solvents favor the structure **II** (**Fig 2.2**) i.e. increasing the electron density on oxygen whereas increasing the spin density on nitrogen. According to the theory of Karplus and Fraenkel[76]

$$\mathbf{A_N = (S^N + Q_{NO}{}^N + 2Q_{NC}{}^N)\rho_N{}^\pi + Q_{ON}{}^N\rho_O{}^\pi + 2Q_{CN}{}^N\rho_C{}^\pi}$$

where $\rho_N{}^\pi$, $\rho_O{}^\pi$, $\rho_C{}^\pi$ are the π-electron spin densities at the nitrogen, oxygen, and adjacent carbon atoms, respectively; S^N represents the contribution to the splitting from the nitrogen 1s electrons; and the Q's represent the contributions of the 2s electrons (e.g., $Q_{ON}{}^N$ is the π-σ parameter for the nucleus of the nitrogen resulting from the interaction between the ON bond and the π-electron density on the oxygen). In this case increasing the spin density on nitrogen and decreasing it on oxygen would increase the magnitude of A_N. Thus, changing the solvent in which the nitroxide is dissolved from one which is less polar to one which is more polar should increase the magnitude of A_N. According to 2I+1 rule, EPR spectrum of ^{14}N nitroxide (I= 1) splits into three lines and A_N value is calculated as follows (**Fig 2.3**):

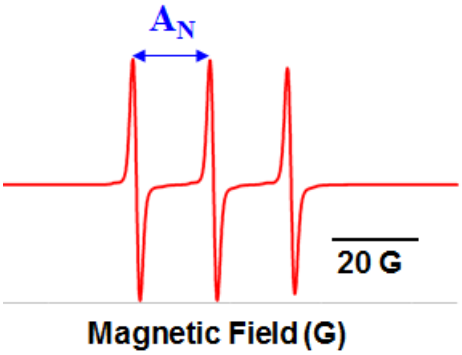

Figure 2.3 EPR spectrum of ^{14}N nitroxide

Rotational Correlation Time (τ_{perp})

Rotational correlation time is the time it takes for a molecule to rotate one radian, on average. Rotational correlation time of probe molecules with unpaired electron is measured from the line-widths of electron spin resonances. Brownian motion is assumed in the calculation of the main component of the correlation time, that is, the perpendicular one (τ_{perp}). **Fig 2.4** shows the schematic diagram of τ_{perp} of the nitroxide.

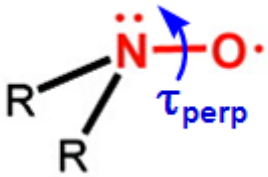

Figure 2.4 Schematic diagram of τ_{perp} of the nitroxide

The τ_{perp} value increases with increasing the mobility of the probe. τ_{perp} is an important parameter to assign the location of the guest molecule (with unpaired electron) in a supramolecular system. When the guest molecule is within a host molecule, its mobility is restricted and hence τ_{perp} is found to be enhanced compared to the guest in solution. The value of τ_{perp} can be calculated from the experimental EPR spectrum (**Fig 2.5**):

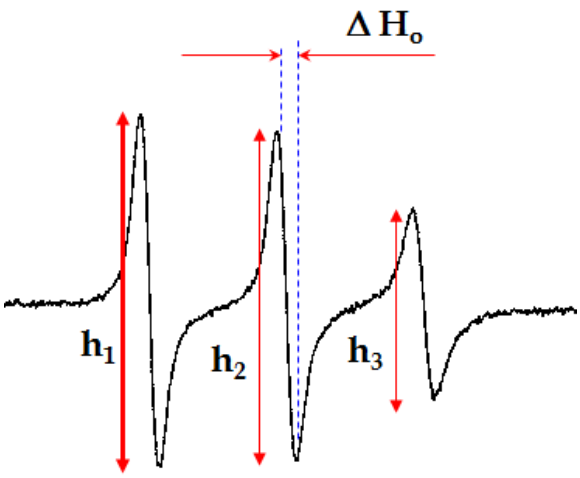

Figure 2.5 Calculation of τ_{perp} from EPR spectrum of nitroxide

τ_{perp} is calculated from **Fig 2.5** as follows:

$$\tau_{perp} = 6.5 \times 10^{-10} \Delta H_0 [(h_2/h_3)^{1/2} + (h_2/h_1)^{1/2} - 2]$$

The simulation of EPR spectra was carried out by Prof. Maria Francesca Ottaviani (University of Urbino, Italy) and without her kind help EPR studies were impossible.

2.6.2 Time resolved EPR

Time-resolved electron paramagnetic resonance (TR EPR) is used to study the phenomena involving electron spin polarization, particularly in the area of electron polarization transfer. Electron spin polarization transfer studies provide the information concerning the details of the mechanism involved in polarization creation. The various reactive and nonreactive phenomenon producing electron spin polarization are commonly gathered together under the term of chemically induced dynamic electron polarization (CIDEP), even for systems not involving chemical reactions. The two most frequently invoked mechanisms for generating CIDEP[1-6] are (i) the radical pair mechanism (RPM) and (ii) the triplet mechanism (TM).[77-80]

In the RPM, the observed CIDEP occurs after the radicals are produced and the polarization is generated by radical pair interactions modulated by exchange interactions and the hyperfine selective reactivity of the pair. Pure RPM is characterized by CIDEP spectra which appear partially in emission and partially in absorption (so-called multiplet spectra). In the TM, the observed CIDEP occurs before the radicals are produced and the polarization is generated in two steps. In the first step, the triplet sublevels are polarized by (spin-orbit induced) sublevel selective S_1 – T_1 intersystem crossing; then the polarization generated in the triplet manifold is transferred by rapid reaction to form the radicals (**Figure 2.6**). Pure TM is characterized by CIDEP spectra which appear as pure emission or pure absorption (so-called net spectra, **Figure 2.6**). In many experimental examples,[77-80] the observed CIDEP spectra are superimpositions of the RPM and TM generated polarizations.

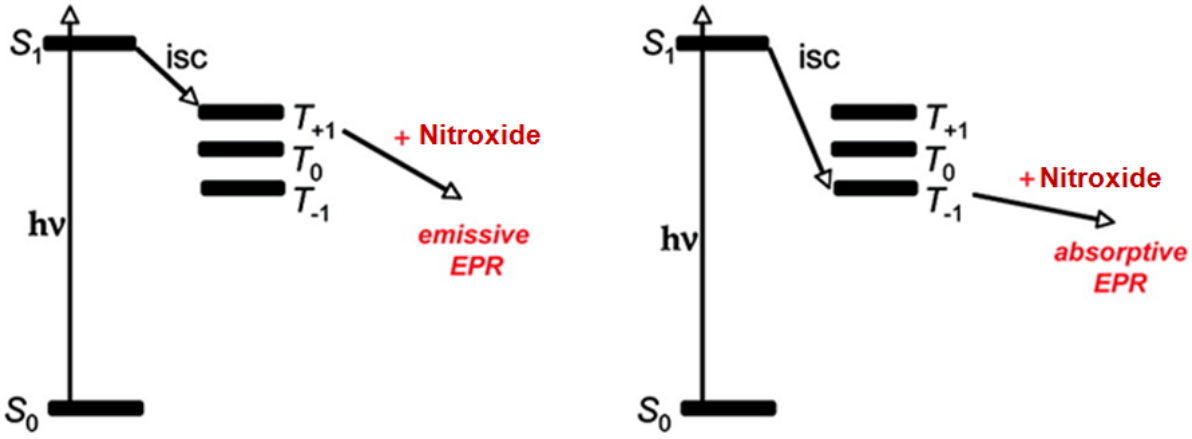

Figure 2.6 Triplet Sublevel Selective Intersystem Crossing Generating Spin-Polarized Triplet States

Pure RTPM is characterized by pure emissive or pure absorptive polarization, but in contrast to the situation for TM, the sign of the polarization is independent of the selectivity of the triplet sublevel population. The CIDEP generated by TM may be transferred to radicals, and a number of examples of such transfer to stable nitroxyl radicals have been proposed (**Figure 2.6**).[77,81,82] The absorptive and emissive polarization transfer can easily be monitored by TR-EPR spectra (**Fig 2.7**).

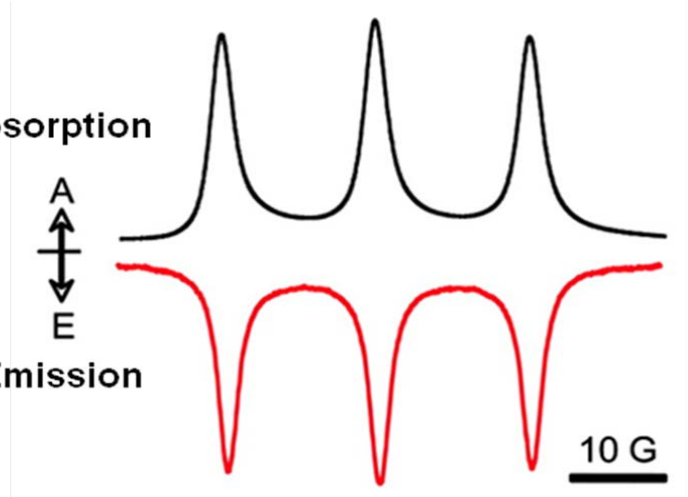

Figure 2.7 The absorptive and emissive TR-EPR spectra in electron spin polarization transfer

CHAPTER 3

Investigation of Micropolarity inside Octa Acid Capsule

3.1 Overview

The importance of supramolecular assemblies to control the excited and ground-state processes of organic molecules has received continued interest during the last three decades.[83-87] A variety of organized assemblies such as micelles, dendrimers, liquid crystals, polymers, gels, crystals, and both organic and inorganic hosts (cyclodextrins (CD), cucurbiturils (CB), calixarenes (CA), cavitands, cholic acids, clay, zeolites, mesoporous materials, etc.) have been explored, in particular, as reaction media with the main goal of identifying the common features, and comparing the properties of their reaction cavities.[88-98] Recently a synthetic cavitand octa acid (OA) (**Scheme 3.1**) has been added to the arsenal of supramolecular hosts.[40,99] The eight carboxylic acids on both the top and bottom rims of OA solubilize it in water under basic (pH ≈ 9.0) conditions. We were interested to explore this host as a photochemical reaction cavity for manipulating photochemical and photophysical properties of organic molecules based on our experimental setup.[100-102] A detailed understanding of the internal characteristics of the OA cavity was needed to rationalize the selectivity within the cavity. This urge prompted us to study its molecular properties such as micropolarity inside OA cavity.

The organic guest molecule forms a capsuleplex with two OA molecules in aqueous media. So the question arises whether water molecules are present inside the OA capsule in order to predict the effect of the host cavity on photochemical transformations of a guest. This knowledge would also help us to understand the driving force for the complexation process including weak interactions between the host and the guest. In this study we used phenanthrene (**1a**, **Scheme 3.1**) to show how an organic guest forms capsuleplex with OA. Five organic molecules (pyrene,[103-105] pyrenealdehyde,[106-110] 2-

acetylanthracene,[111,112] coumarin-1,[113,114] and 7-*O*-propylcoumarin[115-118] (**Scheme 3.1** as **1b-f**) known as polarity probes were used to monitor the polarity of the interior of the guest-occupied OA capsule. The absorption and emission maxima, intensity of emission and its vibrational pattern, and the excited singlet lifetime of these probes are controlled by the polarity of the medium in which they are present. As the size of all these five probes were similar with phenanthrene, they were expected to form complex with OA and thus would be excellent candidates to monitor the micropolarity within OA capsule.

^{1}H NMR studies were performed to establish the nature of the OA−probe complexation process. It is important to know the exact location of these probes during their emissive process. 2D COSY and 2D NOESY experiments were carried out to investigate the orientation of the probe inside OA capsule. We have monitored the micropolarity of the interior of the cavitand by recording the fluorescence of five different organic probes (**1b-f**) in absence and presence of OA.

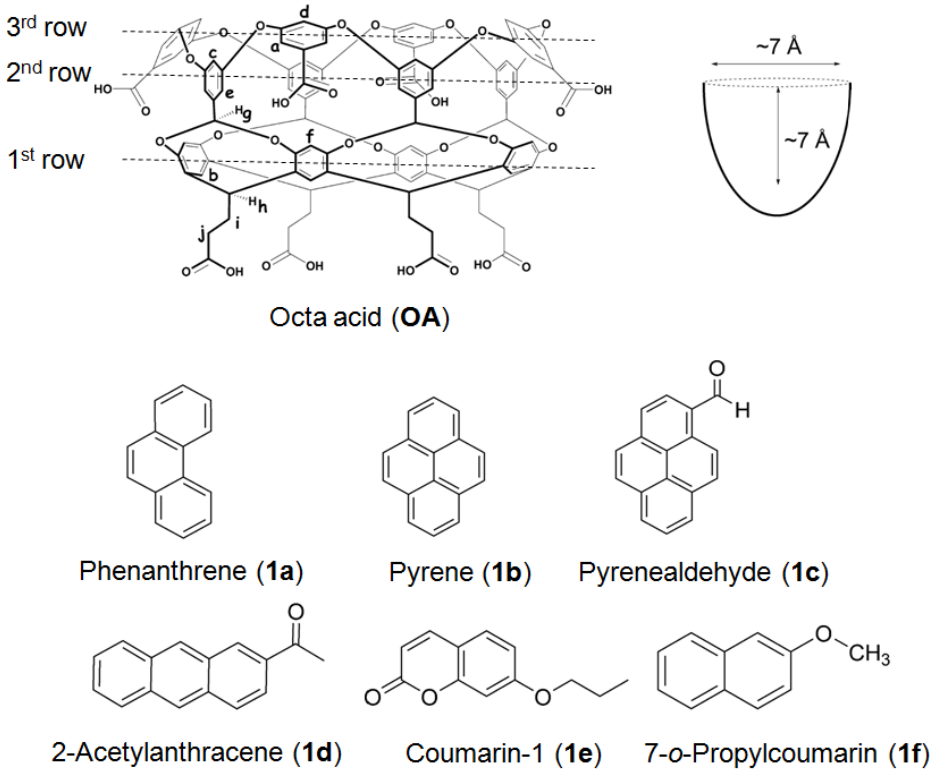

Scheme 3.1 Structures of host (octa acid, OA) and organic molecules (**1a-f**) used as probes.

3.2 Results and discussion

3.2.1 Complexation studies of phenanthrene (1a) with OA

We used fluorescence spectroscopy to investigate the inclusion of phenanthrene (**1a, Scheme 3.1**) within the host molecule by monitoring the change in its emission properties. Aromatic molecules are known to aggregate in water and show distinct emission behavior (different range of wavelength) of monomers and aggregates.[119-122] The emission of aggregates reverts to that of the monomer on dispersion. We utilized this feature to investigate if **1a** could be included within the OA capsule. As shown in **Fig 3.1**, emission spectra of **1a** in water in the presence and absence of OA were very different. A

weak emission between 370-470 nm was observed upon excitation at 300 nm to a suspension of **1a** in borate buffer (10^{-5} M) due to its aggregate formation. After addition of 2 equiv of OA (2×10^{-5} M) to this turbid solution it became clearer indicating the solubiliziation of **1a** in water by the host OA. In presence of OA, the emission spectrum of **1a** became intense, structured, and blue-shifted (**Fig 3.1**).

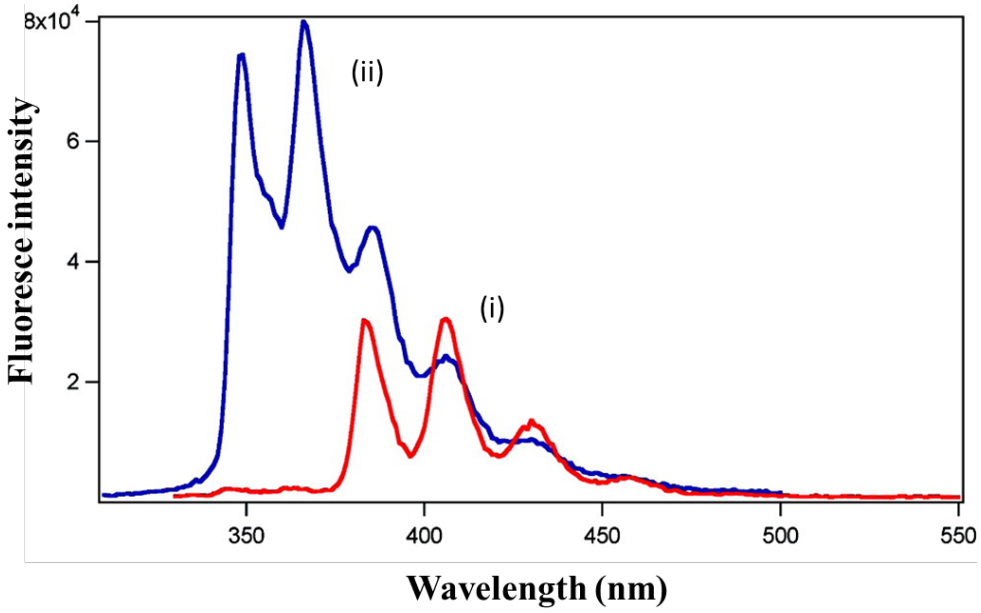

Figure 3.1 Fluorescence emission spectra of (i) **1a** in borate buffer (1×10^{-5} M, pH ≈ 9.0) and (ii) **1a**@OA_2 in borate buffer (pH ≈ 9.0), Excitation wavelength: 300 nm.

We were not able to record ^{1}H NMR spectrum of **1a** in D_2O due to the poor solubility in water resulting from its highly hydrophobic nature. However, upon addition of 2 equiv of OA (1 mM in 20 mM borate buffer in D_2O) to the suspension of **1a** (0.5 mM) in D_2O, the solution became clear and allowed us to perform the ^{1}H NMR experiment. The upfield-shift of the **1a** proton signals in presence of OA suggested that it formed a 2:1 (host: guest) capsule with OA (**Fig 3.2**).

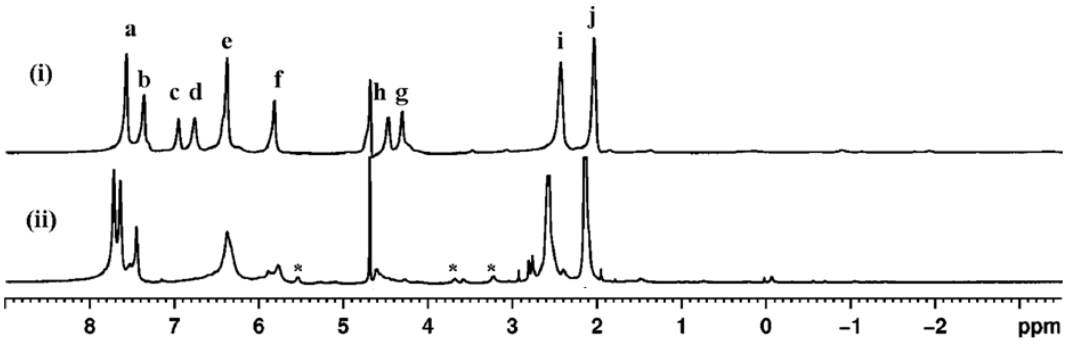

Figure 3.2 ^{1}H NMR spectra (500 MHz) of (i) OA and (ii) **1a**@OA_2 [OA] = 1 mM in 10 mM borate buffered D_2O, [**1a**] = 0.5 mM. Guest signals are marked with * and those due to the host are labeled with letters.

Further to confirm the complexation between **1a** and OA we conducted two-dimensional correlation spectroscopy (2D COSY) and two-dimensional nuclear overhauser spectroscopy (2D NOESY) experiments of **1a**@OA_2 capsuleplex. 2D COSY spectra shows the correlation between two hydrogens of the adjacent carbon atoms and allows one to conclude the connectivity of a molecule by determining which protons are spin-spin coupled. 2D COSY spectrum of **1a**@OA_2 capsuleplex (see **Fig 3.3**) allowed us to rationale the proton signals of **1a** inside OA capsule.

2D NOESY provided further confirmation of encapsulation of **1a** within the confined space of the complex by through-space interactions between host and guest protons. As illustrated in **Fig 3.4**, the guest protons "H_1" and "H_2" were strongly correlated with the host protons "H_g" and "H_d". In addition there was also correlation between the guest proton "H_1" and host proton "H_a". Those 2D NOESY correlations between the host and guest protons also confirmed that **1a** was confined within OA capsule.

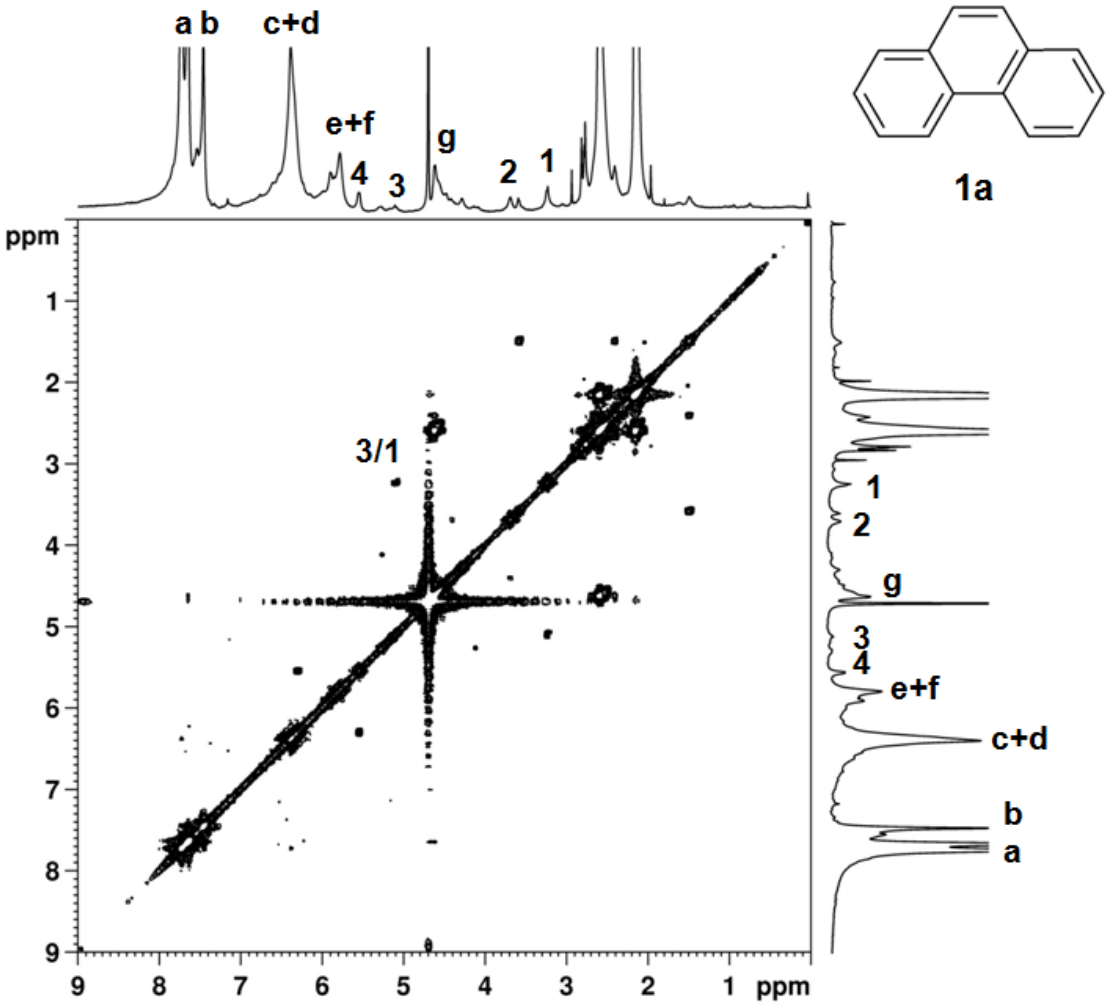

Figure 3.3 2D COSY spectrum (500 MHz, 5 mM) of **1a**@OA_2 in buffered D_2O (50 mM) (OA peaks marked as a-f and guest peaks marked as 1-4).

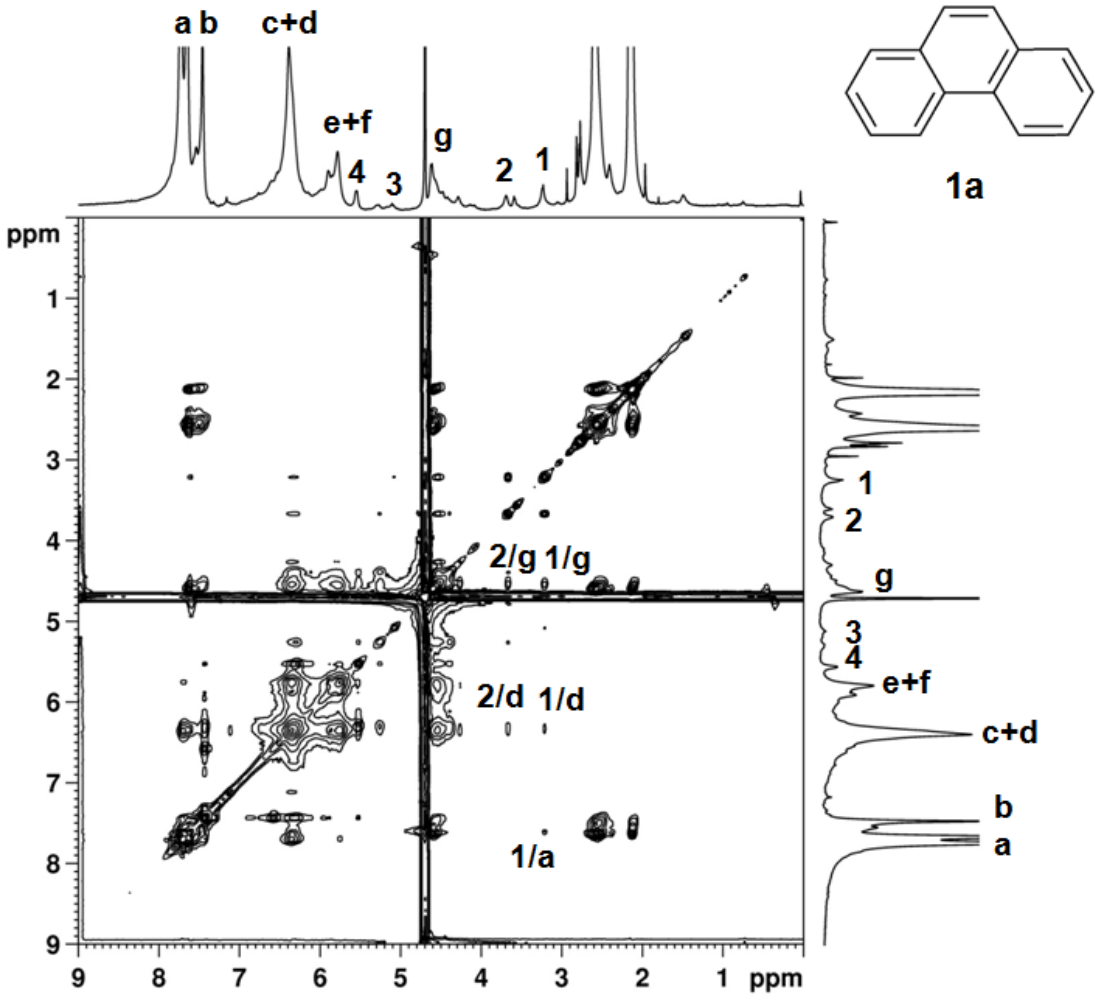

Figure 3.4 2D NOESY spectrum (500 MHz, 5 mM) of **1a**@$(OA)_2$ in buffered D_2O (50 mM).(OA peaks marked as a-f and guest peaks marked as 1-4).

3.2.2 NMR experiments to reveal 1c-f/OA complex

Next we aimed to study the inclusion of the micropolarity indicators **1b**−**f** within the OA host and the stoichiometry of host to guest (H/G) complexes by recording their ^{1}H NMR spectra. It is reported that **1b** forms a strong capsuleplex with OA.[123] ^{1}H NMR studies of other four probes (**1c-f, Scheme 3.1**) in the absence and presence of OA in sodium tetraborate buffer (pH ~ 9) were carried out to confirm the host/guest complex

formation. In the ^{1}H NMR spectra, an upfield shift of the guest proton signals caused by the magnetic shielding provided by the aromatic walls of the host interior served as an experimental test for encapsulation of a guest within the OA cavity.[102,123,124] We observed such upfield shifts for all the complexes of OA with **1b-f**.

For example, ^{1}H NMR signal due to -CHO of **1c** that appears at ~10 ppm in chloroform was upfield shifted to 8.5 ppm in aqueous solution containing OA (4×10^{-3} M) and **1c** (2×10^{-3} M) (**Fig 3.5ii**). Similarly, there was an upfield shift in the ^{1}H NMR signals due to **1d** (1×10^{-3} M) in presence of 2 equiv of OA in D_2O (2×10^{-3} M, 10 mM borate buffer, pH ≈ 9.0) (**Fig 3.5iii**). The ^{1}H NMR signal due to $-COCH_3$ group of **1d** that appeared at 2.5 ppm in chloroform was significantly upfield shifted (−0.5 ppm) in the presence of OA. An upfield shift of $\Delta\delta \approx 3$ ppm suggested that the molecule was encapsulated within the OA capsule. The upfield shift of the signals due to alkyl chains in **1e** and **1f** in presence of OA (**Fig 3.5 iv** and **v**) indicated their inclusion within the OA capsule.

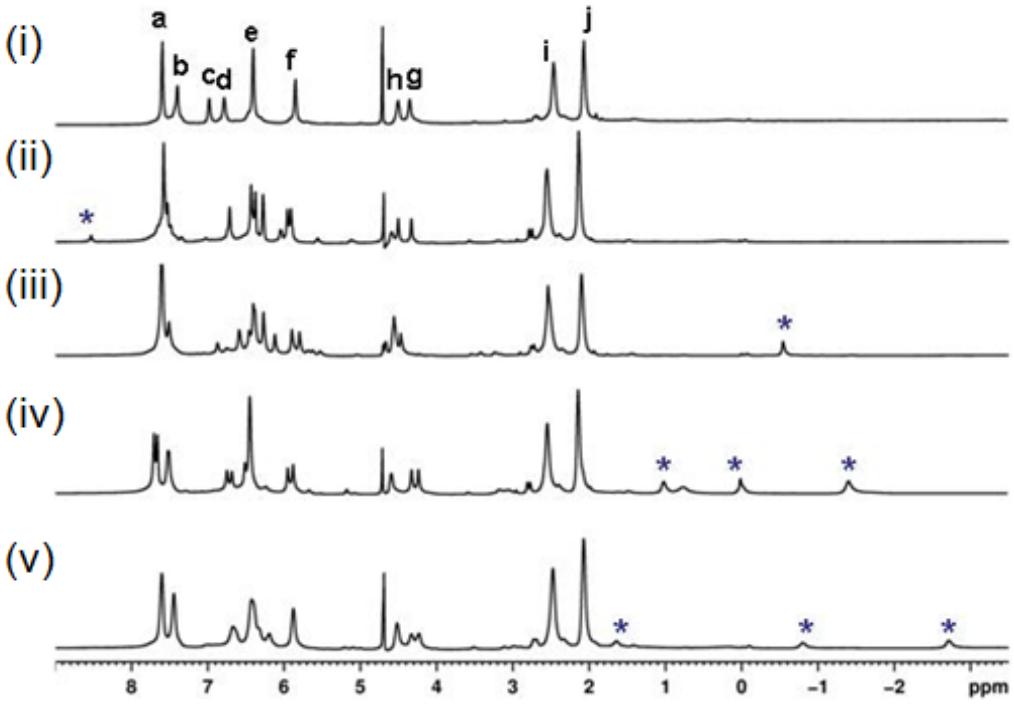

Figure 3.5 ^{1}H NMR spectra of (i) OA (1 mM), (ii) **1c**@OA_2, (iii) **1d**@OA_2, (iv) **1e**@OA_2 and (v) **1f**@OA_2. [OA] = 1 mM in 10 mM borate buffered D_2O, [Guest] = 0.5 mM. Guest signals are marked with *.

The stoichiometry of the complexes (H/G ratio) was determined through titration experiments. Addition of guests **1b−f** to a host solution beyond a 2:1 ratio (H/G) resulted in a turbid solution, indicating that excess probe molecules remained in water as aggregates. This also suggested a 2:1 complex of host/guest in each case. As the guests (**1c-f**) are dissymmetric, the capsule formed by them with two identical OA molecules would be lacking symmetry with different capsular top and bottom halves and that could lead to different chemical shifts for identical hydrogens of OA. For example, with **1c** as the guest, the signals due to H_e, H_f, and H_g were split (**Fig 3.5(ii)**). In the case of **1d**, splitting of H_f and H_g ^{1}H signals was noted (**Fig 3.5(iii)**). Similar splitting of signals due

to host $H_{a,c,f,g}$ protons in the case of unsymmetrical **1e** (**Fig 3.5iv**) and H_{a-g} protons of **1f** were observed (**Fig 3.5v**). Hence, the ^1H NMR studies clearly established that all five probes (**1b-f**) were located as single molecule within the capsule formed by two molecules of OA.

We performed the pulse gradient spin−echo diffusion (PGSE) NMR experiments to obtain the diffusion constants for the OA complexes with **1a−e** (**Table 3.1**). The diffusion constant (D) were calculated using the following equation:

$$D = kT/6\ \pi\eta R_h$$

R_h is the hydrodynamic radius of the sphere (the host-guest complex is considered as a sphere), k is the Boltzmann constant, T is the temperature in K, and η is the solvent viscosity. The 2:1 complexes had low diffusion constant than free OA in water (**Table 3.1**). This was also an indication of the formation of capsular assembly as the hydrodynamic radius of capsular complex is expected to be larger than that of free OA cavitand. Hence the diffusion constant of a capsuleplex was less than that of OA cavity. The values were in the same range obtained from the previous report for 2:1 complex of OA with other guests. [34−37]

Table 3.1 Diffusion constant (D) for the capsular assemblies of polarity probes with OA

Complex[a]	**Diffusion constant (cm^2/s)**
1**a**@OA_2	1.45×10^{-6}
1**b**@OA_2	1.46×10^{-6}
1**c**@OA_2	1.33×10^{-6}
1**d**@OA_2	1.59×10^{-6}
1**e**@OA_2	1.52×10^{-6}
OA	1.88×10^{-6}

[a] [OA]=1 mM in 10 mM buffer; room temperature.

Structures of all host/guest complexes were characterized by 2D COSY and 2D NOESY NMR experiments. The guest protons were assigned from 2D COSY spectra of the capsuleplexes (**Fig 3.6**, **Fig 3.8** and **Fig 3.10**). 2D NOESY spectra of the capsuleplexes presented the host-guest interaction. As illustrated in **Fig 3.7**, The -CHO proton signal (at 8.5 ppm) of **1c** within OA capsule showed NOE correlation with 'H_b' signal of host, which is present at the 1st row (bottom) of the OA suggesting that -CHO group of **1c** was located in the deep of the OA capsule (see **Scheme 3.1**).

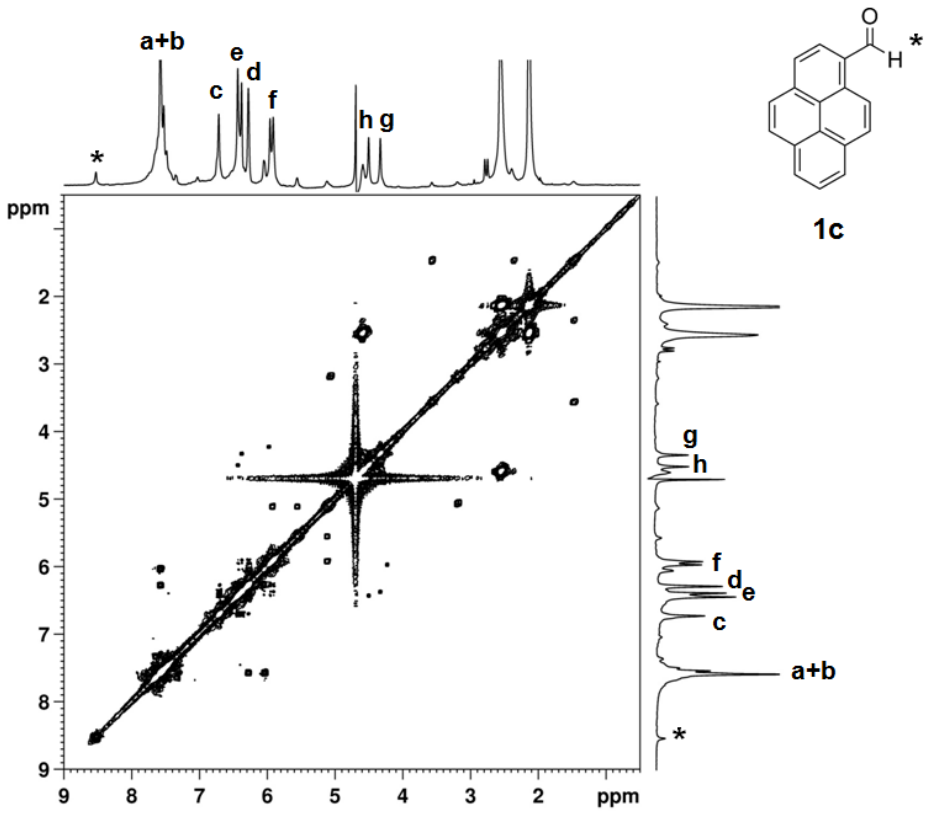

Figure 3.6 2D COSY spectrum (500 MHz) of **1c**@OA_2 in buffered D_2O (50 mM). OA peaks are marked from a-f and guest peak marked by *.[OA] = 5 mM

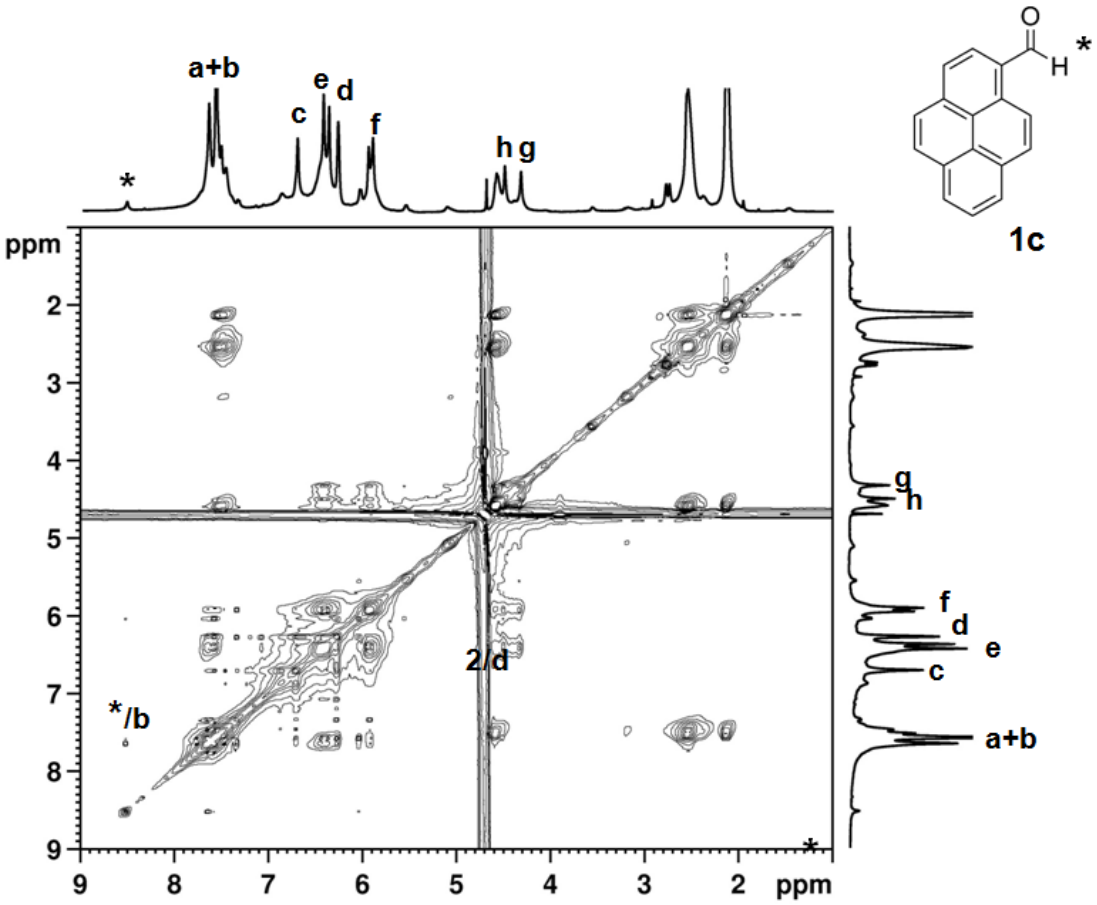

Figure 3.7 2D NOESY spectrum (500 MHz) of **1c**@OA_2 in buffered D_2O (50 mM). OA peaks are marked from a-f and guest peak marked by *. [OA] = 5 mM

In the case of **1d**@OA_2 capsuleplex, we found NOE correlation between -$COCH_3$ group and 'H_d', 'H_f' and 'H_g' of the host protons confirming that the guest was confined within OA capsule (**Fig 3.9**).

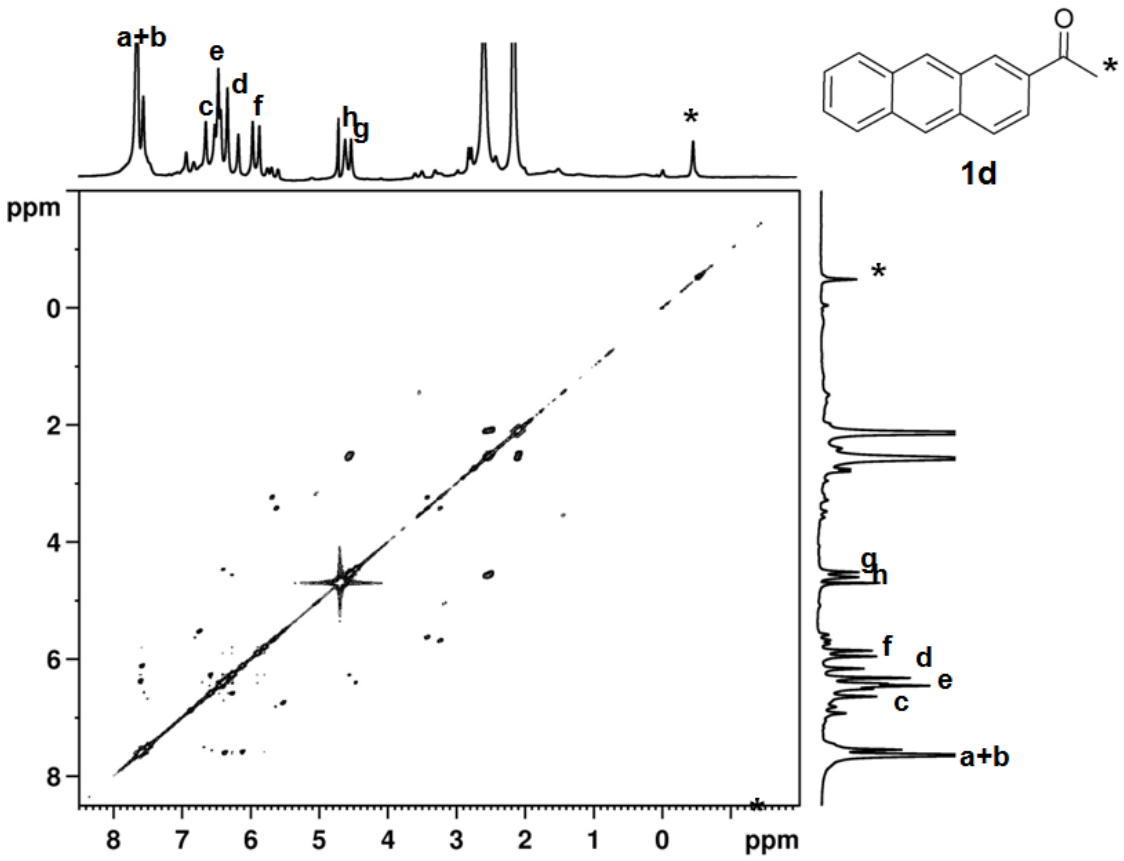

Figure 3.8 2D COSY spectrum (500 MHz) of **1d**@OA_2 in buffered D_2O (50 mM). OA peaks are marked from a-f and guest peak marked by *. [OA] = 5 mM.

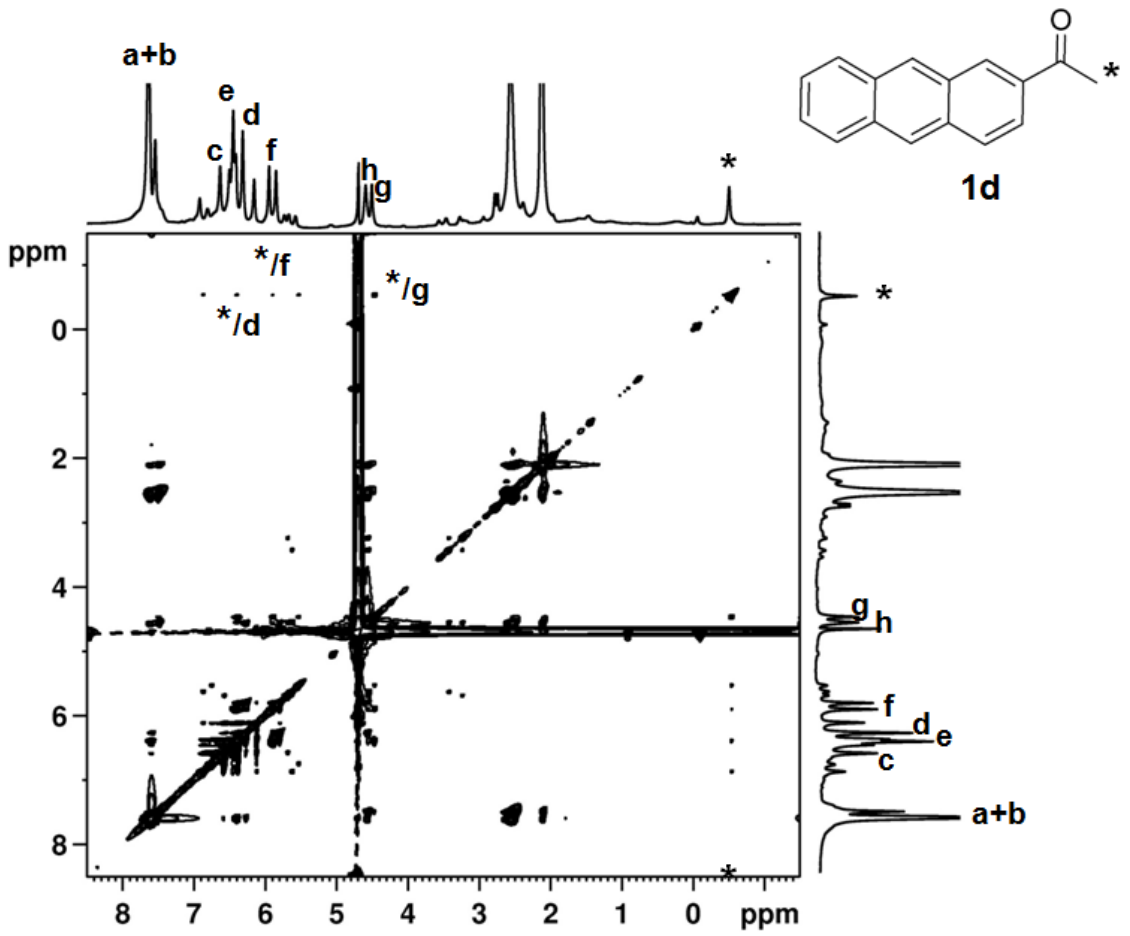

Figure 3.9 2D NOESY spectrum (500 MHz) of **1d**@OA_2 in buffered D_2O (50 mM). OA peaks are marked from a-f and guest peak marked by *. [OA] = 5 mM

We were able to assign all the aliphatic protons of **1e** by 2D COSY spectrum of **1e**@OA_2 (**Fig 3.10**). The correlation between the protons 'H_1' and 'H_3' of **1e** suggested that these protons belongs to $–CH_2CH_3$ group. Examination of 2D NOESY spectra of **1e**@OA_2 (**Fig 3.11)** revealed that 'H_2' showed interaction with 'H_d' that is present at the top rim of OA indicating that this part of the guest was at the middle of the capsule.

Whereas the protons 'H_1' and 'H_3' of **1e** interacted with 'H_d' as well as 'H_g' (2nd row) of OA indicating that the $–CH_2CH_3$ group was deep inside the cavity.

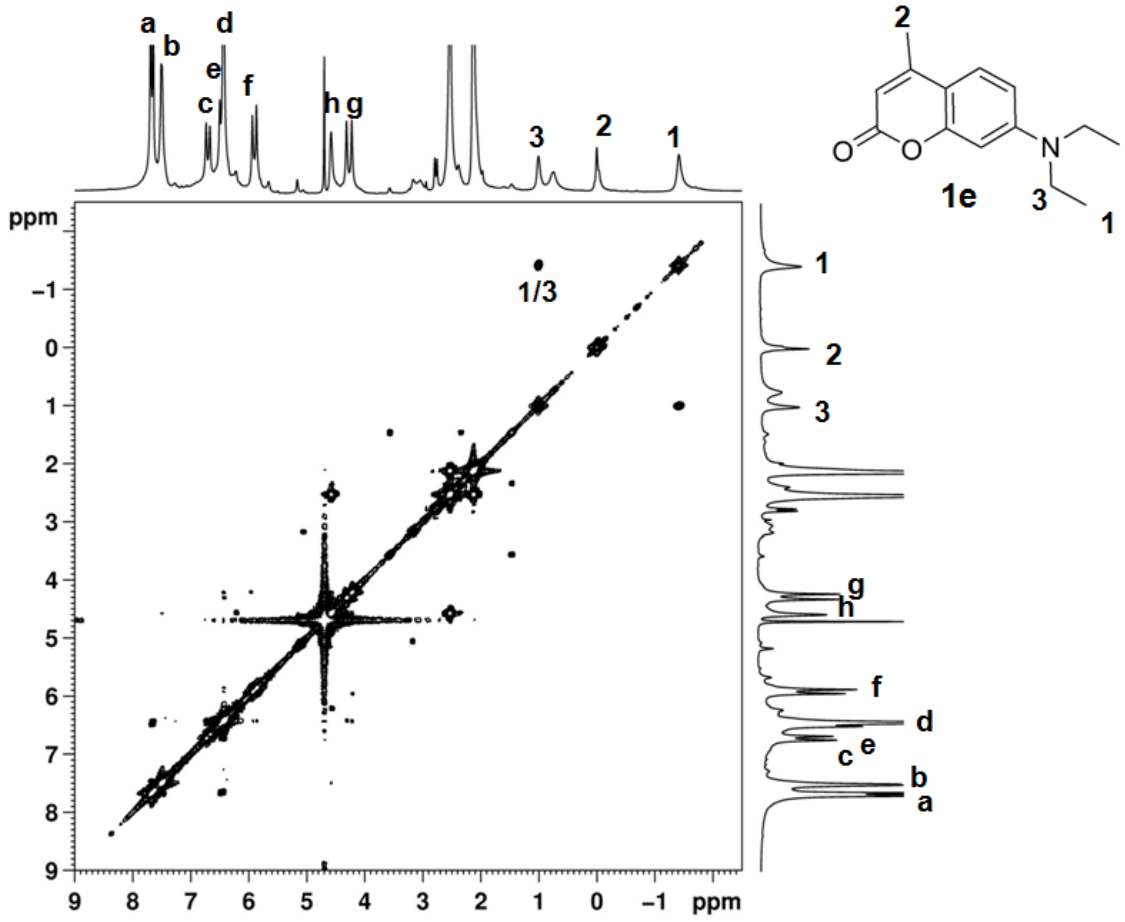

Figure 3.10 2D COSY spectrum (500 MHz) of **1e**@OA_2 in buffered D_2O (50 mM). OA peaks are marked from a-f and guest peaks marked from 1-3. [OA] = 5 mM.

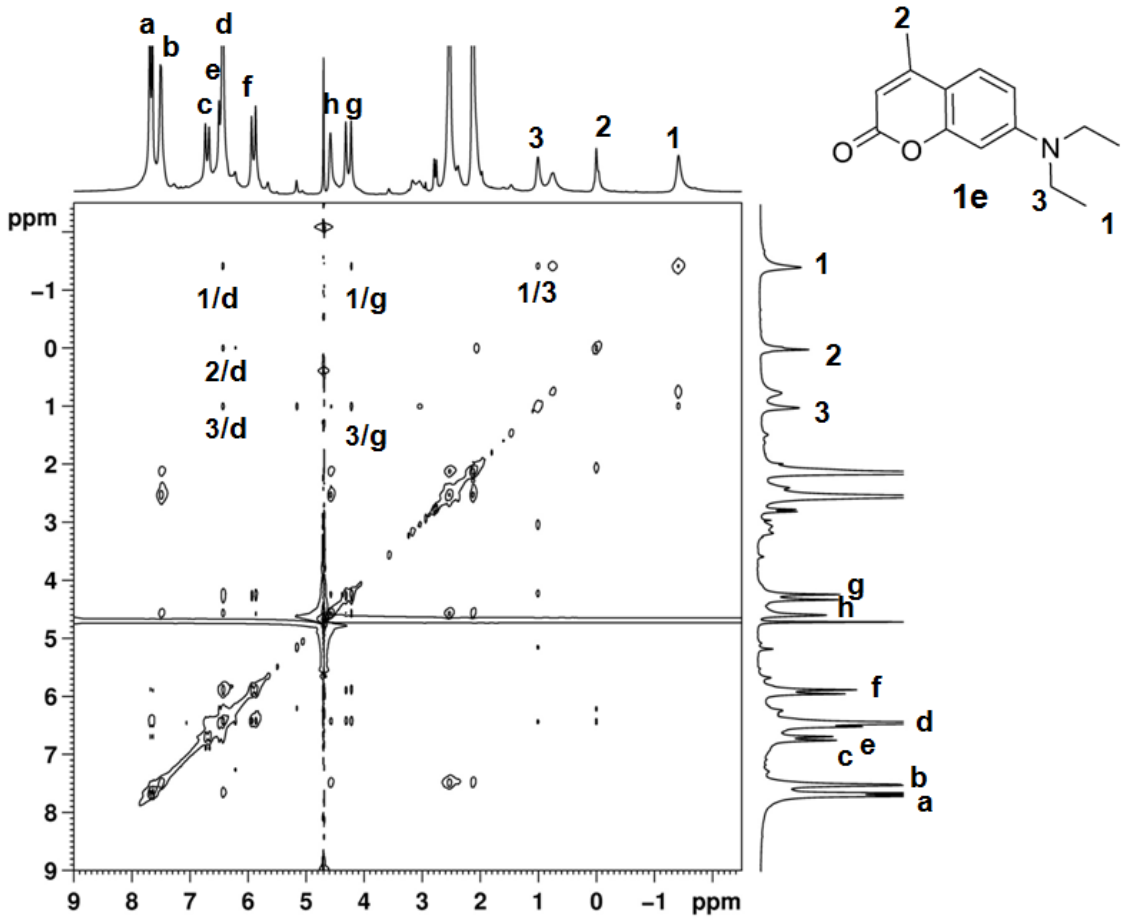

Figure 3.11 2D NOESY spectrum (500 MHz) of **1e**@OA_2 in buffered D_2O (50 mM). OA peaks are marked from a-f and guest peaks marked from 1-3. [OA] = 5 mM.

3.2.3 Emission studies on the aromatic probes to explore their micropolarity inside OA

After confirming the capsuleplex formation of the above mentioned polarity probes with OA by NMR studies, we carried out emission experiments to explore the microenvironment inside the capsule. First we addressed the question: "Is the capsule occupied by an aromatic probe molecule dry or wet?" To accomplish with that, we carried out emission experiments with five polarity probes to reveal their photophysical

properties confined in OA capsule. The results from the probes are discussed individually to reach a final conclusion about the microenvironment of the OA capsule.

Pyrene (**1b**) is a widely used probe molecule to determine the micropolarity of the environment in which it resides.[22-24] Pyrene shows various vibronic bands in its fluorescence spectrum and the relative intensities of those bands, most importantly I_1 and I_3 bands, provide information about the polarity. It is known that I_1/I_3 is greater in a polar medium than in a nonpolar environment.[22-24] Hence, pyrene that formed a stable 2:1 capsule with OA seemed ideal to probe the interior of the capsule. Pyrene was soluble in water at a concentration of 1×10^{-5} M upon sonication. As shown in **Fig 3.12a**, the fluorescence spectrum of pyrene in borate buffer (1×10^{-5} M) consists of a monomer emission between 360−420 nm and a weak excimer emission with a maximum at 470 nm due to pyrene aggregates. Addition of 2 equiv of OA (2×10^{-5} M) completely displaced the later weak emission with an intense monomer emission (**Fig 3.12b**).

In borate buffer solution, the I_1/I_3 ratio of the monomer emission of pyrene was 1.8 which is consistent with the value for pyrene emitting in water.[23] In presence of OA, the monomer emission with I_1/I_3 ratio of 1.01 was an indication that pyrene was emitting from an environment where there were no water molecules. Comparing I_1/I_3 value obtained in OA with those in different solvents reported in the literature, we concluded that the polarity of the host/guest capsule is similar to that of benzene. [23] Considering the 24 benzene rings of the OA capsule, it is quite expected that the polarity interior OA capsule is benzene like.

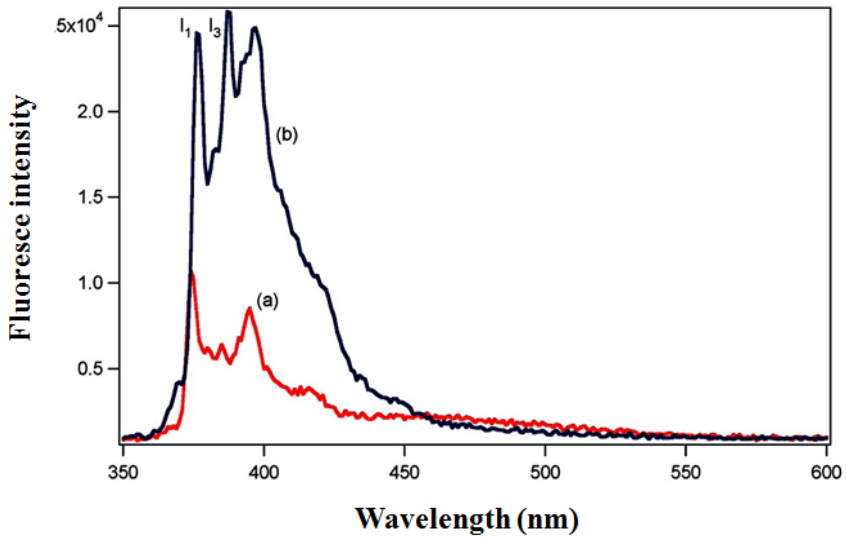

Figure 3.12 Fluorescence emission spectra in borate buffer (pH ≈ 9) of (a) 1×10^{-5} M pyrene and (b) pyrene@OA_2. Note the relative intensities of I_1 to I_3 in the two cases. Excitation wavelength: 320 nm.

It is established that pyrenealdehyde (**1c**) shows emission due to its two emitting states of $\pi\pi^*$ and $n\pi^*$ in polar and nonpolar enviornment, respectively.[25-29] Such a switch in the emitting species results in a shift in the wavelength maximum of emission as well as alters in vibrational structure in the emission spectrum. The fluorescence spectrum of pyrenealdehyde is broad and red shifted in the polar media whereas structured and blue shifted in the nonpolar media. The emission spectra of pyrenealdehyde in the presence and absence of OA in water are shown in **Fig 3.13**. We observed a broad emission with wavelength maximum at 480 nm in water (**Fig 3.13a**). The recorded structured, blue-shifted fluorescence emission of pyrenealdehyde encapsulated within OA indicated that the emission was from its $n\pi^*$ state (**Fig 3.13b**). These observed emission characteristics confirmed that the probe molecule within OA capsule was present in a nonpolar environment.

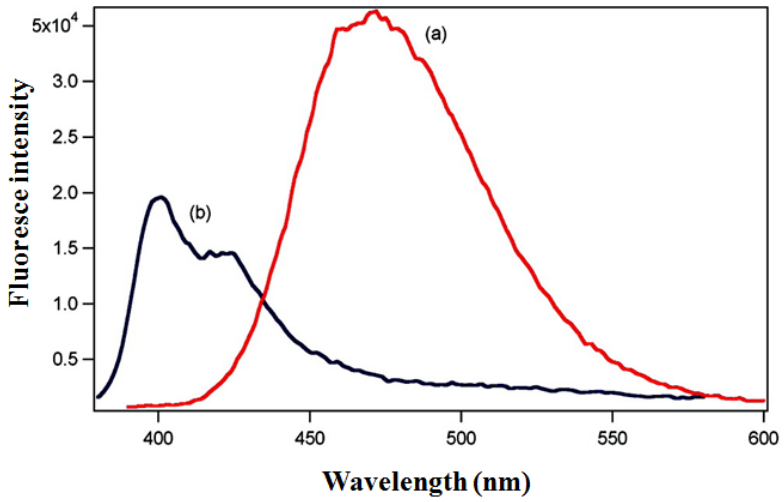

Figure 3.13 Fluorescence emission spectra in borate buffer (pH ≈ 9) of (a) 1×10^{-5} M pyrenealdehyde and (b) pyrenealdehyde@OA_2. Excitation wavelength: 330 nm.

2-Acetylanthracene (**1d**) is known to show fluorescence in different wavelength regions in polar and nonpolar media.[30,31] The structureless emission in polar media changes to structured and blue-shifted in nonpolar solvents. Fluorescence emission of 2-acetylanthracene (1×10^{-5} M) in borate buffer was weak and broad (420−550 nm), a characteristic of polar environment (**Fig 3.14a**). Remarkably, fluorescence emission of 2-acetylanthracene@OA_2 ([**1d**] = 1×10^{-5} M; [OA] = 2×10^{-5} M) was intense, structured, and blue-shifted (400−500 nm; **Fig 3.14b**). On the basis of the above results we confirmed that 2-acetylanthracene was present in a nonpolar environment within the OA capsule. An overlay of the emission spectra of 2-acetylanthracene in benzene and inside OA capsule in water (**Fig 3.15**) supported the earlier conclusion that the polarity of the interior of the OA capsule is similar to that of benzene.

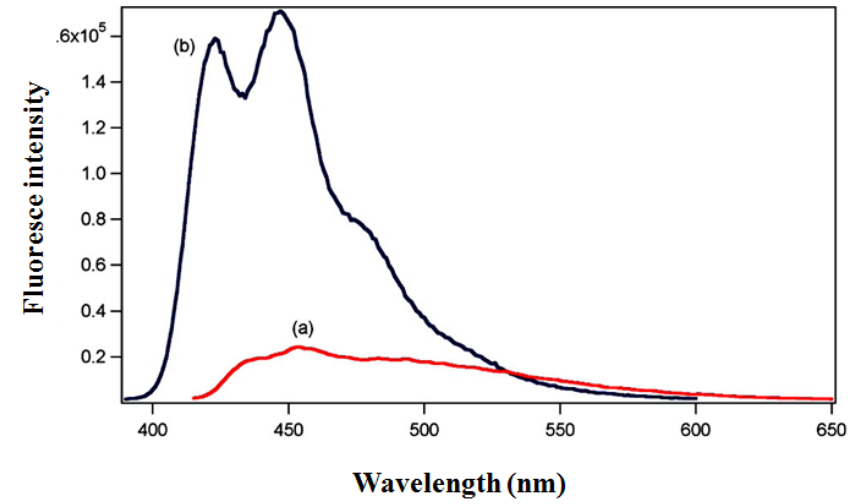

Figure 3.14 Fluorescence emission spectra in borate buffer (pH ≈ 9) of (a) 2-acetylanthracene and (b) 2-acetylanthracene@OA_2. Excitation wavelength: 330 nm.

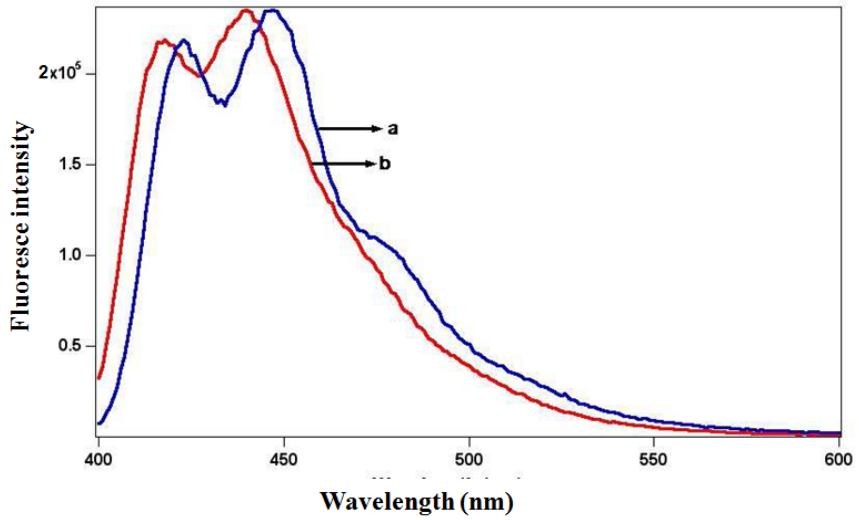

Figure 3.15 Fluorescence emission spectrum of **1d** (10^{-5} M) in (a) octa acid (2×10^{-5} M in10^{-3} M borate buffer) and (b) benzene.

Coumarin-1 (**1e**) belongs to a family of laser dyes whose fluorescence quantum yield increases and wavelength maximum blue shifts with a decrease in solvent polarity. [32,33] For example, fluorescence spectra of coumarin-1 in three solvents with different polarity such as water, methanol and benzene are shown in **Fig 3.16**. It was clear that

with the decrease in polarity (water > methanol > benzene), the fluorescence intensity enhanced with a blue shift. As shown in **Fig 3.17a**, excitation of coumarin-1 at 350 nm in borate buffer showed a weak broad emission between 440 and 540 nm. The significant enhancement in fluorescence and blue shift in the emission of coumarin-1 in the presence of OA ([**1e**] = 1×10^{-5} M; [OA] = 2×10^{-5} M, **Fig 3.17b**) suggested the hydrophobicity inside OA capsule. As illustrated in **Fig 3.18**, the fluorescence titration showed spectral changes due to the addition of small increments of OA to coumarin-1 solution in borate buffer. These experiments unequivocally ascertained that, with incremental addition of OA, the probe was transferred from the polar (aqueous) to the nonpolar (OA capsule) environment. Fluorescence spectrum of coumarin-1 inside OA capsule superimposed with that in benzene is shown in **Fig 3.18**. Similar to the other probes, coumarin-1 also confirmed that the capsule interior was water free; offered a benzene like microenvironment.

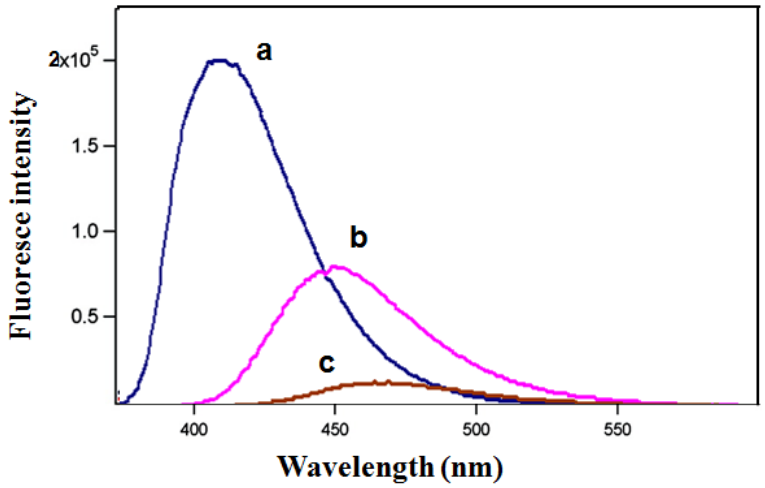

Figure 3.16 Fluorescence emission spectra of coumarin-1 in (a) benzene, (b) methanol and (c) water, [coumarin-1] = 10^{-5} M, Excitation wavelength: 350 nm.

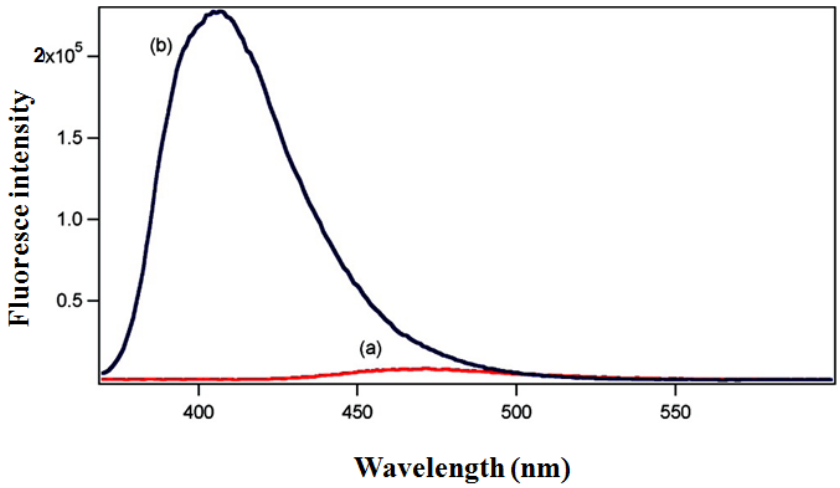

Figure 3.17 Fluorescence emission spectra in borate buffer (pH ≈ 9) of (a) coumarin-1 and (b) coumarin-1@OA_2. Excitation wavelength: 350 nm.

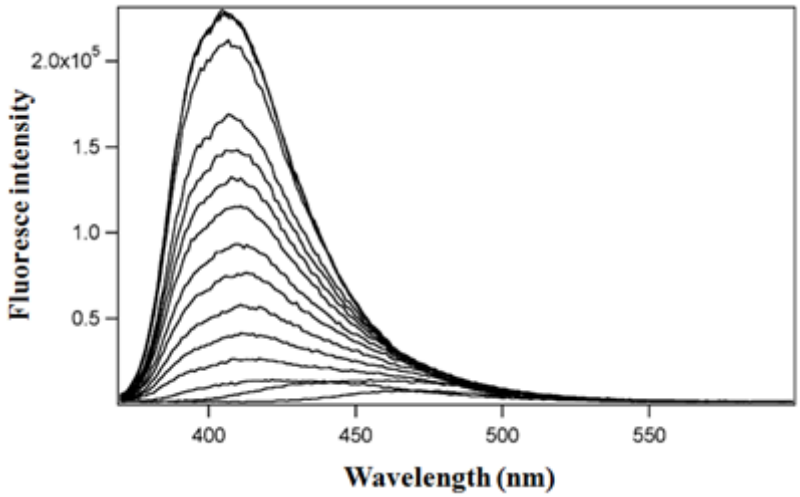

Figure 3.18 Variation in fluorescence of coumarin-1 (1×10^{-5} M; pH ≈ 9.0, 10 mM borate buffer) with increased addition (from bottom to top) of OA in borate buffer (1×10^{-6} to 3×10^{-5} M). Note the shift in the maxima as well as increase in the intensity with increased concentrations of OA. Excitation wavelength: 350 nm.

The last probe molecule we used was 7-*O*-propylcoumarin (**1f**). Unlike Coumarin 1, 7-*O*-propylcoumarin emits weakly in nonpolar media and strongly in polar, without any change in the emission maxima.[34-37] The fluorescence titration spectra of **1f** with increasing concentration of OA leading to fluorescence suppression are shown in **Fig**

3.19. 7-*O*-propylcoumarin also confirmed that the interior of OA capsule made with a small organic guest molecule and two OA cavities was completely nonpolar though the complex was prepared in water.

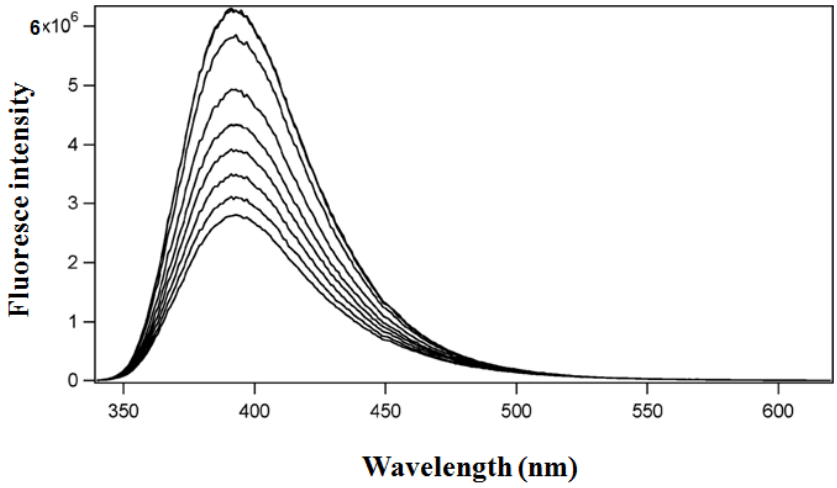

Figure 3.19 Variation in fluorescence of 7-*O*-propyl coumarin (2×10^{-5} M) with increased addition of OA in borate buffer (1×10^{-5} to 6×10^{-5} M, from top to bottom). Excitation wavelength: 320 nm.

3.3 Conclusion

^{1}H NMR studies on the guest **1a-f** (**Scheme 3.1**) in presence and absence of OA revealed that all of them were encapsulated inside OA capsule. 2D COSY and 2D NOESY experiments on the capsuleplexes suggested the orientation of the guest within the capsule. The polarity probes (**1b-f**, **Scheme 3.1**) significantly altered their emission behavior in presence of OA with respect to water.

The individual result from the probes brought a final conclusion that the interior of the OA capsule where the organic guest molecule resides was nonpolar, and most

likely no water molecules were present. It was interesting to notice that the water used to dissolve the guest OA was excluded from its cavity (**Scheme 3.2**).

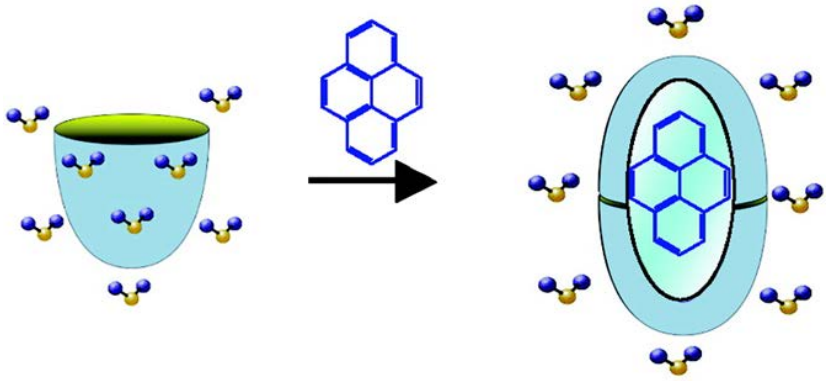

Scheme 3.2 Schematic representation of the formation of a calsuleplex with an organic guest and two OA molecules

3.4 Experimental Section

Materials and Methods

All probe molecules used in this study were purchased from Sigma-Aldrich/Acros Organics and were recrystallized twice prior to use. Octa acid (OA) was synthesized following a literature procedure.[17] Fluorescence spectra were recorded using an Edinburgh FC900 spectrofluorometer equipped with a xenon lamp. Fluorescence lifetime measurements were made using an Edinburgh single photon counter, fitted with a hydrogen arc lamp. All ^{1}HNMR spectra were recorded using a Bruker 500 MHz NMR at 27 °C. Spectral plots were generated using Igor Pro software. Diffusion constant measurements were made using a Bruker 500 MHz NMR spectrometer at 27 °C. Data were collected by using 'stebpg1s' pulse sequence (eight scans) and processed by T_1/T_2 relaxation module in the TOPSIN 2.1 software.

Photophysical Studies

A 1 mM stock solution of OA was made in 10 mM sodium tetraborate in water. Guest stock solutions (1 mM) were made in spectrophotometric grade chloroform. To chloroform evaporated (by bubbling nitrogen) were added appropriate amounts of each guest to a test tube with the required amounts of borate buffer and OA stock solution such that the guest and OA were at 1×10^{-5} M and 2×10^{-5} M concentrations, respectively. The same concentration and procedure was adopted for all seven guests.

General Protocol for Binding Studies by NMR

A ^{1}H NMR spectrum of 600 μL of 2 mM OA in 20 mM sodium borate buffer in D_2O was recorded. To this solution was added 0.25 equiv of guest (5 μL of a 120 mM solution in DMSO-d_6) in four stages, the mixture was shaken well for about 5 min, and spectra were recorded after each addition. Each sample was also examined 24 h later. No differences were noticed between 5 min and 24 h spectra. In all cases complete complexation was observed upon addition of 0.5 equiv of guest. Further addition resulted in a turbid solution, and the NMR spectrum revealed the presence of both free and complexed guest. All 2D ^{1}H NMR experiments were carried out with samples containing 5 mM OA and 2.5 mM guest in 50 mM sodium tetraborate buffer in D_2O.

CHAPTER 4

Nature of Supramolecular Complexes and Dynamics of the Guest Molecules within the Capsuleplex of Octa Acid

4.1 Overview

In **Chapter 3** we demonstrated how different hydrophobic probes (pyrene, pyrenealdehyde, 2-acetylanthracene, coumarin-1, and 7-*O*-propylcoumarin) of various dimensions can fit inside OA capsuleplex. Those probes were too large to fit within the cavity of a single OA molecule and formed a 2:1(host: guest) complex with it. Now the question is: What happens if the guest molecule is small; will it form a 2:2 or 1:1 complex? Would a more water-soluble (hydrophilic) molecule complex with OA? How strong would such a complex be? To address these questions we studied in details the nature of supramolecular complexes of OA controlled by the structure of the guest molecules. Three probe molecules were chosen with different size and hydrophobicity: a small guest 2-methoxynapthalene (**1a, Scheme 4.1**), a larger guest 2-hexyloxynaphthalene (**1b, Scheme 4.1**), and a guest with ionic head group 2-naphthoic acid (**1c**, **Scheme 4.1**). The complexation properties were investigated by employing NMR and emission spectroscopy on these probes.

Previous studies in our group in collaboration with Gibb's group have shown that on the inclusion of aromatic molecules within OA, anthracene (**1d**) and naphthalene (**1e**) formed 2:2 capsuleplex while pyrene and tetracene formed 2:1 capsuleplex.[103] Recently, Jayaraj *et al.* have elucidated an interesting feature of OA-guest complexation using 1,4-dialkyl benzenes as guest molecules that if the guest is small enough, it can form both 2:1 and 2:2 capsuleplexes depending on the relative concentrations of host and guest in solution.[125] This observation is particularly useful when planning reactions of small molecules within OA. Given the similarity in size of anthracene and naphthalene to 1,4-

diethylbenezene we became interested to study their complexation with OA in detail, particularly at relatively lower concentrations of the aromatic molecules.

Our interest in organic capsules relates to their use as reaction cavities for manipulating photochemical processes. In this context, we were further interested in understanding the dynamics of the host, the guest, and the host-guest complex on the excited-state timescale. It is also important to note that the dynamics of host-guest assemblies are time-dependent. The system may be static on one timescale but dynamic on a different timescale. As NMR and EPR work at different time scale, millisecond and nanosecond respectively, these two techniques might be useful to monitor the dynamics of the guest molecules within the capsuleplex. Based on this premise, we probed the mobility of guests within the OA capsule by NMR and EPR techniques.

Scheme 4.2 presents a cartoon depiction of the two types of motion of the 2:1 capsuleplex. The three axes of the guest are defined in **Scheme 4.2a**. A free guest could undergo overall rotation along the *x*, *y*, and *z* axes (**Scheme 4.2b, c**). We visualized two types of guest rotational motion in a capsuleplex: (1) guest rotation along its *x* axis (**Scheme 4.2d**), a motion that would not lead to major changes in the structure of the host−guest complex and (2) guest motion along the *y* or *z* axis (**Scheme 4.2e**), a motion that would, especially with an unsymmetrical guest, displace the two ends (arbitrarily named its head and tail) from one part of the capsule to a different one (arbitrarily named the top and bottom of the capsule). It should be noted that the possible rotations of the capsuleplex as a whole along the *x*, *y*, or *z* axis would not alter the relative orientation of the guest with respect to the host.

Our group had already established the rotation of the guest along *y* or *z* axis on the NMR timescale (ms).[126] In this chapter we will focus on the analysis of EPR spectra of OA-bound nitroxide probes (**1f-i**) that suggested the rotation along the *x* axis occurs on the nanosecond timescale.

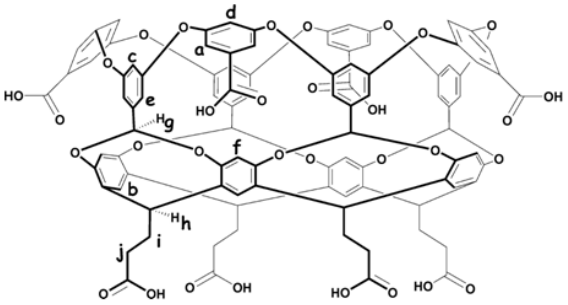

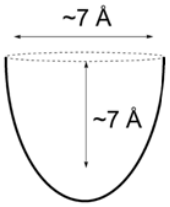

Octa acid (**OA**)

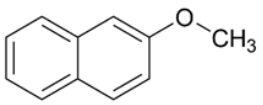

2-Methoxynapthalene (**1a**)

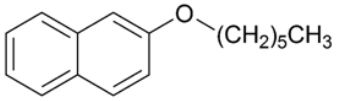

2-Hexyloxynapthalene (**1b**)

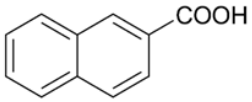

2-Napthoic acid (**1c**)

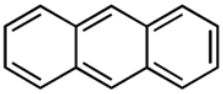

Anthracene (**1d**)

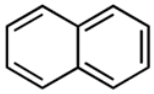

Naphthalene (**1e**)

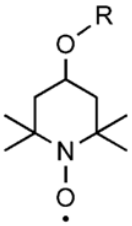

1f, R = n-Pr
1g, R = n-Hexyl
1h, R = n-Octyl
1i, R = n-Decyl

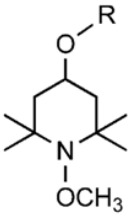

1g', R = n-Hexyl

Scheme 4.1 Structure of the host and guests in this study

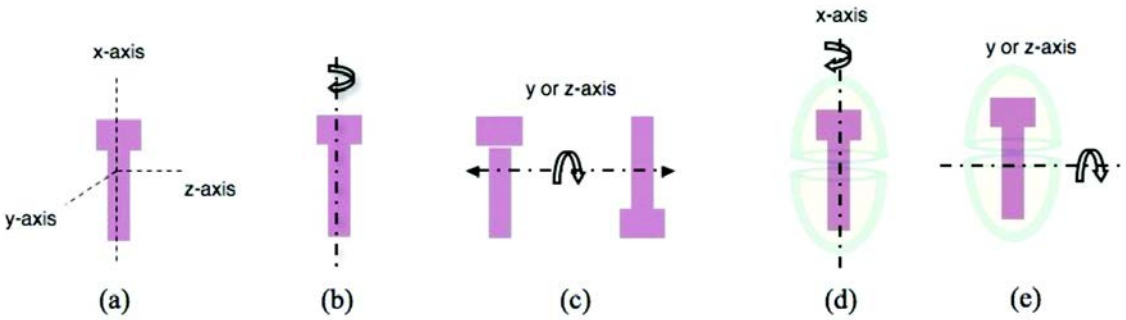

Scheme 4.2 Cartoon representations of (a) the three axes of the guest and (b−e) various motions of host−guest complexes being investigated.

4.2 Results and discussion

4.2.1 Stoichiometry of guest-dependent host/guest complex of OA

We carried out ^{1}H NMR titration of OA with the guest molecule to investigate the stoichiometry of the host/guest complex. The ^{1}H NMR titration spectra of 2-methoxynaphthalene (**1a**) with OA is shown in **Fig 4.1**. The upfield shift (δ −0.75) of the methyl group signal indicated the location of the methoxy group at the narrower end of OA capsule. The chemical shift of the methoxy group did not alter with varying the amount of guest to a host solution. This suggested that the complex was stable in the NMR time scale (compare with **Fig 4.10**). The lack of change in the spectra on further addition of the guest beyond host: guest = 1:1 ratio suggested the formation of either 1:1 cavitandplex or 2:2 capsuleplex. A symmetrical guest-host complex (2:2) formation, possible only through accommodation of two guest molecules within a capsule, was inferred from the absence of splitting of any of the host signals. The complex formation of **1a** with OA was further conformed by two-dimensional correlation spectroscopy (2D COSY) (**Fig 4.2**) and two-dimensional nuclear overhauser spectroscopy (2D NOESY)

(**Fig 4.3**) experiments on **1a**$_2$@OA$_2$. 2D COSY spectra shows the correlation between two hydrogens of the adjacent carbon atoms and allows one to conclude the connectivity of a molecule by determining which protons are spin-spin coupled. On the other hand NOESY spectra provides about the through space interaction. As illustrated in **Fig 4.3**, the methoxy proton showed interaction with the host protons such as H_g, H_e and H_f confirming that **1a** was located inside OA capsule. The diffusion constant was measured by 2D DOSY NMR experiment and found to be 1.38×10^{-6} cm^2/s which was consistent with the diffusion constant value of a capsuleplex.[127]

Figure 4.1 ^{1}H NMR titration experiments of 2-methoxynaphthalene (**1a**) with host OA. (i) OA (1 mM in 10 mM buffered D_2O), OA/2-methoxynaphthalene at (ii) 4:1, (iii) 4:2, (iv) 4:3, and (v) 4:4. Aliphatic guest resonances are marked with *.

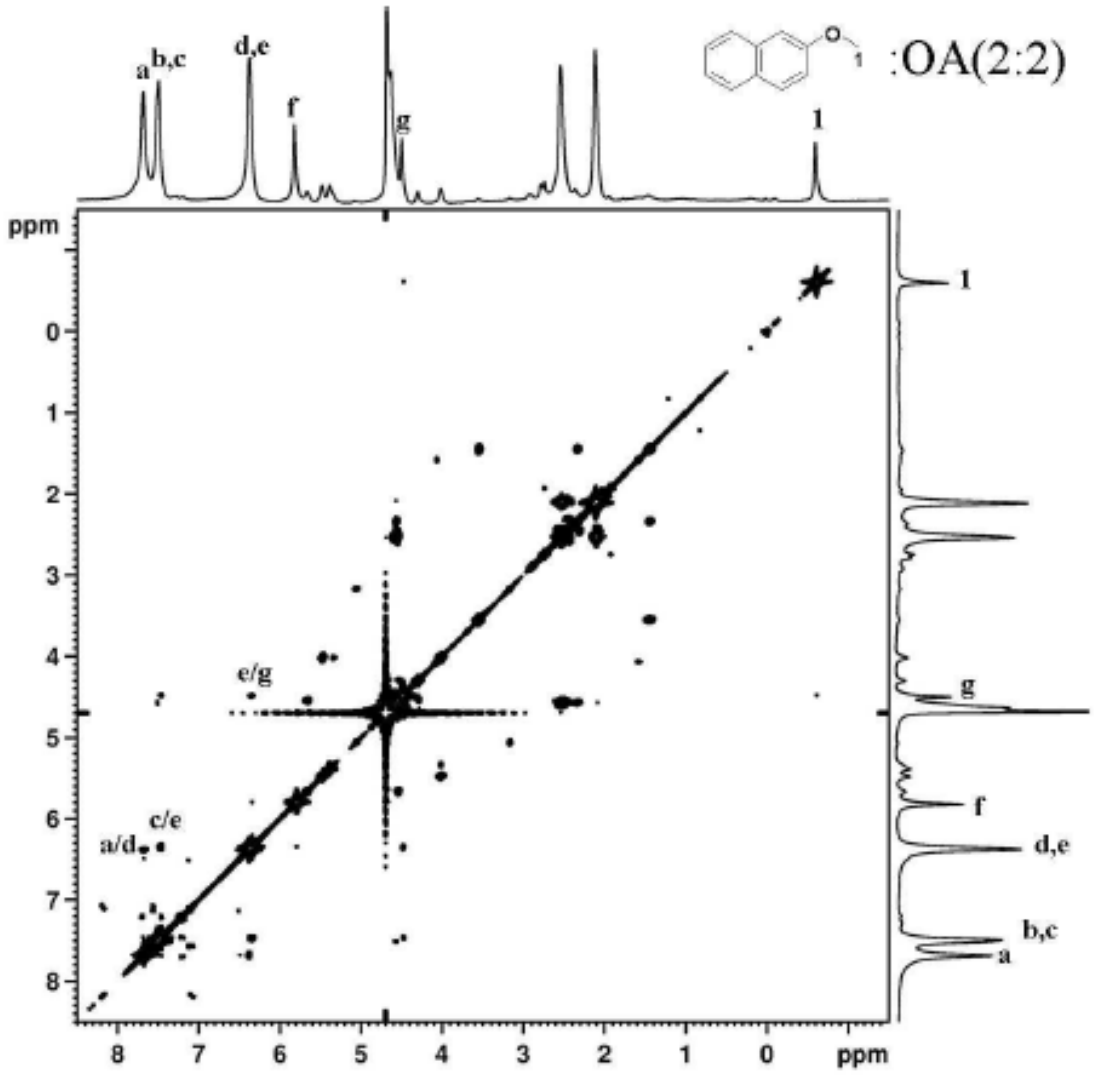

Figure 4.2 2D-COSY spectrum (500 MHz, 5 mM) of (**1a**)$_2$@(OA)$_2$ in buffered D_2O (50 mM)(OA peaks are marked from a-f and guest peak is marked by 1).

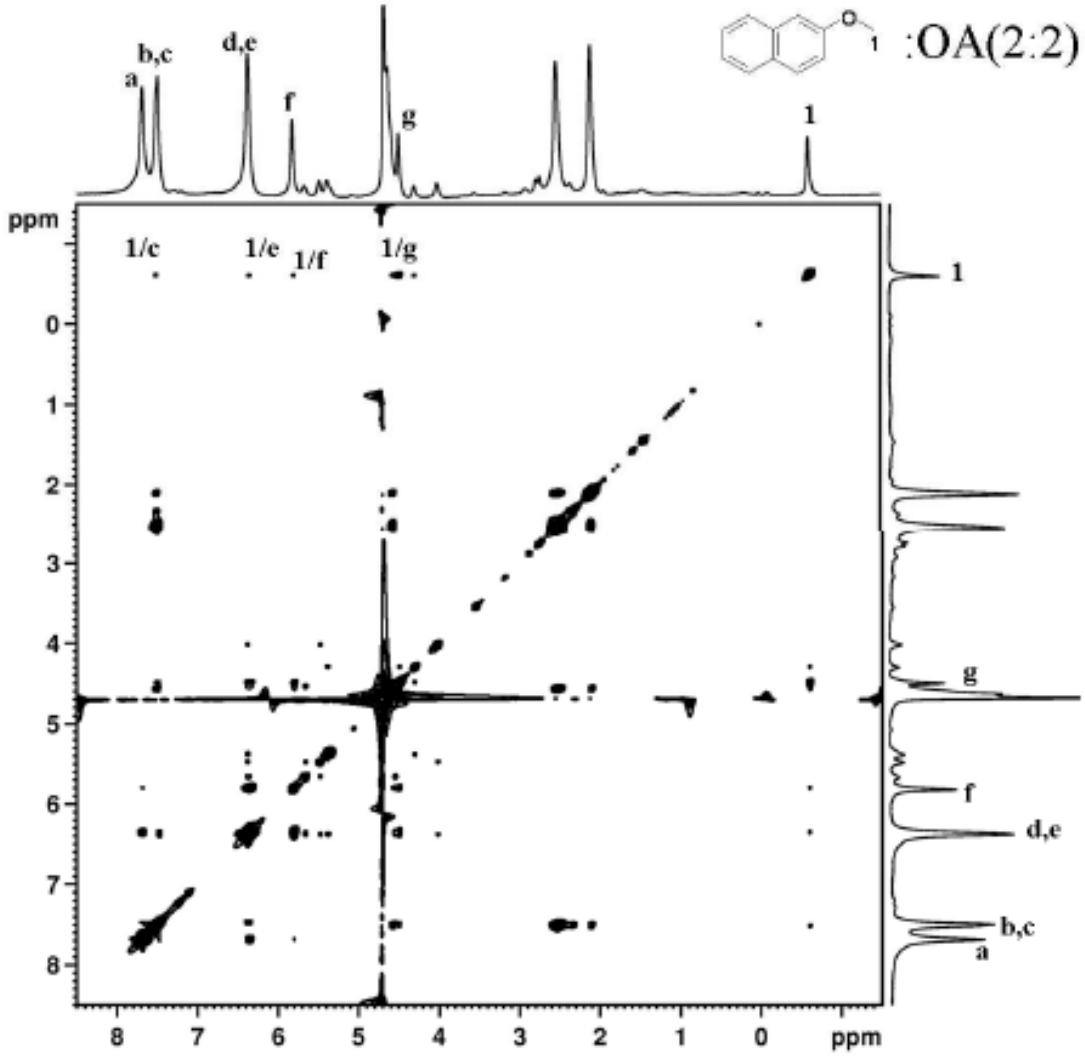

Figure 4.3 2D-NOESY spectrum (500 MHz, 5 mM) of (**1a**)$_2$@(OA)$_2$ in buffered D$_2$O (50 mM)(OA peaks are marked from a-f and guest peak is marked by 1).

The above observation was further confirmed by the results of emission studies. Emission spectra of 2-methoxynaphthalene (**1a**) in water upon addition of various amounts of OA are provided in **Fig 4.4**. The change from the exclusive emission from the monomer of 2-methoxynaphthalene (**1a**) at a concentration of 2×10^{-5} M in water to the emission from both the monomer and excimer upon addition of OA resulted from the inclusion of two molecules of the host within OA guest. This emission titration result confirmed that 2-methoxynaphthalene formed 2:2 (host: guest) capsuleplex with OA. The excimer was longer lived (39 ns, **Scheme 4.5(ii)**) than the monomer (11 ns, **Scheme 4.5(i)**) inside OA capsule.

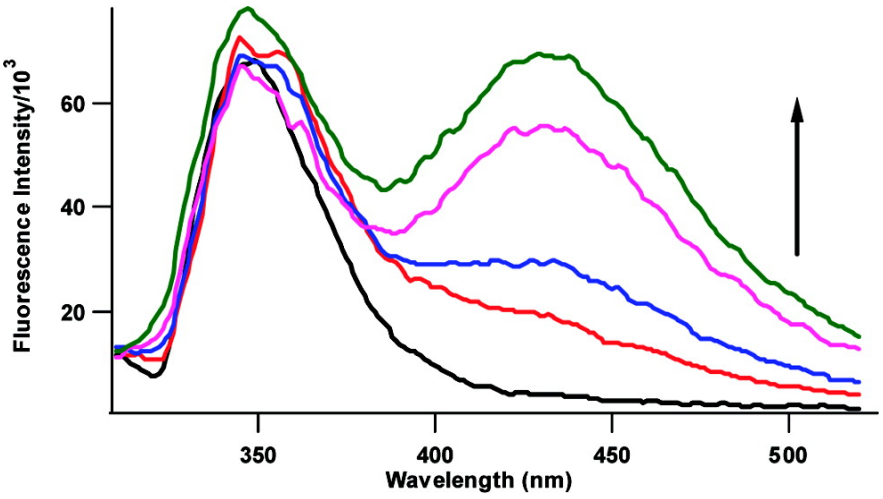

Figure 4.4 Fluorescence titration experiments of 2-methoxynaphthalene (**1a**) (2×10^{-5}M) with OA host in borate buffer (10 mM), with varying concentration of OA from (bottom to top) 0 to 4×10^{-5}M. Excitation was carried out at 270 nm.

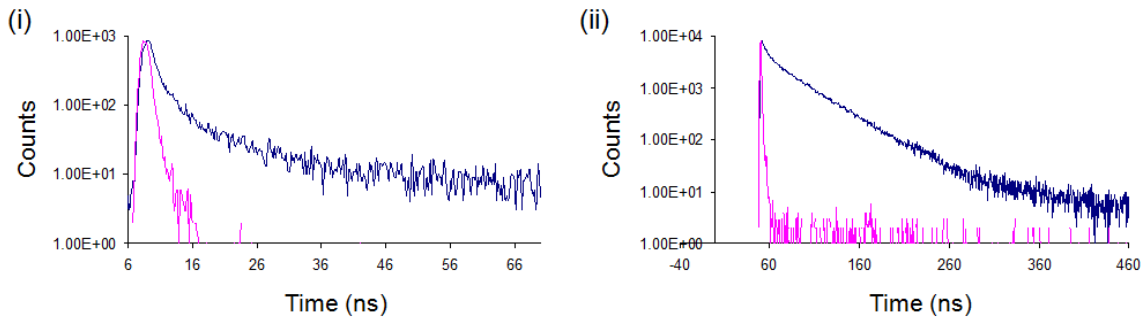

Figure 4.5 Life time of 2-Methoxynaphthalene in oata acid for (i) monomer, 11 ns, λ_{em} = 350 nm; (ii) excimer, 39 ns, λ_{em} = 430 nm. In both cases λ_{ex} = 270 nm.

In contrast to the above results, a 2:1 capsule was formed with 2-hexyloxynaphthalene (**1b**), a molecule longer than 2-methoxynaphthalene (**1a**). ^{1}H NMR titration spectra of 2-hexyloxynaphthalene (**1b**) with OA are shown in **Fig 4.4**. Inclusion of **1b** within OA capsule was evident from the upfield shift of the ^{1}H NMR signals due to the alkyl chain. Further, the chemical shift of the alkyl chain was independent of the amount of guest and host present in solution suggesting that the host/guest complex was stable in the NMR time scale. This observation was similar to that noted with 2-methoxynaphthalene (**1a**). An important observation was that addition of 2-hexyloxynaphthalene (**1b**) beyond 0.5 equiv of the host solution resulted in the complete disappearance of the signals due to uncomplexed host indicative of this guest forming a 2:1 capsule with OA (**Fig 4.6**). Consistent with this result, the $^1H_{a-g}$ signals due to the host were split, suggesting that in presence of 2-hexyloxynaphthalene (**1b**) the top and bottom halves of the capsule were not symmetrically identical. The proton signals of **1b** were assigned by 2D COSY correlations (**Fig 4.7**). As shown in **Fig 4.8**, all the alkyl protons of **1b** showed NOE interactions with the host protons confirming that the guest

2b was inside OA capsuleplex. Consistent with the 2:1 complexation, the diffusion constant was measured to be 1.26×10^{-6} cm^2/s.

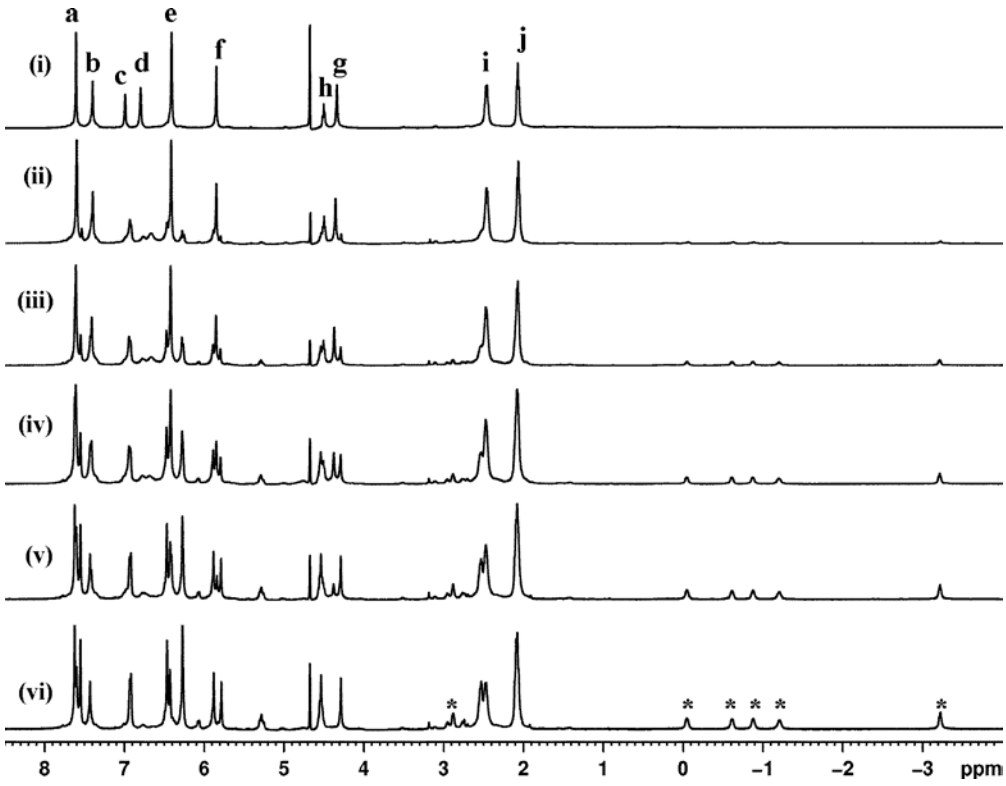

Figure 4.6 ^{1}H NMR titration experiments of 2-hexyloxynaphthalene (**1b**) with host OA. (i) OA (2 mM in 20 mM buffered D_2O), OA/2-hexyloxynaphthalene at (ii) 10:1, (iii) 5:1, (iv) 3:1, (v) 2.5:1 and (vi) 2:1. Aliphatic guest resonances are marked with *.

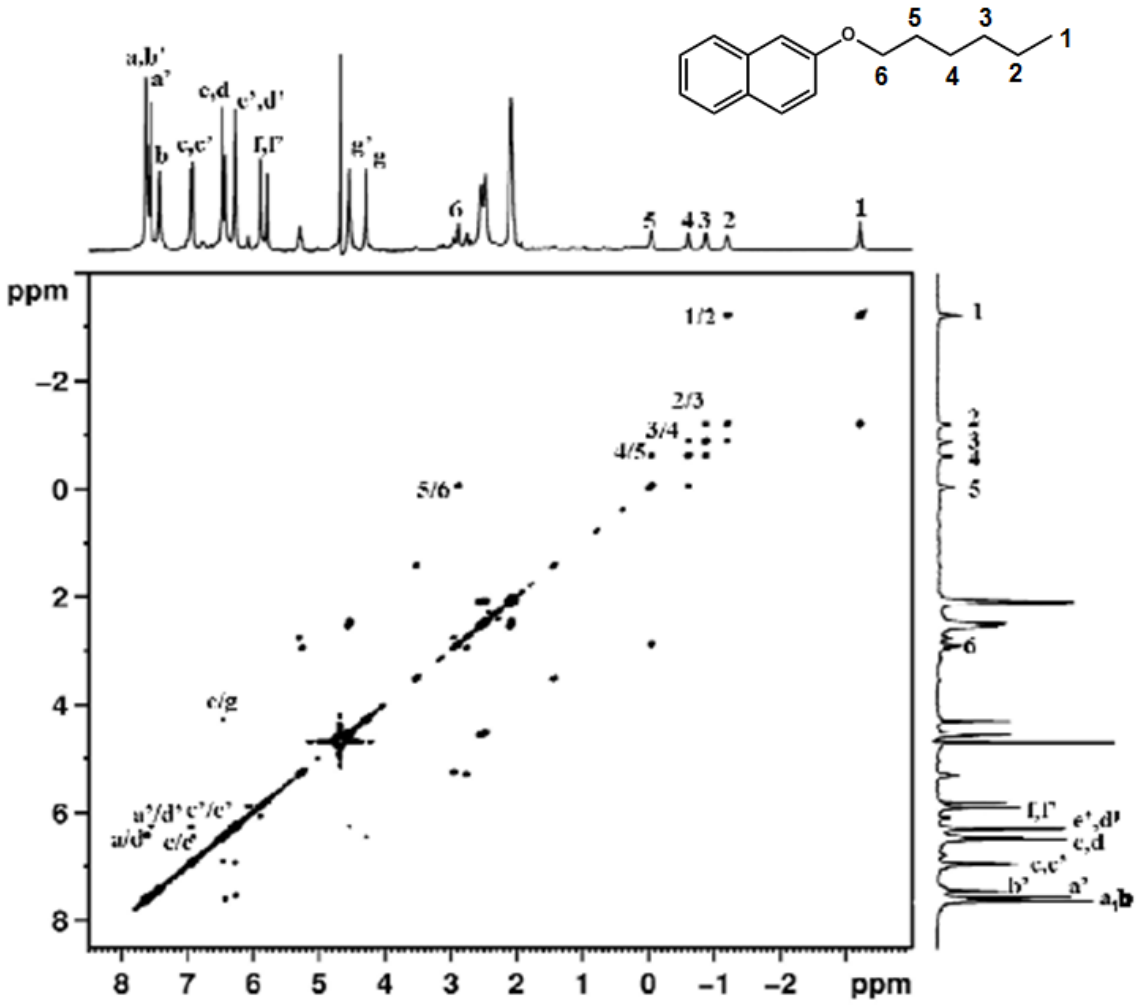

Figure 4.7 2D-COSY spectrum (500 MHz, 5 mM) of **1b**@$(OA)_2$ in buffered D_2O (50 mM)(OA peaks are marked from a-f and guest peaks marked by 1-6).

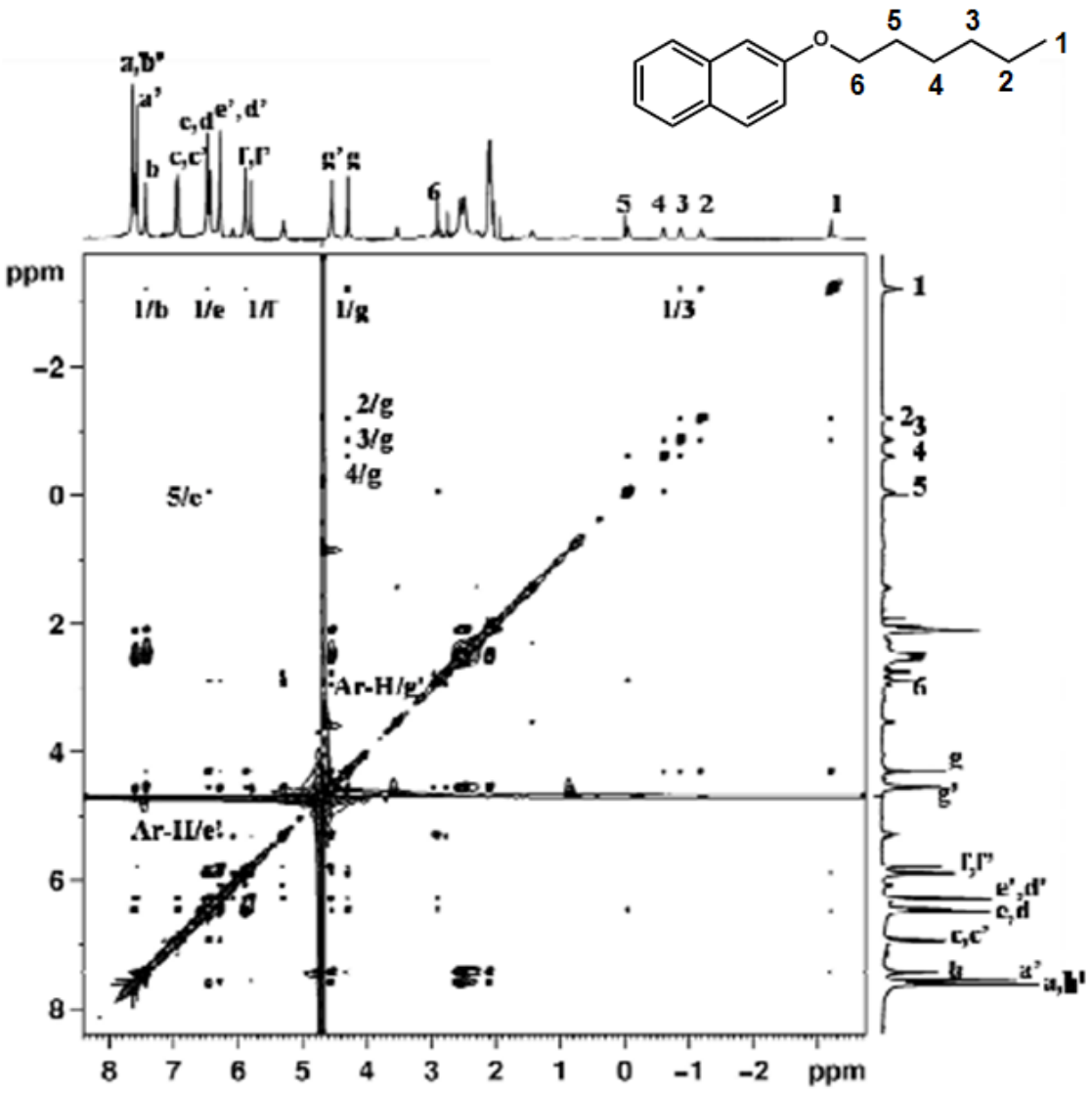

Figure 4.8 2D-NOESY spectrum (500 MHz, 5 mM) of **1b**@$(OA)_2$ in buffered D_2O (50 mM)(OA peaks are marked from a-f and guest peaks marked by 1-6).

In support of the inference that, unlike **1a** (2-methoxy), **1b** (2-hexyloxy naphthalene) formed a 2:1 complex, its emission spectrum in the presence of OA was also different. The weak monomer emission, observed with the poorly water-soluble 2-hexyloxynaphthalene (**1b**), intensified upon addition of OA to the solution (**Fig 4.9**). Most importantly, emission due to excimer was absent (**Fig 4.9**). This difference in the nature of the emission between 2-methoxy- and 2-hexyloxynaphthalenes in presence of OA convincingly demonstrated the crucial role of the molecular size of the guest in complexation with the host.

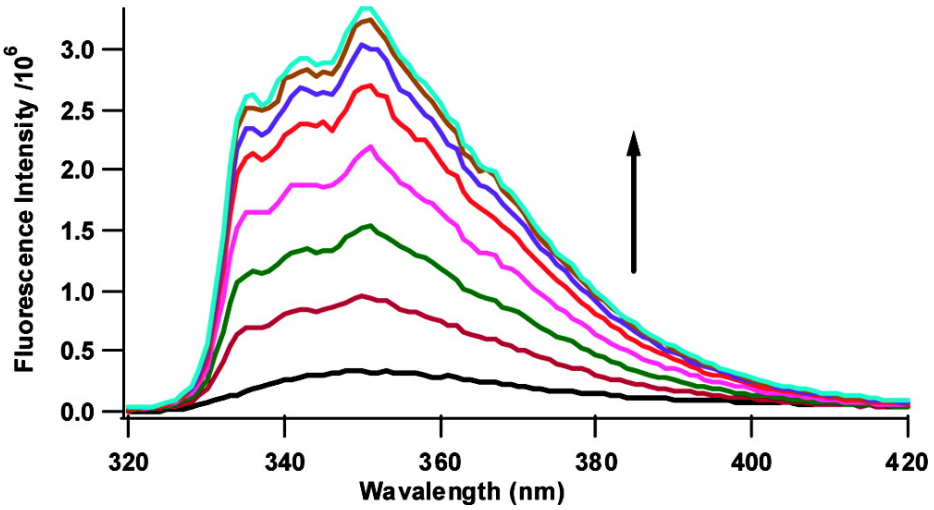

Figure 4.9 Fluorescence spectra of 2-hexyloxynaphthalene (**1b**) (2×10^{-5} M) with OA host in borate buffer (10 mM) at concentrations varying from (bottom to top) 0 to 1.4×10^{-4} M. Excitation was carried out at 270 nm.

In contrast to the above two 2-alkoxynaphthalenes, more hydrophilic and water soluble 2-naphthoic acid (**1c, Scheme 4.1**) exhibited a different behavior. The ^{1}H NMR titration spectra are provided in **Fig 4.10**. Here we focused on two specific signals, one

due to the guest (H_1) and another due to the host (H_e) (see **Fig 4.10**). Unlike the two 2-alkoxynaphthalenes discussed above, the chemical shifts of the above two signals in the 2-naphthoic acid (**1c**)/OA complex were not constant but changed with addition of different amount of the host OA to a guest solution. As shown in **Fig 4.11** the differences in the chemical shifts of H_1 (in the presence and absence of OA in buffer) were plotted with respect to the host/guest ratio. We observed a continuous shift in the signal position with the increased addition of OA. Even at 2:1 ratio (H/G) the chemical shift did not reach a plateau, and it was still shifting upfield. This was an indication that OA/**1c** complex was not stable in the NMR time scale; there was an exchange between free and complexed states. This was quite different from what we found with the two 2-alkoxynaphthalenes (**1a** and **1b**) where the host/guest complexes (2:2 and 2:1) remained intact during the NMR time scale. The diffusion constants for the guest and host molecules for various host/guest ratios are shown in **Fig 4.10**. Once again the diffusion constants were dependent on the amount of the host/guest ratio in solution. In fact the diffusion constant of the guest, although decreased from 5.36×10^{-6} cm^2/s to 4.32×10^{-6} cm^2/s (**Fig 4.10**), did not reach that expected of a host/guest complex. Both chemical shift and diffusion constants that we measured at various host/guest ratios were an average of the ones due to free and complexed species. Water solubility and hydrophilicity of 2-naphthoic acid made the host/guest complex less stable on the NMR time scale. Since even with 3 equiv of the host the saturation limit was not reached, we could not estimate the binding constant for this system. Depending upon the above discussion it was clear that the OA forms a 1:1 cavitandplex with 2-naphthoic acid.

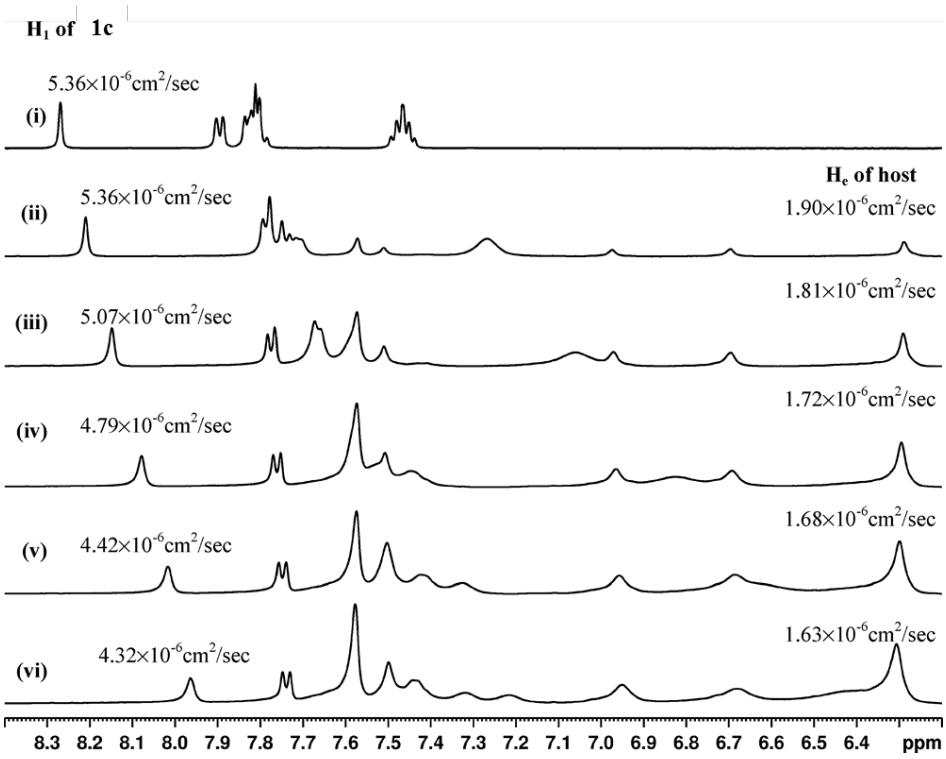

Figure 4.10 ^{1}H NMR titration experiments of 2-naphthoic acid (**1c**) with host OA. (i) 2-naphthoic acid (1 mM in 10 mM buffered D_2O), (ii) 2-naphthoic acid/OA 1:0.2, (iii) 2-naphthoic acid/OA 1:0.4, (iv) 2-naphthoic acid/OA 1:0.6, (v) 2-naphthoic acid/OA 1:0.8, and (v) 2-naphthoic acid/OA 1:1. Diffusion constant for the H_1 resonance of the guest and H_e resonance of the host are indicated at each host/guest ratio.

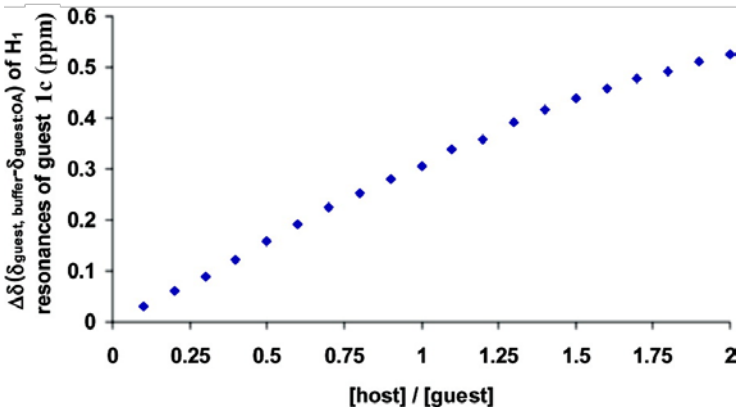

Figure 4.11 Variation of H_1 proton resonance of **1c** upon the addition of OA. [**1c**] = 1 mM.

It was concluded from the above results that the nature of the host/guest complex is dependent on the structure and hydrophobicity of the guest. Structures we visualized for the three guests are represented in **Scheme 4.3**. It is important to recognize that the structure of host/guest complex depends on a number of factors. Currently we identified two of these, size and shape of the guest and its solubility (hydrophobicity) in water.

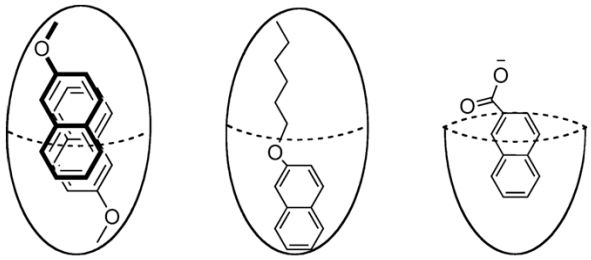

Scheme 4.3 Cartoon representations of capsular assemblies of naphthalene derivatives **1a-c** with OA.

4.2.2 Complexation of anthracene and naphthalene with OA

Our next experiments aimed to investigate the nature of the capsuleplex formation (Host: guest = 2:1 or 2:2 or both) in details depending upon the size of the hydrophobic guests. We chose anthracene and naphthalene for this study. The ^{1}H NMR titration spectra of anthracene (**1d**) with OA are presented in **Fig 4.12**. The five signals due to anthracene noncovalent dimer are marked with a triangle (**Fig 4.12(v)**), confirmed by the earlier literature.[123] However, at very low concentrations of anthracene, none of these signals were seen (**Fig 4.12(ii)**); instead, new ^{1}H signals due to OA (in addition to free OA) were found, suggesting a complex formation with anthracene but not a 2:2 capsuleplex. Careful examination of the spectra revealed three signals due to anthracene

(marked with filled circles) were correspond to a 2:1 OA-anthracene capsuleplex (**Fig 4.12(ii)**).

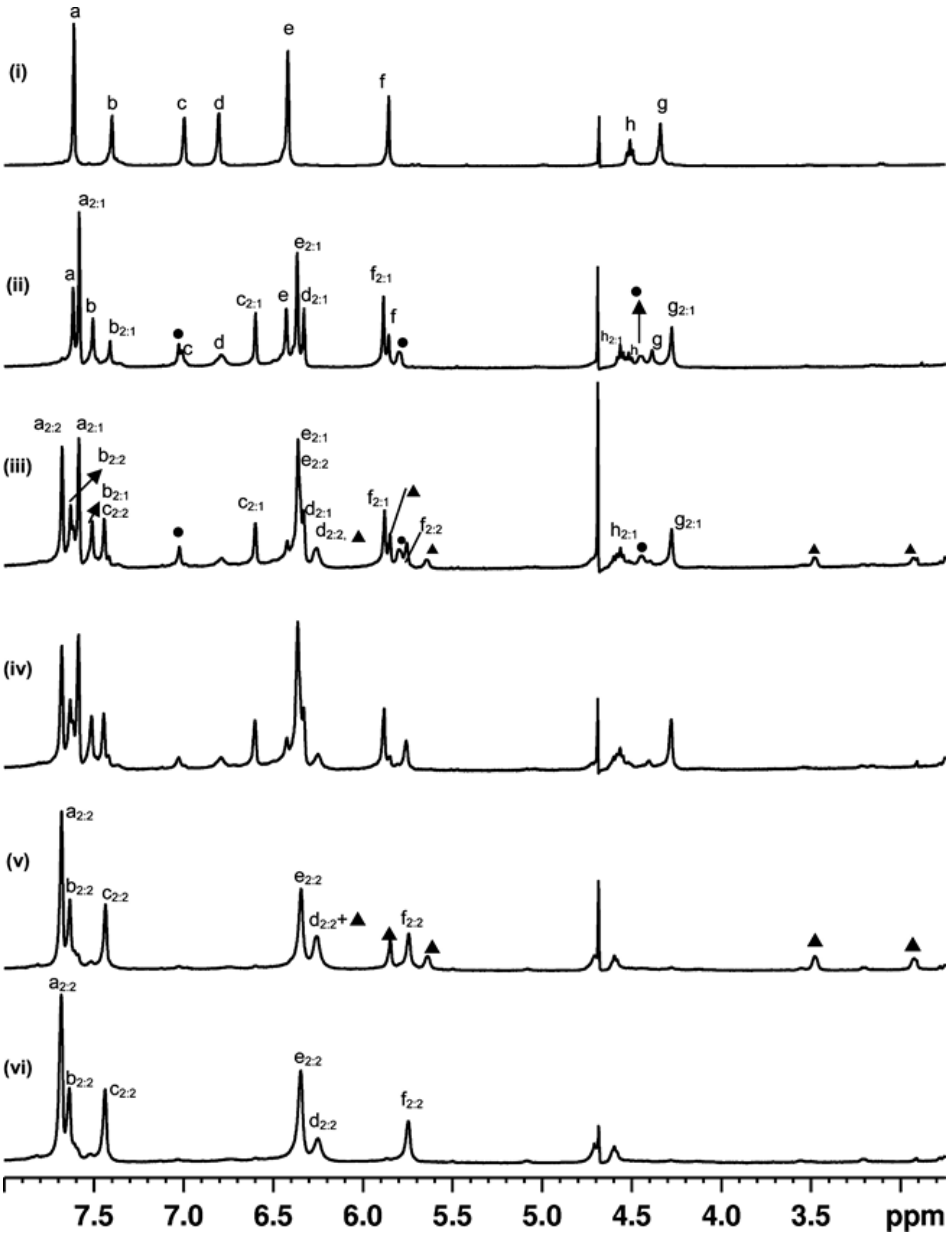

Figure 4.12 ^{1}H NMR spectra of anthracene in octa acid. (i) OA (1 mM in 10 mM buffered D_2O), (ii) OA:anthracene 10:2, (iii) OA:anthracene 10:6, (iv) OA:anthracene-d_{10} 10:6, (v) OA:anthracene 10:10, and (vi) OA:anthracene-d_{10} 10:10. The aromatic host resonances of free OA, 2:1 (H:G), and 2:2 capsular assemblies are denoted by a-h, (●) represents the guest resonances of 2:1 (H:G) assembly, and (▲) represents the guest resonances of 2:2 capsular assembly.

Upon further addition of anthracene, these signals and the expected five signals due to 2:2 capsuleplex were found in the ^{1}H NMR spectrum (**Fig 4.12**, (iii)); likewise, ^{1}H NMR OA signals corresponding to OA due to both 2:2 and 2:1 capsuleplexes were visible. A comparison of traces iii and iv in **Fig 4.12** representing anthracene and anthracene-d_{10}, respectively, established the existence of the two sets of OA signals. It should be noted that the ^{1}H NMR signals of anthracene was absence in trace iv, **Fig 4.12**. The 2D-COSY correlation spectrum shown in **Fig 4.13** illustrated that, at an OA to antharcene concentration ratio of 1.7 to 1, the two types of capsuleplexes (2:1 and 2:2) coexisted. From the signals due to 2:1 complex and 2:2 complex in one NMR spectrum, it became clear that the capsuleplexes correlate well among themselves but not with each other.

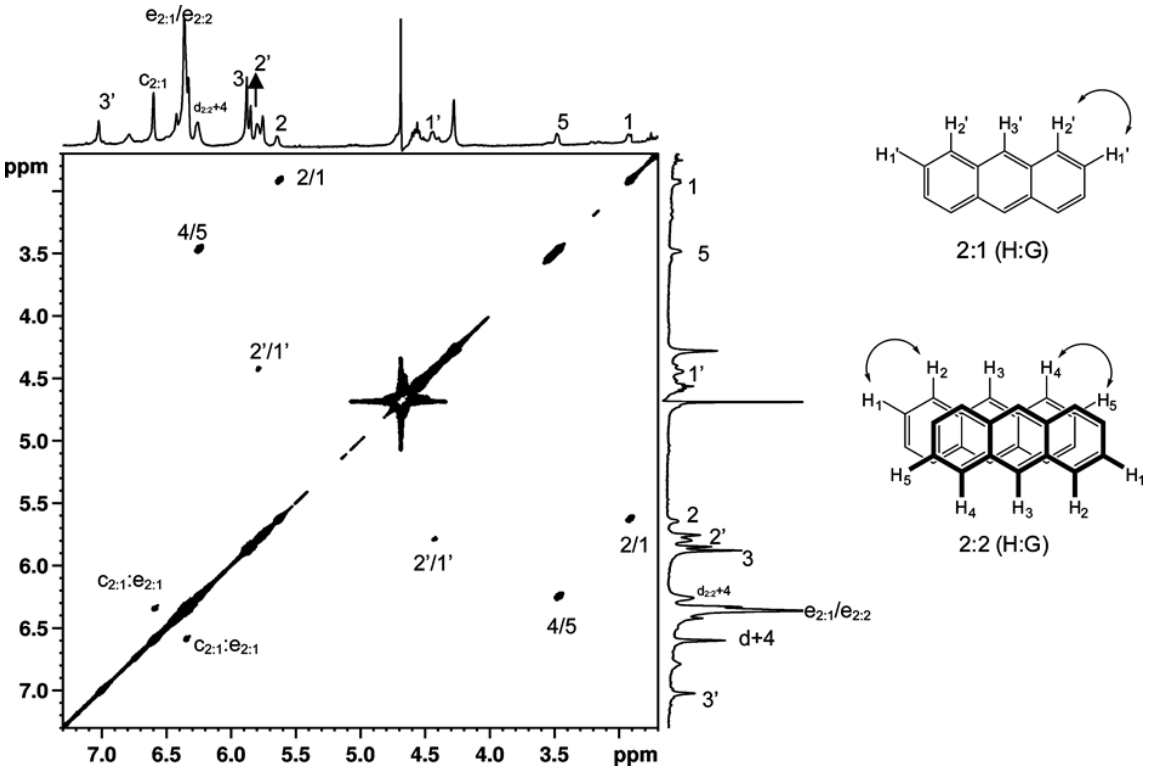

Figure 4.13 2D-COSY NMR spectrum of a solution containing 2:1 (H:G) and 2:2 capsular assemblies of OA:anthracene. [OA] = 5 mM and [anthracene] = 3 mM.

Emission spectra of anthracene recorded at different OA-anthracene concentrations provided the final confirmation for the existence of 2:1 capsuleplex (**Fig 4.14**). The emission was observed mainly from excimer with OA to **1d** at a concentration ratio of 1:1. Upon further addition of OA, emission spectrum changed to the mostly monomer emission at 5:1 ratio (**Fig 4.14**). This change suggested that, at high and low concentrations of anthracene relative to OA, 2:2 and 2:1 capsuleplexes were preferred, respectively. The NMR and emission data presented above suggest that anthracene formed two types of capsuleplexs (2:1 and 2:2) depending on the host-guest concentrations.

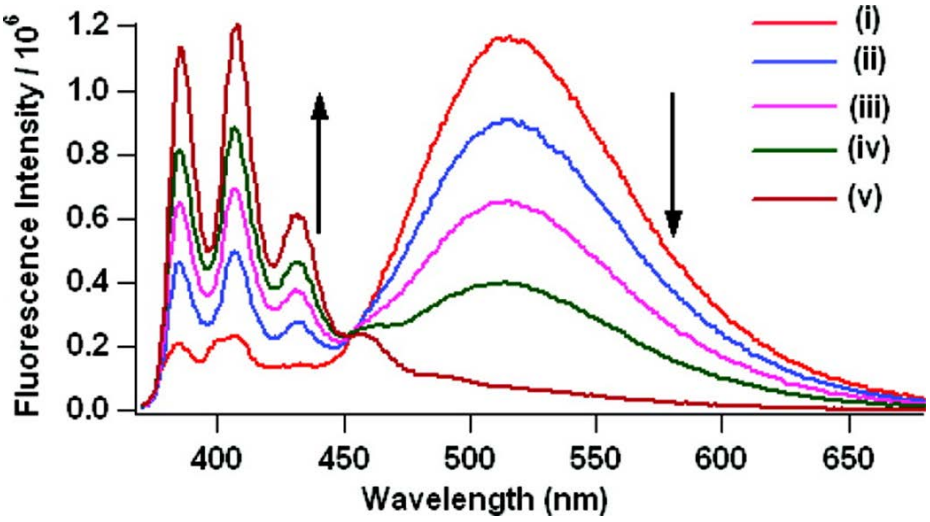

Figure 4.14 Emission spectra of anthracene (**1d**) in octa acid. (i) OA:anthracene 1:1, (ii) OA:anthracene 2:1, (iii) OA:anthracene 3:1, (iv) OA:anthracene 4:1, and (v) OA:anthracene 5:1. [Anthracene] = 10^{-5} M. λ_{ex} = 350 nm.

The above results as well as previous report[125] from our group established that the three guest molecules, all smaller/closer to the depth of the OA cavity, namely, adamantane (5 Å), 1,4-diethylbenezene (9.8 Å), and anthracene (9.2 Å), form both 2:1

and 2:2 capsuleplexes. Based on these results, we expected naphthalene (**1e**) (6.8 Å), smaller than 1,4-diethylbenezene and anthracene, would form both 2:1 and 2:2 capsuleplexes with OA. But, contrary to our expectation we found that naphthalene would only form the 2:2 capsuleplexes with OA at all host-guest concentrations. As shown in **Fig 4.15**, ^{1}H NMR signals of naphthalene (black filled circles) only due to 2:2 capsuleplex with OA were observed.

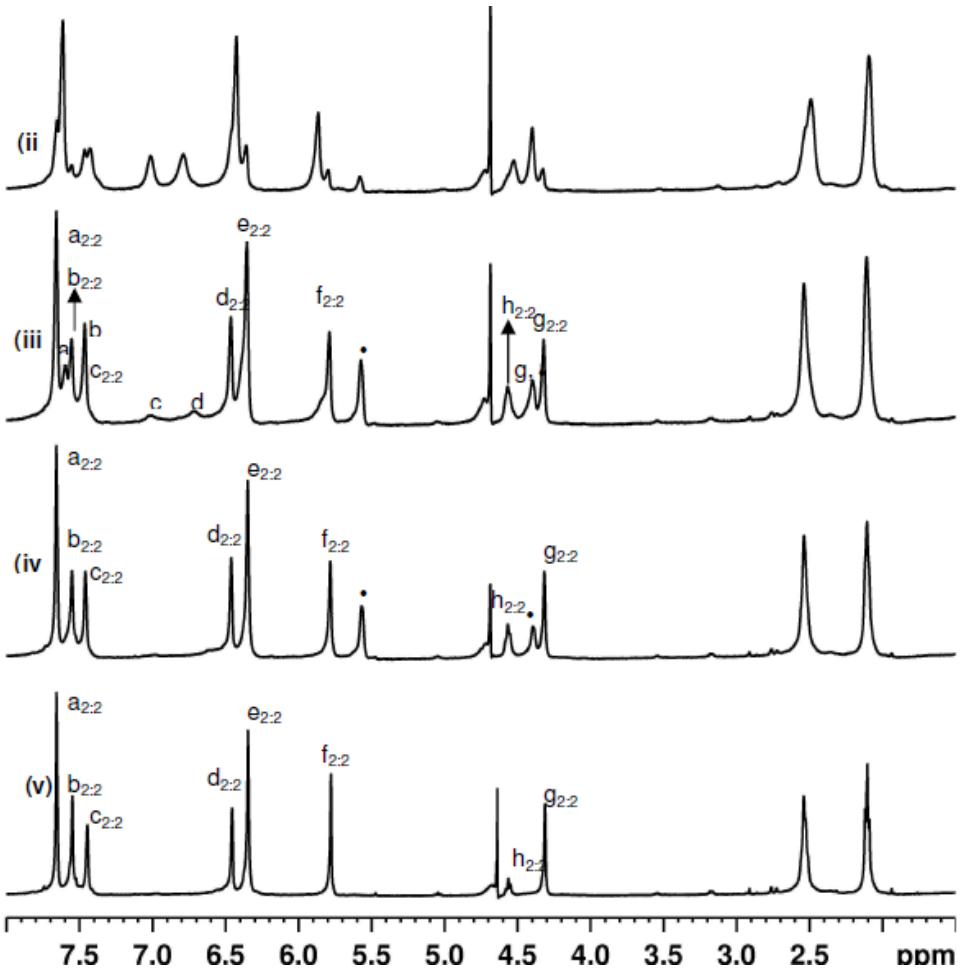

Figure 4.15 ^{1}H NMR spectra of naphthalene (**1e**) in octa acid (i) OA (1 mM in 10 mM buffered D_2O, (ii) OA: Naphthalene 10:2, (iii) OA: Naphthalene 10:6, (iv) OA : Naphthalene 10:10 and (v) OA : Naphthalene-d_8 10:10. The aromatic host resonances of free OA and 2:2 capsular assemblies were denoted by a-h, "●" represents the guest resonances of 2:2 (H:G) assembly.

The above observations suggested that the molecular dimension alone was insufficient to predict whether a given molecule would form 2:1 or 2:2 capsuleplex. Weak interactions between host−guest, guest−guest, and guest−medium might have a role in determining the nature of the complex formed.

4.2.3 Guest rotation within a capsuleplex along the X axis monitored by EPR spectroscopy

In the earlier section we established that, depending upon the structure of the guest, the stoichiometry of OA−guest complexes could have a host/guest ratio of 1:1, 2:1, 2:2 or both 2:1 and 2:2. We further became interested to explore the dynamics of a guest molecule within OA capsuleplex, the 2:1 complex in particular. It was established that guest molecules rotate within the capsule faster (along the molecular *x* axis) than the NMR timescale.[126] Therefore, we probed this motion through the EPR technique where the timescale is much shorter (ns). To monitor the guest rotational motion, the EPR spectra of paramagnetic probes **1f-i** (**Scheme 4.1**) were recorded at room temperature. The three-line EPR spectra (three hyperfine lines: $2I_N + 1 = 3$, I = 1 for ^{14}N) were simulated by the well-established procedure of Freed and co-workers[128] and matched the experimental spectra. There were two main input parameters: (i) the A_{ii} principal values of the A_N tensor for the coupling between electron and nuclear spins, which were taken to be $A_N = (A_{xx} + A_{yy} + A_{zz})/3$. An increase in the environmental polarity enhances the A_N tensor components owing to the increased electron spin density on the nitrogen nucleus of the NO group of the nitroxide probe.[129,130] Monitoring the A_N tensor helped us to ascertain the location of guests in the presence of OA. (ii) The correlation time (τ) for

the rotational diffusion motion of the spin probe provided information about the guest rotation within the capsule. Brownian motion was assumed in the calculation of the main component of the correlation time, that is, the perpendicular one (τ_{perp}) [for details see Chapter 2].

We will focus on **1g** first to explain the host/guest complex formation with OA using EPR spectroscopy and then use that information in the case of the other paramagnetic guests (**1f**, **1h** and **1i**, **Scheme 4.3**). **Fig 4.16(i)** provides EPR spectra for **1g** at different OA/**1g** molar ratios. It was clear that the EPR spectra of samples containing OA/**1g** < 2 consist of two components. In the spectra, the high-field hyperfine line was split into two. One of these corresponded to the uncomplexed guest, and the other to the complexed guest. At OA/**1g** = 4:1, the component due to complexed guest was predominant. In **Fig 4.16(ii)**, experimental (recorded in the absence and in the presence of 4 equiv of OA) and simulated spectra of **1g** are provided. It is important to note that both the A_N (polarity) and τ_{perp} (rotational mobility) parameters for **1g** in the absence and in the presence of 4 equiv of OA were significantly different (**Fig 4.16(ii)**). A sharp reduction in polarity, that is, a decrease in A_N, and in mobility, that is, an increase in τ_{perp}, for OA/**1g** = 4 with respect to OA/**1g** = 0 suggested that the probe at OA/**1g** = 4 was fully included within OA. The environmental polarity measured by A_N for **1g** @OA_2 was close to that of benzene.[127,129-131] This is consistent with the micropolarity measured earlier for the OA capsule with various fluorescence probes (see **Chapter 3**).[127] As shown in **Fig 4.17**, The A_N parameters measured for **1f**, **1g**, **1h**, and **1i** at a host to guest ratio of 4:1 were 15.83, 15.52, 15.93, and 16.0 G, respectively indicated that at a host to

guest ratio of 4:1 **1f**−**1i** exist as complexes with OA. These numbers were smaller than the value measured in water in the absence of OA (17.02 G).

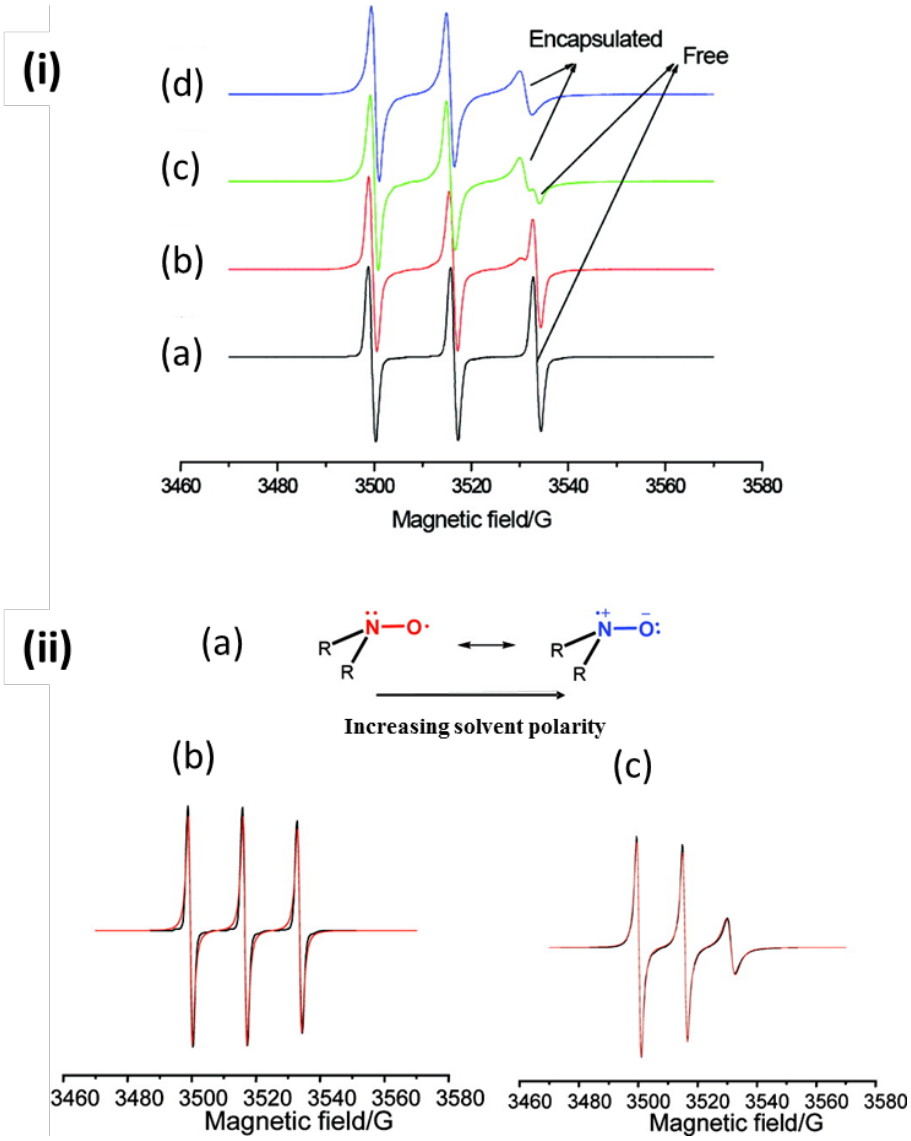

Figure 4.16 (i) EPR experimental spectra of **1g** at various OA concentrations (in 20 mM sodium tetraborate buffer): (a) OA/**1g** (0:1), (b) OA/**1g** (1:1), (c) OA/**1g** (2:1), and (d) OA/**1g** (4:1). [**1g**] = Amount corresponding to 1 mM in water, and it was partially solubilized; the addition of OA increases the solubility of **1g** in water. The high-field hyperfine lines of the encapsulated and free components are indicated by arrows. (ii) (a) Resonance structures of nitroxide derivatives depending upon the polarity of the medium; the distribution depends on the polarity of the medium. (b) EPR spectra of **1g** in water corresponding to the free component (simulated spectrum shown in red) with A_N = 17.02

G; and τ_{perp}= 0.031 ns. (c) EPR spectra of OA/**1g** (4:1) corresponding to the encapsulated component (simulated spectrum shown in red) with A_N = 15.52 G; and τ_{perp}= 0.66 ns.

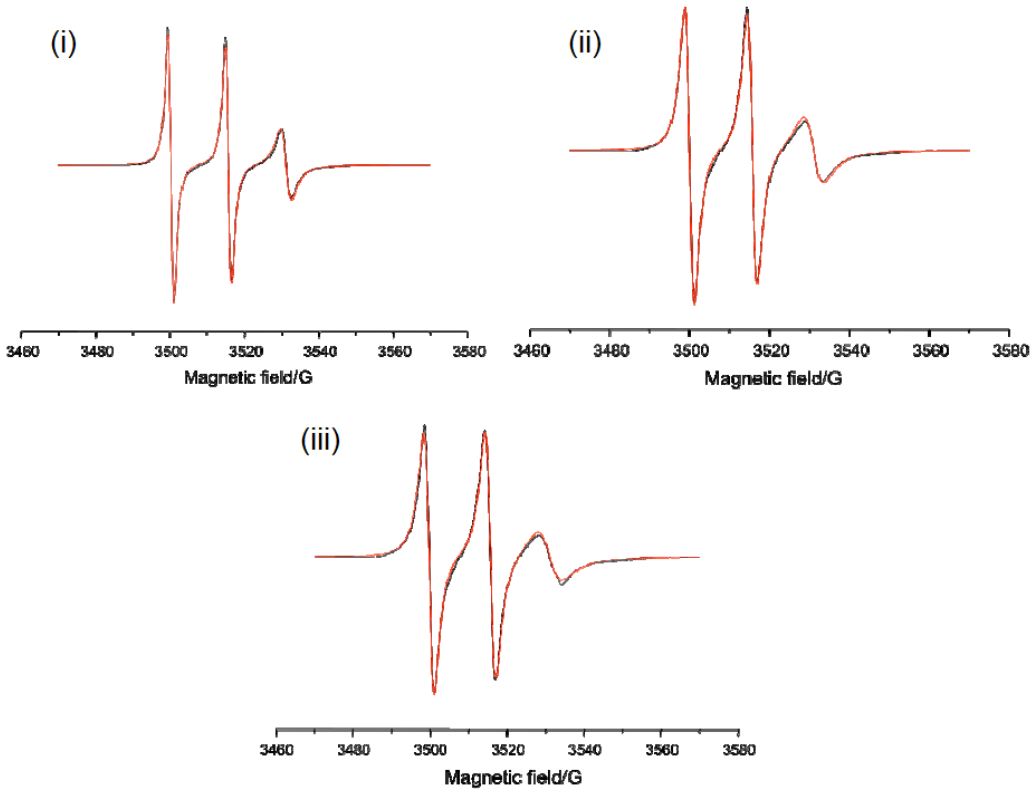

Figure 4.17 EPR spectra of (i) **1f**: OA (1:4), A_N= 15.8 G; τ_{perp}= 0.26 ns, (ii) **1h**: OA (1:4), A_N= 15.9 G; τ_{perp}= 1.18 ns and (iii) **1i**: OA (1:4), A_N= 16 G; τ_{perp}= 1.5ns; simulated spectrum was shown in red color, [guest] = 1 mM.

Because the host−guest complexes of the above paramagnetic probes gave extremely broad ^{1}H NMR spectra, we could not ascertain the complex formation by NMR. Therefore, we synthesized methylated derivative (N−O replaced with N−OMe; see **1g'** in **Scheme 4.1**) of **1g** and monitored its comlexation with OA by NMR. ^{1}H NMR titration spectra for **1g'** are provided in **Fig 4.18**. The upfield shift of the alkyl guest protons of **1g'** in presence of OA indicated that **1g'** formed complex with OA. Upon addition of 0.5 equivalent of **1g'** to OA solution, all the uncomplexed host signals disappeared suggesting that **1g'** formed 2:1 capsuleplexes. This NMR results indirectly

suggested that **1g** also formed 2:1 complex with OA. Similarity of the EPR results (mainly A_N values as it informs about the polarity surrounding the probe) of **1f**, **1h** and **1f** with **1g** suggested that they also formed 2:1 capsuleplex with OA.

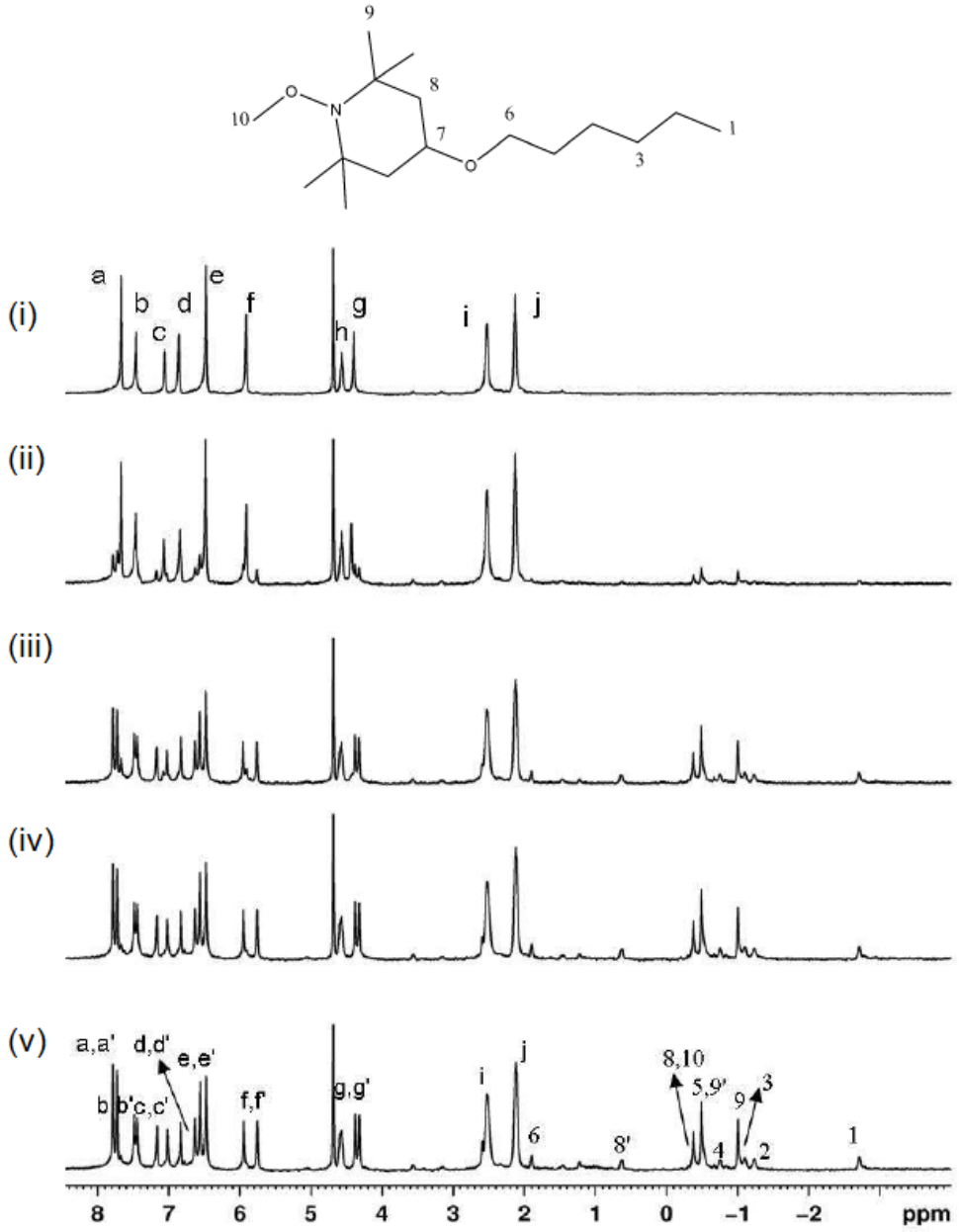

Figure 4.18 ^{1}NMR (500 HHz, D_2O) titration of **1g'** with OA (i) OA (1mM, 10 mM borate buffer), (ii) OA: **1g'** =1:0.1, (iii) OA: **1g'** =1:0.3, (iv) OA: **1g'** =1:0.4, (v) OA: **1g'**=1:0.5. Numbering for the guest was shown above the figure.

We were able to assign the guest protons in **1g'**@OA_2 complex by 2D COSY NMR (**Fig 4.19**). As illustrated in **Fig 4.20**, all the alkyl protons of **1g'**showed NOE correlation with the host protons and that also was an indication of the complex formation of **1g'** with OA.

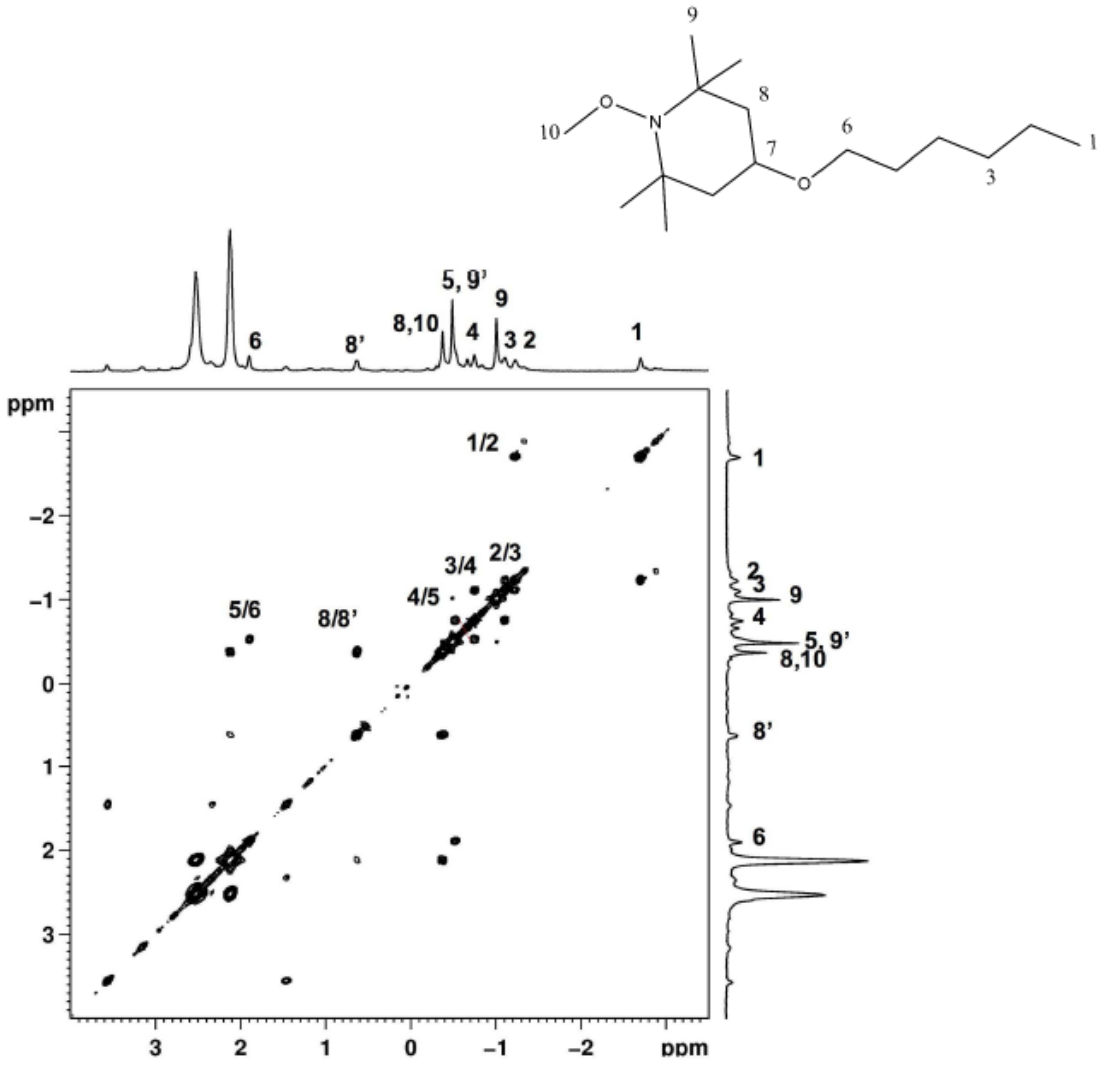

Figure 4.19 Partial 2D-COSY spectrum of **1g'**@OA_2. ([OA] = 5 mM in 50 mM sodium tetraborate buffer, [**1g'**] = 2.5 mM. Aromatic resonances of host are labeled from 'a-f' and encapsulated guest resonances are marked as 1-10).

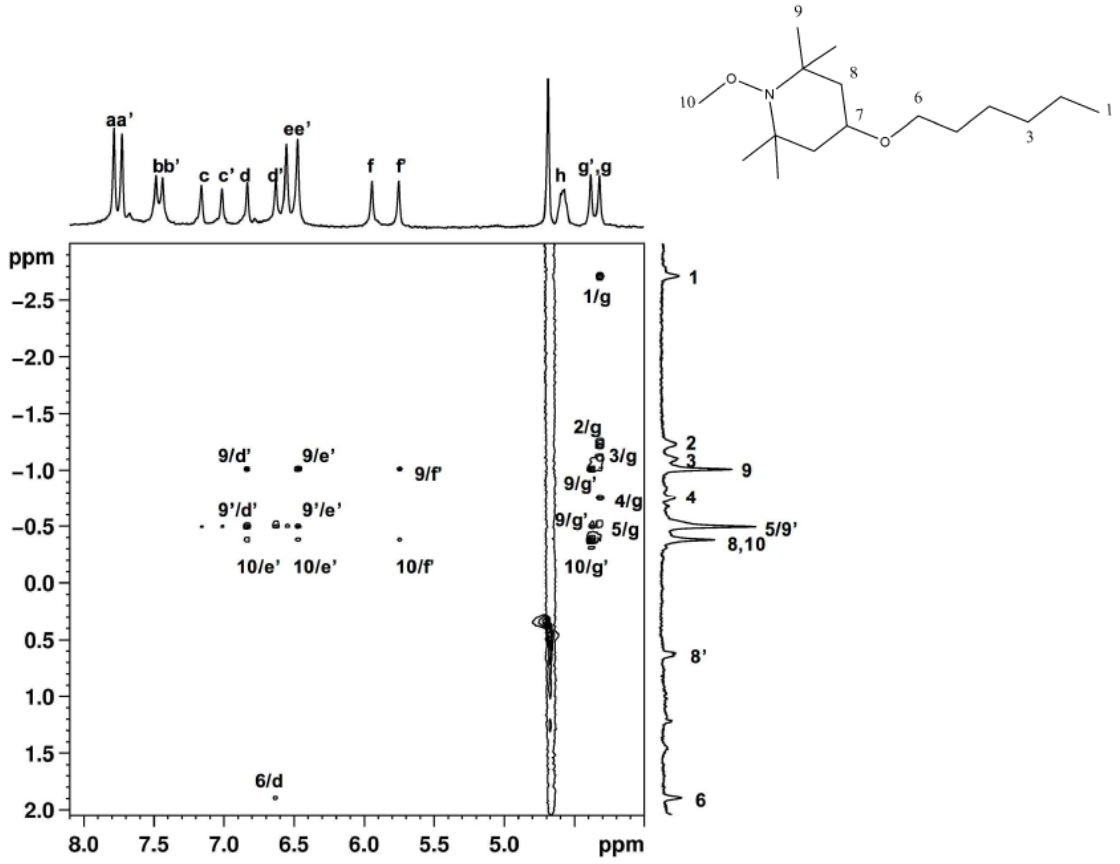

Figure 4.20 Partial 2D-NOESY spectrum of **1g'**@OA2. ([OA] = 5 mM in 50 mM sodium tetraborate buffer, [**1g'**] = 2.5 mM. Aromatic resonances of host are labeled from 'a-f' and encapsulated guest resonances are marked as 1-10). Mixing time 300 ms.

A plot of τ_{perp} measured from the simulated spectra at a host to guest ratio of 4:1 versus the chain length of the guests is provided in **Fig 4.21**. The Figure also includes the definition of τ_{perp}, which is the rotational diffusion mobility of the probes along the magnetic *x* axis (see **Fig 4.21(i)**). It was observed that τ_{perp} value for the probe in water was about 0.03 ns (**Fig 4.16).** However, for all probes within the OA capsule, τ_{perp} values were an order of magnitude longer than in pure water, suggesting that rotation was restricted within the OA capsule (**Fig 4.16 and 3.17**). Interestingly, τ_{perp} was dependent on the alkyl chain length. For example, for O-propyl, O-hexyl, O-octyl and O-decyl the numbers were 0.26, 0.66, 1.18, and 1.5 ns, respectively. On the basis of the EPR data, we

conclude that paramagnetic guest molecules undergo rotation along the molecular *x* axis within the capsule and that their rotational motion is dependent on the length of the alkyl chain. Importantly, the rotation of the probes was restricted within the capsule compared to that in water.

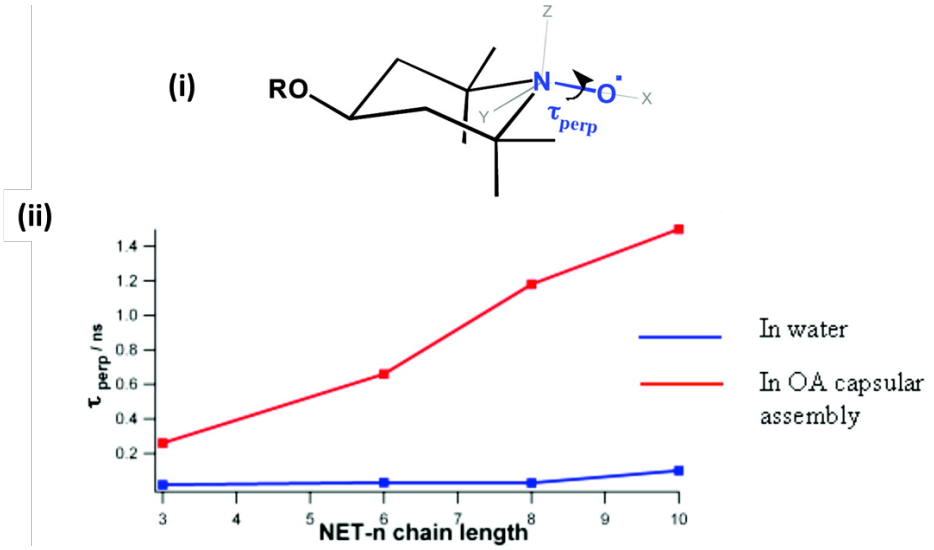

Figure 4.21(i) Reference frame that describes the rotational correlation time (τ_{perp}). (ii) Rotational correlation times of **1f**, **1g, 1h**, and **1i** included within OA.

4.3 Conclusion

The NMR and emission studies on 2-alkoxynaphthalnes (**1a-1b**) with varying chain length have shown that 2-methoxynaphthalne (**1a**) formed a 2:2 complex while 2-hexyloxynaphthalene (**1b**) formed a 2:1 capsuleplex. In contrast, 2-naphthoic acid formed 1.1 cavitandplex with OA.[105] Hence based on the above results it was concluded that the length and hydrophobicity of the molecule determines whether a given guest forms a 2:1 or 2:2 or 1:1 complex. On the other hand, anthracene was able to offer enough stabilization energy to form both 2:1 and 2:2 complexes, where as naphthalene formed only 2:2 complex.

Using a series of paramagnetic guest, we confirmed that the guest molecule rotates (in EPR time scale, ns) along its molecular axis inside the capsule, but its rotation is restricted inside OA capsule with respect to water. Varying the chain length of the guests we confirmed that their rotational motion is dependent with the size of the guest.

4.4 Experimental Section

Materials and Methods

All probe molecules used in this study were purchased from Sigma-Aldrich/Acros Organics and were recrystallized twice prior to use. Octa acid (OA) was synthesized following a literature procedure.[83] Fluorescence spectra were recorded using an Edinburgh FC900 spectrofluorometer equipped with a xenon lamp. Fluorescence lifetime measurements were made using an Edinburgh single photon counter, fitted with a hydrogen arc lamp. All ^{1}HNMR spectra were recorded using a Bruker 500 MHz NMR at 27 °C. Spectral plots were generated using Igor Pro software. Diffusion constant measurements were made using a Bruker 500 MHz NMR spectrometer at 27 °C. Data were collected by using 'stebpg1s' pulse sequence (eight scans) and processed by T_1/T_2 relaxation module in the TOPSIN 2.1 software.

Photophysical Studies

A 1 mM stock solution of OA was made in 10 mM sodium tetraborate in water. Guest stock solutions (1 mM) were made in spectrophotometric grade chloroform. To chloroform evaporated (by bubbling nitrogen) were added appropriate amounts of each guest to a test tube with the required amounts of borate buffer and OA stock solution such

that the guest and OA were at 1×10^{-5} M and 2×10^{-5} M concentrations, respectively. The same concentration and procedure was adopted for all seven guests.

General Protocol for Binding Studies by NMR

A ^{1}H NMR spectrum of 600 μL of 2 mM OA in 20 mM sodium borate buffer in D_2O was recorded. To this solution was added 0.25 equiv of guest (5 μL of a 120 mM solution in DMSO-d_6) in four stages, the mixture was shaken well for about 5 min, and spectra were recorded after each addition. Each sample was also examined 24 h later. No differences were noticed between 5 min and 24 h spectra. In all cases complete complexation was observed upon addition of 0.5 equiv of guest. Further addition resulted in a turbid solution, and the NMR spectrum revealed the presence of both free and complexed guest. All 2D ^{1}H NMR experiments were carried out with samples containing 5 mM OA and 2.5 mM guest in 50 mM sodium tetraborate buffer in D_2O.

General Protocol for EPR Study:

Preparation of host/guest complex at different concentration: Stock solution of guest (20 mM) was prepared in chloroform (**1f-i**). Host stock solution (5 mM) was prepared in water. Required amount of water, host and guest solutions were added and shaken by a mechanical shaker for 15 h. The same procedure was adopted for all guests.

CHAPTER 5

Photoinduced Electron Transfer from an Encapsulated Donor to a Free Acceptor through Capsular Wall

5.1 Overview

Electron transfer is the process by which an electron moves from one entity (an atom or a molecule) to another. The importance and complexity of electron transfer reactions are very nicely exhibited in Nature. Many biological processes, including oxygen binding, photosynthesis, respiration, and detoxification, utilize electron transfer reactions as a key mechanism to operate their housekeeping machineries. The mechanistic concept of electron transfer has been thoroughly studied in the last few decades.[57] A significant portion of this effort has been devoted to investigate the photoinduced charge separation reactions to capture and store the solar energy. *Photoinduced electron transfer* is an electron transfer process that occurs when photoactive materials interact with light. When a molecule is excited by a photon, an electron in a ground state orbital is excited to a higher energy orbital. This excited state generates a vacancy in a ground state orbital which can be filled by an electron donor. On the other hand an excited molecule places an electron in a high energy orbital that can be donated to an electron acceptor. In these respects a photoexcited molecule can act as a good oxidizing agent or a good reducing agent. A comprehensive understanding of photoinduced electron transfer reactions will enable researchers to design a chemical assembly for the conversion of solar energy into chemical potential. Electron transfer reactions commonly involve transition metal complexes, but there is an emerging trend of organic molecules behaving as electron transfer agents.

A critical part of this type of study is the design and synthesis of the molecular systems which are comprised of electron donors and acceptors. In previous chapters, we

established the analytical tools needed to understand and explore the supramolecular complexation of host and guest systems. In this section we showed the photoinduced electron transfer from the encapsulated donor molecules to a free acceptor in a supramolecular assembly. 4, 4' Dimethyl stilbene (DMS, **Scheme 5.1**) was chosen as electron donor. Methyl vilogen (MV^{2+}) and N-Me-pyridinium iodide (Py^{+}) (**Scheme 5.1**) were selected as electron acceptors. The donor-acceptor pairs were selected based on the well-established literature reports defining the exothermic photoinduced electron transfer from stilbene to the aforementioned acceptors in solution.[132,133] It has also been reported that DMS forms a strong 2:1 (H: G) complex with octa acid (OA, **Scheme 5.1**).[134] The OA-complex has been studied at pH ~ 9 (sodium tetraborate buffer) and at this pH carboxyl acid groups convert to negatively charged carboxylates and thus the whole complex become negatively charged. Generally electron transfer is more efficient if the donor and the acceptor are in close contact. Due to this reason cationic charged acceptors were selected as they can come close to the negatively charged DMS@OA_2 complex by electrostatic interaction. Moreover there is an important requirement for electron transfer process. The total energy for oxidation potential of the donor and reduction potential of the acceptor should be lower than the energy for excitation. The oxidation potential of DMS is 1.5 eV and the reduction potentials of MV^{2+} and Py^{+} are -0.69 eV and -1.5 eV respectively; the S_1 energy of DMS is 3.5 eV. [135-137] From the above values, it was calculated that electron transfer for both the cases should be exothermic (~1.3 eV in the case of MV^{2+} and ~0.5 eV in the case of Py^{+}). Another host cucurbit[7]uril (CB7) (**Scheme 5.1**) was used as it forms good complex with both the acceptors, MV^{2+} and Py^{+}. The idea behind using CB7 was that it would dissociate the acceptor from DMS@OA_2

complex and thus restrict the electron transfer process. This strategy was used as an indirect proof of the electron transfer process from DMS to MV^{2+}/Py^{+} across OA wall.

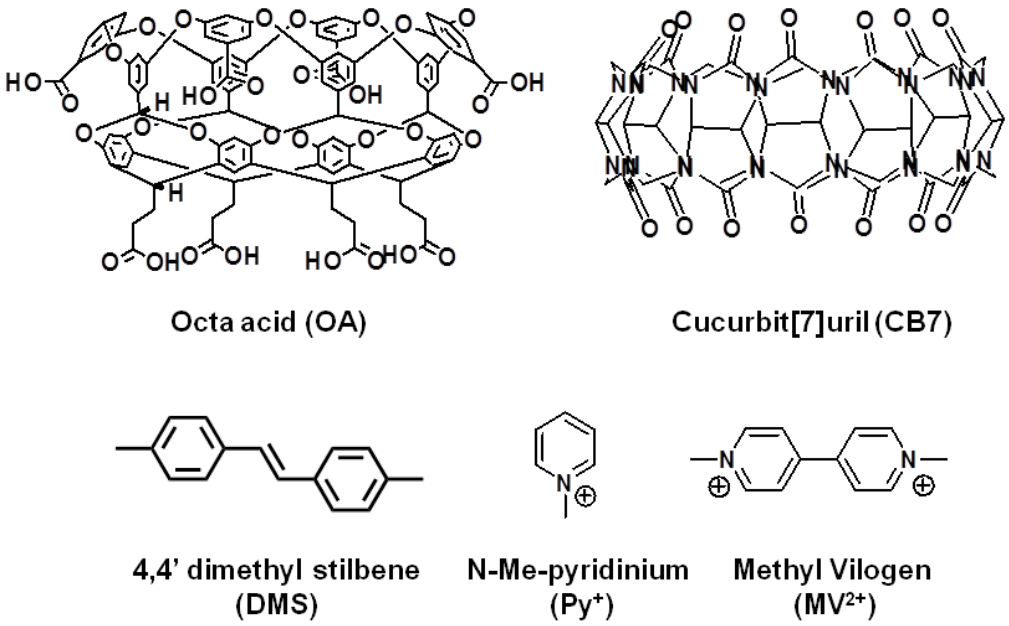

Scheme 5.1 Structures of the hosts (OA and CB7) and guests (DMS, Py^{+} and MV^{2+})

5.2 Results and discussion

5.2.1 ^{1}H NMR and 2D-DOSY studies

We performed ^{1}H NMR study to confirm the complex formation of DMS with OA. As we discussed in the previous chapter (**Chapter 3**), when a guest molecule forms complex with OA its proton signals are up-field shifted because of the shielding effect of the benzene rings in the interior cavity of OA. **Fig 5.1(i)** shows ^{1}H NMR spectra of DMS@OA_2. In presence of OA upfield shift of $-CH_3$ group of DMS suggests that DMS was inside OA capsule. The DMS@OA_2 complex was already reported[134] and we have

followed the same procedure to make the complex. **Fig 5.1(ii)** and **Fig 5.1(iii)** represent the ^{1}H NMR spectra of DMS@OA_2 + MV^{2+} and DMS@OA_2 + MV^{2+}@CB7. Large upfield shift of 4-methyl group of DMS and corresponding small shifts of the methyl groups of MV^{2+} in the presence and absence of OA suggested that DMS was encapsulated within OA capsule and MV^{2+} was located outside the capsule. After addition of one equivalent (with respect to MV^{2+}) CB7, methyl signals of MV^{2+} were up-field shifted suggesting that MV^{2+} was encapsulated within CB7.

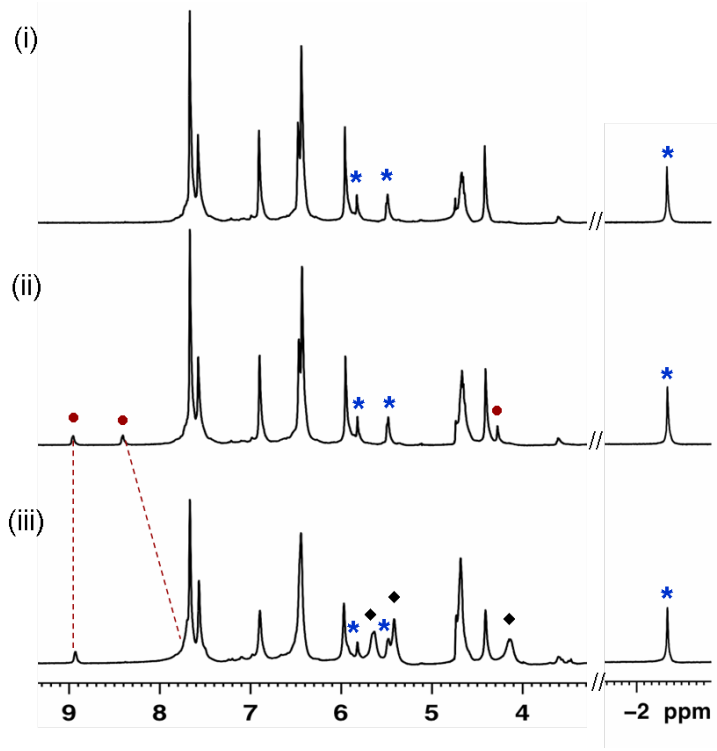

Figure 5.1 ^{1}H NMR (500 MHz, D_2O) spectra of (i) DMS@OA_2, (ii) DMS@OA_2 + MV^{2+} and (iii) DMS@OA_2 + MV^{2+}@CB7; [DMS]= 1 mM, [OA]=2 mM, [MV^{2+}]= 1 mM and [CB7]=1 mM; "*", "●" and "♦" represent bound DMS proton, MV^{2+} and CB7 proton signals.

Having shown that MV^{2+} resided outside the DMS@OA_2 capsule, we wanted to make sure that there was an assembly of (DMS@OA_2)@MV^{2+} due to electrostatic interaction between negatively charged DMS@OA_2 complex and positively charged MV^{2+}. One simple tool to examine this is to measure the diffusion constant of the individual molecule in the assembly. 2D-DOSY experiments were carried out to measure diffusion coefficient of the molecules in this system. This technique tells us the size and shape of the molecule. Diffusion constant of DMS@OA_2 was in accord with the reported value, 1.2×10^{-10} m^2 s^{-1}.[134] From 2D-DOSY experiment of DMS@OA_2 + MV^{2+}, it was observed that MV^{2+} had identical diffusion constant (1.2×10^{-10} m^2 s^{-1}) to that of DMS@OA_2. This indicated that DMS, OA and MV^{2+} moved together in aqueous solution (**Fig 5.2**).

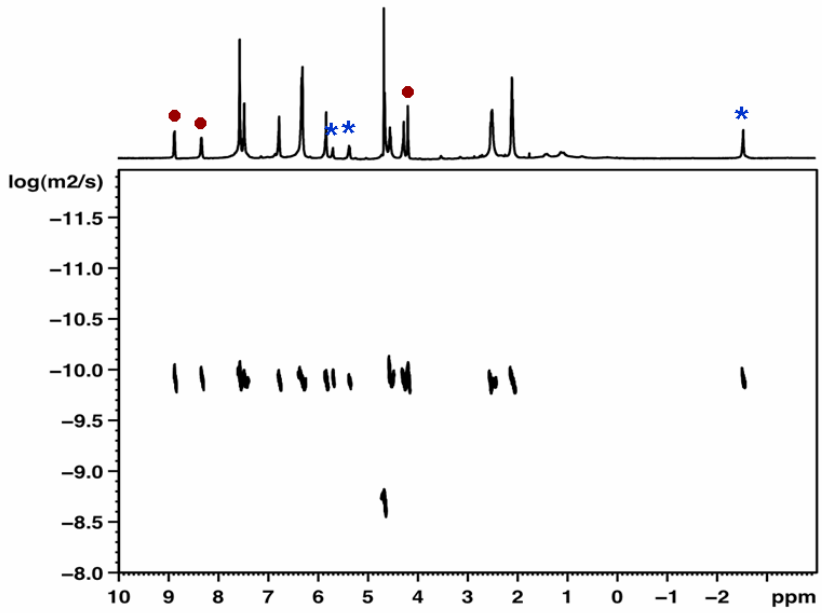

Figure 5.2 2D DOSY (500 MHz, D_2O) spectra of DMS@OA_2 + MV^{2+}; [DMS]= 0.5 mM, [OA]=1 mM, [MV^{2+}]= 0.5 mM; "*" and "•" represent bound DMS proton and MV^{2+} proton signals, diffusion constant of DMS@OA_2 and MV^{2+} are 1.25×10^{-10} m^2/s and 1.17×10^{-10} m^2/s respectively.

Similar results were found in the case of DMS@OA_2 + Py^+ system. From **Fig 5.3**, it is clear that 4-methyl group of DMS was upfield shifted whereas there was no significant change in methyl signal of Py^+ in the presence and absence of OA. This indicates that DMS was encapsulated within OA capsule and Py^+ was located outside the capsule. After addition of one equivalent (with respect to Py^+) of CB7, methyl signals of Py^+ were upfield shifted suggesting that Py^+ was encapsulated within CB7. The diffusion constant of Py^+ in the presence of OA was reduced from 8.9×10^{-10} m^2 s^{-1} to 4.8×10^{-10} m^2 s^{-1} (**Fig 5.4**). Though the diffusion constant of Py^+ was not exactly same as DMS@OA_2, it was significantly reduced in presence of DMS@OA_2 indicating that Py^+ interacted with DMS@OA_2 complex.

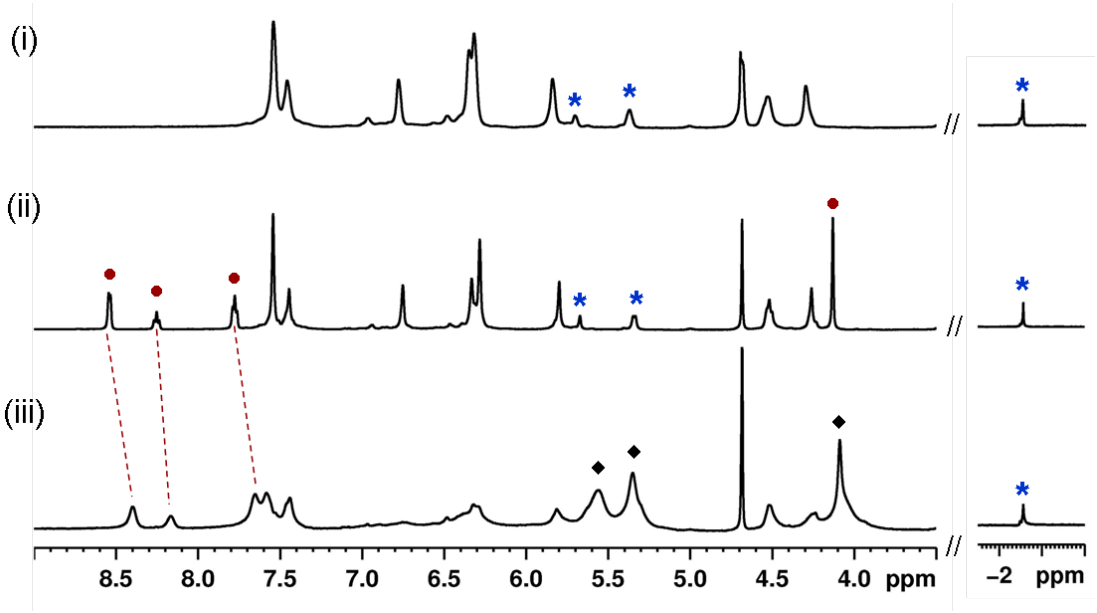

Figure 5.3 ^1H NMR (500 MHz, D_2O) spectra of (i) DMS@OA_2 (ii) DMS@OA_2 + Py^+ (iii) DMS@OA_2 + Py^+@CB7; [DMS] = 0.5 mM, [OA] = 1 mM, [Py^+] = 1 mM and [CB7]= 1 mM; "*", "●" and "♦" represent bound DMS proton, Py^+ and CB7 proton signals.

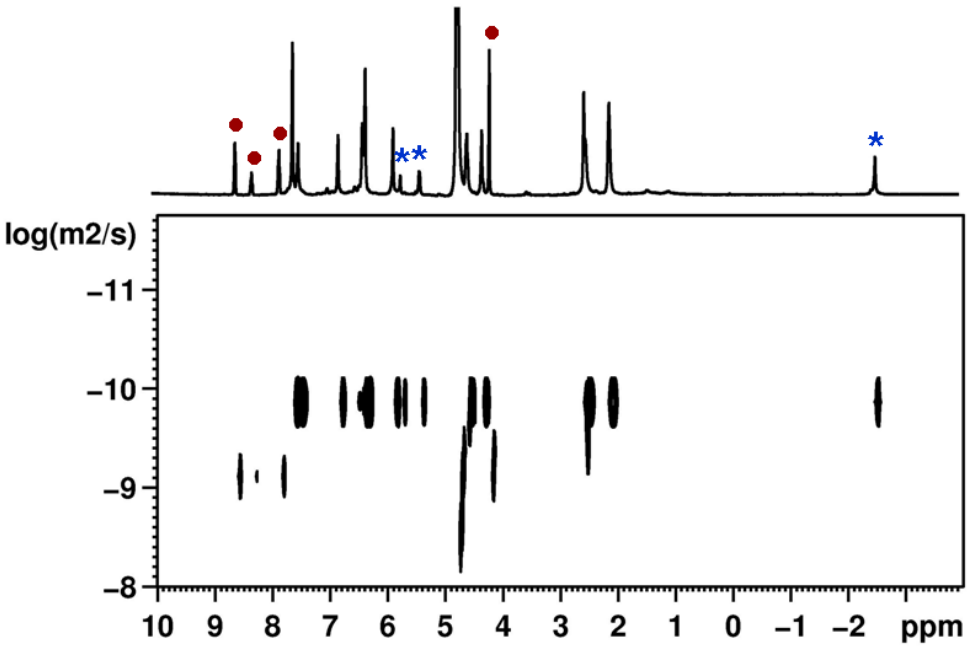

Figure 5.4 2D DOSY (500 MHz, D_2O) spectra of DMS@OA_2 + Py^+; [DMS]= 0.5 mM, [OA]=1 mM, [Py^+]= 1 mM; "*" and "•" represent bound DMS proton and Py^+ proton signals, diffusion constant of DMS@OA_2 and Py^+ are 1.2×10^{-10} m^2/s and 4.8×10^{-10} m^2/s respectively.

Based on the 2D-DOSY data we concluded that the cationic acceptors MV^{2+} and Py^+ remain associated with DMS@OA_2 due to electrostatic interaction between their cationic pyridyl parts and the carboxylate anion groups of OA. Apparently, Py^+ was not associated to the capsule as strongly as MV^{2+}.

5.2.2 Photophysical study

We performed steady state emission study to show the interaction between excited DMS encapsulated within OA capsule and free Py^+ or MV^{2+}. DMS has strong fluorescence. After transferring one electron to the accepter, DMS generates radical cation ($DMS^{+\cdot}$) which is not emissive. Thus electron transfer from DMS can be monitored by quenching the DMS fluorescence. It is also important to assure that DMS

should be excited selectively in presence of acceptor otherwise competitive absorption might be the partial reason for the quenching of DMS fluorescence by the acceptor. **Fig 5.5** shows the UV-Vis spectra of DMS@OA_2, OA and Py^+. The excitation wavelength for the fluorescence quenching study was chosen at 320 nm as DMS@OA_2 could selectively be excited at this wavelength without any interference of Py^+ absorption.

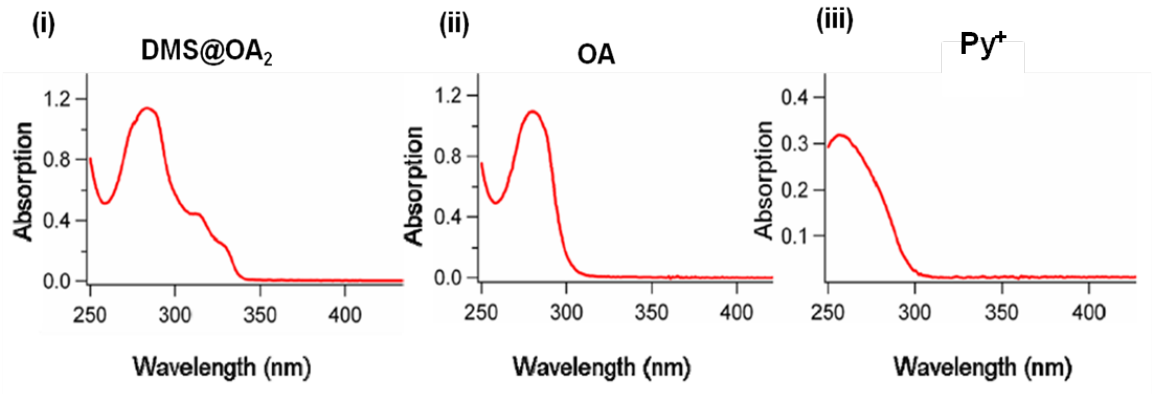

Figure 5.5 UV-Vis spectra of (i) DMS@OA_2; (ii) OA and (iii) Py^+; [OA] = 6×10^{-5} M, [DMS] = 3×10^{-5} M and [Py^+] = 6×10^{-5} M in 10 mM sodium tetraborate buffer.

With increasing the concentration of Py^+, fluorescence of DMS@OA_2 was quenched (**Fig 5.6**). Time resolved titration experiment was performed to see whether the quenching was static or dynamic. If the quenching is dynamic the Stern-Volmer plots based on steady state emission intensity and lifetime measurements should fully overlap. In case the quenching is fully static lifetime won't change with increasing concentration of the quencher. As shown in **Fig 5.7(i)**, the lifetime of excited DMS was reduced slightly in presence of Py^+. Comparison of Stern-volmer plot of I_0/I *vs* [Py^+]/[DMS@OA_2] and τ_0/τ *vs* [Py^+]/[DMS@OA_2] revealed that the quenching of DMS@OA_2 with Py^+ was mostly static, with a little dynamic component. As CB7 (one equivalent with respect to

Py^+) was added in the solution of DMS@OA_2 + Py^+, the quenched fluorescence of DMS@OA_2 by Py^+ was recovered (**Fig 5.8**). This is due to the fact that CB7 formed complex with Py^+ and therefore separated from DMS@OA_2 complex.

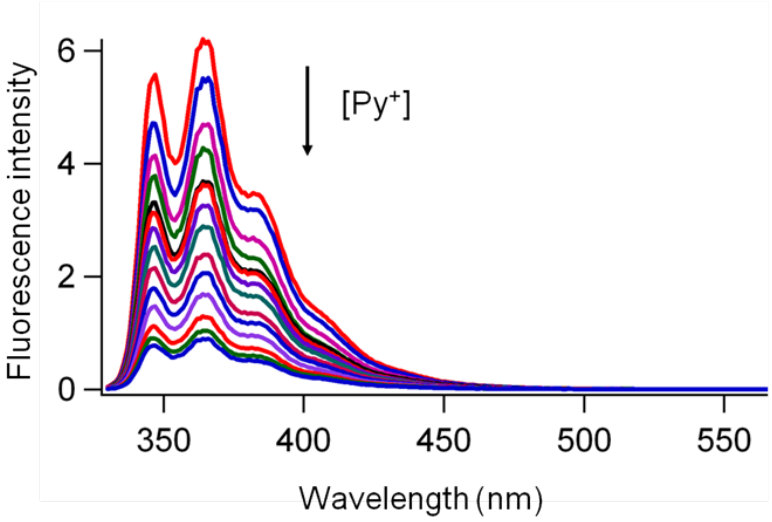

Figure 5.6 Fluorescence quenching titration of DMS@OA_2 with Py^+; λ_{ex}= 320 nm; [DMS]=1.25×10^{-5} M, [OA]=2.5×10^{-5} M and [Py^+]=0 to 31.75×10^{-5} M in 10 mM sodium tetraborate buffer.

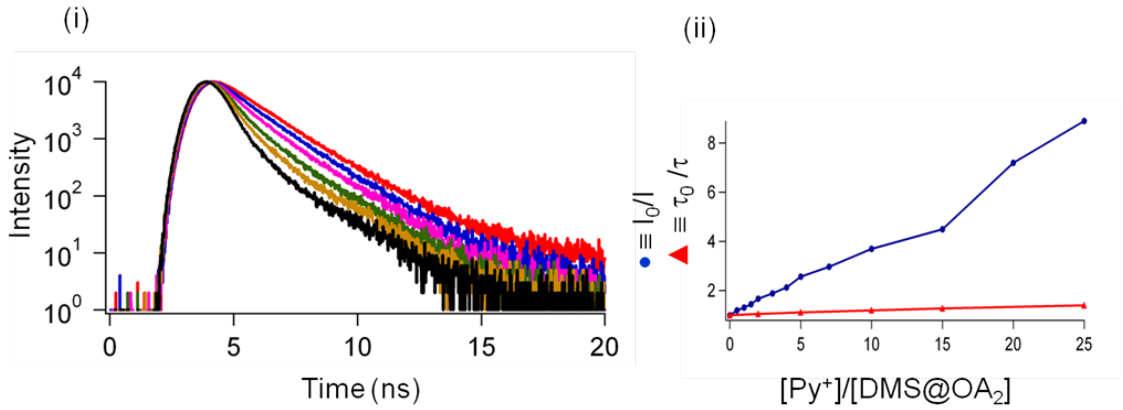

Figure 5.7 (i) Time resolved quenching titration of DMS@OA_2 with Py^+ and (ii) Stern-Volmer plot for quenching titration of DMS@OA_2 with Py^+; λ_{ex}= 320 nm, λ_{em}= 365 nm; [DMS]=1.25×10^{-5} M, [OA]=2.5×10^{-5} M and [Py^+]=0 to 31.75×10^{-5} M and in 10 mM sodium tetraborate buffer.

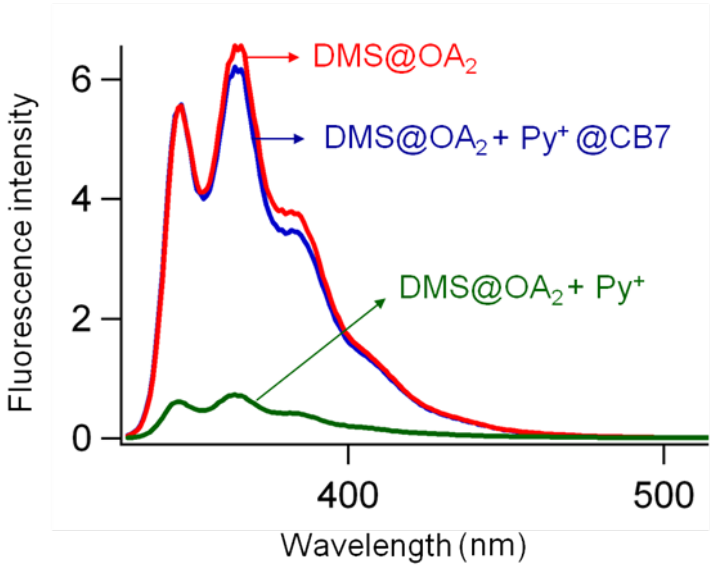

Figure 5.8 Fluorescence spectra of DMS@OA_2, DMS@OA_2 + Py^+ and DMS@OA_2 + Py^+@CB7; [DMS]=1.25×10^{-5} M, [OA]=2.5×10^{-5} M, [Py^+]=31.75×10^{-5} M and [CB7]=31.75×10^{-5} M in 10 mM sodium tetraborate buffer; λ_{ex}= 320 nm.

Similar results were observed in the case of MV^{2+}. With increasing concentration of MV^{2+}, fluorescence of DMS@OA_2 was quenched (**Fig 5.9**). As lifetime of DMS@OA_2 did not change with increasing concentration of MV^{2+}, quenching of DMS@OA_2 with MV^{2+} was completely static (**Fig 5.10**). Examination of Stern-Volmer plots shown in **Fig 5.11** suggested that quenching is much more efficient in the case of MV^{2+} compared to Py^+. Being doubly cationic charged, MV^{2+} bound more strongly to negatively charged exterior walls of OA than mono-cation Py^+. Due to this reason quenching process in the case of Py^+ was less efficient than in the case of MV^{2+}. As CB7 (one equivalent with respect to MV^{2+}) was added in the solution of DMS@OA_2 + MV^{2+}, the quenched fluorescence of DMS@OA_2 by MV^{2+} was recovered (**Fig 5.12**) indicating that quenching did not occur as MV^{2+} was encapsulated within CB7.[138]

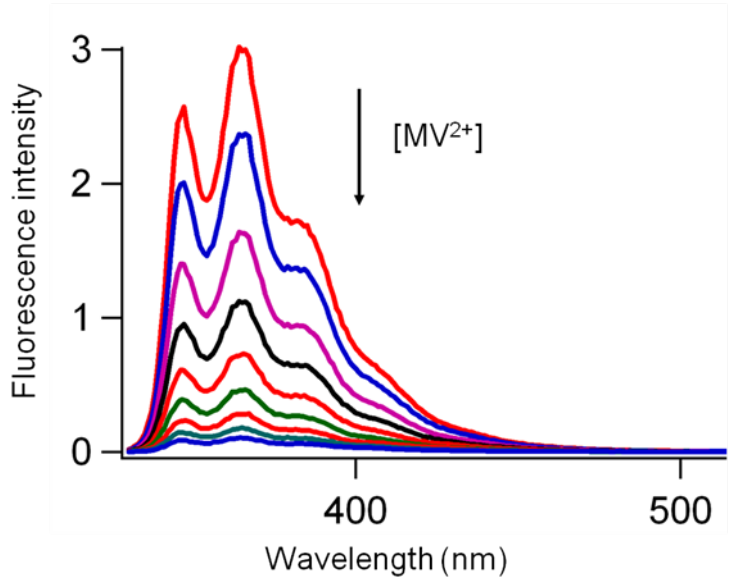

Figure 5.9 Fluorescence quenching titration of DMS@OA_2 with MV^{2+}, [DMS] = 1.25×10^{-5} M, [OA]=2.5×10^{-5} M and [MV^{2+}]=0 to 2.5×10^{-5} M in 10 mM sodium tetraborate buffer.

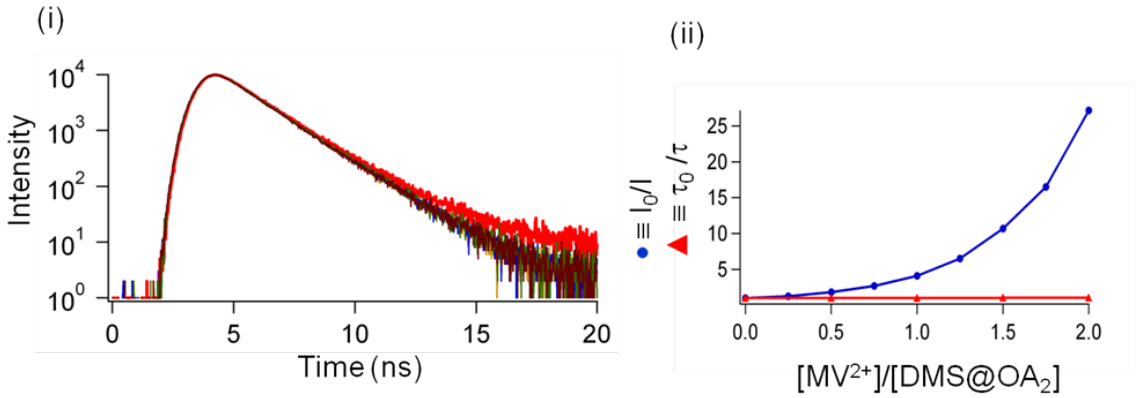

Figure 5.10 (i) Time resolved quenching titration of DMS@OA_2 with MV^{2+} and (ii) Stern-Volmer plot for quenching titration of DMS@OA_2 with MV^{2+}; [DMS]=1.25×10^{-5} M, [OA]=2.5×10^{-5} M and [MV^{2+}]=0 to 2.5×10^{-5} M in 10 mM sodium tetraborate buffer.

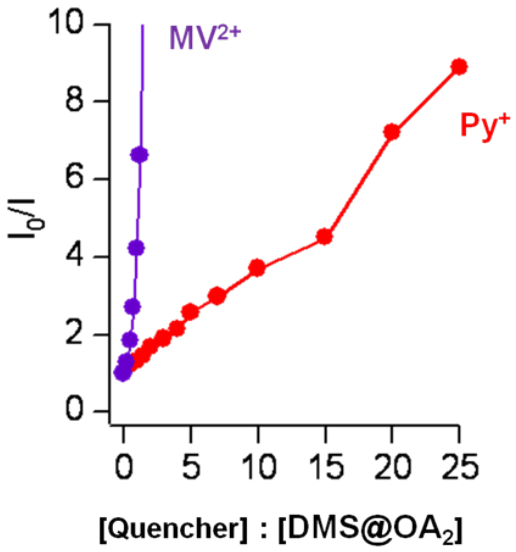

Figure 5.11 Stern-Volmer plot for quenching titration of DMS@OA_2 with Py^+ and MV^{2+}; λ_{ex}= 320 nm, λ_{em}= 365 nm; [DMS]=1.25×10^{-5} M, [OA]=2.5×10^{-5} M, [Py^+]=0 to 31.75×10^{-5} M and [MV^{2+}]=0 to 2×10^{-5} M in 10 mM sodium tetraborate buffer.

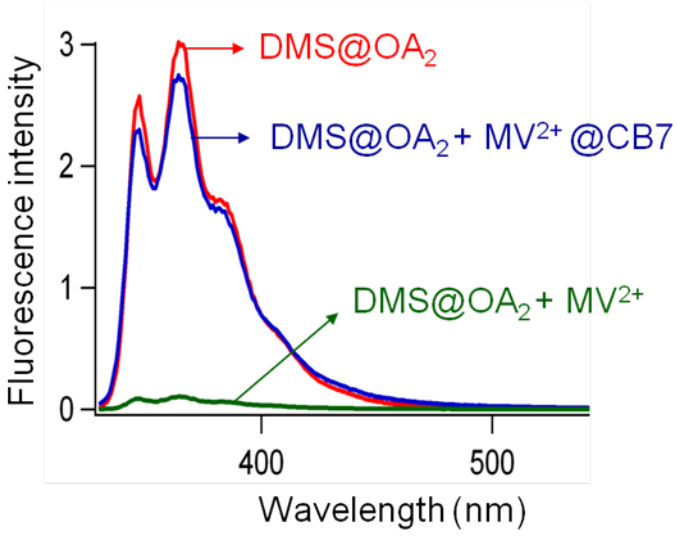

Figure 5.12 Fluorescence spectra of DMS@OA_2, DMS@OA_2 + MV^{2+} and DMS@OA_2 + MV^{2+}@CB7; [DMS]=1.25×10^{-5} M, [OA]=2.5×10^{-5} M, [MV^{2+}]=2.5×10^{-5} M and [CB7]=2.5×10^{-5} M in 10 mM sodium tetraborate buffer; λ_{ex}= 320 nm.

5.2.3 Steady state and time resolved transient absorption study

The next experiments aimed to find out the origin of the quenching. We used laser flash photolysis to record the absorption spectra of the transient intermediates of DMS@OA_2 in the presence and absence of Py^+ and MV^{2+}. Laser pulse of 308 nm was used for excitation. From **Fig 5.5**, the molar extinction co-efficient of DMS@OA_2 (7500 M^{-1} cm^{-1}) was calculated to be higher than OA (530 M^{-1} cm^{-1}) and MV^{2+} (200 M^{-1} cm^{-1}) at 308 nm. As shown in **Fig 5.13** transient absorption spectrum of electron transfer product, radical cation of DMS ($DMS^{+\bullet}$) encapsulated within OA in presence of Py^+ was observed. Transient spectra at 510 nm and > 700 nm were assigned to $DMS^{+\bullet}$ based on the previously reported transient absorption of $DMS^{+\bullet}$.[132,133] An excellent correlation was observed between the bleaching of DMS (observed at 320 nm) and the generation of $DMS^{+\bullet}$ suggesting that the observed transient spectrum was not an artifact (**Fig 5.14**). However N-methyl pyridinium radical ($Py^\bullet$ generated from Py^+) could not be detected as it does not possess detectable absorption between 350 and 800 nm.[139] From the time resolved transient spectrum in **Fig 5.14(i)**, life time of radical cation of DMS within OA was 4.6 μs. **Fig 5.15** presents transient absorption spectra of $DMS^{+\bullet}$ in the absence and presence of oxygen. There was no quenching of transient absorption of $DMS^{+\bullet}$ in oxygen saturated solution. It was observed that in presence of CB7, there was no transient absorption from $DMS^{+\bullet}$ (510 nm, **Fig 5.16(i)**) and no bleaching of the DMS ground state

(320 nm, **Fig 5.16(ii)**). This is consistent with the steady state fluorescence result. CB7 forms complex with Py^+ and thus inhibits electron transfer process.

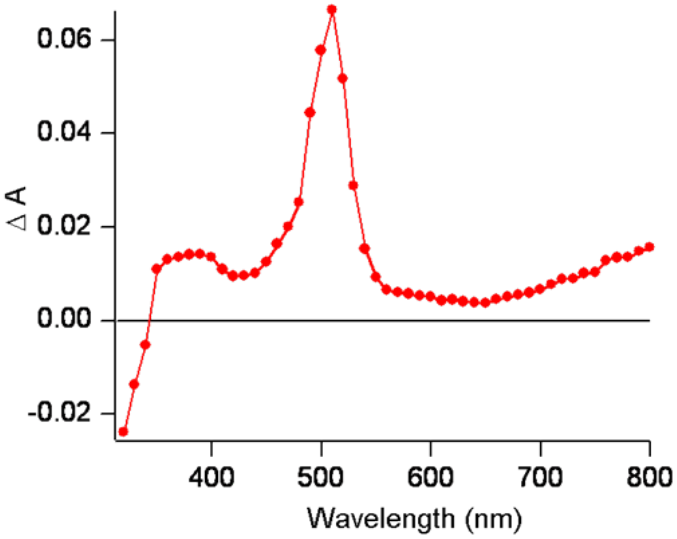

Figure 5.13 Transient absorption spectrum of the cation radical of DMS encapsulated within OA in presence of Py^+; [DMS]=1.25×10^{-5} M, [OA]=2.5×10^{-5} M and [Py^+]=31.25×10^{-5} M in 10 mM sodium tetraborate buffer; Laser pulse: 308 nm, pulse width: 15 ns.

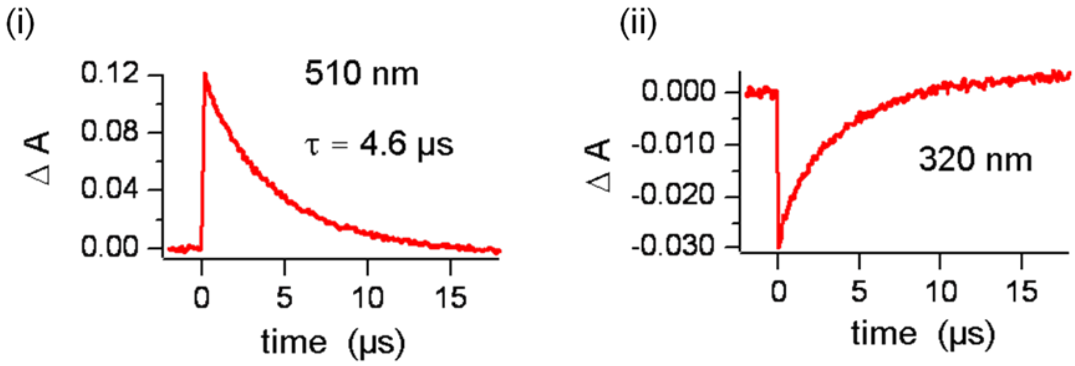

Figure 5.14 Decay traces of (i) cation radical generation from DMS and (ii) bleaching of DMS within OA in presence of Py^+; [DMS]=1.25×10^{-5} M, [OA]=2.5×10^{-5} M and [Py^+]=31.25×10^{-5} M in 10 mM sodium tetraborate buffer; Laser pulse= 308 nm, pulse width= 15 ns.

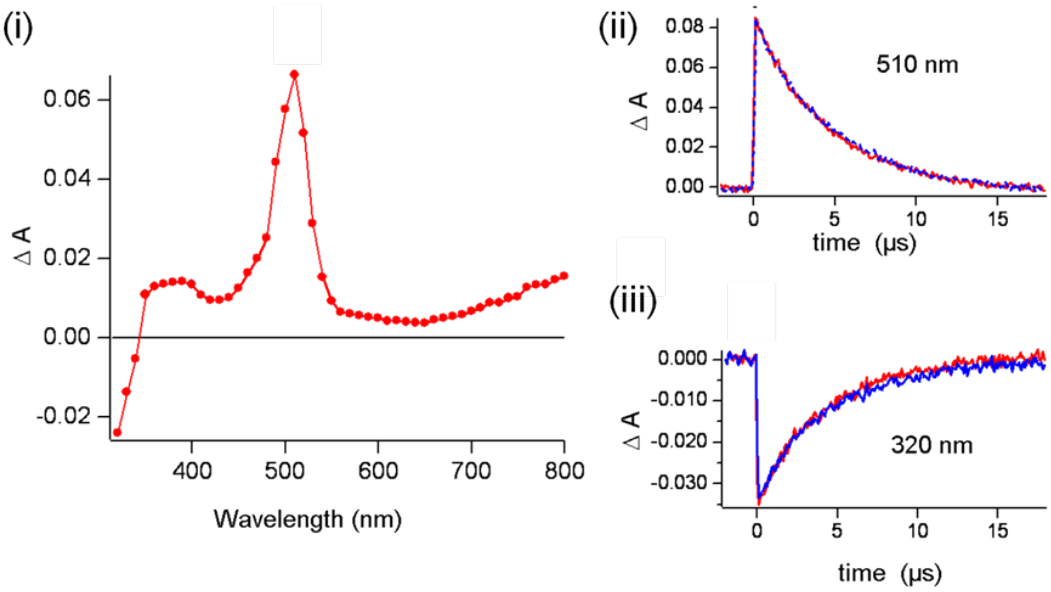

Figure 5.15 (i) Transient absorption spectrum of the cation radical of DMS encapsulated within OA in presence of Py^+; Decay traces of cation radical generation from DMS (ii) and bleaching of DMS (iii) within OA in presence of Py^+ in argon (blue) and oxygen (red) atmosphere; [DMS]=1.25×10^{-5} M, [OA]=2.5×10^{-5} M and [Py^+]=31.25×10^{-5} M in 10 mM sodium tetraborate buffer; Laser pulse= 308 nm, pulse width= 15 ns.

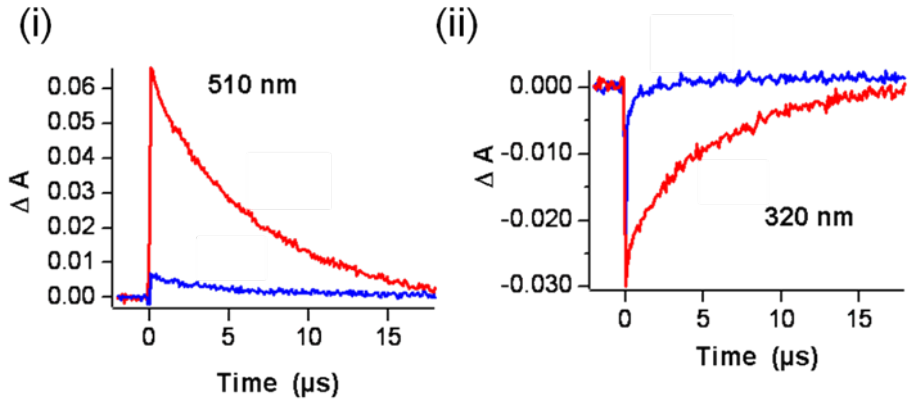

Figure 5.16 Transient absorption decay traces of (i) cation radical formation of DMS and (ii) bleaching of DMS in the absence (red) and presence of CB7 (blue); [DMS]=1.25×10^{-5} M, [OA]=2.5×10^{-5} M, [Py^+]=31.25×10^{-5} M and [CB7]=31.25×10^{-5} M in 10 mM sodium tetraborate buffer; λ_{ex}: 320 nm, Laser pulse= 308 nm, pulse width= 15 ns.

In the case of electron transfer from DMS@OA_2 to MV^{2+}, both the products of electron transfer, namely $DMS^{+\bullet}$ and radical cation of methyl vilogen, $MV^{+\bullet}$ were detected. Most importantly, transient absorption spectrum of radical cation of methyl vilogen provided unequivocal support for electron transfer across the capsular wall. The absorption maximum for $MV^{+\bullet}$ appeared at 400 nm and 600 nm (**Fig 5.17**).[140] **Fig 5.18** shows the bleaching of DMS and the decay traces of $DMS^{+\bullet}$ and $MV^{+\bullet}$. Lifetime of $DMS^{+\bullet}$ after transferring electron to MV^{2+} was less than 20 ns.

Comparison of transient absorption of $DMS^{+\bullet}$ at 0 min and 100 min reveals that even after the complete decay of $DMS^{+\cdot}$, some amount of $MV^{+\cdot}$ was left in solution (**Fig 5.17**). This result indicates that OA itself might act as a donor. This was probed by exciting a solution of OA/MV^{2+} with laser pulse of 308 nm. In this case the observed transient absporption of $MV^{+\cdot}$ (**Fig 5.19**) suggested that OA also acted as electron donor. However, the signal intensity of $MV^{+\cdot}$ was weaker in the absence of DMS. DMS has a much higher absorption co-efficient than OA at 308 nm. This suggested that the direct electron transfer from OA to Py^+ / MV^{2+} played a minor role under this condition.

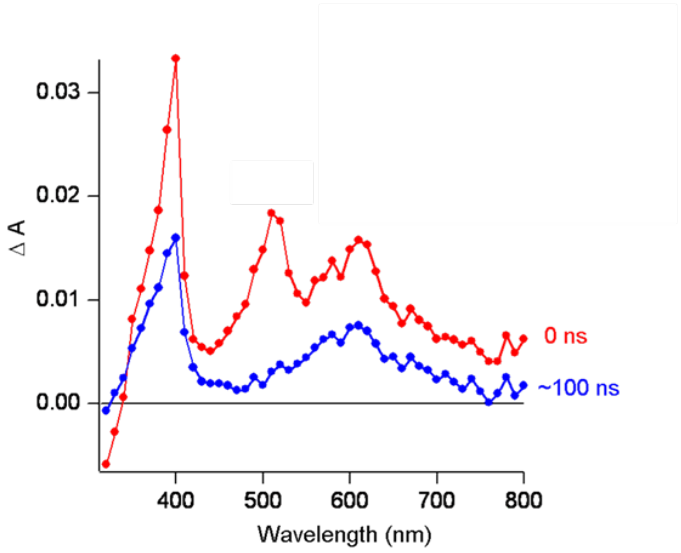

Figure 5.17 Transient absorption spectra of the cation radical of DMS encapsulated within OA in presence of MV^{2+}; [DMS]=1.25×10^{-5} M, [OA]=2.5×10^{-5} M and [MV^{2+}]= 2.5×10^{-5} M in 10 mM sodium tetraborate buffer; Laser pulse= 308 nm, pulse width= 15 ns.

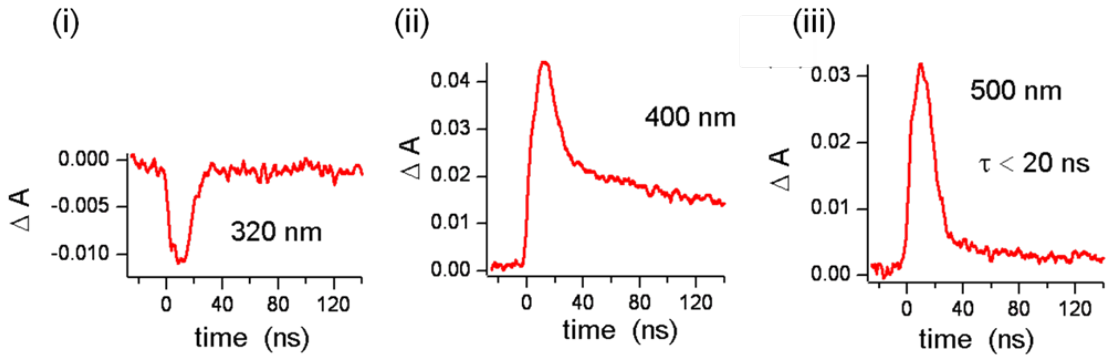

Figure 5.18 Decay traces of (i) bleaching of DMS**,** (ii) cation radical generation from MV^{2+}**,** and (iii) cation radical generation from DMS within OA in presence of MV^{2+}; [DMS]=1.25×10^{-5} M, [OA]=2.5×10^{-5} M and [MV^{2+}]=2.5×10^{-5} M in 10 mM sodium tetraborate buffer; Laser pulse= 308 nm, pulse width= 15 ns.

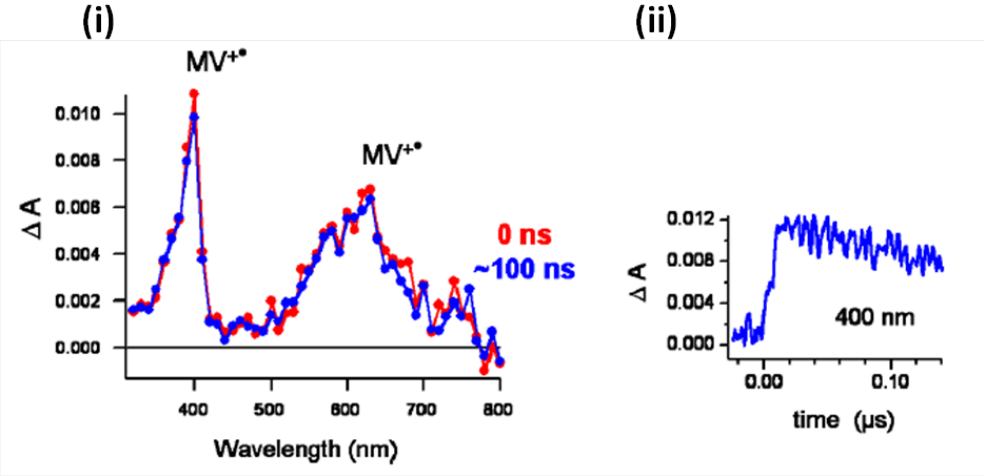

Figure 5.19 (i) Transient absorption spectra and (ii) decay trace of $MV^{+\cdot}$ generated by laser excitation (308 nm, pulse width 15 ns) of argon saturated solutions of OA (2.5×10^{-5} M) in the presence of MV^{2+} (2.5×10^{-5} M); sodium tetraborate buffer solution (10 mM).

The most important phenomenon was noticed regarding the back electron transfer process to regenerate the original states of DMS, Py^{+} and MV^{2+}. It was shown that $DMS^{+\cdot}$ had lifetime 4.6 μs and < 20 ns as generated via electron transfer to Py^{+} and MV^{2+}, respectively. As shown in **Scheme 5.2**, Py^{+} yielded $Py^{\bullet}$ which is neutral radical after accepting one electron. On the other hand MV^{2+} upon acceptance one electron converts to $MV^{+\bullet}$ that is a mono-cationic radical. Positively charged $MV^{+\bullet}$ is still expected to stick to negatively charged OA complex where as $Py^{\bullet}$ would not be associated with the capsule. Due to this difference, back electron transfer rate constants were different in the above two cases. From **Scheme 5.2**, signal from $DMS^{+\bullet}$ is weaker in case of MV^{2+} than that in the case of Py^{+}. This variation is understandable from the rate of back electron transfer. As $MV^{+\bullet}$ was associated to OA complex, back electron transfer from $MV^{+\bullet}$ to $DMS^{+\bullet}$ was

faster occurring in the nanosecond timescale during the laser pulse (laser pulse width 15 ns).

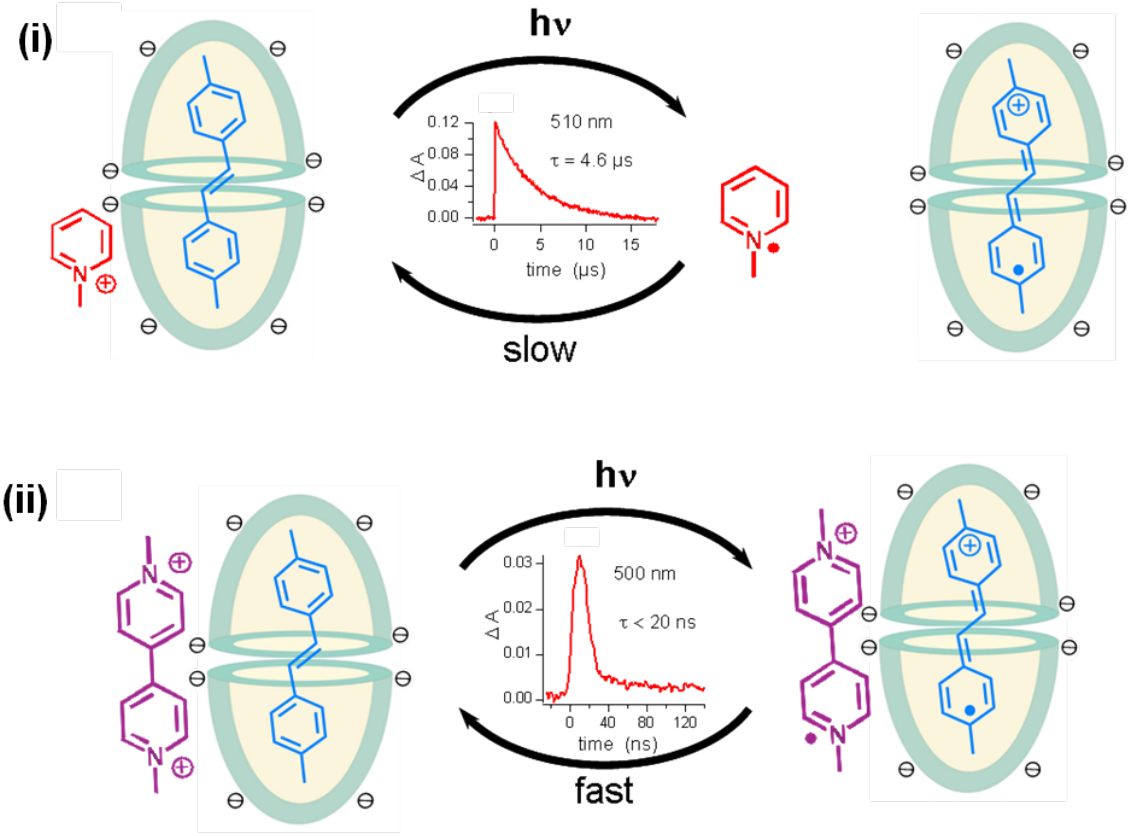

Scheme 5.2 Forward and back electron transfer from DMS@OA_2 to (i) Py^+ and (ii) MV^{2+}.

In our systems, the weak electronic coupling between the excited donor and the acceptor through the capsular wall was compensated by the strong association of the acceptors (Py^+ or MV^{2+}) to the negatively charged external wall of the capsule (that contained the donor) through electrostatic attraction.

5.3 Conclusion

Formation of DMS@OA_2 complex was confirmed by ^{1}H NMR. From 2D DOSY experiment it was revealed that MV^{2+} was strongly associated with the complex due to electrostatic interaction of positively charged MV^{2+} and negatively charged DMS@OA_2 complex. Despite the diffusion constant of Py^+ was not exactly same as DMS@OA_2, it was significantly reduced in presence of the complex indicating that Py^+ interacts with DMS@OA_2 complex. By ^{1}H NMR study it was also noticed that CB7 forms complex with both MV^{2+} and Py^+.

Steady state fluorescence study was performed to yield the S_1 excited state quenching of DMS by MV^{2+} and Py^+. It was presented that the amount of Py^+ needed was more than that of MV^{2+} to do the same extend of quenching. After addition of CB7, the quenched fluorescence was recovered due to the complex formation between CB7 and MV^{2+}/Py^+. Time resolved emission study of DMS@OA_2 with the acceptor (MV^{2+}/Py^+) suggests that the quenching was static in both the cases as life time of the donor was not changed with increasing concentration of the acceptor. The rate constant of quenching could not be measured because of the static nature of the quenching.

The products from the electron transfer process were monitored by flash photolysis transient absorption study. In the case of Py^+, radical cation of DMS ($DMS^{+\bullet}$) was detected at 510 nm and its life time was measured as 4.6 μs. Transient absorption of $Py^{\cdot}$ was not observed as it does not absorb in the window from 350 nm to 800 nm. In case of MV^{2+}, radical cations of both the donor ($DMS^{+\bullet}$; 510 nm) and acceptor ($MV^{+\bullet}$; 400 nm and 600 nm) were detected. This provides a direct proof of electron transfer from DMS

encapsulated within OA to MV^{2+}. The lifetime of $DMS^{+\bullet}$ was less than 20 ns in this case. There was a perfect correlation between the bleaching of DMS and the formation of $DMS^{+\bullet}$. The difference between lifetime of $DMS^{+\bullet}$ in the case of monocation and dication acceptor is an interesting phenomenon. After receiving one electron monocation becomes neutral and thus becomes isolated from the complex. The back electron transfer from $Py^{\bullet}$ to $DMS^{+\bullet}$ was not strong enough and hence made it more stable. On the other hand MV^{2+} generates $MV^{+\bullet}$ after accepting one electron. Being still cationic $MV^{+\bullet}$ associated with negatively charged $DMS@OA_2$ complex that makes the back electron transfer from $MV^{+\bullet}$ to $DMS^{+\bullet}$ favorable. Due to the efficient back electron transfer, lifetime of $DMS^{+\bullet}$ was very short in the case of MV^{2+}.

It was also interesting to see that after addition of CB7, transient absorption of $DMS^{+\bullet}$ completely disappeared. This is because CB7 formed complex with the acceptor and thus inhibited electron transfer process.

The above project concludes that electron transfer occurs between incarcerated and free molecules. The back electron transfer rate in photoinduced electron transfer process was controlled by applying supramolecular concepts.

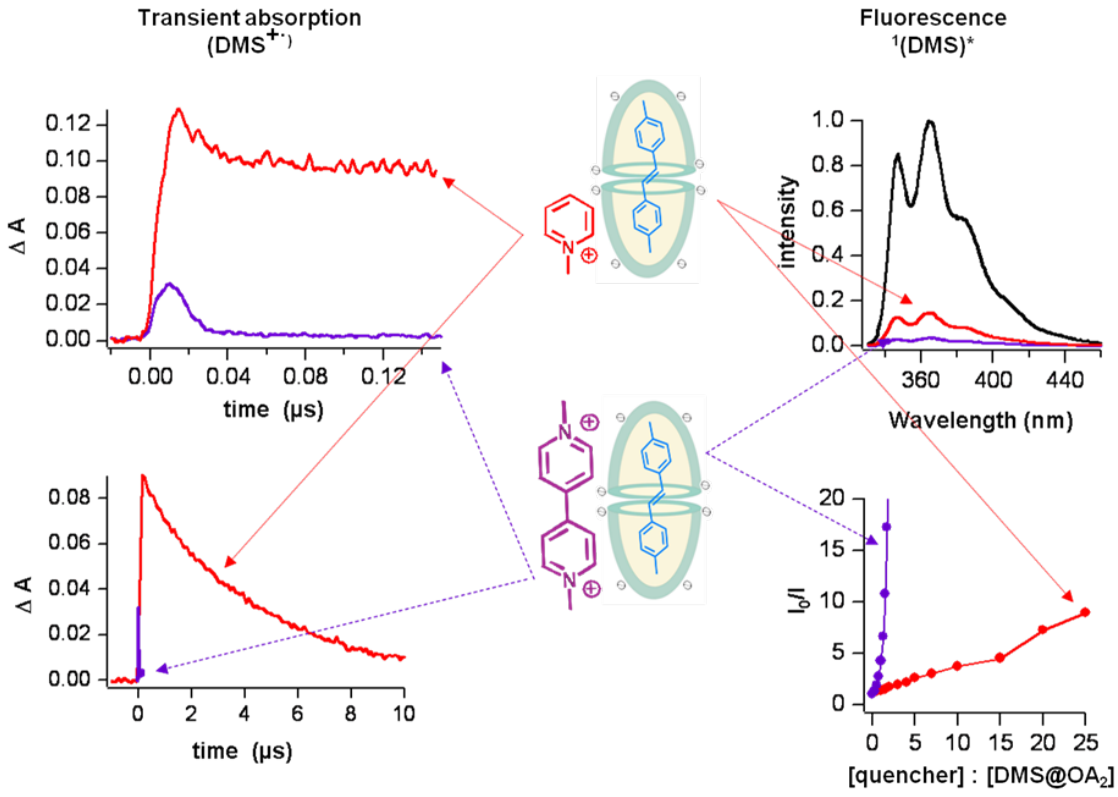

Scheme 5.3 Comparison between electron transfer processes from DMS@OA_2 to Py^+ (top) and MV^{2+} (bottom) by transient absorption of $DMS^{+\bullet}$ and fluorescence of DMS.

5.4 Experimental Section

Materials and Methods:

The hosts octa acid,[40] cucurbit[7]uril[141] were synthesized following published procedures. The guest DMS was synthesized following the published procedure [142] and MV^{2+} was used as received from Sigma-Aldrich/Acros.

Synthesis of Py^+I^-:

Equal molar equivalents of pyridine and methyl iodide were dissolved in acetonitrile and refluxed at 80 ºC for 16 h. The reaction mixture was cooled to room temperature and then

ethyl acetate was added slowly until precipitation was observed. The precipitate was washed with ethyl acetate and dried under vacuum. The purity was checked by ^{1}H NMR.

General protocol for NMR study:

^{1}H NMR studies were carried out on a Bruker 500 MHz NMR spectrometer at 25 °C. 600 μL of a D_2O solution of host OA (1mM OA in 10 mM $Na_2B_4O_7$) was taken in a NMR tube and to this 0.5 equivalent increments of DMS (5 μL of a 60 mM solution in DMSO-d_6) was added. The ^{1}H NMR experiments were carried out after shaking the NMR tube for 5 min after addition. Completion of complexation was monitored by the disappearance of the free host OA signals upon addition of guest. The required amount of quencher solution (Py^+ and MV^{2+}; stock solutions of 30 mM were prepared in D_2O) was added and ^{1}H NMR was recorded after shaking the NMR tube for 5 min. For experiments in the presence of CB7, the calculated amount of CB7 (solid) was added to DMS@OA_2 + quencher solutions and shaken properly before ^{1}H NMR spectra were recorded.

General protocol for fluorescence study:

Fluorescence emission spectra were recorded on a FS920CDT Edinburgh steady-state fluorimeter and the lifetime measurements on FL900CDT fluorescence lifetime spectrometer. Capsular assemblies (0.5 mM) were made by adding 5 μL of 60 mM solution of DMS (in DMSO solution) to 0.6 mL of 1 mM OA in 10 mM borate buffer in H_2O. It was diluted appropriately with 10 mM buffer solution to have the required concentration of host/guest complex. Calculated amounts of quencher solution (stock solutions in H_2O) were added and mixed thoroughly and then the fluorescence spectra were recorded. The required amount of CB7 (stock solution was prepared in H_2O) was added to the solution (host/guest + quencher) and fluorescence spectra were recorded.

General protocol for transient absorption study:

Laser flash photolysis experiments employed the pulses from a Lambda Physik Lextra 50 excimer laser (308 nm, pulse width 15 ns) and a home built system.[143]

CHAPTER 6

Photoinduced Electron Transfer from Coumarin Dyes to Methyl Viologen and TiO_2 across a Molecular Wall

6.1 Overview

Photoinduced electron transfer plays an important role in a number of fundamental chemical and biological transformations, and commercial applications including capture and storage of solar energy.[144-147] Despite the ease of synthesis or commercial availability of different organic dyes, their use as electron donors/acceptors has not been fully explored because of their tendency to aggregate and photodegrade upon exposure to light.[141,148-151] In the previous chapter (**Chapter 5**) we have shown the feasibility of electron transfer between two molecules; one trapped within an organic capsule while the other is free in solution. The observations suggested that the recombination rates in photoinduced electron transfer processes can be controlled by applying supramolecular concepts. Despite elucidating a number of key features regarding photoinduced electron transfer in supramolecular assembly, some other relevant facts, such as electron transfer and recombination rates etc. remained yet to be measured. Electron transfer occurs on the picosecond time scale or faster.[152] The nanosecond laser pulse (detailed in **Chapter 5**) did not allow us to measure the electron transfer rate constant. To fully elucidate the electron transfer process in the supramolecular system we switched from nanosecond to femtosecond laser excitation. Femtosecond transient absorption measurements enabled us to monitor both the electron transfer and recombination rates from incarcerated donor to free acceptor. We also carried out the similar experiments on the electron transfer process from the same donor and acceptor in solution. Comparison of the electron transfer process between the solution and the supramolecular assembly demonstrated the advantage of using a host molecule in between the donor and acceptor.

The femtosecond laser instrument that we used had a limitation of the excitation wavelength at 390 nm or more. Hence our previously used donor molecule, 4,4' dimethyl stilbene (**Chapter 5**) could not be used in this condition as it absorbs < 390 nm (see **Fig 5.5** in **Chapter 5**). Instead we chose coumarin dyes (coumarin 153, coumarin 480 and coumarin 1, **Scheme 6.1**) as the donor in our current study as they absorb at 390 nm. 4,4' dimethyl viologen (MV^{2+}, **Scheme 6.1**) was used as acceptor. The donor-acceptor pairs were selected based on the well-established literature reports defining the exothermic photoinduced electron transfer from coumarin to MV^{2+} in solution.[153] It has also been reported that the selected coumarin derivatives form strong 2:1 (H:G) complex with octa acid (OA, **Scheme 6.1**). Moreover there is an essential requirement for electron transfer process: The total energy for oxidation potential of the donor and reduction potential of the acceptor should be lower than the energy for excitation.[6] Oxidation potentials of C153, C1 and C480 are 0.89 V, 1.09 V and 0.72 V, respectively; and reduction potential of MV^{2+} is −0.69 V; S_1 energies of the three coumarins are >2.7 eV and S_1 energy of MV^{2+} is ~4 eV.[153] Based on the oxidation potentials and the excited state (S_1) energies of coumarins, reduction potential and the excited state (S_1) energy of MV^{2+}, it was expected that the fluorescence of the coumarins would be quenched by MV^{2+} via electron transfer and not by singlet–singlet energy transfer.[154] Another host cucurbit[7]uril (CB7) (**Scheme 6.1**) was used as it forms good complex with both the acceptors, MV^{2+}. The idea behind using CB7 was that it would dissociate the acceptor from coumarin@OA_2 complex and thus restrict the electron transfer process. This strategy was used as an indirect proof of the electron transfer process from coumarin to MV^{2+} across OA wall.

After studying the electron transfer process from encapsulated donor to free accepter in solution, we were interested to explore the electron injection from incarcerated donor to the semiconductor. We have chosen TiO_2 as semiconductor as it is well known semiconductor used in dye sensitized solar cells.[146] There are some additional advantages of OA over other previously used molecular hosts such as cyclodextrins, cucurbiturils, and hemicarcerands on TiO_2 surface.[155] For example, OA has multiple COOH groups on its periphery and they can interact with the TiO_2 surface more strongly than the other hosts having OH (cyclodextrins) and C═O (cucurbiturils) functionalities. We studied the adsorption of C153@OA_2 complex on TiO_2 surface and the electron transfer from encapsulated C153 to TiO_2 semiconductor.

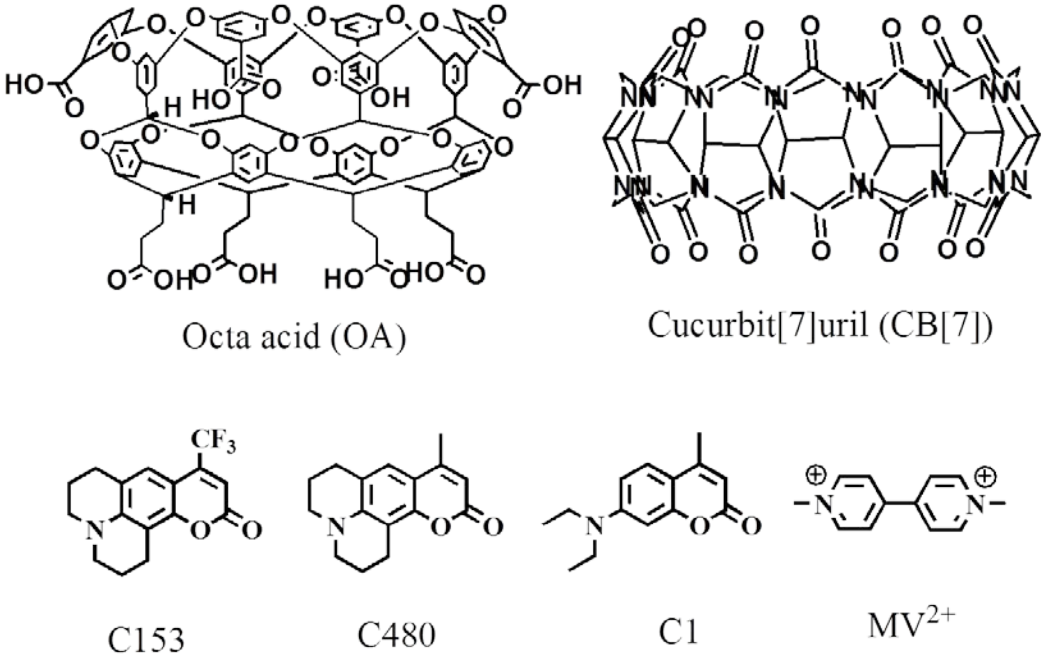

Scheme 6.1 Structure of host and guest molecules

6.2 Results and Discussion

6.2.1 ^{1}H NMR and 2D- DOSY experiment on the systems

We performed ^{1}H NMR study to confirm the complex formation of coumarin with OA. As shown in **Fig 6.1,** the upfield shift of C153 signals and the disappearance of uncomplexed OA signals indicated the formation of C153@OA_2 complex.

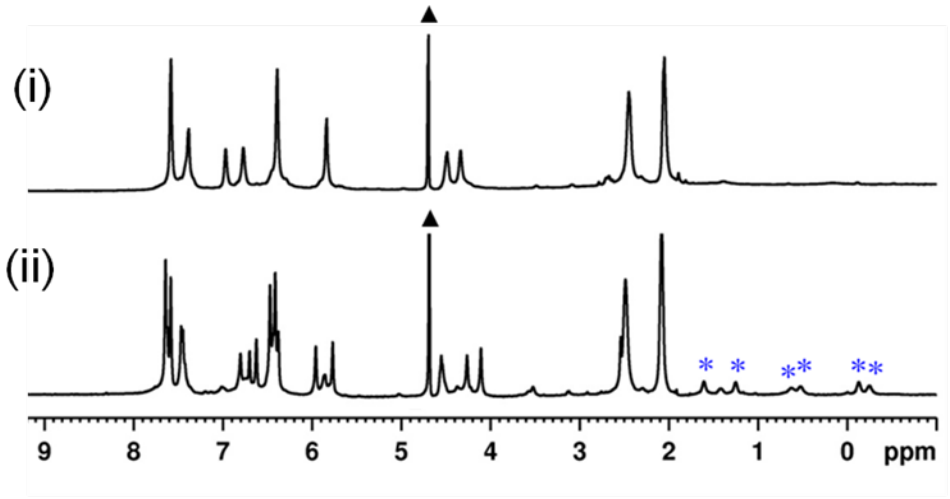

Figure 6.1 ^{1}H NMR (500 MHz, D_2O) spectra of (i) OA and (ii) C153@OA_2; [C153]= 0.5 mM and [OA]=1 mM in 10 mM sodium tetraborate buffer; "*", and "▲"represent bound C153 protons and residual proton signal in D_2O respectively.

As mentioned in the previous chapters, OA complex was prepared in basic medium (pH ~ 9). In the basic condition –COOH groups are converted to $–COO^-$ groups and hold positively charged MV^{2+} on the exterior walls of OA capsule through Columbic interaction. To probe the location of MV^{2+} in the presence of C153@OA_2,^{1}H NMR spectra of a solution containing the capsule with MV^{2+} was recorded (**Fig 6.2**). ^{1}H NMR signals of MV^{2+} were unaffected in presence of C153@OA_2 indicating that MV^{2+} remained outside the capsule. MV^{2+} and C153@OA_2 were found to have identical

diffusion constants which imply the strong association of the two (**Fig 6.3**). Based on the above data it was concluded that the donor C153 was inside the capsule and the acceptor MV^{2+} was held on the exterior of the capsule through electrostatic interaction between the cationic MV^{2+} and the anionic C153@OA_2 capsule. After addition of one equivalent CB7 (with respect of MV^{2+}), ^1H NMR signals of MV^{2+} were upfield shifted indicating that MV^{2+} formed complex with CB7 (**Fig 6.4**).

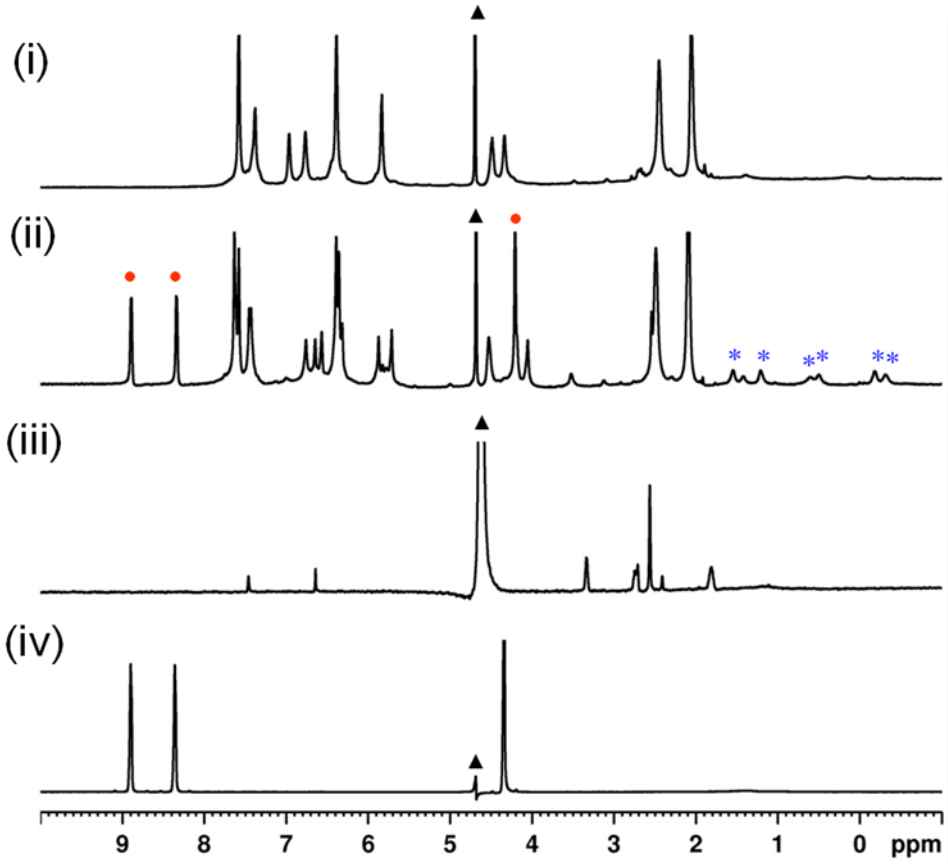

Figure 6.2 ^1H NMR (500 MHz, D_2O) spectra of (i) OA, (ii) C153@OA_2 + MV^{2+}, (iii) C153 and (iv) MV^{2+}; [C153]= 0.5 mM, [OA]=1 mM, [MV^{2+}]= 1 mM and in 10 mM sodium tetraborate buffer; "∗", "•"and "▲"represent bound C153 protons, MV^{2+} protons and residual proton signal in D_2O respectively.

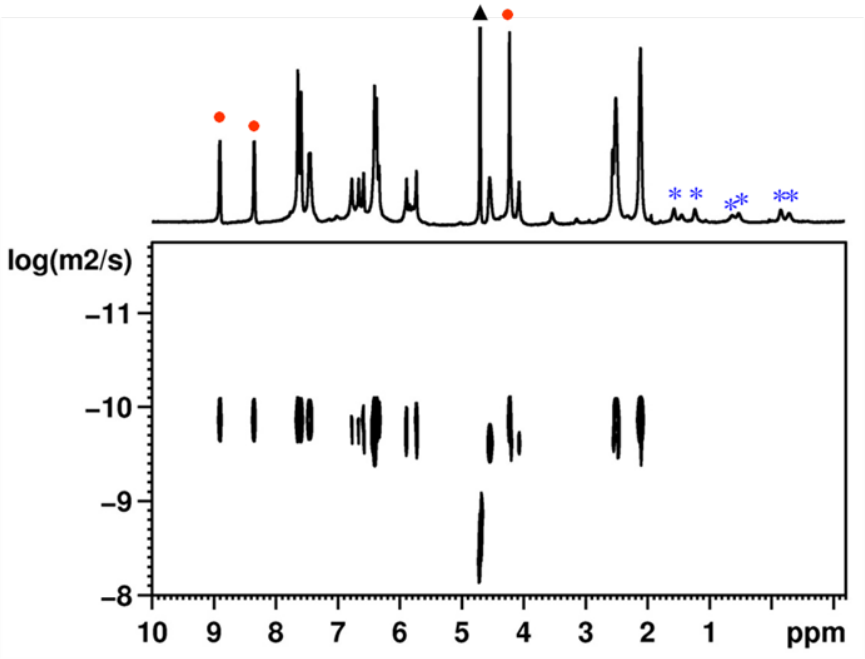

Figure 6.3 2D DOSY (500 MHz, D_2O) spectra of C153@OA_2 + MV^{2+}; [C153]= 0.5 mM, [OA]=1 mM, [MV^{2+}]= 1 mM; "∗" and "●" represent bound C153 and MV^{2+} proton signals, diffusion constant of C153@OA_2 and MV^{2+} are 1.19×10^{-10} m^2/s and 1.2×10^{-10} m^2/s respectively.

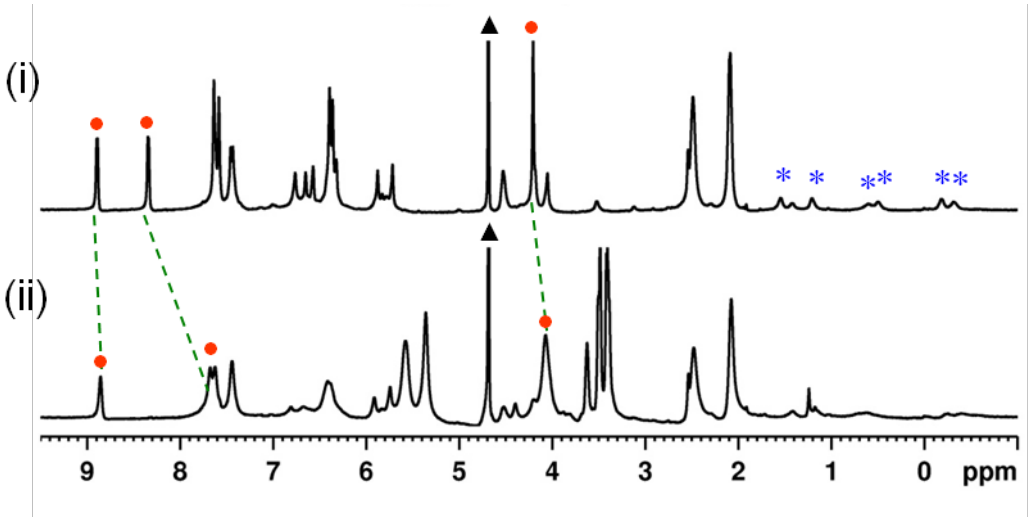

Figure 6.4 ^1H NMR (500 MHz, D_2O) spectra of (i) C153@OA_2 + $MV^{2+}$and (ii) C153@OA_2 + MV^{2+}@CB7; [C153]= 0.5 mM, [OA]=1 mM, [MV^{2+}]= 1 mM and [CB7]= 1 mM in 10 mM sodium tetraborate buffer; "∗", "●"and "▲"represent bound C153 protons, MV^{2+} protons and residual proton signal in D_2O respectively.

6.2.2 Photophysical study

We performed emission study to probe the interaction between OA-trapped photoexcited C153 and free MV^{2+}. Coumarin has strong fluorescence. After transferring one electron to the accepter, coumarin generates radical cation ($coumarin^{+\cdot}$) which is not emissive. Thus electron transfer from coumarin can be monitored by the quenching of coumarin fluorescence. It is also important to assure that coumarin was excited selectively in presence of acceptor otherwise competitive absorption might be the partial reason for the quenching of coumarin fluorescence by the acceptor. UV-Visible spectra of coumarin@OA_2 complex and MV^{2+} are shown in **Fig 6.5** to **Fig 6.7**. The excitation wavelengths for the fluorescence quenching study of C153@OA_2, C480@OA_2 and C1@OA_2 were chosen at 420 nm, 380 nm and 350 nm, respectively. Coumarin@OA_2 can selectively be excited at those wavelengths without any interference of MV^{2+} absorption.

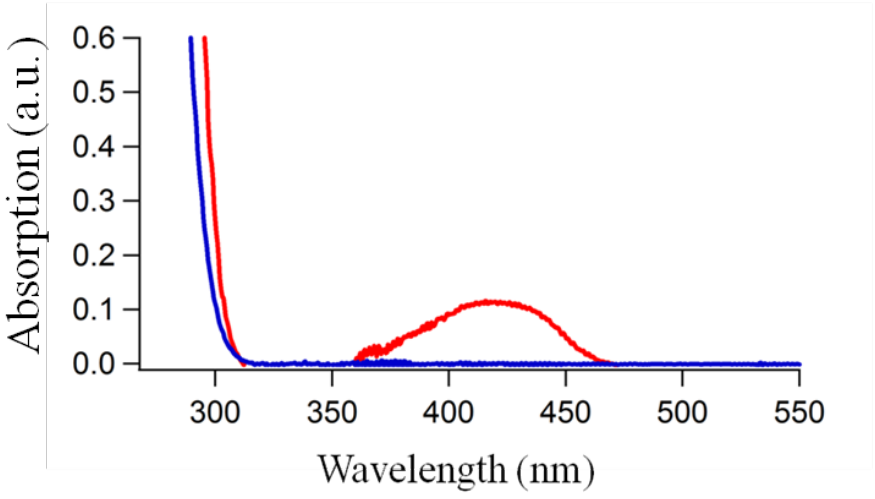

Figure 6.5 UV-visible spectra of C153@OA_2 (red) and MV^{2+} (blue); [C153] = 1.5×10^{-5} M, [OA] = 1×10^{-4} M and [MV^{2+}] = 1.5×10^{-5} M to 7.5×10^{-5} M in 10 mM sodium tetraborate buffer.

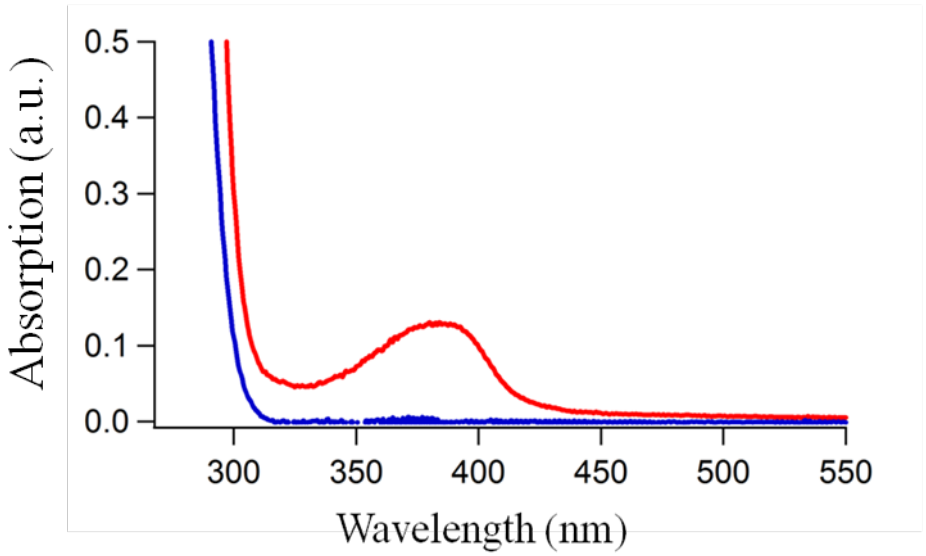

Figure 6.6 UV-visible spectra of C480@OA_2 (red) and MV^{2+} (blue); [C480] = 2×10^{-5} M, [OA] = 1×10^{-4} M, and [MV^{2+}] = 1.5×10^{-5} M to 5×10^{-5} M in 10 mM sodium tetraborate buffer.

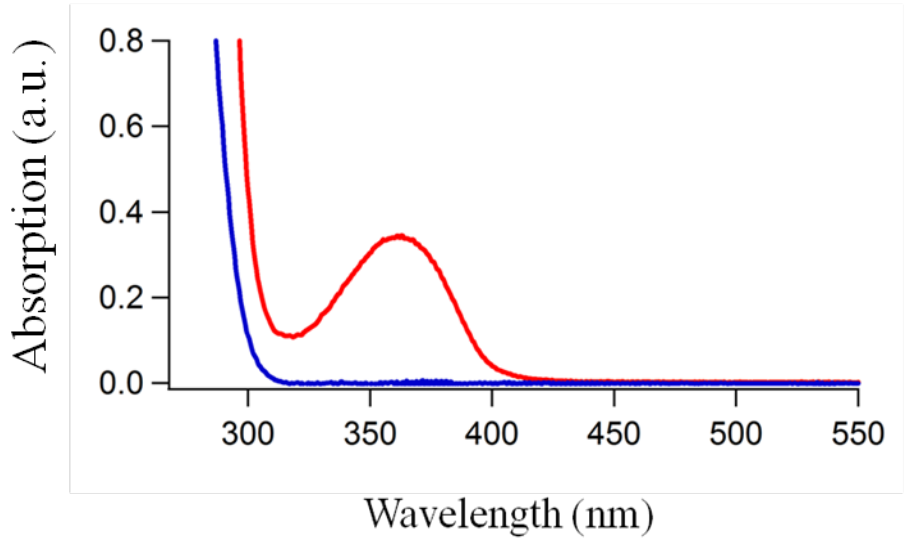

Figure 6.7 UV-visible spectra of C480@OA_2 (red) and MV^{2+} (blue); [C1] = 1.2×10^{-5} M, [OA] = 1.5×10^{-4} M, and [MV^{2+}] = 0 M to 5.8×10^{-5} M in 10 mM sodium tetraborate buffer.

As illustrated in **Fig 6.8**, the increasing concentration of MV^{2+} gradually quenched the fluorescence spectra of C153@OA_2. Lifetime of C153@OA_2 was not changed in presence of MV^{2+} (**Fig 6.9** (left)). The Stern–Volmer plots, I_o/I and τ_o/τ vs. MV^{2+} concentration (**Fig 6.9**, right) shows that it was a static quenching as dynamic quenching would have resulted in overlapping the Stern–Volmer plots based on steady state fluorescence intensity and lifetime measurements. Measurement of the quenching rate constant was not possible due to the static nature of the quenching. A second host CB7 (**Scheme 6.1**) was introduced to explore whether the quenching process would be affected by moving the acceptor away from the capsular wall. From the NMR study it was observed that MV^{2+} formed strong complex with CB7 (**Fig 6.4**). Upon addition of CB7, the fluorescence of C153@OA_2 was recovered (**Fig 6.10**) indicating that the acceptor must be next to the capsule for efficient quenching.

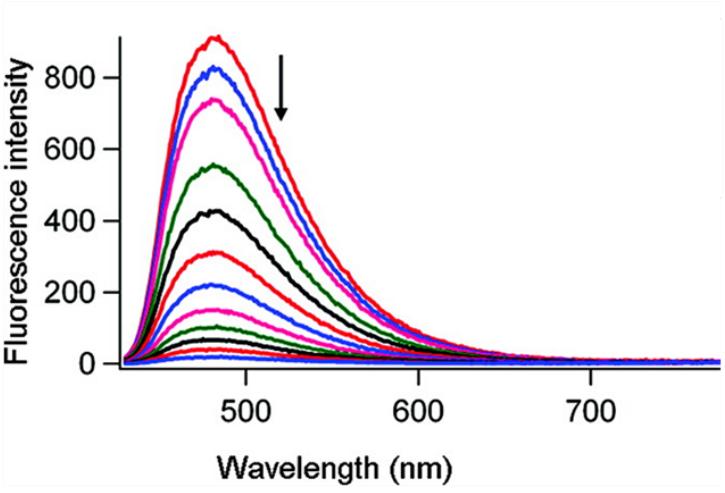

Figure 6.8 Fluorescence titration spectra of C153@OA_2 with MV^{2+}; λ_{ex} = 420 nm; [C153] = 1.5×10^{-5} M, [OA] = 1×10^{-4} M and [MV^{2+}] = 1.5×10^{-5} M to 7.5×10^{-5} M in 10 mM sodium tetraborate buffer.

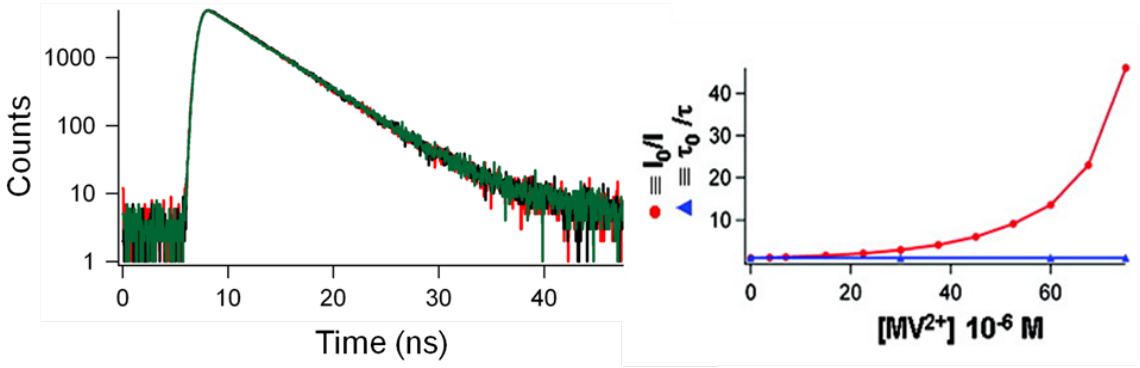

Figure 6.9 Fluorescence lifetime titration spectra of C153@OA_2 with MV^{2+} (left) and Stern-volmer plot of steady state and time resolved quenching experiment of C153@OA_2 with MV^{2+} (right), λ_{ex} = 420 nm; λ_{em} = 480 nm; [C153] = 1.5 × 10^{-5} M, [OA] = 1 × 10^{-4} M and $[MV^{2+}]$ = 1.5 × 10^{-5} M to 7.5 × 10^{-5} M in 10 mM sodium tetraborate buffer.

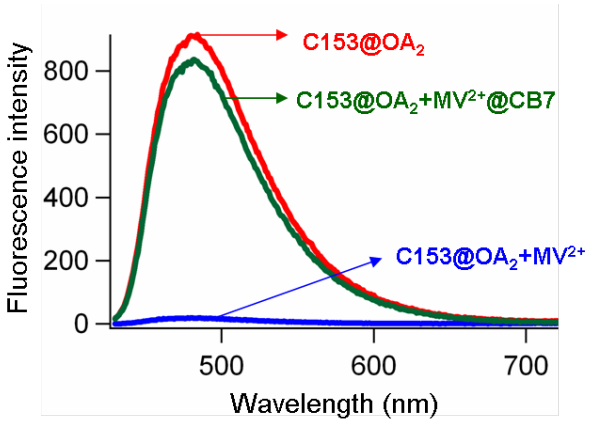

Figure 6.10 Fluorescence spectra of C153@OA_2 in presence of MV^{2+} and MV^{2+}@CB7, λ_{ex} = 420 nm; [C153] = 1.5 × 10^{-5} M, [OA] = 1 × 10^{-4} M and $[MV^{2+}]$ = 7.5 × 10^{-5} M and [CB7] = 7.5 × 10^{-5} M in 10 mM sodium tetraborate buffer.

Fluorescence quenching experiments were carried out with other two coumarin derivatives (C480 and C1, **Scheme 6.1**) encapsulated within OA capsule with MV^{2+}. From the steady state fluorescence titration, it was observed that fluorescence of coumarin dyes were quenched in presence of MV^{2+} (**Fig 6.11** and **Fig 6.14**) in both the cases. Time resolved titrations of C480@OA_2 and C1@OA_2 with MV^{2+} confirmed the

static nature of the quenching (**Fig 6.12** and **Fig 6.15**). After addition of CB7, quenched fluorescence was recovered (**Fig 6.13** and **Fig 6.16**) suggesting that quenching was inhibited in presence of two molecular walls.

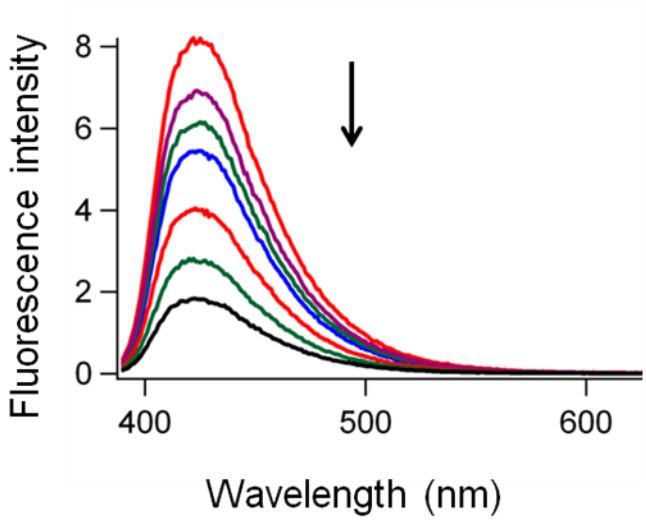

Figure 6.11 Fluorescence titration spectra of C480@OA_2 with $MV^{2+;}$ λ_{ex} = 380 nm; [C480] = 2×10^{-5} M, [OA] = 1×10^{-4} M, and [MV^{2+}] = 1.5×10^{-5} M to 5×10^{-5} M in 10 mM sodium tetraborate buffer.

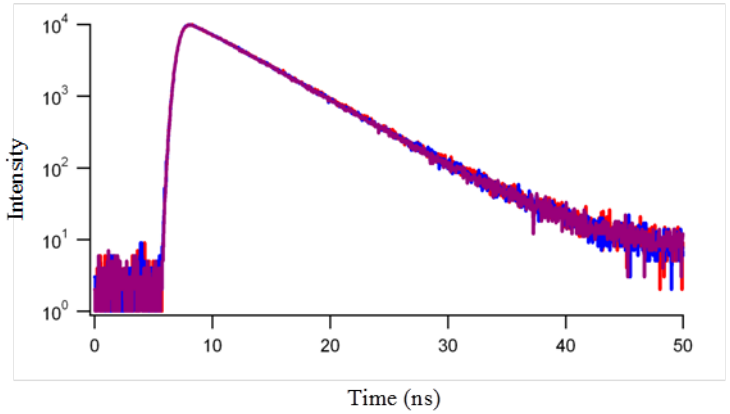

Figure 6.12 Fluorescence lifetime titration spectra of C480@OA_2 with MV^{2+}; λ_{ex} = 380 nm, λ_{ex} = 430 nm; [C480] = 2×10^{-5} M, [OA] = 1×10^{-4} M and [MV^{2+}] = 1.5×10^{-5} M to 5×10^{-5} M sodium tetraborate buffer.

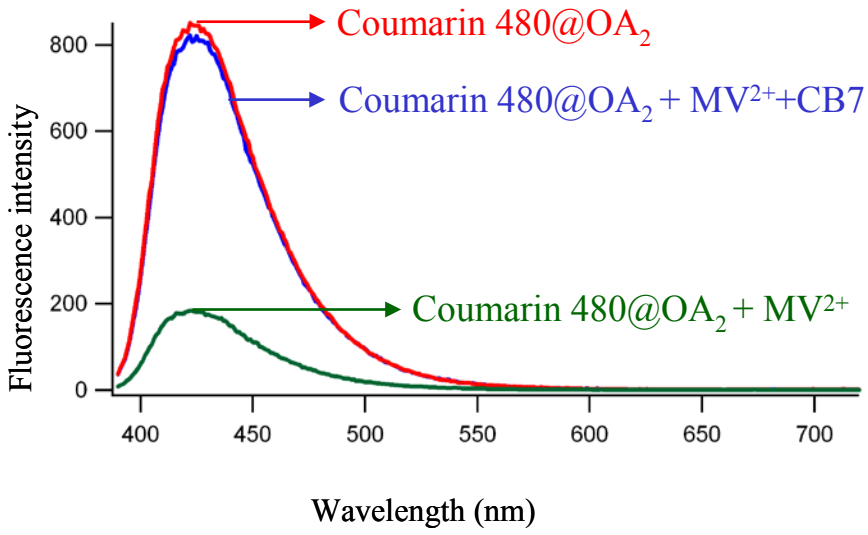

Figure 6.13 Fluorescence lifetime titration spectra of C480@OA_2 in presence of MV^{2+} and MV^{2+}@CB7; λ_{ex} = 380 nm; [C480] = 2×10^{-5} M, [OA] = 1×10^{-4} M, [MV^{2+}] = 1.5×10^{-5} M to 5×10^{-5} M and [CB7] = 5×10^{-5} M in 10 mM sodium tetraborate buffer.

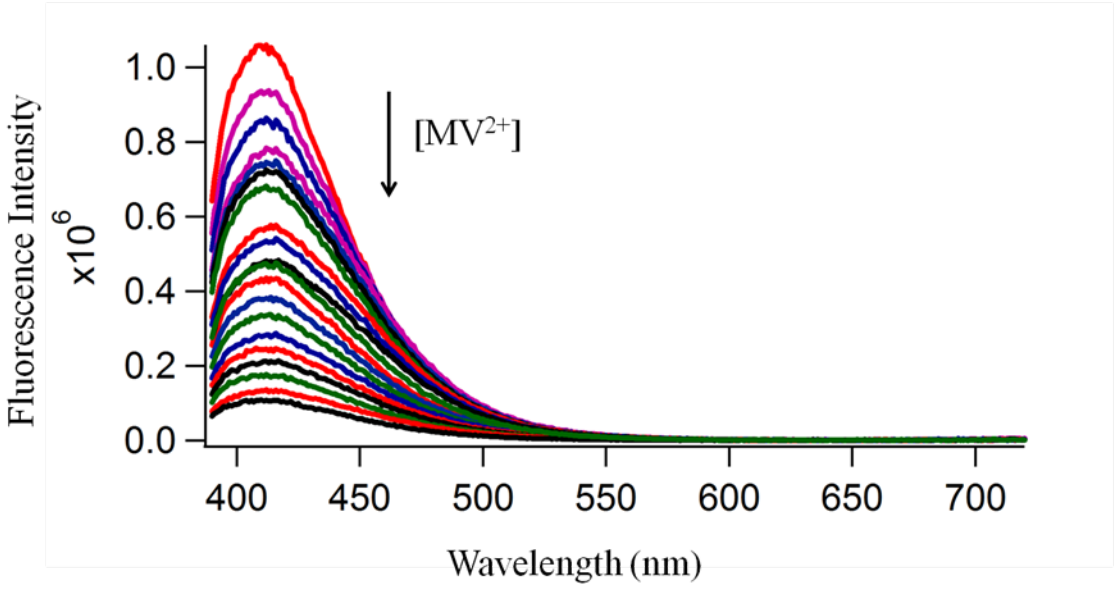

Figure 6.14 Fluorescence titration spectra of C1@OA_2 with $MV^{2+;}$ λ_{ex} = 350 nm; [C1] = 1.2×10^{-5} M, [OA] = 1.5×10^{-4} M, and [MV^{2+}] = 0 M to 5.8×10^{-5} M in 10 mM sodium tetraborate buffer.

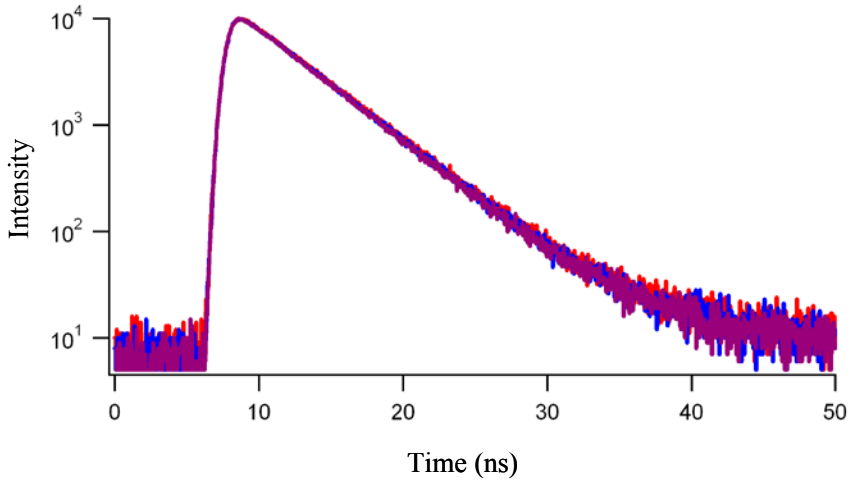

Figure 6.15 Fluorescence lifetime titration spectra of C1@OA_2 with MV^{2+}; λ_{ex} = 350 nm, λ_{em} = 410 nm; [C1] = 1.2×10^{-5} M, [OA] = 1.5×10^{-4} M and [MV^{2+}] = 0 to 5.8×10^{-5} M sodium tetraborate buffer.

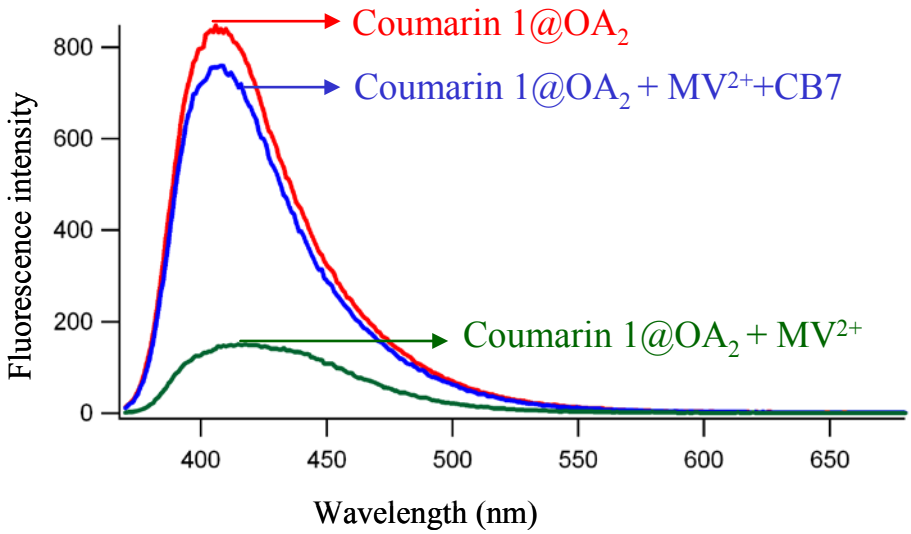

Figure 6.16 Fluorescence titration spectra of C1@OA_2 with $MV^{2+;}$ λ_{ex} = 350 nm; [C1] = 1.2×10^{-5} M, [OA] = 1.5×10^{-4} M, [MV^{2+}] = 5×10^{-5} M and [CB7] = 5×10^{-5} M in 10 mM sodium tetraborate buffer.

From the above study it was concluded that fluorescence quenching of an encapsulated dye is possible when the quencher is associated with the capsule. Quenching is inhibited when both the donor and the acceptor are included within organic hosts.

6.2.3 Steady state and time resolved transient absorption study

Our next experiments aimed to find out the origin of the quenching of coumarin@OA_2 with MV^{2+}. The origin of the quenching became clear from the absorption spectra of the transient intermediates of C153@OA_2 in the presence of MV^{2+} recorded by femtosecond pump-probe spectroscopy. Transient absorption in the range from 550 to 700 nm is shown in **Fig 6.17(i)**, which was assigned to the radical cation of MV^{2+} ($MV^{+\cdot}$) based on the previously reported transient absorption spectrum of $MV^{+\cdot}$. [156] The formation of $MV^{+\cdot}$ resulting from the electron injection from C153 to MV^{2+} provided unequivocal support of electron transfer across the capsular wall (**Scheme 6.2**). At the first few ps of the experiment, intensity of the transient absorption of $MV^{+\cdot}$ increased indicating the accumulation of $MV^{+\cdot}$ (**Fig 6.17(i)**). The laser induced fluorescence of C153 was consistent with the formation of $MV^{+\cdot}$ as a result of electron transfer (**Fig 6.17(i)**). We were also able to monitor the decay of $MV^{+\cdot}$ during the charge recombination process (**Fig 6.17(i)**).

The lifetime of the resulting charge transfer state was measured after selectively probing the $MV^{+\cdot}$. **Fig 6.17(ii)** shows the decay $MV^{+\cdot}$ due to recombination process. The recombination kinetics was very well reproduced by a single exponential with τ = 724 ps ± 38. An excellent correlation was observed between the time constant of the bleaching

of C153 excited state (τ = 18 ps ± 2) and formation of $MV^{+\cdot}$ (τ = 20 ps ± 0.8, see the inset of **Fig 6.17(ii)**). Interestingly, encapsulation within the host cavity abruptly slowed down the recombination rate and extends the lifetime of charge transfer species.

To rule out the possibility of OA acting as the electron donor in the above described experiment, we performed the transient absorption measurements exciting *trans*-dehydrosterone@OA_2 capsuleplex with 390 nm in the presence of MV^{2+}. *Trans*-dehydrosterone was reported to form a strong 2:1 (host:guest) complex with OA and it does not absorb at 390 nm.[40] The absence of any transient absorption in this case (**Fig 6.18**) confirmed that the afformentioned electron transfer from C153 to MV^{2+} through OA wall was free from interference of OA.

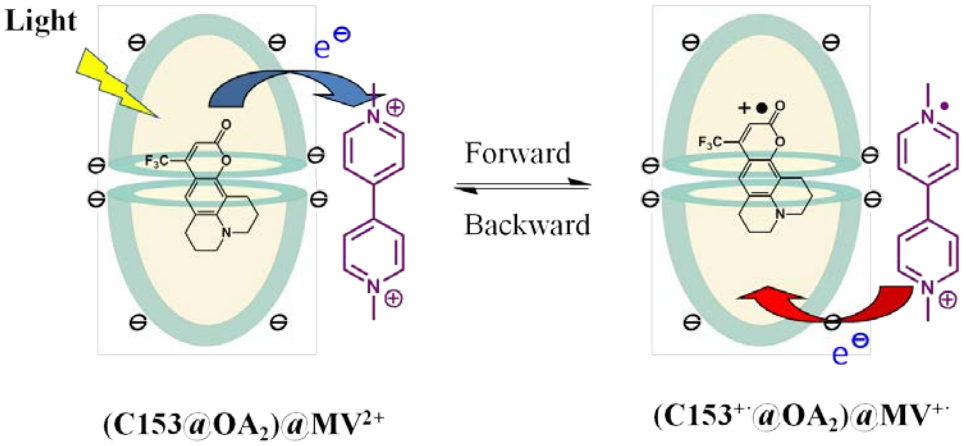

Scheme 6.2 Schematic representation of forard and backward electron transfer from C153 to MV^{2+} through OA wall.

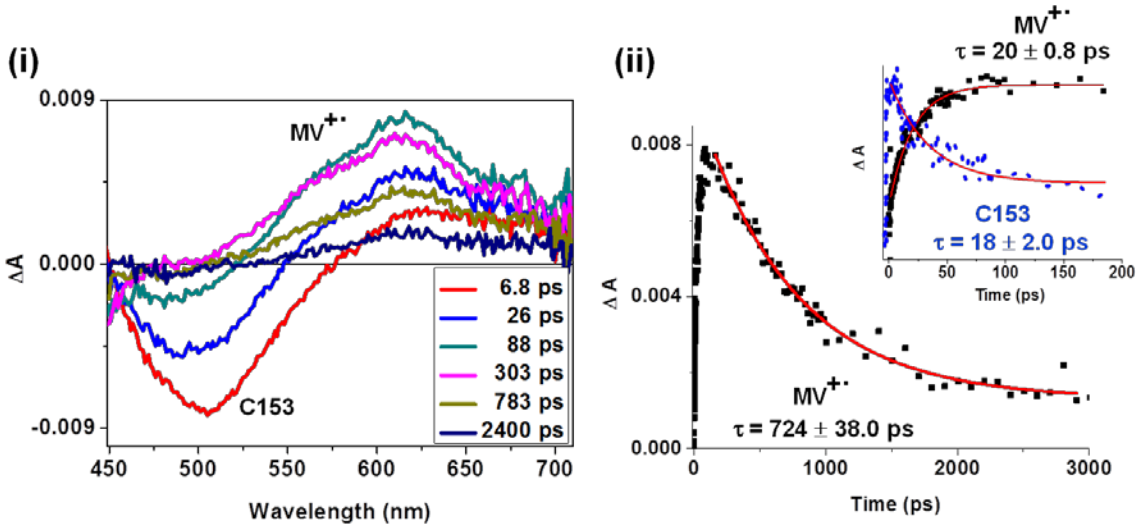

Figure 6.17 (i) Transient absorption spectra of the methyl viologen radical cation ($MV^{+\cdot}$) upon electron transfer from C153@OA_2 and (ii) TR-TA kinetics of $MV^{+\cdot}$, inset: rise of $MV^{+\cdot}$ (black) and Laser induced fluorescence dynamics of the photoexcited C153 (blue); rise and decay of $MV^{+\cdot}$ and bleaching of C153 were monitored at 625 nm and 500 nm, respectively; $[MV^{2+}] = 6\times10^{-4}$ M, $[C153] = 6\times10^{-5}$ M and $[OA] = 4\times10^{-4}$ M in 10 mM sodium tetraborate buffer; Laser pulse = 390 nm, pulse width = 150 fs.

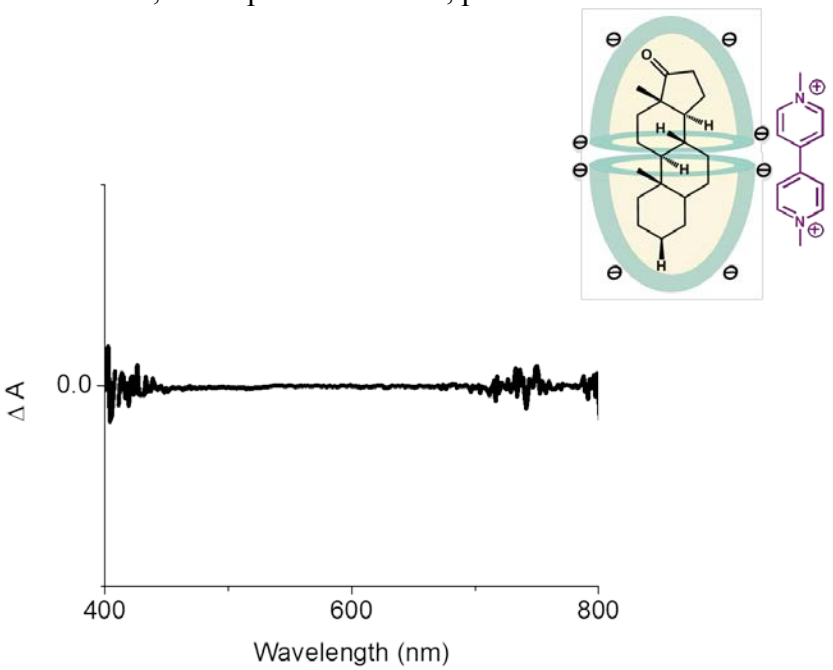

Figure 6.18 Lack of any transient signal of *trans*-dehydroandrosterone@OA_2 in presence of MV^{2+}; $[MV^{2+}] = 1\times10^{-3}$ M, [*trans*-dehydroandrosterone] = 5×10^{-5} M and $[OA] = 1\times10^{-4}$ M in 10 mM sodium tetraborate buffer; Laser pulse = 390 nm, pulse width = 150 fs. This shows that the OA capsule itself is not causing any electron transfer to MV^{2+}.

To compare the electron transfer between electron donor and free acceptor we carried out femtosecond transient absorption measurements exciting C153 in the presence of MV^{2+} in 30% acetonitrile in water. Fluorescence of C153 wsa quenched in presence of MV^{2+} (**Fig 6.19**). Transient spectra of the C153 excited state due to electron transfer from C153 to MV^{2+} in solution are shown in **Fig 6.20 (i)**. The time constant of the electron transfer, τ = 630 ps ± 50, was obtained from the transient spectra of the C153 excited state shown in **Fig 6.20 (ii)** at λ_{obs} = 625 nm. Due to its completely diffusion controlled nature, the electron transfer rate in solution was slower and almost identical to the recombination rate. The charged transfer intermediate ($MV^{+\cdot}$) was not sufficiently accumulated in solution and hence the absence of $MV^{+\cdot}$ absorption in the femtosecond transient spectra (**Fig 6.20 (i)**). On the other hand due to Coulombic attraction between negatively charged C153@OA_2 and positively charged MV^{2+}, the donor and acceptor associate tightly, even through the OA wall, which accelerated the electron transfer process by a factor ~ 300.

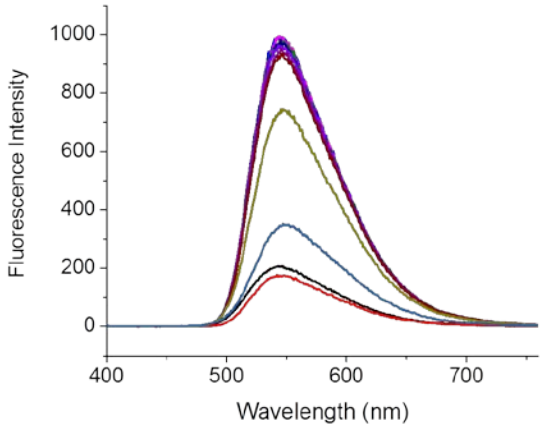

Fig 6.19 Fluorescence titration spectra of C153 with MV^{2+} in 30% acetonitrile in water; λ_{ex} = 420 nm; [C153] = 5×10^{-4} M and [MV^{2+}] = 0 to 7×10^{-3} M.

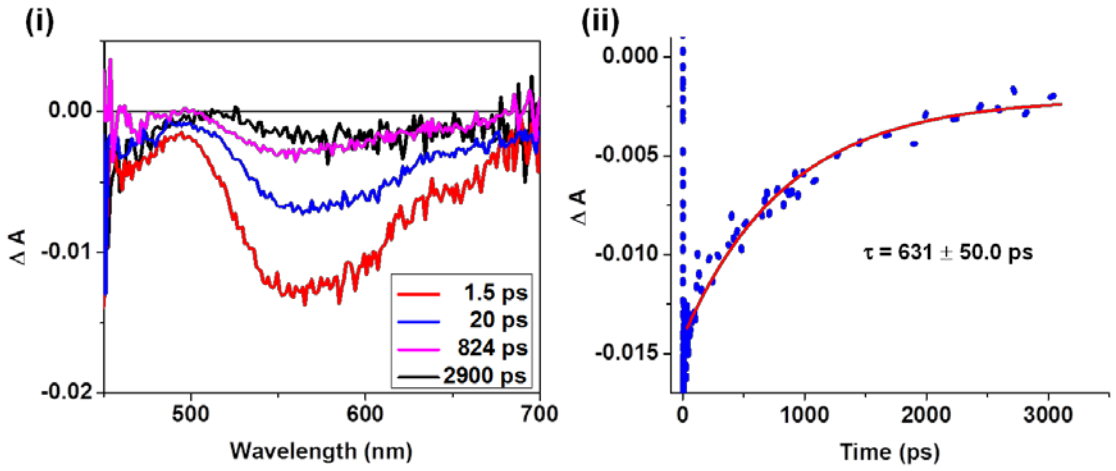

Fig 6.20 (i) Transient absorption spectra (ii) fluorescence decay kinetics of C153 in the presence of MV^{2+} in 30% acetonitrile in water; decay of C153 fluorescence was monitored at 560 nm; [C153] = 5×10^{-4} M and [MV^{2+}] = 7×10^{-3} M; Laser pulse = 390 nm, pulse width = 150 fs. Forward electron transfer in solution is slow (τ_{et} = 1700 ps) and consequently accumulation of the formed MV^{+} is not observed.

Similar results were observed in the cases of C480 and C1. Formation of $MV^{+\cdot}$ resulting from the electron transfer from coumarin to MV^{2+} across OA wall and its decay due to recombination process were observed in both the systems, C480@OA_2+MV^{2+} (**Fig 6.21(i)**) and C1@OA_2+MV^{2+} (**Fig 6.22(i)**). The time constant of the electron transfer from C480 to MV^{2+} and that of recombination were 1.2 ps ± 0.1 and 575 ps ± 17, respecctively (**Fig 6.21(ii)**).C1 transferred electron to MV^{2+} through OA wall with a rate constant as 2.3 ps ± 0.3 and the recombination rate constant was 1003 ps ± 60 (**Fig 6.22(ii)**).

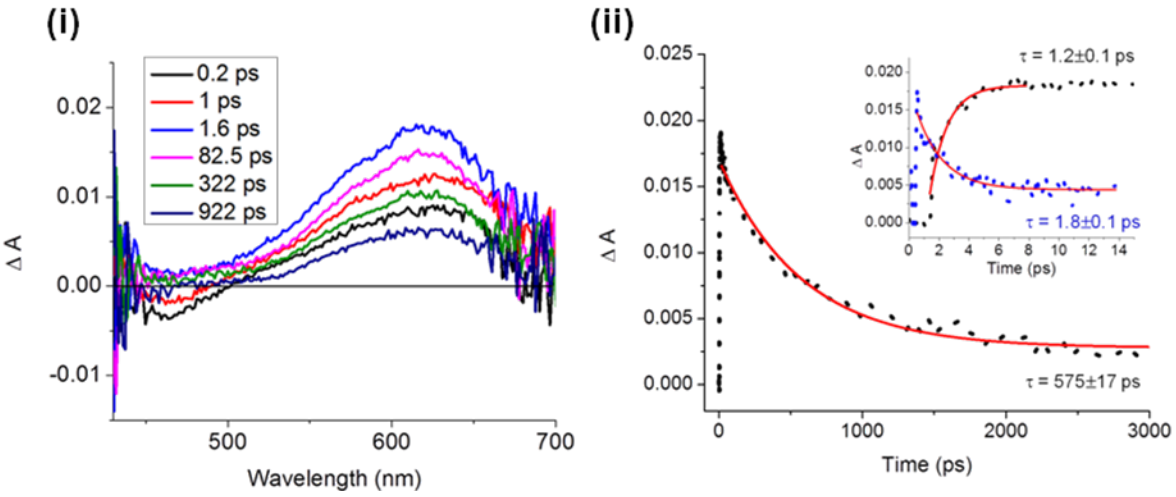

Figure 6.21 (i) Transient absorption spectra of the methyl viologen radical cation ($MV^{+\cdot}$) upon electron transfer from C480@OA_2 and (ii) TR-TA kinetics of $MV^{+\cdot}$, inset: rise of $MV^{+\cdot}$ (black) and Laser induced fluorescence dynamics of the photoexcited C480 (blue); rise and decay of $MV^{+\cdot}$ and bleaching of C480 were monitored at 625 nm and 470 nm, respectively; $[MV^{2+}] = 2\times10^{-3}$ M, $[C480] = 6\times10^{-5}$ M and $[OA] = 5\times10^{-4}$ M in 10 mM sodium tetraborate buffer; Laser pulse = 390 nm, pulse width = 150 fs.

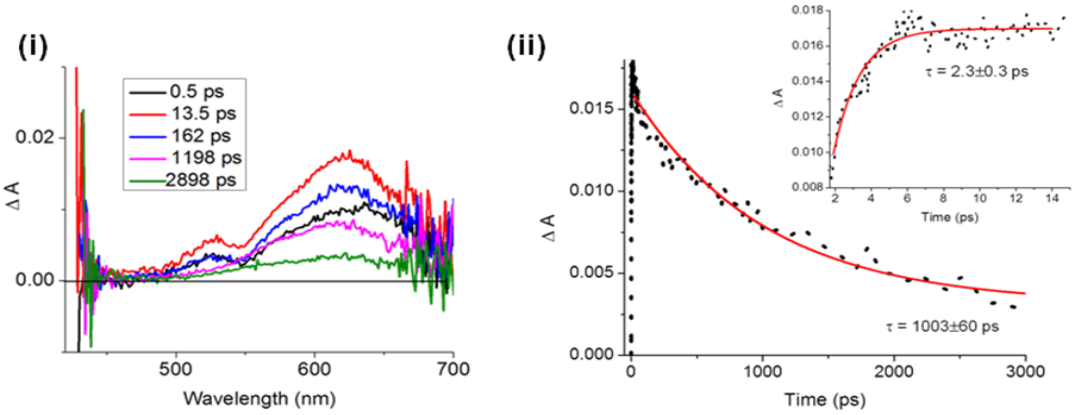

Figure 6.22 (i) Transient absorption spectra of the methyl viologen radical cation ($MV^{+\cdot}$) upon electron transfer from C1@OA_2 and (ii) TR-TA kinetics of $MV^{+\cdot}$, inset: rise of $MV^{+\cdot}$; rise and decay of $MV^{+\cdot}$ were monitored at 625, respectively; $[MV^{2+}] = 2\times10^{-3}$ M, $[C1] = 6\times10^{-5}$ M and $[OA] = 3\times10^{-4}$ M in 10 mM sodium tetraborate buffer; Laser pulse = 390 nm, pulse width = 150 fs.

Table 6.1 Time constants of the rise and decay of $MV^{+\cdot}$ and bleaching of coumarin in femtosecond laser excitation on coumarin@OA_2 complex in presence of MV^{2+}

Solution	$MV^{+\cdot}$	Time Constant (ps)	Coumarin	Time Constant (ps)
C153@OA_2+MV^{2+}	Rise	20 ± 0.8	Decay	18 ± 2
	Decay	724 ± 38		
C480@OA_2+MV^{2+}	Rise	1.2 ± 0.1	Decay	1.8 ± 0.1
	Decay	575 ± 17		
C1@OA_2+MV^{2+}	Rise	2.3 ± 0.3	Decay	----------
	Decay	1003 ± 60		

In this section, we demonstrated that Coulombic attraction between the C153@OA_2 complex and MV^{2+} accelerated electron transfer process faster than in solution without the OA host molecule. In addition, the presence of the molecular wall between the donor and acceptor dramatically slowed down the recombination rate (**Table 6.1**).

6.2.4 Supramolecular assembly on TiO_2 surface

After studying the electron transfer process from encapsulated donor to free acceptor through OA wall, we further wanted to explore electron injection from the same donor to semiconductor, TiO_2. Electron transfer study from C153@OA_2 to TiO_2 was performed with two types of nanostructured TiO_2: TiO_2 film and a colloidal aqueous suspension of TiO_2. **Scheme 6.3** represents the different approaches for the binding of dye molecule on the TiO_2 surface. Sometimes dye might aggregate and degrade on TiO_2

surface as shown in **Scheme 6.3(i)**. Various derivatives of the dye molecules have been synthesized to anchor it on the surface (**Scheme 6.3(ii)**). There are some functional groups that preferentially attach on some specific surfaces, such as –COOH group for TiO_2 surface, -SH group for gold surface etc. Another approach of binding dye to the surface is illustrated in **Scheme 6.3(iii).** A dye molecule is encapsulated inside a host and attached on the surface with the host-anchoring group.

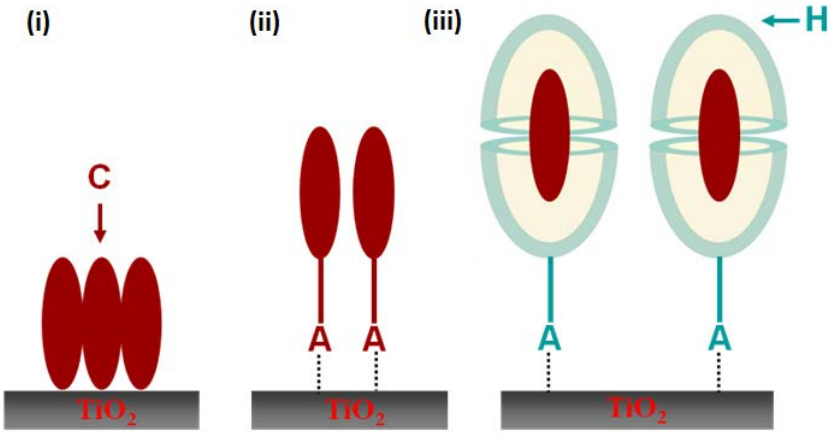

Scheme 6.3 Schematic illustration of chromophore (i) aggregated, (ii) directly bound through a linker-anchor group and (iii) chromophore@host bound though the host to metal oxide semiconductor surfaces, C: chromophore, H: host and A: anchoring group.

The advantages of using a host to anchor the dye molecule on the surface over attaching the dye molecule itself are:

(i) Synthesis of the structurally modified dye molecule is not needed as binding occurs through the host.

(ii) Encapsulation of the dye within a host molecule prevents the aggregate formation on the surface.

(iii) Encapsulation sometimes leads to significant changes in dye's chemical, photophysical and electrochemical properties, such as enhancing fluorescence lifetime of the dye, preventing excited state quenching due to dye-dye close contact, increase chemical stability etc.[157]

Despite having a number of advantages, this approach is limited by the properties of the guest and host including size and lipophilicity and their ability to form stable complexes. However, the complexation chemistry of many organic macrocycles and supramolecular cages is well known, and it is possible to select matching hosts for a variety of chromophores, and many other classes of molecules. In many cases the binding constants are high, leading to stable host@guest complexes.

TiO_2 has the fundamental absorption up to ~400 nm. As C480 and C1 absorb below 400 nm, they cannot be selectively excited in presence of TiO_2 (**Fig 6.6** and **Fig 6.7**). Hence they are not suitable for transferring an electron to TiO_2. Only C153 was focused in this study as its absorption spectrum (λ_{max} = 420 nm) was not obscured by the semiconductor-absorption (**Fig 6.5**). Nanostructured ZrO_2 was used as a control due to the following reasons: (i) ZrO_2 has wider band gap than TiO_2. The energy of band gap, (E_{bg}) of ZrO_2 is ~5.0 eV where as that of TiO_2 is ~3.2 eV. Due to the wider band gap electron injection from C153@OA_2 to ZrO_2 is not possible. (ii) ZrO_2 has the morphology resembling closely to that of TiO_2 films.

Careful consideration of both the capsular stability and energy levels of TiO_2 was required to examine whether C153 incarcerated within OA capsule would transfer an electron to TiO_2. It is reported that COOH adsorbs well on TiO_2 rather than COO^-.[158-160]

It has been demonstrated that potential determining ions, as well as addition of acids or bases, result in a dramatic shift of the TiO_2 conduction band edge,[161,162] a Nernstian shift of ~59 mV/pH, thereby influencing theinjection process. In general, acidic conditions lower the energy of the E_{cb} (energy level of the conduction band) thus favoring injection from a photoreductant dye, whereas strongly basic conditions have the opposite effect, and may inhibit charge injection of a dye with an excited state close to the E_{cb}.[161,162] These observations necessitated neutral or acidic rather than basic conditions. However, OA is readily soluble in basic medium (pH ~ 9). To examine pH dependence of the stability of the capsule, fluorescence spectra of C153@OA_2 was recorded at various pH in water. It is reported that fluorescence maxima of C153 in polarity dependent.[163] Fluorescence maxima of C153 is 547 nm in water and 483 nm when encapsulated within OA.[164] The polarity dependent fluorescence maximum was used to locate the probe relative to the capsule with changing the polarity of the medium. **Fig 6.23** represents the fluorescence spectra of C153@OA_2 at different pH. The emission maximum at 483 nm at pH 9, similar to the value observed in benzene, and consistent with C153 being within the lipophilic capsule interior shifted to 535 nm, closer to that in water (547 nm) in pH 6 suggesting that the capsule had dissociated under acidic conditions. The observed shift in the emission maximum for C153 was inferred to result from the pH dependent stability of the complex as the emission maximum of C153 alone (in the absence of OA) was independent of the pH (**Fig 6.24**). We concluded that the capsule dissociated below pH ~ 7 based on the emission spectra recorded under various pH conditions, and carried out all experiments with TiO_2 at pH 7.

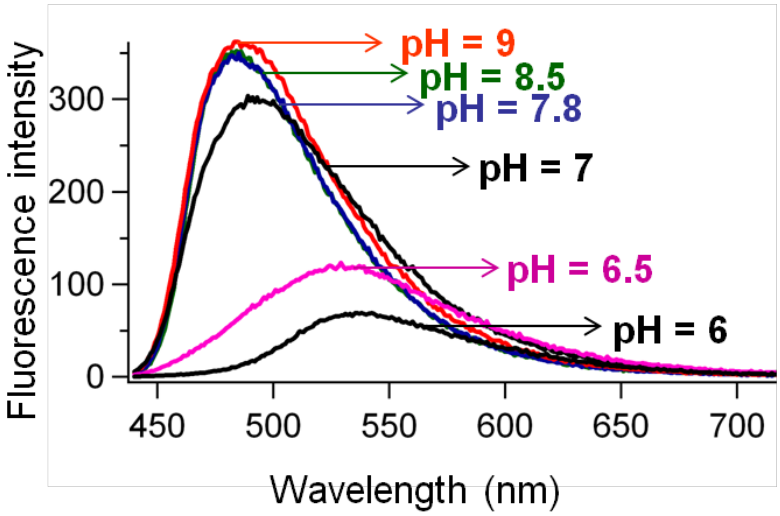

Figure 6.23 Fluorescence spectra of C153@OA_2 at different pH; λ_{ex} = 420 nm; [C153] = 1.5×10^{-5} M, [OA] = 1×10^{-4} M in 10 mM sodium tetraborate buffer.

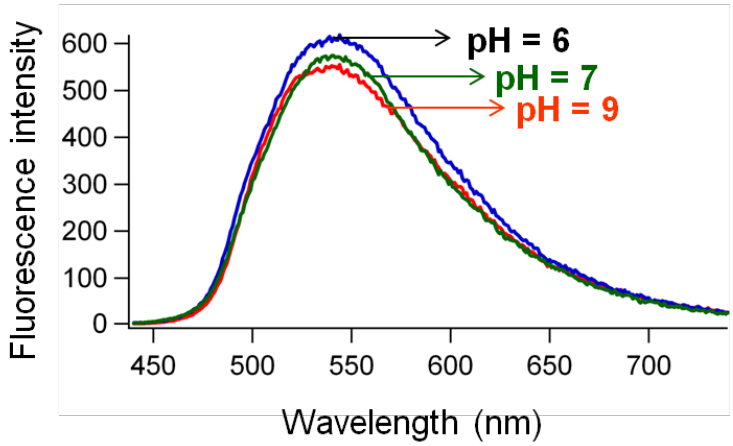

Figure 6.24 Fluorescence spectra of C153 at different pH; λ_{ex} = 420 nm; [C153] = 1.5×10^{-5} M, [OA] = 1×10^{-4} M in 10 mM sodium tetraborate buffer.

Adsorption of the complex on the films were carried out by immersing the film in 1 mM aqueous solution of C153@OA_2 at pH = 7. We used Fourier Transformed Attenuated Total Reflection Infrared (FT-ATR-IR) spectroscopy to monitor the adsorption of the complex on TiO_2 and ZrO_2 film. FT-ATR-IR spectra of TiO_2 (**Fig**

6.25) and ZrO_2 (**Fig 6.26**) films coated with C153@OA_2 complex showed some specific characterized bands:

(a) 1707 cm^{-1} due to the ν(C═O) stretch of unbound COOH groups

(b) broad, intense bands in the 1500–1650 cm^{-1} region assigned to the ν(O⎓C⎓O) stretch of bound carboxylate groups

(c) 1298 cm^{-1} due to the *ν*(C–O) stretch of the carboxylic acid

(d) broad O–H stretch above 3000 cm^{-1}

FT-ATR-IR spectrum of solid OA was also recorded (**Fig 6.27**) and that contained similar band as mentioned above. Comparison of the spectra of TiO_2 and ZrO_2 films coated with C153@OA_2 and solid OA indicated that C153@OA_2 was bound to both the films.

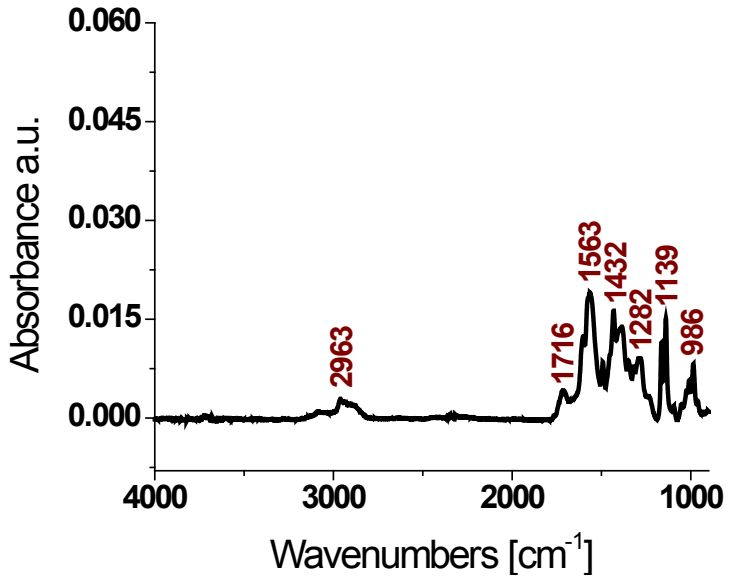

Figure 6.25 FT-ATR-IR spectra of C153@OA_2 on TiO_2

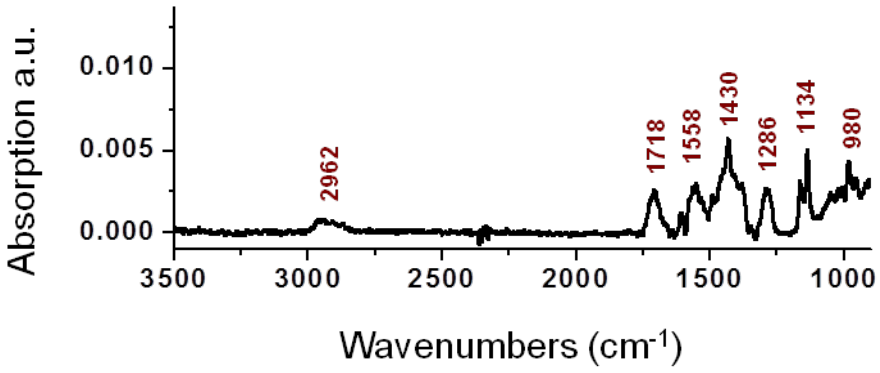

Figure 6.26 FT-ATR-IR spectra of C153@OA_2 on ZrO_2

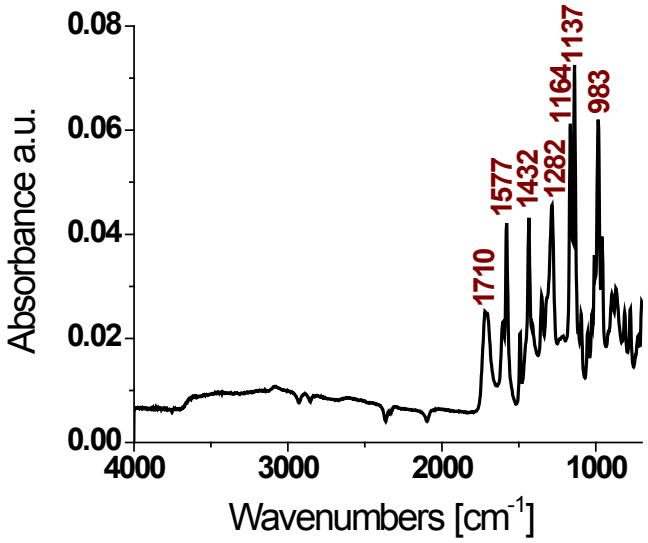

Figure 6.27 FT-ATR-IR spectra of OA (solid)

Emission spectra of TiO_2 and ZrO_2 films adsorbed with the C153@OA_2 complex have been shown in **Fig 6.32**. Excitation of the ZrO_2 films at 420 nm gave the fluorescence at 500 nm that resembles with the emission of C153@OA_2 complex in

solution suggesting that C153 was encapsulated and shielded from the polar environment on ZrO_2 film. On the other hand emission of C153 was fully quenched on TiO_2 film. Quenching of C153@OA_2 fluorescence on TiO_2 surface indicates that electron transfer occurred from encapsulated C153 to TiO_2. This preliminary observation signifies the importance of OA type cavitands in the problems related to the charge separation and dye shielding from heterogeneous environment of a semiconductor surface.

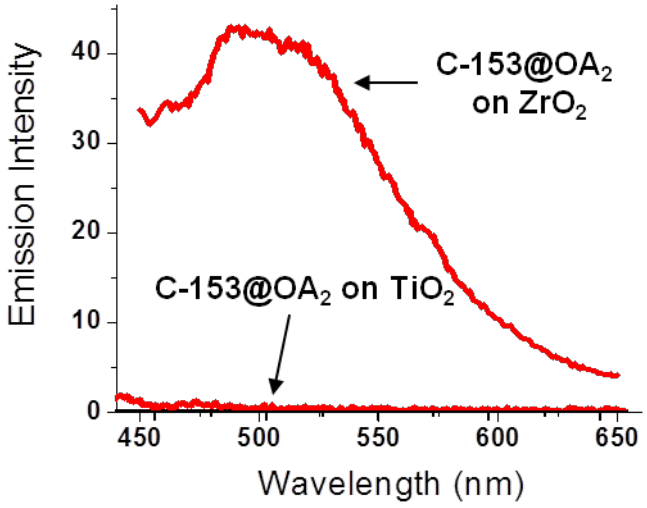

Figure 6.28 Fluorescence spectra of C153@OA_2 on TiO_2 and ZrO_2 film; λ_{ex} = 420 nm.

Since the fluorescence of C153@OA_2 was completely quenched on TiO_2 films, we further wanted to examine the possibility of controlling the quenching by adjusting the concentration of TiO_2. For this purpose aqueous colloidal TiO_2 was employed as the quencher. Thus the studies were conducted in solution, not in films. The emission spectra of C153@OA_2 were recorded in presence of increasing concentrations of TiO_2 (**Fig 6.29**). The fluorescence intensity of C153@OA_2 was reduced with increasing concentration of TiO_2. The same emission titration was done with ZrO_2 colloidal solution

as a control. As illustrated in **Fig 6.30,** colloidal ZrO_2 did not show any effect on the emission intensity. The above observations indicate that emission quenching in TiO_2 film is the result of electron transfer from physisorbed C153@OA_2 complex to the TiO_2 surface.

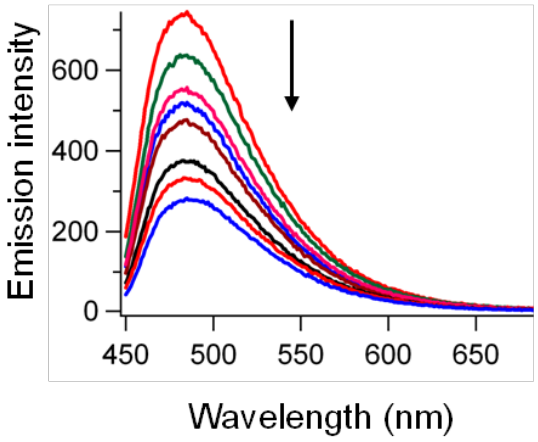

Figure 6.29 Fluorescence titration spectra of C153@OA_2 with TiO_2 solution; λ_{ex} = 440 nm; [C153] = 1.5 × 10^{-5} M, [OA] = 1 × 10^{-4} M in water.

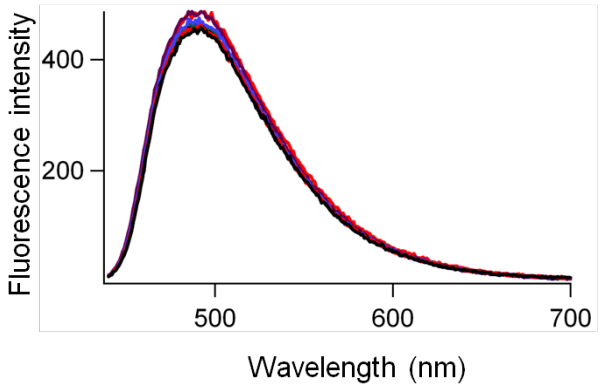

Figure 6.30 Fluorescence titration spectra of C153@OA_2 with ZrO_2; λ_{ex} = 440 nm; [C153] = 1.5 × 10^{-5} M, [OA] = 1 × 10^{-4} M in water.

6.3 Conclusion

In this work we have concluded that electron transfer occurs from an encapsulated dye molecule to an acceptor. Host@guest complex formation was confirmed by ^{1}H NMR study. Association of the complex and MV^{2+} was proved by 2D-DOSY experiment. Steady state fluorescence of coumarin dyes encapsulated within OA capsules was quenched with the addition of MV^{2+}. No change in lifetime of the dye in presence of MV^{2+} confirmed that the quenching was static in the cases of all three coumarin derivatives. By femtosecond laser excitation we confirmed that the quenching was due to electron transfer from encapsulated coumarin dyes to the acceptor. Electron transfer was faster than the recombination process. Introduction of CB7 in the solution of coumarin@OA_2 in presence of MV^{2+}, quenched fluorescence was recovered suggesting that the quenching was prevented in presence of CB7. The above visualized electron transfer process is schematically illustrated below (**Scheme 6.4**).

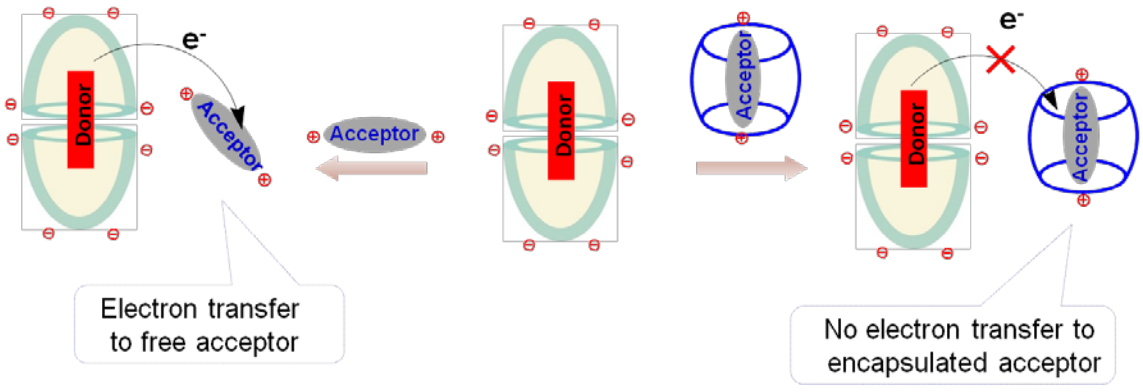

Scheme 6.4 Schematic representation of electron transfer process in supramolecular assembly in solution

Adsorption of the C153@OA_2 complex on TiO_2 surface was monitored by FTIR-ATR. Nanostructured ZrO_2 was used as a control. Emission of C153@OA_2 was fully quenched on TiO_2 surface indicating that electron was transferred from C153 to TiO_2 across OA wall (**Scheme 6.5**). Whereas no electron transfer occurs from C153 to ZrO_2 as ZrO_2 is an insulator. With the increase in concentration of TiO_2 nanoparticles, fluorescence intensity of C153@OA_2 was gradually decreased indicating the electron transfer from C153 to TiO_2 nanoparticle in solution. In summary we have shown that encapsulated guest within OA capsule can be used as an electron donor to a free acceptor in solution as well as to the semiconductor.

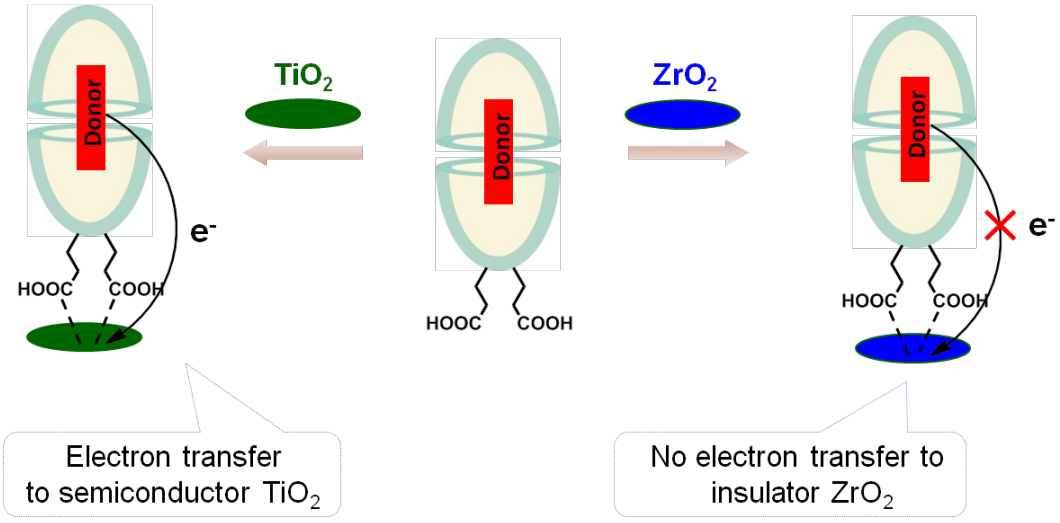

Scheme 6.5 Schematic representation of electron transfer process in supramolecular assembly on surface

6.4 Experimental Section

Material:

The hosts octa acid,[40] cucurbit[7]uril[141] were synthesized following published procedures. Laser grade coumarin 153 (C153), coumarin 1 (C1) and coumarin 480 (C480) were used as received from Sigma-Aldrich/Acros.

General protocol for NMR study:

^{1}H NMR studies were carried out on a Bruker 500 MHz NMR spectrometer at 25 °C. 600 μL of a D_2O solution of host OA (1mM OA in 10 mM $Na_2B_4O_7$) was taken in a NMR tube and to these 0.5 equivalent increments of coumarin (5 μL of a 60 mM solution in DMSO-d_6) was added. The ^{1}H NMR experiments were carried out after shaking the NMR tube for 5 min after addition. Completion of complexation was monitored by the disappearance of the free host OA signals upon addition of guest. The required amount of quencher solution (MV^{2+}; stock solutions of 30 mM were prepared in D_2O) was added and ^{1}H NMR was recorded after shaking the NMR tube for 5 min. For experiments in the presence of CB7, the calculated amount of CB7 (solid) was added to coumarin@OA_2 + quencher solutions and shaken properly before ^{1}H NMR spectra were recorded.

General protocol for fluorescence study:

Fluorescence emission spectra were recorded on a FS920CDT Edinburgh steady-state fluorimeter and the lifetime measurements on FL900CDT fluorescence lifetime spectrometer. A 30 mM stock solution of the guest was prepared in $CHCl_3$. The host (OA) aqueous solution was prepared in 10 mM sodium tetraborate buffer (1 mM). The complex solutions were prepared by adding required amount of guest solution in a vial,

evaporating the solvent, and adding to the vial 2.5 mL of the host solution. The resulting aqueous solution was sonicated for 30 min. Calculated amounts of quencher solution (aqueous MV^{2+} solution, TiO_2 and ZrO_2 colloidal solution) were added and mixed thoroughly and then the fluorescence spectra were recorded. The required amount of CB7 was added to the solution (host/guest + MV^{2+}), sonicated and fluorescence spectra were recorded.

pH adjustment:

Capsular assembly (C153@OA_2) was made in sodium tetraborate buffer (pH~9) and its emission was recorded. At each step of the acid-titration, aqueous HCl was added drop wise and pH of the solution was checked. After adjusting a certain pH, emission of the solution was recorded. It was observed that up to pH~7, λ_{max} of complex emission remain almost same. From pH=7, λ_{max} was gradually red shifted with increasing pH of the solution indicating that C153 was decomplexing from OA capsule. Depending upon this result pH of C153@OA_2 was fixed at 7 for binding study with TiO_2.

Mesoporous metal oxide film preparation and binding:

Binding was done on semiconducting TiO_2 (E_b = 3.2 eV) films, as well as insulating ZrO_2 (E_b = 5 eV) films to study excited states. Synthesis of TiO_2 / ZrO_2 nanoparticles were carried out by acidic hydrolysis of titanium(IV) iso-propoxide and zirconium(IV) propoxide under nitrogen atmosphere and autoclaved at 200 °C for 8 hours as previously described.[165,166] Poly(ethylene glycol) (PEG 2,000) was added (6g/L) to the colloidal pastes of TiO_2/ $ZrO_2$to optimize the solution viscosity of the pastes. The pastes were applied to a micro cover glass (VWR) or a conductive glass (FTO, TEC 7 by Pilkington, with 8 – 10 Ω/sq resistance of the sheet). The TiO_2/ZrO_2 pastes were spread on a

conductive glass by using a glass test tube and holding the edge of a conductive glass by the tape. The films were air dried and then sintered in the oven at 450 °C for 30 minutes under oxygen flow. Then, the films were cooled down before using, or stored in a desiccator in dark.

The binding of C153@OA_2 complexes onto TiO_2 and ZrO_2 films was performed by immersing the MO_n films in 1 mM aqueous solutions of the complex overnight in the dark. The functionalized films were rinsed with water, dried, and then used for the spectroscopic measurements.

General protocol for FTIR-ATR study of the films:

All FTIR-ATR spectra for OA (solid) and C153@OA_2 (at pH=7) on TiO_2/ZrO_2 films were recorded on a Thermo Scientific, Nicolet 6700Ft-IR. The films were dried by heating in the oven to 110 °C for 30 minutes before all measurements.

General protocol for emission study of the films:

Fluorescence emission spectra of the C153@OA_2 (at pH=7) binding on TiO_2/ ZrO_2 films were collected on a Cary Eclipse, Varian fluorescence spectrometer. The fluorescence spectra were recorded at λ_{ex} = 420 nm. Before the spectroscopic measurements all films were heated in the oven to 110 °C for 30 minutes to remove moisture.

General protocol for transient absorption study:

Femtosecond transient absorption (TA) measurements were conducted using a Clark MXR 2001 femtosecond laser system producing 780 nm, 150 fs pulses from a regenerative amplifier.[1-3] The laser pulse train was split to generate a white light continuum probe pulse in a sapphire crystal and a 390 nm pump pulse using second harmonic generation. The excitation power of ~ 5 mJ / cm^2 per pulse fluence was

controlled carefully. All femtosecond laser experiments were carried out in a 2 mm quartz cuvette at room temperature. The instrumental time resolution was determined to ~150 fs via a pump-probe cross-correlation analysis.

CHAPTER 7

Communication between Encapsulated Excited Organic Molecules and Free Nitroxides Across a Molecular Wall

7.1 Overview

In **Chapters 5** and **6**, we established that an excited donor molecule that was incarcerated within OA capsule could transfer an electron to an acceptor free in water. The feasibility of electron–electron spin communication between two nitroxide molecules separated by molecular wall has been explored through steady state and time-resolved EPR experiments.[167,168] Our group has also demonstrated the ultrafast Forster resonance energy transfer (FRET) between a confined excited donor and a free acceptor using the well-established FRET pair, coumarin dyes-rhodamine 6G.[154] It is interesting that these types of molecular communications continue between the molecules despite one being held tightly within a molecular capsule and the other just outside. A literature review suggests that the deactivation of excited molecules by nitroxides results from exchange and/or charge transfer processes, and both require close contact between the excited guest and the nitroxide.[169-175] Based on the above two reports, we became interested to study the electron-electron spin communication between an excited molecule and a ground state paramagnetic molecule such as nitroxide separated by a molecular wall. The excited molecule was trapped within an organic capsule and nitroxide was positioned outside the complex in aqueous solution. The guest and host molecules for this study are presented in **Scheme 7.1** and **Scheme 7.2,** respectively. We have used three different paramagnetic nitroxides; cationic, anionic, neutral (**Scheme 7.1**) along with nine other guest molecules to probe the inside-outside spin communication.

In this study, we have probed the spin communication by monitoring the quenching of excited singlet or triplet states of guest molecules (**Scheme 7.1**) present inside a capsule by paramagnetic nitroxide that was present outside the capsule. The

quenching rate was calculated by monitoring the fluorescence/phosphorescence intensity or the excited state lifetimes of guest molecules in the presence of different concentrations of nitroxide. Guest molecules were chosen such that they either fluoresce or phosphoresce.

The rationale behind choosing the cationic ($T^{\oplus}$), anionic ($T^{\ominus}$) and neural (T) nitroxides for the current study was rooted in the well-known fact that spin communication becomes efficient when the two molecules come closer. The host@guest complex was prepared at basic pH ~ 9. At this condition the –COOH groups of the host deprotonate and convert to $–COO^-$. So the overall complex becomes negatively charged. As a result of the electrostatic interaction, $T^{\oplus}$ is expected to associate to the complex more tightly than other two whereas $T^{\ominus}$ would prefer to stay as far away as possible. This approach allowed us to monitor the spin communication as a function of the distance between the two molecules.

It is reported that, the triplet quenching and spin polarization occurred during collisions of freely diffusing excited ketones and nitroxides or with the nitroxide that was covalently linked to the ketone.[176,177] The establishment of the spin communication between an excited guest molecule incarcerated within OA capsule and the free nitroxide in the bulk water prompted us to explore the polarization transfer from a spin polarized excited triplet state of an incarcerated guest within OA capsule to the cationic nitroxide associated on the surface of the capsule.

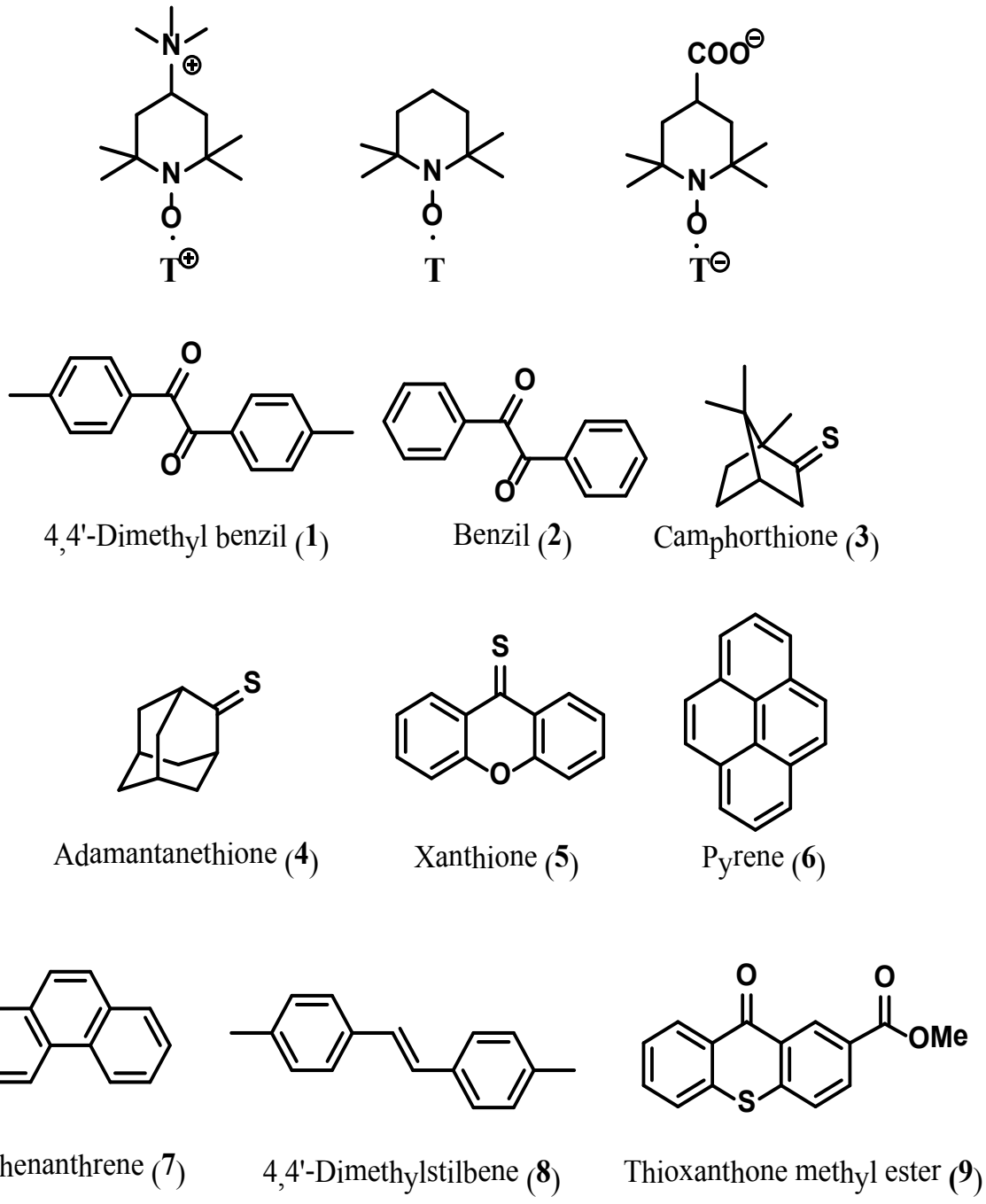

Scheme 7.1 Structures guests examined in this study.

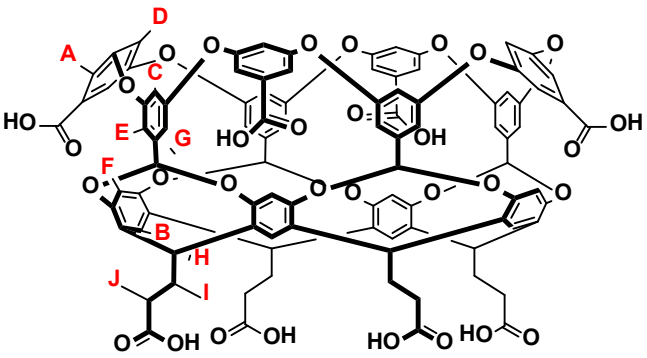

Octa acid (OA)

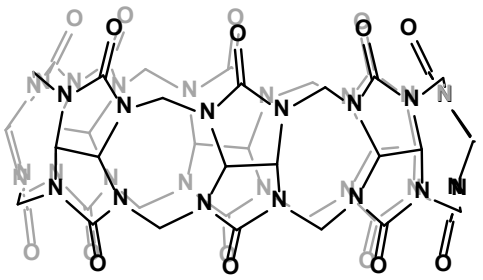

Cucurbit[8]uril (CB8)

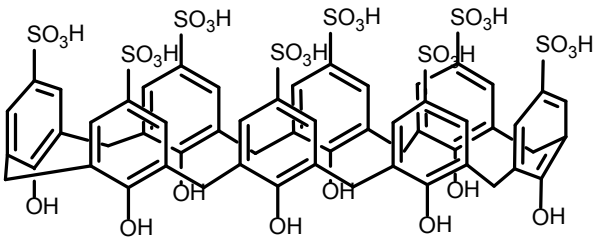

Calixarene octa sulfonic acid (CA8)

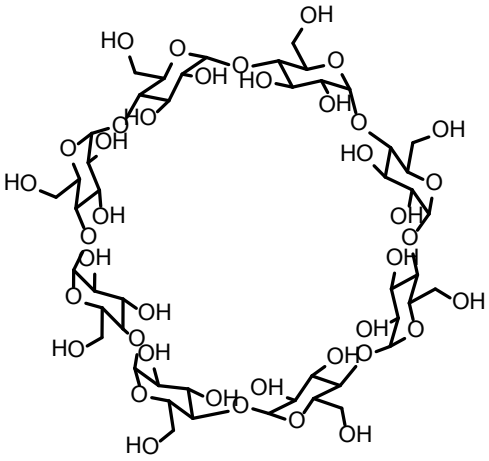

γ–Cyclodextrin (γ–CD)

Scheme 7.2 Structures of hosts examined in this study. The letters "A" to "J" in OA represent the corresponding protons.

7.2 Results and discussion

7.2.1 ^{1}H NMR study

The complexes of the guests **1-8** with OA were prepared in 10 mM sodium tetraborate buffer (pH ~ 9) following the literature procedure. Jayaraj *et al.* have already established that camphorthione (**3**) and adamantinethione (**4**) form 2:2 (H:G) complex while the rest of the guest molecules form 2:1 (H:G) complexes with OA.[178] In this work, we conducted ^{1}H NMR studies to find out the relative location of the nitroxides with respect to the capsuleplex.

^{1}H NMR spectra of OA and **1**@OA_2 in absence and presence of $T^{\oplus}$ are provided in **Fig 7.1**. Upfield shift of $-CH_3$ proton of the guest suggested that **1** was included within OA. Upon increasing the concentration of $T^{\oplus}$, ^{1}H NMR signals of the protons of the host (OA) as well as the guest (**1**) were broadened indicating that $T^{\oplus}$ was associated with **1**@OA_2 complex. This is expected as the presence of a paramagnetic substance reduces the relaxation time of a ^{1}H NMR signal.[179] So the observed broadening of the signal indicated that $T^{\oplus}$ was closely associated with the capsule. At basic pH, OA has eight $-COO^{-}$ groups in its periphery. The electrostatic interaction further appreciate the close contact of $T^{\oplus}$ with OA. It was also observed that the broadening of the OA signals was more than for the guest **1** suggesting that $T^{\oplus}$ was closer to OA than to the guest **1**. While broadening of NMR signals of OA by $T^{\oplus}$ was observed, differential broadening of signals due to various protons suggested $T^{\oplus}$ to adopt a specific orientation with respect to the cavity. The detailed information on the location of $T^{\oplus}$ with respect to OA cavity was obtained from ^{1}H relaxation study and that will be discussed in the next section.

In contrast, upon addition of T^{Θ} to a **1**@OA_2 solution, the ^{1}H NMR signals of OA as well as $-CH_3$ of the guest **1** remained unchanged (**Fig 7.2**). Due to the electrostatic repulsion between T^{Θ} and negatively charged **1**@OA_2 complex, T^{Θ} was located far apart from the complex. This observation suggest that the broadening of the host/guest proton signals was due to the close contact of **1**@OA_2 and $T^{\oplus}$.

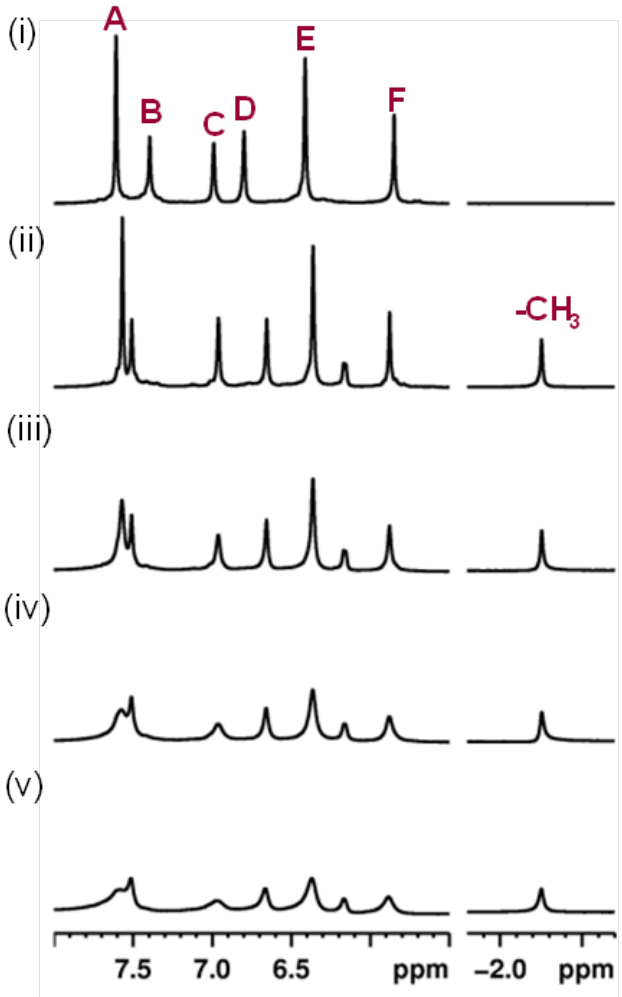

Figure 7.1 ^{1}H NMR spectra (500 MHz, D_2O) of (i) OA, (ii) **1**/OA(1:2), (iii) **1**/OA/$\mathbf{T}^{\oplus}$ (1:2:1), (iv) **1**/OA/$\mathbf{T}^{\oplus}$ (1:2:2), (v) **1**/OA/$\mathbf{T}^{\oplus}$ (1:2:3). [**1**] = 0.5 mM, [OA] = 1 mM and [$\mathbf{T}^{\oplus}$] = 0.5 mM to 1.5 mM in 10 mM borate buffered D_2O.

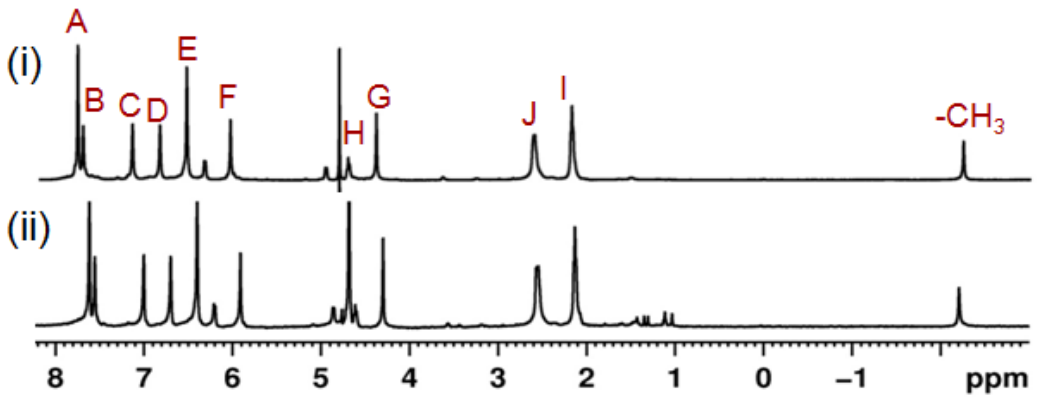

Figure 7.2 ^{1}H NMR spectra (500 MHz, D_2O) of (i) **1**/OA(1:2), and (ii) **1**/OA/$\mathbf{T}^{\Theta}$ (1:2:5), [**1**] = 0.5 mM, [OA] = 1 mM and [$\mathbf{T}^{\Theta}$] = 2.5 mM in 10 mM borate buffered D_2O.

As shown in **Fig 7.3**, upon addition of CB8 to the solution of **1**@OA_2 + $T^{\oplus}$, the line shape of the ^{1}H NMR signals of the host as well as –CH_3 of the guest were recovered suggesting that spin-spin communication was suppressed in presence of CB8. It is reported that CB8 forms a cavitandplex with $T^{\oplus}$ (represented as $T^{\oplus}$@CB8).[180,181] In presence of CB8, $T^{\oplus}$ was encapsulated within CB8 and hence became dissociated from **1**@OA_2 complex. Therefore the presence of two host walls (OA and CB8) between **1** and $T^{\oplus}$ hinders the spin-spin communication between them resulting in the sharpening of the proton NMR signals (**Fig 7.3(iv)**).

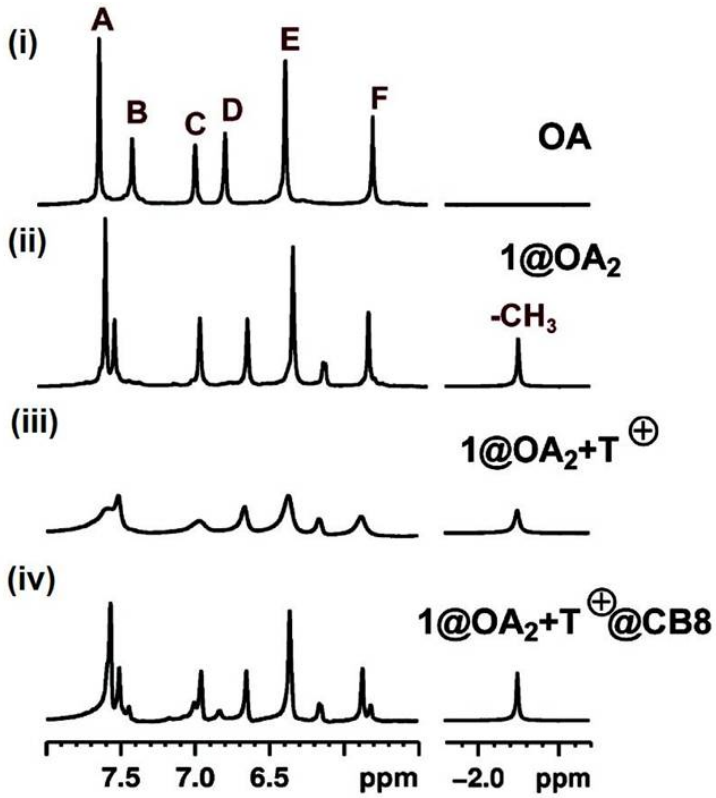

Figure 7.3 ^{1}H NMR spectra (500 MHz, D_2O) of (i) OA, (ii) **1**@OA_2, (iii) **1**@OA_2+ $T^{\oplus}$, and (iv) **1**@OA_2+ $T^{\oplus}$@CB8; [1] = 0.5 mM, [OA] = 1 mM, [$T^{\oplus}$] = 1 mM, and [CB8] = 1 mM in 10 mM borate buffered D_2O.

After we found that $T^{\oplus}$ was associated on the OA wall, the same idea was applied to the other host namely calixarene octasulfonic acid (CA8, **Scheme 7.2**). As $T^{\oplus}$ was added to CA8 solution in 10 mM sodium tetraborate buffer solution (pH ~ 9), the ^{1}H NMR signals of CA8 was broadened indicating that $T^{\oplus}$ was associated with CA8 wall due to electrostatic interaction of $T^{\oplus}$ and the sulfonate groups of CA8 in basic media (**Fig 7.4**). Upon addition of CA8 to the solution of **1**@OA_2 + $T^{\oplus}$, the line shape of the ^{1}H NMR signals of the host as well as $–CH_3$ of the guest was recovered suggesting that spin-spin communication was inhibited in presence of CA8 (**Fig 7.5**).

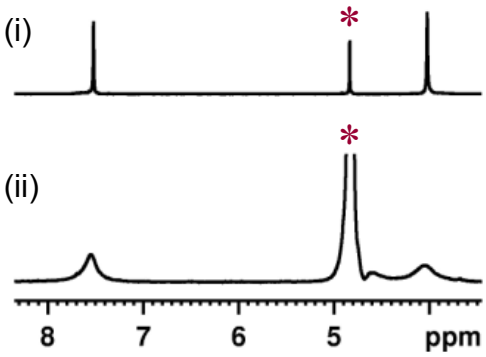

Figure 7.4 ^{1}H NMR spectra (500 MHz, D_2O) of (i) CA8 and (ii) $\mathbf{T}^{\oplus}$/CA8 (1:1); [$\mathbf{T}^{\oplus}$] = 1 mM and [CA8] = 1 mM in 10 mM borate buffered D_2O, "*" represents residual H_2O proton resonances.

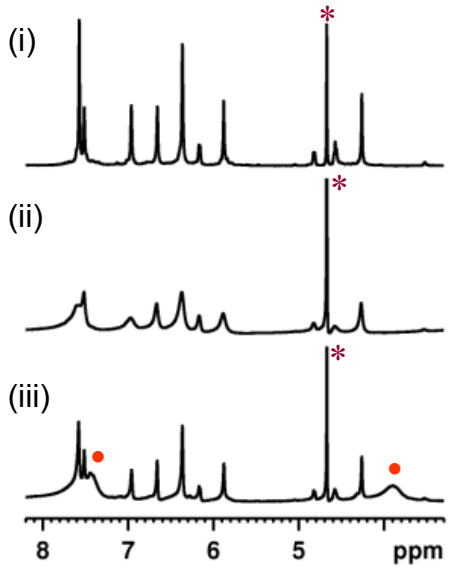

Figure 7.5 ^{1}H NMR spectra (500 MHz, D_2O) of (i) **1**/OA (1:2) , (ii) **1**/OA/$\mathbf{T}^{\oplus}$ (1:2:2), (iii) **1**/OA/ $\mathbf{T}^{\oplus}$/CA8 (1:2:2:2), [**1**]=0.5 mM, [OA] = 1 mM, [$\mathbf{T}^{\oplus}$] = 1 mM and [CA8] = 1 mM in 10 mM borate buffered D_2O, "•" represents CA8 proton resonances, "*" represents residual H_2O proton resonances.

Unlike the case of CB8 and CA8, addition of γ-CD to the solution of **1**@OA_2 + $T^{\oplus}$ did not change the line shape of the ^{1}H NMR signals of the host as well as the guest indicating that spin-spin communication was not affected in presence of γ-CD (**Fig 7.6**).

The result with γ-CD suggests that the recovery of ^{1}H NMR signals of the host and the guest in presence of CB8 and CA8 was not an artifact.

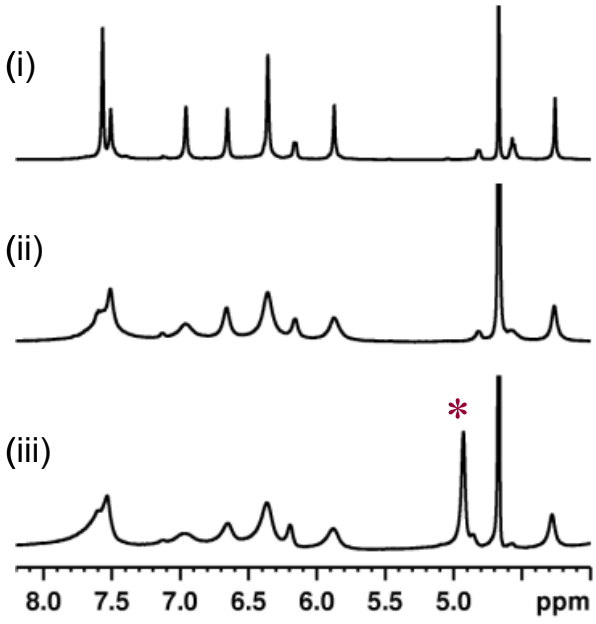

Figure 7.6 ^{1}H NMR spectra (500 MHz, D_2O) of (i) **1**/OA (1:2), (ii) **1**/OA/ $\mathbf{T}^{\oplus}$ (1:2:2) and (iii) **1**/OA/$\mathbf{T}^{\oplus}$/γ-CD (1:2:2:2), [**1**]=0.5 mM, [OA] = 1 mM, [$\mathbf{T}^{\oplus}$] = 1 mM and [γ-CD] = 1 mM in 10 mM borate buffered D_2O, "*" represents γ-CD proton NMR signal.

7.2.2 ^{1}H NMR relaxation study

The relative location of nitroxide with respect to the capsule was obtained from its signature on the relaxation time of ^{1}H NMR signals of the guest and the host in water. Relaxation times of methyl proton of guest **1** and each proton of the host in absence ($T_{1,d}$) and presence ($T_{1,obs}$) of nitroxides were measured by the inversion recovery method to quantify the influence of nitroxide. $1/T_{1,p}$ (relaxivity by nitroxide) values for the protons were calculated according to Solomon-Bloembergen equation as listed in **Table 7.1**.[179,182,183] According to the Solomon-Bloembergen equation, the relaxivity ($1/T_{1,p}$) is

proportional to the reciprocal of the sixth power of the distance between the proton and the paramagnetic center, in our case, nitroxide. It was observed that $T^{\oplus}$ had a major influence on H_A and H_C protons of OA that are present at the wider rim of the OA cavitand. All other host protons were affected by $T^{\oplus}$ to a smaller extend than H_A and H_C, signifying that $T^{\oplus}$ was located closer to the middle region of the capsuleplex by Coulombic interactions with benzoate anions (**Fig 7.7**). Consistent with this model, $T^{\oplus}$ had only a small effect on the methyl proton of guest **1**. This is because the methyl proton was positioned at the narrower end and far from the wider middle region of the capsule (**Table 7.1**). In line with the expectation that the anionic nitroxide and capsuleplex would be repelled as they both are negatively charged. As shown in **Table 7.1**, T^{Θ} had smaller $1/T_{1,p}$ values for all protons. Interestingly, its effect on H_A and H_C of OA was very small compared to $T^{\oplus}$ as shown in **Table 7.1**. Taken together, it suggested that T^{Θ} avoided the wider rim that is substituted with benzoate anions while approaching towards the capsuleplex. Finally the influence of neutral T on the capsuleplex was examined. $1/T_{1,p}$ values listed in **Table 7.1** for T were much smaller than that for $T^{\oplus}$ and slightly larger than that for T^{Θ} suggesting that T approached the capsule randomly, closer than T^{Θ}. In addition it was also observed that its effect on all the hydrogens of OA were almost similar (see $1/T_{1,p}$ values) indicating that T has no specific interaction with **1**@OA_2.

Table 7.1 ^{1}H relaxation time (T_1) for OA (host) and **1** (guest) in presence of nitroxide radicals ($T^{\oplus}$, T and $T^{\ominus}$, see **Scheme 7.1**)

Protons	$(T_{1,d})^a$	$(T_{1,obs})^b$ $[T^+]$	$(1/T_{1,p})^c$ $[T^+]$	$(T_{1,obs})$ [T]	$(1/T_{1,p})$ [T]	$(T_{1,obs})$ $[T^-]$	$(1/T_{1,p})$ $[T^-]$
H_A	2.42	0.07	14.28	0.31	2.86	2.09	0.07
H_B	0.56	0.23	2.56	0.32	1.33	0.54	0.07
H_C	0.76	0.08	11.11	0.24	2.86	0.7	0.11
H_D	0.35	0.15	2.85	0.19	2.38	0.31	0.37
H_E	1.14	0.14	6.25	0.31	2.33	0.96	0.16
H_F	1.11	0.14	6.25	0.3	2.44	0.88	0.24
H_I	0.38	0.19	2.63	0.26	1.22	0.36	0.15
H_J	0.35	0.12	5.56	0.23	1.49	0.32	0.26
H_{-CH3}	0.82	0.38	1.43	0.5	0.78	0.78	0.06

Note:

[a] $T_{1,d}$ = relaxation time in absence of the paramagnetic center

[b] $T_{1,obs}$= observed relaxation time in presence of paramagnetic center

[c] $T_{1,p}$= relaxation time caused by the paramagnetic species

$1/T_{1,p} = 1/T_{1,obs} - 1/T_{1,d}$

$1/T_{1,p} \propto r^{-6}$, r=distance between nucleus and paramagnetic center.

[1] = 0.5 mM, [OA] = 1 mM, $[T^{\oplus}] = [T] = [T^{\ominus}]$ = 0.5 mM, in 10 mM borate buffered D_2O.

Relaxation time for H_G and H_H could not be measured as these proton signals merged with residual H_2O signal.

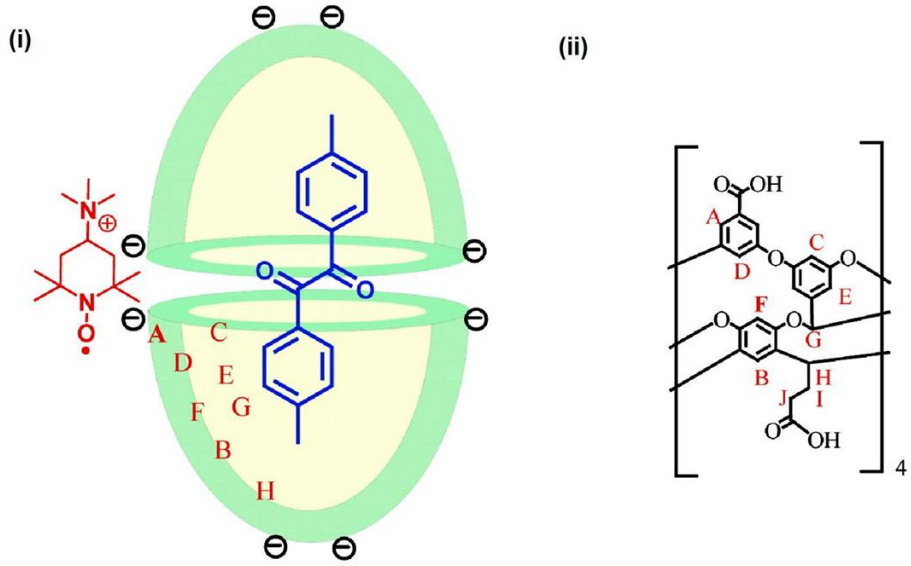

Figure 7.7 (i) Cartoon representation of [1@OA_2]-$T^{\oplus}$ complex and (ii) partial chemical structure of OA. The letters A-J in OA represent relative positions of corresponding protons.

As mentioned above cavitand CB8 strongly binds $T^{\oplus}$. Upon addition of CB8, the $1/T_{1,p}$ values for all host protons were much smaller (compare data in **Table 7.1** and **Table 7.2**). Inclusion of $T^{\oplus}$ within CB8 was already confirmed by ^1H NMR study discussed above (**Fig 7.3**). CA8 was effective to some extent, though not as powerful as CB8 to dissociate $T^{\oplus}$ from the capsulplex (**Table 7.2**). γ-CD was unable to displace $T^{\oplus}$ from the capsular exterior walls and hence did not change $T_{1,p}$ values (**Table 7.2**).

Table 7.2 ^{1}H relaxation time (T_1) for OA (host) and **1** (guest) in presence of $T^{\oplus}$ (see **Scheme 7.1**) and other hosts (CB8. CA8 and γ-CD)

Protons	$(T_{1,obs})^a$ $[T^+]$ + CB8	$(T_{1,p})^b$ $[T^+]$+ CB8	$(T_{1,obs})^c$ $[T^+]$+ CA8	$(T_{1,p})$ $[T^+]$+ CA8	$(T_{1,obs})$ $[T^+]$+ γ-CD	$(T_{1,p})$ $[T^+]$+ γ-CD
H_A	1.64	0.2	1	0.6	0.15	6.26
H_B	0.52	0.13	0.4	0.71	0.26	2.06
H_C	0.68	0.15	0.66	0.2	0.05	18.68
H_D	0.35	0.03	0.26	0.99	0.13	4.83
H_E	1.06	0.07	1.14	0	0.15	5.79
H_F	1.05	0.05	1.1	0.01	0.28	2.67
H_I	0.35	0.2	0.3	0.7	0.27	1.07
H_J	0.35	0	0.29	0.6	0.1	7.14
H_{-CH3}	0.76	0.09	0.79	0.05	0.37	1.48

Note:

[a] $T_{1,d}$ = relaxation time in absence of the paramagnetic center

[b] $T_{1,obs}$= observed relaxation time in presence of paramagnetic center

[c] $T_{1,p}$= relaxation time caused by the paramagnetic species

$1/T_{1,p} = 1/T_{1,obs} - 1/T_{1,d}$

$1/T_{1,p} \propto r^{-6}$, r=distance between nucleus and paramagnetic center.

[1] = 0.5 mM, [OA] = 1 mM, $[T^{\oplus}]$ = 0.5 mM, [CB8] =0.5 mM, [CA8] = 0.5 mM and [γ-CD] = 0.5 mM in 10 mM borate buffered D_2O.

Relaxation time for H_G and H_H could not be measured as these proton signals merged with residual H_2O signal.

The effect of $T^{\oplus}$ on the relaxation time of -CH_3 proton of three substituted dibenzylketones as guest molecules is shown in **Fig 7.8.** We conducted ^1H NMR experiments (**Fig 7.9**) suggested that those three dibenzylketone derivatives were held in the capsule in the geometry shown in **Fig 7.8**.[88,184] The difference in ^1H NMR chemical shift for the CH_3 signal in $CDCl_3$ in the absence of OA, and in water in the presence of 2 equiv of OA referred to the distinctly different location of CH_3 group in each case. The deeper the -CH_3 group moves from the middle of the capsule, the larger the $\Delta\delta$ for the CH_3 group becomes (**Fig 7.8**). The $\Delta\delta$ value is the difference in ^1H NMR chemical shift for CH_3 signal in $CDCl_3$ in the absence of OA, and in water in the presence of 2 equiv of OA. From the results shown in **Fig 7.8**, it was predicted that the effect of $T^{\oplus}$ on the relaxivity of the -CH_3 group of dibenzylketones would be inversely related to $\Delta\delta$ values. As –CH_3 of α-octyl dibenzylketone went the most deep inside the capsule, it was least effected by $T^{\oplus}$, whereas –CH_3 of methyl dibenzylketone which was at the middle rim of the capsule, was affected most by $T^{\oplus}$.

The relaxivity effects observed with the three systems and also the study with cationic, neutral and anionic nitroxide reflect that not only the orientation of the nitroxide at the exterior of the capsule, but also of the lifetime of the encounter complex between the capsuleplex and the nitroxide influence the relaxivity of the proton of the complex; the longer the lifetime, the larger the effect. On the basis of the extent and specificity of the influence of the three nitroxides on the relaxation of the protons, we reached the

following conclusions: (a) the encounter complex between the capsuleplex and $T^{\oplus}$ has a preferred orientation and longer lifetime. (b) The encounter complex between capsuleplex and T^{Θ} is shorter-lived and the two anionic ends in the complex avoid each other. (c) Encounters between capsuleplex and T are random and the encounter complex has a lifetime intermediate between those of $T^{\oplus}$ and T^{Θ}.

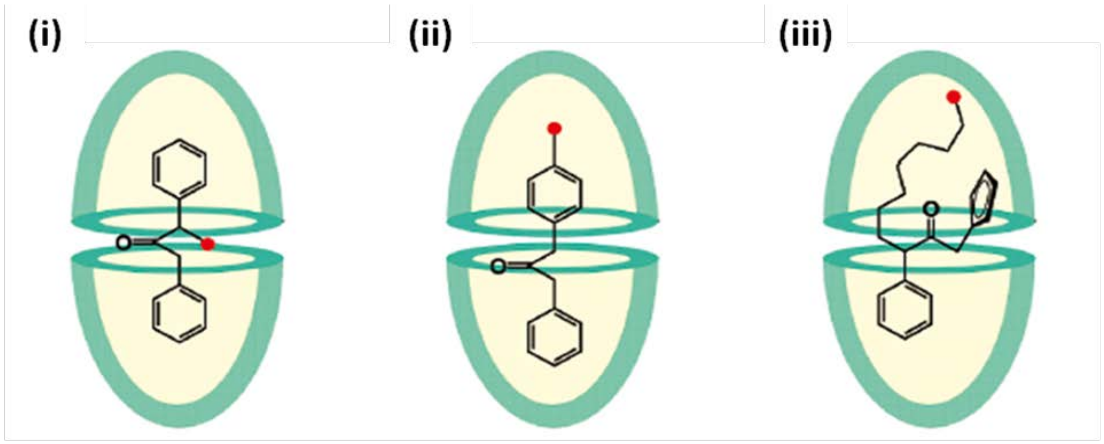

(i)	(ii)	(iii)
$\Delta\delta$ = 0.98 ppm	$\Delta\delta$ = 2.70 ppm	$\Delta\delta$ = 3.60 ppm
$T_{1,d(\text{-Me})}$ = 1.26	$T_{1,d(\text{-Me})}$ = 1.35	$T_{1,d(\text{-Me})}$ = 1.19
$T_{1,obs}[T^{\oplus}]$ = 0.09	$T_{1,obs}[T^{\oplus}]$ = 0.18	$T_{1,obs}[T^{\oplus}]$ = 0.37
$T_{1,p}[T^{\oplus}]$ = 11.03	$T_{1,p}[T^{\oplus}]$ = 4.80	$T_{1,p}[T^{\oplus}]$ = 1.80

Figure 7.8 Cartoon representations of (i) α-methyl dibenzyl ketone@OA_2; (ii) para-methyl dibenzyl ketone@OA_2; and (iii) α-octyl dibenzyl ketone@OA_2. The red ball represents the CH_3 group at the corresponding guest molecule. Relaxation times for -CH_3 protons are given. $\Delta\delta$ is the difference in ^{1}H NMR chemical shift for CH_3 signal in $CDCl_3$ in the absence of OA, and in water in the presence of 2 equiv of OA.

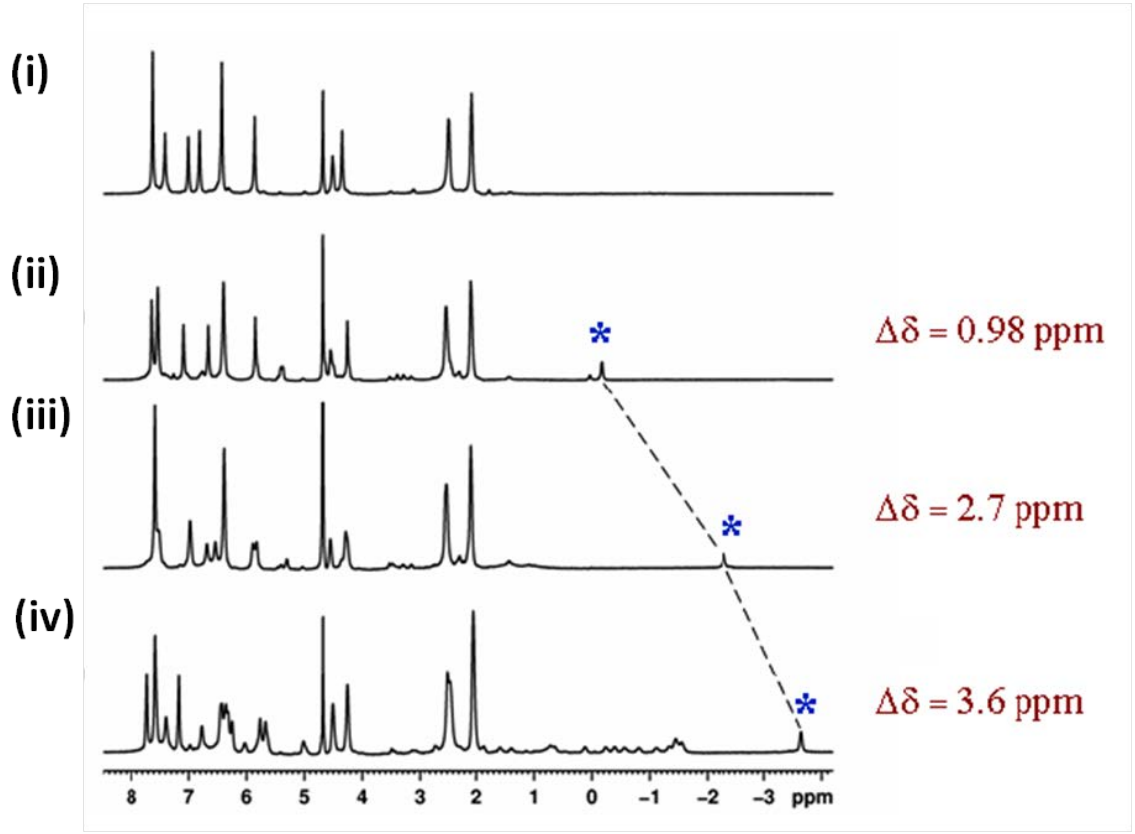

Figure 7.9 ^{1}H NMR spectra (500 MHz, D_2O) of (i) OA, (ii) α-methyl dibenzyl ketone @OA_2, (iii) *para*-methyl dibenzyl ketone @OA_2 and (iv) α-octyl dibenzyl ketone @OA_2; [guest] = 0.5 mM and [OA] = 1 mM in 10 mM borate buffered D_2O. "*" represents $–CH_3$ proton signals of corresponding guest molecule. Δδ is the difference in chemical shift in $–CH_3$ signal in $CDCl_3$ and inside OA capsule.

7.2.3 Emission study

We further explored the spin-spin communication between two molecules, one was singlet or triplet excited and confined within a cage, and the other free and paramagnetic organic radical by emission study. Guest molecules **1** to **5** (**Scheme 7.1**) show phosphorescence at room temperature in aqueous solution as they have very high rate constants of intersystem crossing from S_1 to T_1. On the other hand guests **6** to **8** (**Scheme 7.1**) with low rate constants for intersystem crossing only fluoresce at room

temperature. As pyrene (**6**) does not phosphoresce, quenching of its triplet states was monitored by its T-T absorption. Nitroxides generally quenche the excited singlet and triplet states of aromatics and carbonyl compounds in solution at room temperature with rate constants > 2×10^9 M^{-1} s^{-1}.[169,185-187] The room temperature emission spectrum of **1**@OA_2 in borate buffer consisted of fluorescence, delayed fluorescence (480 to 520 nm), and phosphorescence (530 to 670 nm **Fig 7.10(i)**). The phosphorescence intensity of **1**@OA_2 was significantly reduced with increasing concentration of nitroxide $T^{\oplus}$ in nitrogen saturated buffer solution. Consistent with the steady state emission data, excited triplet state lifetime was also reduced in presence of $T^{\oplus}$ (**Fig 7.11(i)**). The quenching rate constants were calculated from the slope of the plots of the pseudo-first order decay rate constants ($1/\tau$) of **1** triplet states *vs* the $T^{\oplus}$ concentration.

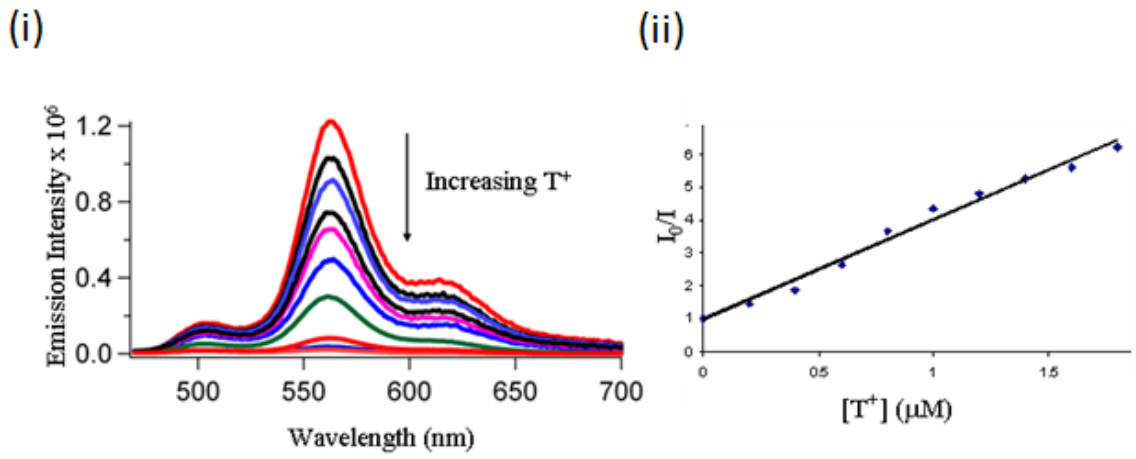

Figure 7.10 (i) Steady state phosphorescence titration of **1**@OA_2 with $T^{\oplus}$and (ii) Stern-Volmer plot for phosphorescence quenching of **1**@ OA_2 by $T^{\oplus}$. λ_{ex} = 320 nm, [**1**]= 1×10^{-5} M, [OA] = 2×10^{-5} M and [$T^{\oplus}$] = 0 to 2 μM.

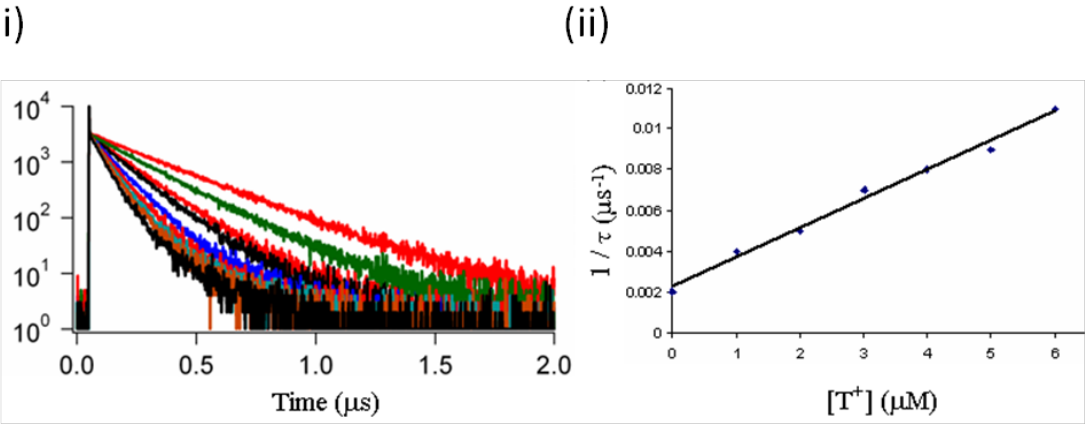

Figure 7.11 (i) Time resolved phosphorescence titration of **1**@OA_2 with $T^{\oplus}$and (ii) phosphorescence decay constant of **1**@OA_2 at different concentration of $T^{\oplus}$. λ_{ex} = 320 nm, λ_{em} = 560 nm, [**1**]= $1x10^{-5}$ M, [OA] = $2x10^{-5}$ M and [$T^{\oplus}$] = 0 to 6 μM.

Quenching rate constants obtained by both the steady state and time resolved methods were identical within the limits of experimental error ($(1.5 \pm 0.2) \times 10^9$ M^{-1} s^{-1}). The linear plots with identical slopes in Stern-Volmer plots of I_0/I *vs* [$T^{\oplus}$] and $1/\tau$ *vs* [$T^{\oplus}$] (**Fig 7.10(ii)** and **Fig 7.11(ii)**) were consistent with a dynamic quenching process. **Fig 7.12** shows the emission of **1**@OA_2 in presence of $T^{\oplus}$ and $T^{\oplus}$@CB8. The phosphorescence of **1**@OA_2 quenched by $T^{\oplus}$ was fully recovered upon addition of CB8 because $T^{\oplus}$@CB8 was unable to interact with excited states of **1** included within OA capsule, thereby signifying that only free $T^{\oplus}$ located at the wall of OA capsule can quench the triplet of **1**.

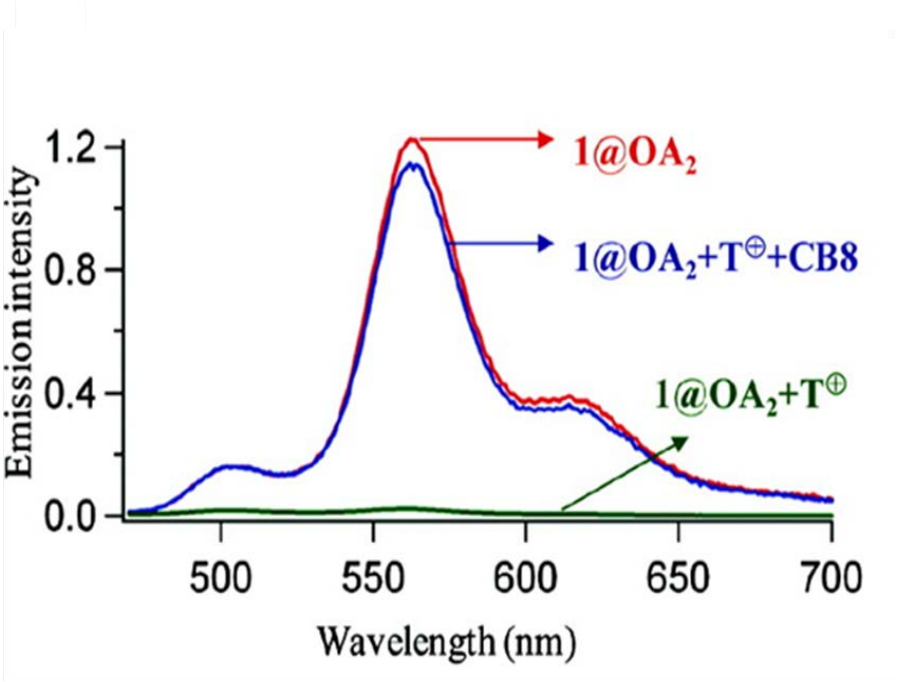

Figure 7.12 Phosphorescence quenching of **1**@OA_2 by $T^{\oplus}$ and recovery of phosphorescence upon addition of CB8; [**1**] = 1×10^{-5} M, [OA] = 2×10^{-5} M, [$T^{\oplus}$] = 2×10^{-5} M, and [CB8] = 2×10^{-5} M

Similar results were observed in the case of guests **2** to **4** (**Scheme 7.1**) probes. In all the cases it was observed that phosphorescence of the probes encapsulated within OA capsule was quenched in presence of $T^{\oplus}$ (**Fig 7.13, Fig 7.15** and **Fig 7.17**). The triplet life time of the guests was also reduced with increasing concentration of $T^{\oplus}$ suggesting that the quenching was dynamic in all the cases of these guests (**Fig 7.14, Fig 7.16** and **Fig 7.18**).

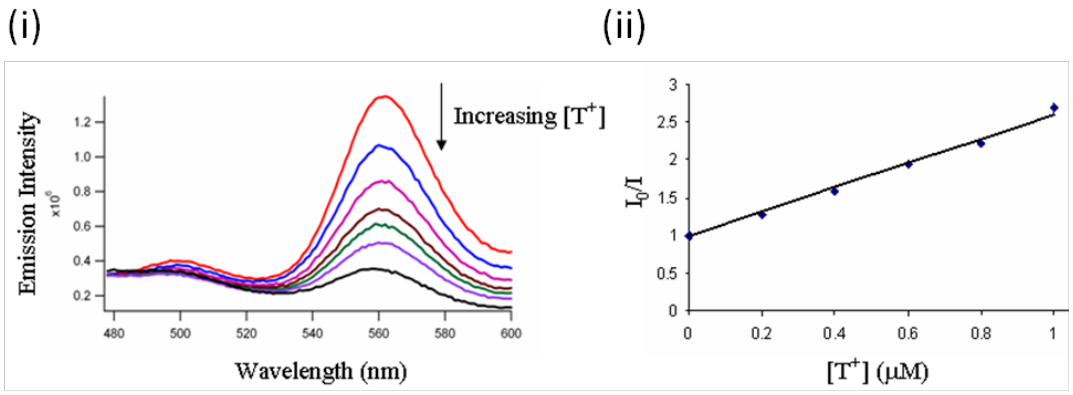

Figure 7.13 (i) Steady state phosphorescence titration of **2**@OA_2 with $T^{\oplus}$and (ii) Stern-Volmer plot for phosphorescence quenching of **2**@ OA_2 by $T^{\oplus}$. λ_{ex} = 300 nm, [**2**]= $1x10^{-5}$ M, [OA] = $2x10^{-5}$ M and [$T^{\oplus}$] = 0 to 1 μM.

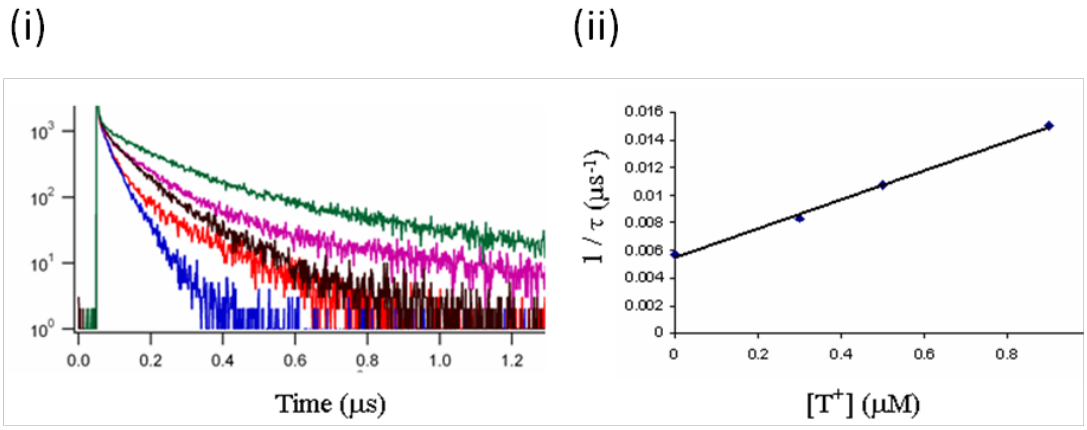

Figure 7.14 (i) Time resolved phosphorescence titration of **2**@OA_2 with $T^{\oplus}$ and (ii) phosphorescence decay constant of **2**@OA_2 at different concentration of $T^{\oplus}$. λ_{ex} = 300 nm, λ_{em} = 560 nm, [**2**]= $1x10^{-5}$ M, [OA] = $2x10^{-5}$ M and [$T^{\oplus}$] = 0 to 1 μM.

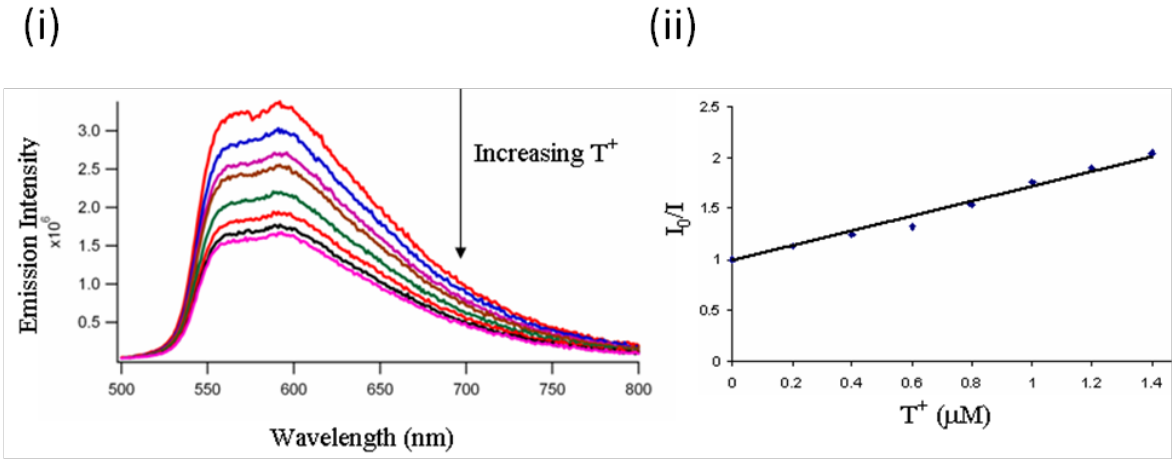

Figure 7.15 (i) Steady state phosphorescence titration of $\mathbf{3}_2$@OA_2 with $T^{\oplus}$ and (ii) Stern-Volmer plot for phosphorescence quenching of $\mathbf{3}_2$@ OA_2 by $T^{\oplus}$. λ_{ex} = 254 nm, [**3**]= $2x10^{-5}$ M, [OA] = $2x10^{-5}$ M and [$T^{\oplus}$] = 0 to 1.4 μM.

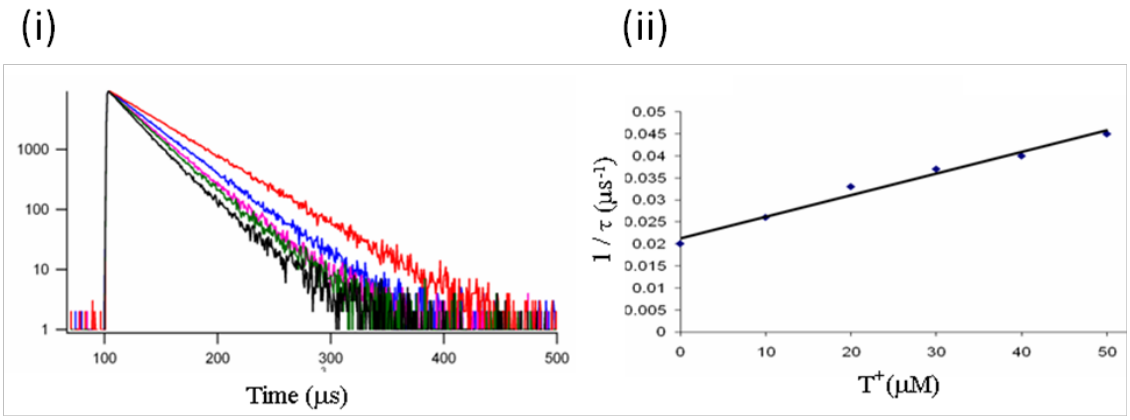

Figure 7.16 (i) Time resolved phosphorescence titration of $\mathbf{3}_2$@OA_2 with $T^{\oplus}$ and (ii) phosphorescence decay constant of $\mathbf{3}_2$@OA_2 at different concentration of $T^{\oplus}$. λ_{ex} = 254 nm, λ_{em} = 600 nm, [**3**]= 10^{-4} M, [OA] = 10^{-4} M and [$T^{\oplus}$] = 0 to 50 μM.

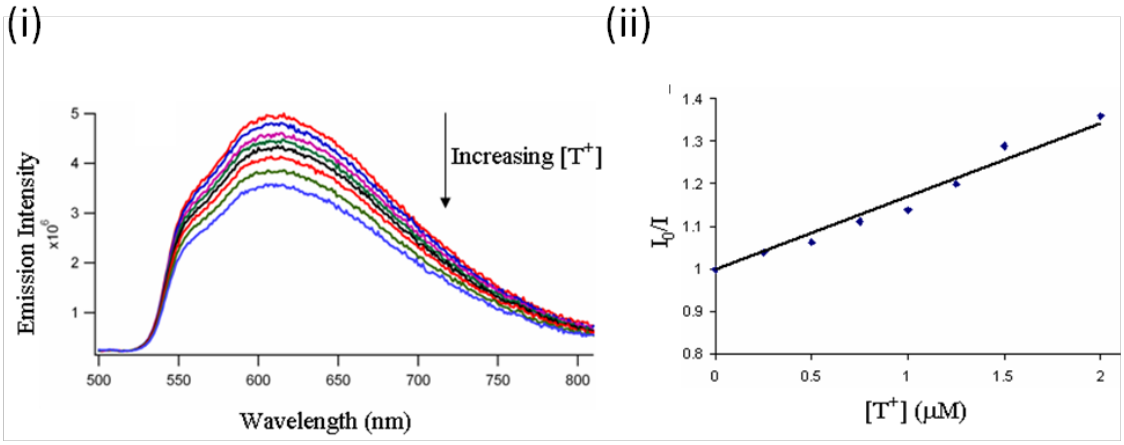

Figure 7.17 (i) Steady state phosphorescence titration of $\mathbf{4}_2$@OA_2 with $T^{\oplus}$ and (ii) Stern-Volmer plot for phosphorescence quenching of $\mathbf{4}_2$@ OA_2 by $\mathbf{T}^{\oplus}$. λ_{ex} = 254 nm, [**4**]= $2x10^{-5}$ M, [OA] = $2x10^{-5}$ M and [$T^{\oplus}$] = 0 to 2 μM.

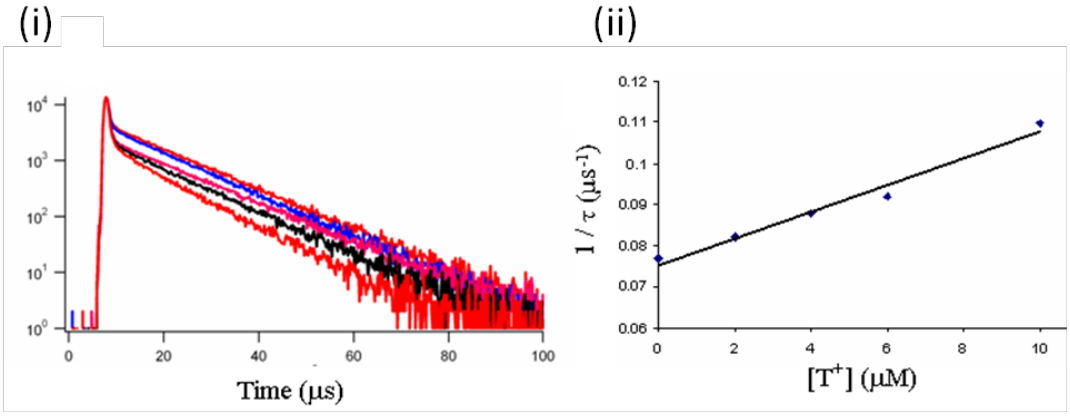

Figure 7.18 (i) Time resolved phosphorescence titration of $\mathbf{4}_2$@OA_2 with $T^{\oplus}$ and (ii) phosphorescence decay constant of $\mathbf{4}_2$@OA_2 at different concentration of $T^{\oplus}$. λ_{ex} = 254 nm, λ_{em} = 600 nm, [**4**]= $2x10^{-5}$ M, [OA] = $2x10^{-5}$ M and [$T^{\oplus}$] = 0 to 10 μM.

On the other hand, in the case of excited triplet **5** and singlet **6** to **8** (**Scheme 7.1**), only the emission intensity and not the excited state lifetime were influenced by the concentration of $T^{\oplus}$ (**Fig 7.19** to **Fig 7.22**). The above results suggested that the quenching of excited triplet **5** and singlet **6** to **8** by $T^{\oplus}$ was a static process.

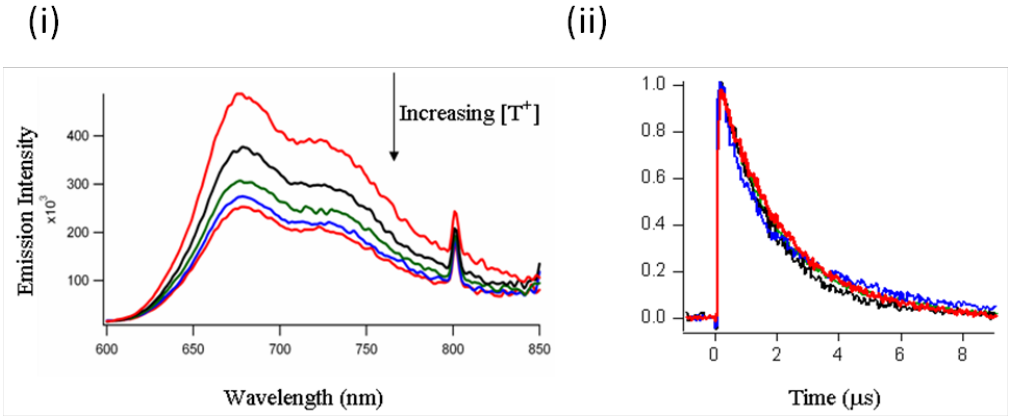

Figure 7.19 (i) Steady state phosphorescence titration of **5**@OA_2 with $T^{\oplus}$ and (ii) time resolved phosphorescence titration of **5**@OA_2 with $T^{\oplus}$. λ_{ex} = 400 nm, λ_{em} = 675 nm, [**5**]= 1x10^{-5} M, [OA] = 2x10^{-5} M and [$T^{\oplus}$] = 0 to 10 μM.

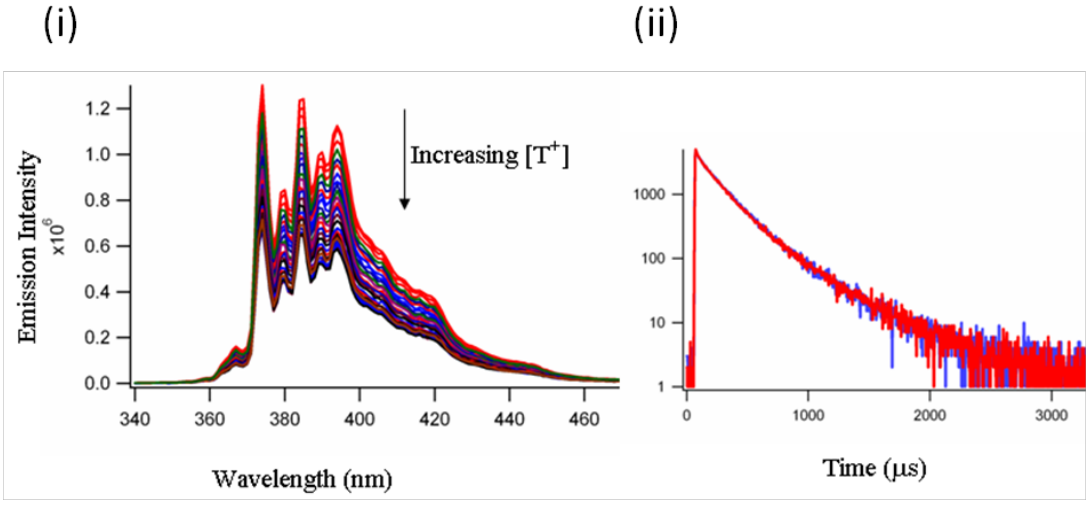

Figure 7.20 (i) Steady state fluorescence titration of **6**@OA_2 with $T^{\oplus}$ and (ii) time resolved phosphorescence titration of **6**@OA_2 with $T^{\oplus}$. λ_{ex} = 320 nm, λ_{em} = 375 nm, [**6**]= 1x10^{-5} M, [OA] = 2x10^{-5} M and [$T^{\oplus}$] = 0 to 20 μM.

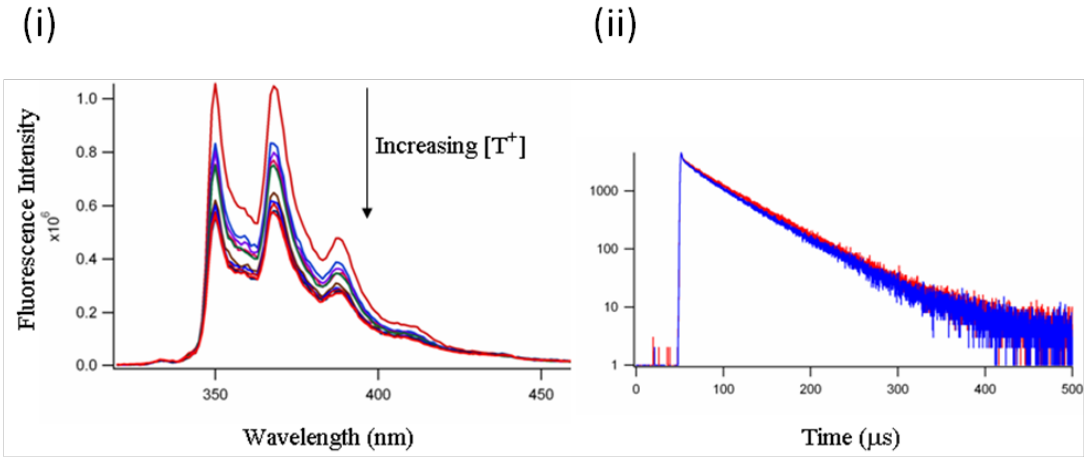

Figure 7.21 (i) Steady state fluorescence titration of **7**@OA_2 with $T^{\oplus}$ and (ii) time resolved phosphorescence quenching of **7**@ OA_2 by $\mathbf{T}^{\oplus}$. λ_{ex} = 300 nm, λ_{em} = 350 nm, [**7**]= $1x10^{-5}$ M, [OA] = $2x10^{-5}$ M and [$T^{\oplus}$] = 0 to 20 μM.

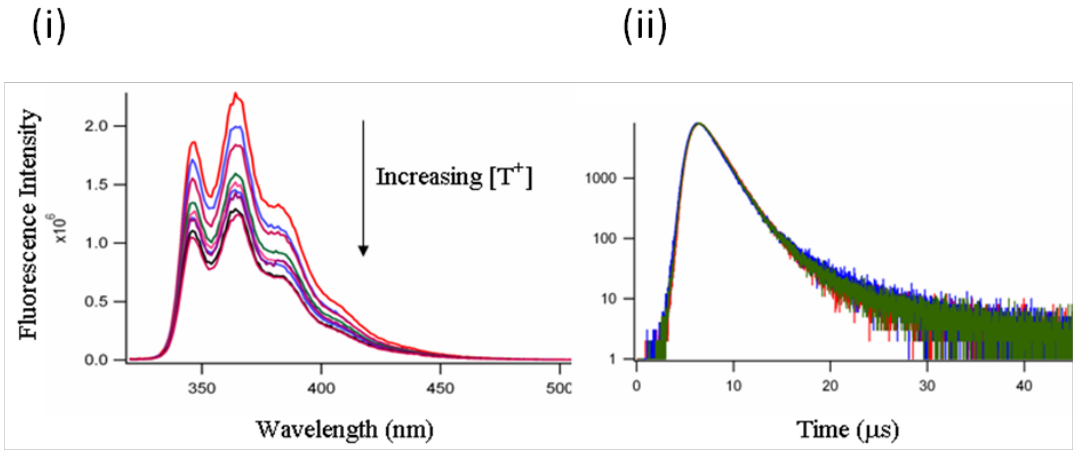

Figure 7.22 (i) Steady state fluorescence titration of **8**@OA_2 with $T^{\oplus}$ and (ii) time resolved fluorescence titration of **8**@OA_2 with $T^{\oplus}$. λ_{ex} = 320 nm, λ_{em} = 350 nm, [**8**]= $1x10^{-5}$ M, [OA] = $2x10^{-5}$ M and [$T^{\oplus}$] = 0 to 20 μM.

Phosphorescence spectra of **1**@OA_2 alone and in the presence of $T^{\oplus}$, T, and $T^{\ominus}$ are presented in **Fig 7.23**. $T^{\oplus}$ quenched the phosphorescence significantly, $T^{\ominus}$ quenched the least and quenching by neutral T was in between that of $T^{\oplus}$ and $T^{\ominus}$. Because of the electrostatic repulsion $T^{\ominus}$ did not interact with **1**@OA_2. As expected, the ability of T to quench was in between that of $T^{\oplus}$ and $T^{\ominus}$.

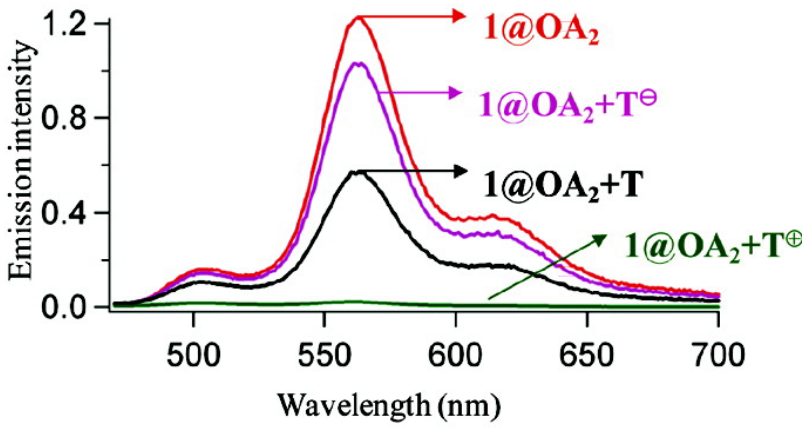

Figure 7.23 Comparison of **1**@OA_2 quenching by $T^{\oplus}$, T, and $T^{\ominus}$; [**1**] = 1×10^{-5} M, [OA] = 2×10^{-5} M, $[T^{\oplus}] = [T] = [T^{\ominus}] = 2 \times 10^{-5}$ M.

The quenching study of the emission of guests **1** to **8** (**Scheme 7.1**) within the OA capsule by T was carried out and results are provided in **Fig 7.24** to **Fig 7.36**. It was observed that both the steady state and the time resolved phosphorescence of the guests **1** to **4** (**Scheme 7.1**), encapsulated within OA capsule, were quenched by T (**Fig 7.24** to **Fig 7.31**). The above results suggested that T quenched the excited triplet of **1** to **4** (**Scheme 7.1**), confined in OA capsule, through a dynamic quenching process. In the case of other guests, **5** to **8** that showed static quenching by $T^{\oplus}$, did not quenched at all by T (**Fig 7.32** to **Fig 7.36**).

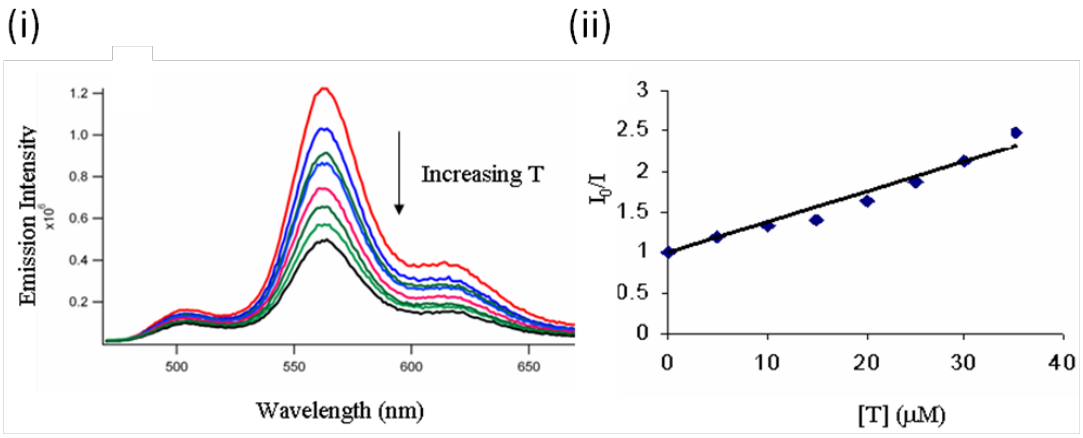

Figure 7.24 (i) Steady state phosphorescence titration of **1**@OA_2 with T and (ii) Stern-Volmer plot for phosphorescence quenching of **1**@ OA_2 by T. λ_{ex} = 320 nm, [**1**]= $1x10^{-5}$ M, [OA] = $2x10^{-5}$ M and [T] = 0 to 35 μM.

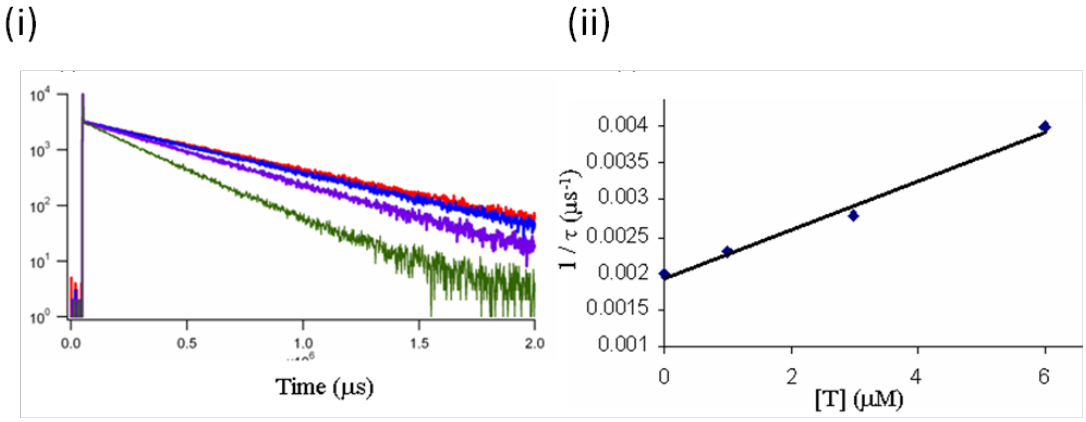

Figure 7.25 (i) Time resolved phosphorescence titration of **1**@OA_2 with T and (ii) phosphorescence decay constant of **1**@OA_2 at different concentration of T. λ_{ex} = 320 nm, λ_{em} = 560 nm, [**1**]= $1x10^{-5}$ M, [OA] = $2x10^{-5}$ M and [T] = 0 to 6 μM.

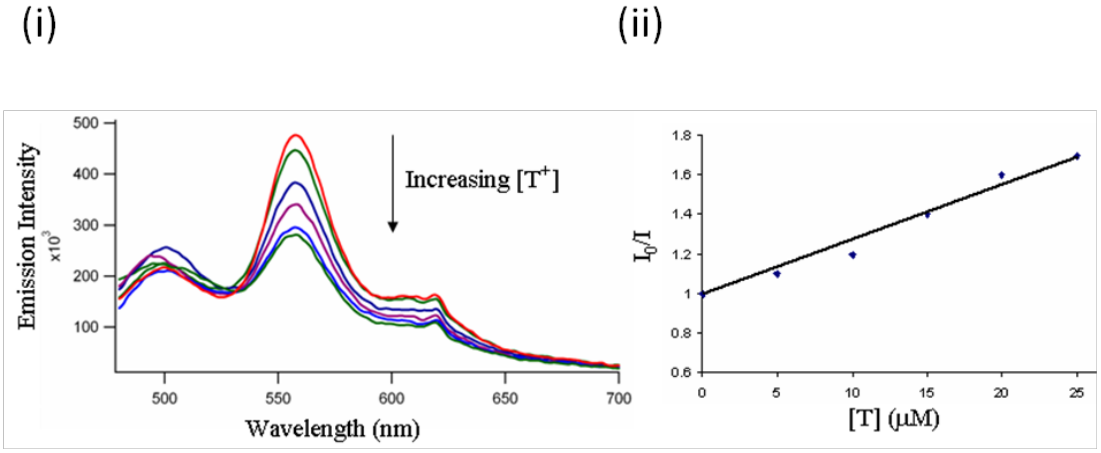

Figure 7.26 (a) Steady state phosphorescence titration of **2**@OA_2 with T and (b) Stern-Volmer plot for phosphorescence quenching of **2**@ OA_2 by T. λ_{ex} = 320 nm, [**2**]= $1x10^{-5}$ M, [OA] = $2x10^{-5}$ M and [T] = 0 to 25 μM.

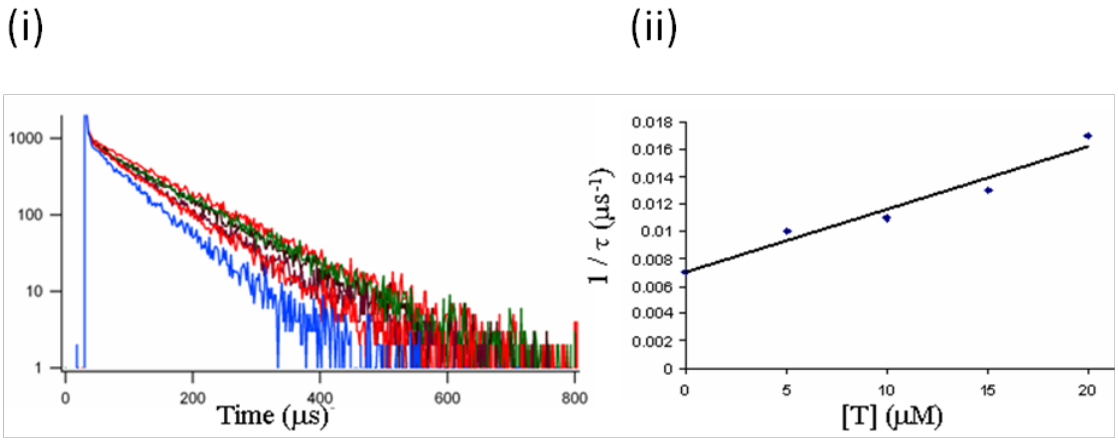

Figure 7.27 (i) Time resolved phosphorescence titration of **2**@OA_2 with T and (ii) phosphorescence decay constant of **2**@OA_2 at different concentration of T. λ_{ex} = 320 nm, λ_{em} = 560 nm, [**2**]= $1x10^{-5}$ M, [OA] = $2x10^{-5}$ M and [T] = 0 to 20 μM.

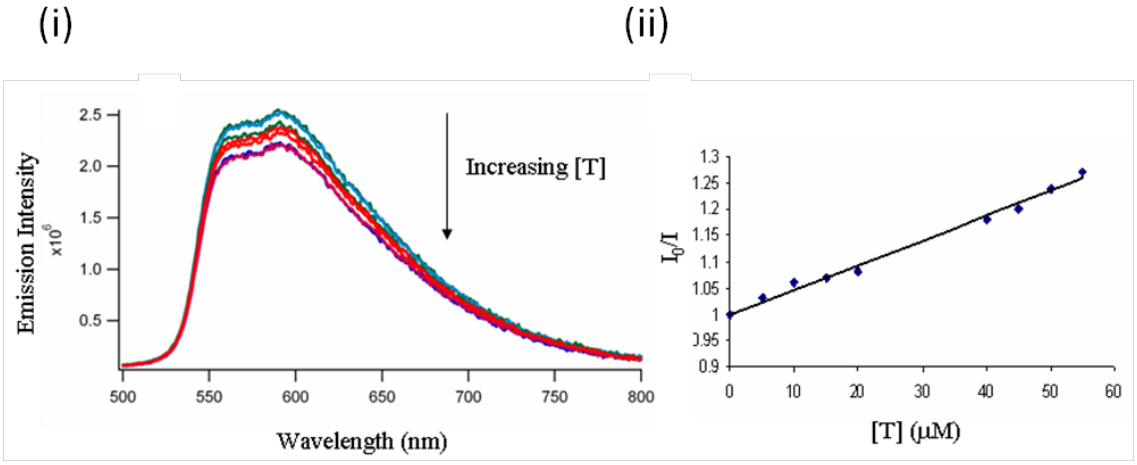

Figure 7.28 (i) Steady state phosphorescence titration of $\mathbf{3}_2$@OA_2 with T and (ii) Stern-Volmer plot for phosphorescence quenching of $\mathbf{3}_2$@ OA_2 by T. λ_{ex} = 254 nm, [**3**]= $2x10^{-5}$ M, [OA] = $2x10^{-5}$ M and [T] = 0 to 60 μM.

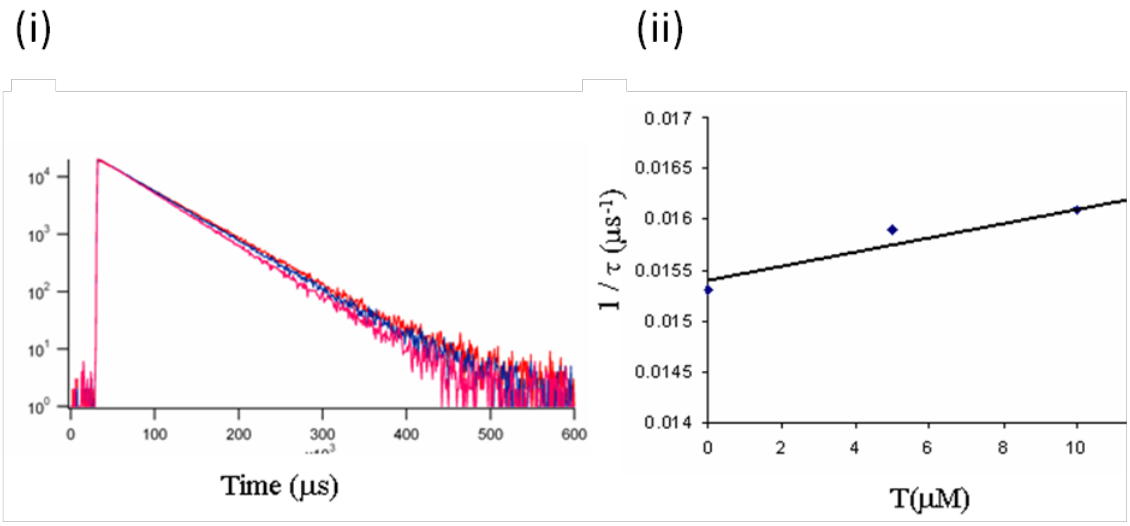

Figure 7.29 (i) Time resolved phosphorescence titration of $\mathbf{3}_2$@OA_2 with T and (ii) phosphorescence decay constant of $\mathbf{3}_2$@OA_2 at different concentration of T. λ_{ex} = 254 nm, λ_{em} = 600 nm, [**3**]= $2x10^{-5}$ M, [OA] = $2x10^{-5}$ M and [T] = 0 to 10 μM.

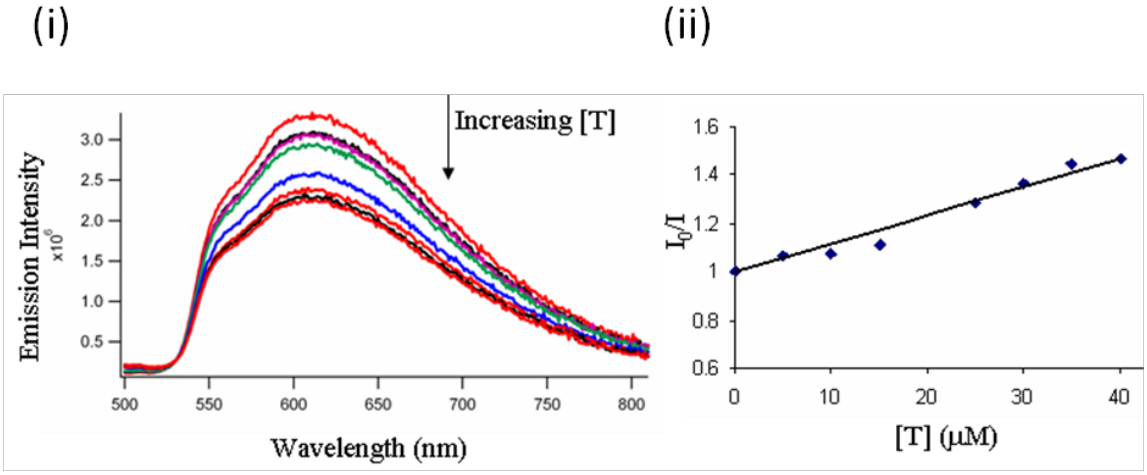

Figure 7.30 (i) Steady state phosphorescence titration of $\mathbf{4}_2$@OA_2 with T and (ii) Stern-Volmer plot for phosphorescence quenching of $\mathbf{4}_2$@ OA_2 by T. λ_{ex} = 254 nm, [**4**]= $2x10^{-5}$ M, [OA] = $2x10^{-5}$ M and [T] = 0 to 40 μM.

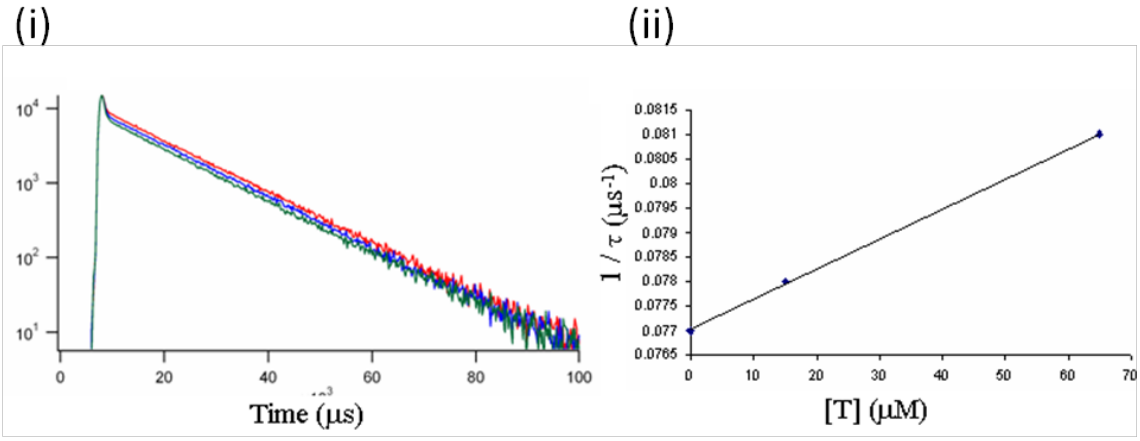

Figure 7.31 (i) Time resolved phosphorescence titration of $\mathbf{4}_2$@OA_2 with T and (ii) phosphorescence decay constant of $\mathbf{4}_2$@OA_2 at different concentration of T. λ_{ex} = 254 nm, λ_{em} = 625 nm, [**4**]= $2x10^{-5}$ M, [OA] = $2x10^{-5}$ M and [T] = 0 to 65 μM.

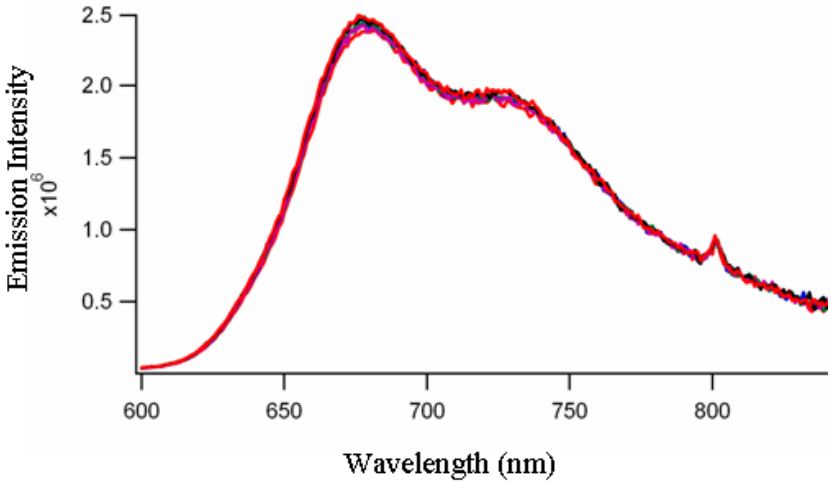

Figure 7.32 Steady state phosphorescence titration of **5**@OA_2 with T. λ_{ex} = 400 nm, [**5**] = $1x10^{-5}$ M, [OA] = $2x10^{-5}$ M and [T] = 0 to 50 μM.

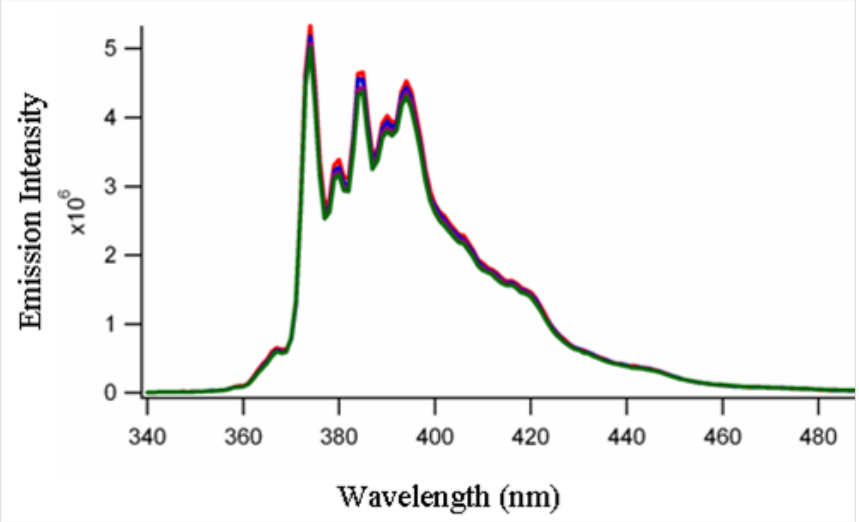

Figure 7.33 Steady state fluorescence titration of **6**@OA_2 with T. λ_{ex} = 320 nm, [**6**] = $1x10^{-5}$ M, [OA] = $2x10^{-5}$ M and [T] = 0 to 50 μM.

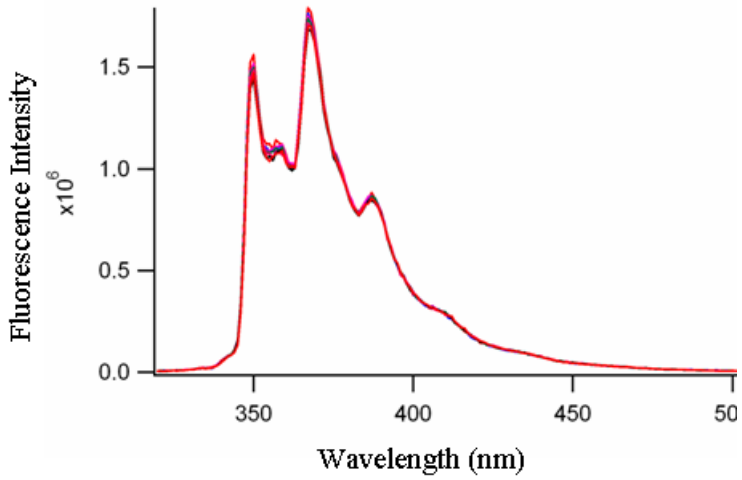

Figure 7.34 Steady state fluorescence titration of **7**@OA_2 with T. λ_{ex} = 300 nm, [**7**] = $1x10^{-5}$ M, [OA] = $2x10^{-5}$ M and [T] = 0 to 50 μM.

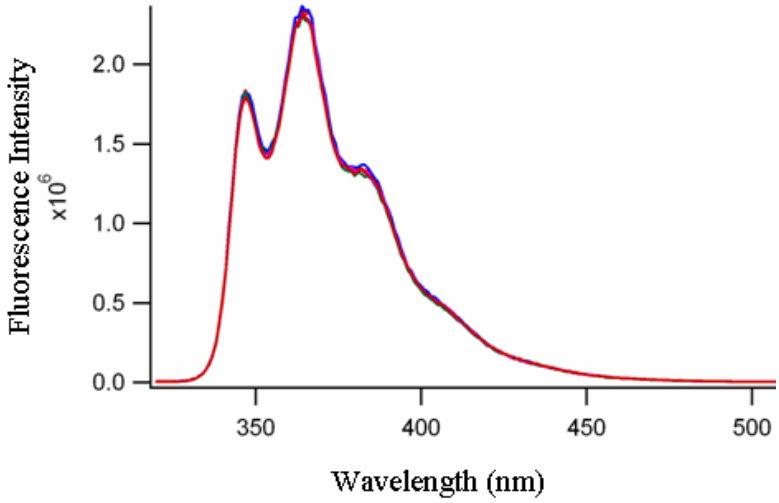

Figure 7.35 Steady state fluorescence titration of **8**@OA_2 with T**.** λ_{ex} = 300 nm, [**8**] = $1x10^{-5}$ M, [OA] = $2x10^{-5}$ M and [T] = 0 to 50 μM.

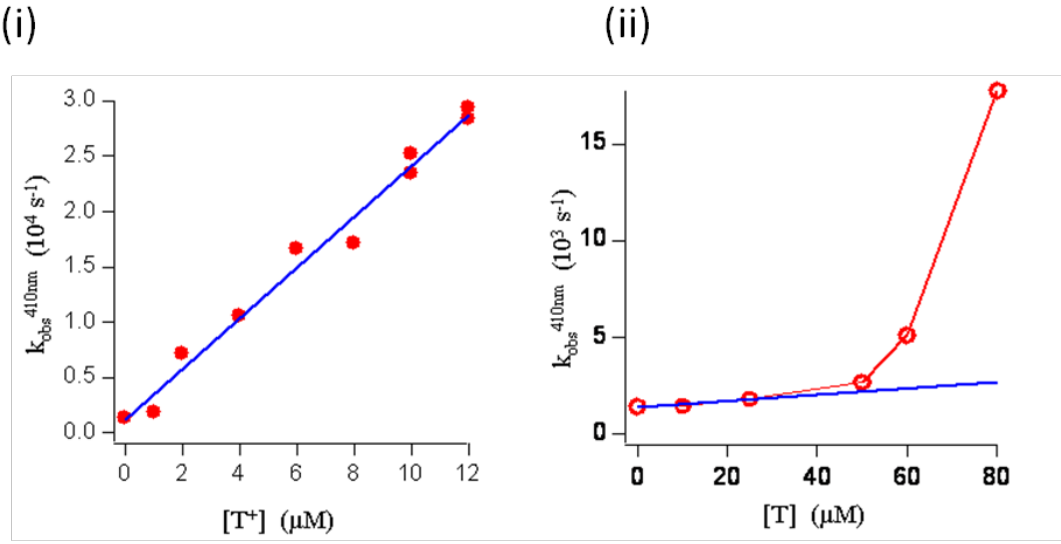

Figure 7.36 Time resolved triplet-triplet absorption titration of **6**@OA_2 with (i) $T^{\oplus}$ and (ii) T, [**6**]= $1x10^{-5}$ M, [OA] = $2x10^{-5}$ M, [$T^{\oplus}$] = 0 to 12 μM and [T] = 0 to 80 μM.

The quenching constant values of all the complexes with $T^{\oplus}$ and T are consolidated in **Table 7.3**. There are two sets of molecules: (i) triplet of **1** to **4** and **6** that were quenched mostly by a dynamic process by $T^{\oplus}$ when enclosed within OA capsule; and (ii) triplet of **5** and excited singlet **6** to **8** enclosed within OA capsule which exhibit quenching by $T^{\oplus}$ from a static process only. All quenching constants in **Table 7.3** are estimated from triplet decays that were monitored by either phosphorescence or T-T absorption corresponding to a dynamic process. Closer examination of **Table 7.3** implies that the lifetime of the excited state of the guests plays a role in the overall deactivation of excited states by $T^{\oplus}$. Guest molecules enclosed within OA capsule with lifetimes shorter than 5 μs were quenched only by a static process. It is also important to note that

the guest molecules, whose lifetimes are in between 17 and 922 μs, were quenched by $T^{\oplus}$ with similar rate constants.

To understand the details of the quenching rate constant (k_q), one needs to know what exactly the measured k_q represents. The deactivation of excited guest by $T^{\oplus}$ presented in **Scheme 7.3** involves the formation of the complex between $T^{\oplus}$ and excited guest@OA capsuleplex controlled by the diffusion constant (k_{diff}). Its decomplexation without quenching is controlled by k_{-diff}; diffusion out of the encounter complex without deactivation. Deactivation of the excited guest by $T^{\oplus}$ within the encounter complex is controlled by k_{deact}.[6,188,189] The measured quenching rate constant k_q is given by equation 1 (**Scheme 7.3**). While k_{diff} would be the diffusion rate constant in water, that is 7.4×10^9 M^{-1} s^{-1} at 25 °C, the k_{-diff} value would be expected to be much smaller than k_{diff} as there is strong Coulombic attraction between the negatively charged capsule and the positively charged $T^{\oplus}$. If we assume that $k_{deact} \gg k_{\_diff}$, then k_q would be given by equation 2. Under this condition, if we take spins of the triplet excited guest and the paramagnetic quencher into account, the measured quenching constant k_q would be expected to be $(1/3)k_{diff}$. The quenching of the triplet by a doublet nitroxide will result in doublet and quartet state collision complexes at the proper spin statistical ratios of 1/3 and 2/3. Among these two types of collision complexes, only the doublet complex that formed at $(1/3)k_{diff}$ will lead to quenching. It is satisfying that the measured quenching constants (kq) for triplets of **1** to **4** and **6** are in this range. Thus, in the case of positively charged quencher, $T^{\oplus}$, 1/3 of encounter leads to quenching. While the lifetime as well as the intensity of emission were dependent on the concentration of $T^{\oplus}$, quenching must be dynamic in character.

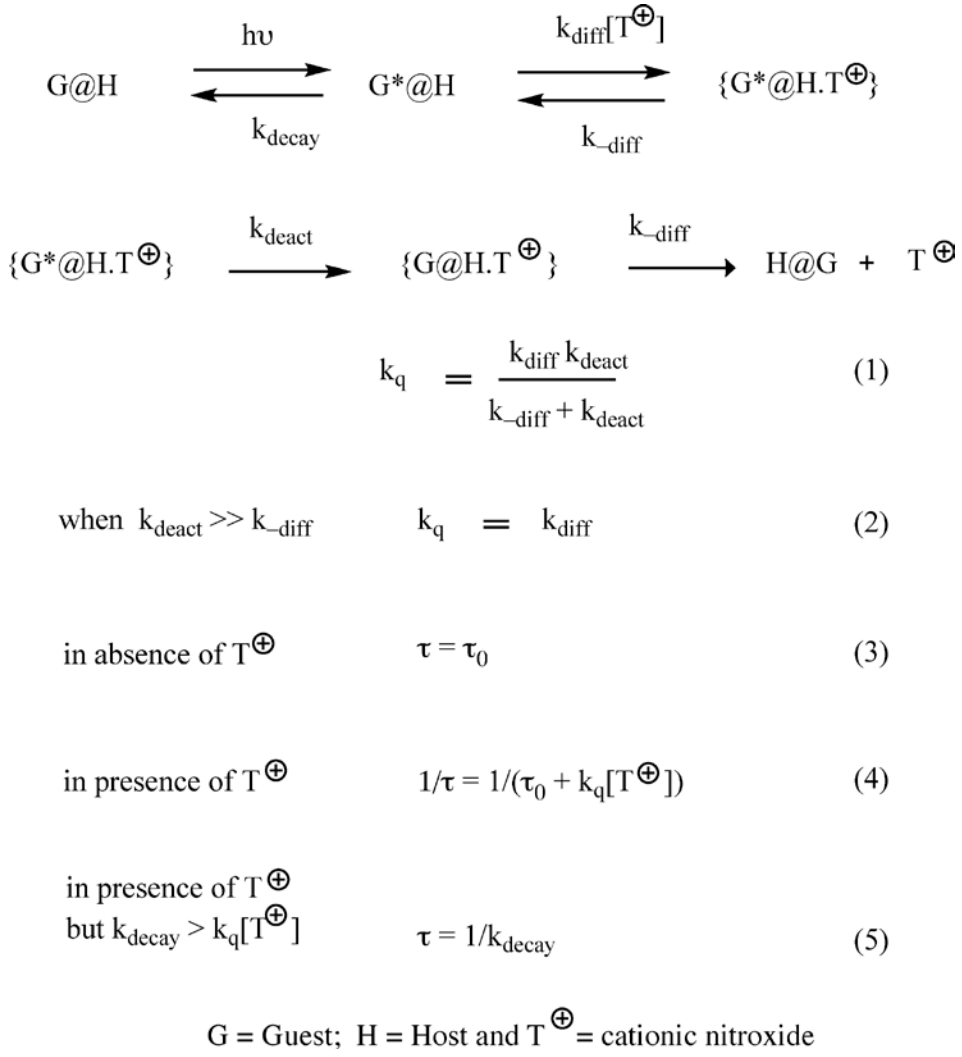

Scheme 7.3 The deactivation pathway of the guest excited state by $T^{\oplus}$

Quenching rate constants of the excited states of **1** to **8** (**Scheme 7.1**) encapsulated within OA capsule by the neutral nitroxide (T) are presented in **Table 7.3**. The quenching of triplet **1**–**4** and **6** included within OA capsule by T was roughly an order of magnitude lower than that by $T^{\oplus}$. In solution where the excited aromatics and ketones are free, the quenching by neutral nitroxides is nearly diffusion controlled and the quenching numbers

for guests enclosed within OA capsule were around two orders of magnitude lower. This lower number is consistent with the predictable lower rate of quenching by a mechanism needed overlap between the excited guest and the quencher (charge transfer and/or exchange process). Results observed here are consistent with the conclusion that nitroxides can quench the excited guest molecule despite they are separated by a molecular wall and the lack of direct orbital overlap between these two molecules. The upper limit for the quenching of triplet **1** to **4** and **6** by anionic nitroxide ($T^{\ominus}$) was estimated to be ~10^5 M^{-1} s^{-1}.

Table 7.3 Excited state lifetime (τ_0) and nitroxide ($T^{\oplus}$ and T, **Scheme 7.1**) quenching data for capsuleplexes made up of OA and organic guests **1-8** listed in **Scheme 7.1.**

Guests	Excited state type	Lifetime in OA (μs)	Quenching by $T^{\oplus}$ in OA (%)[a]	k_q ($T^{\oplus}$) in OA (M^{-1} s^{-1})	Quenching by T in OA (%)[b]	k_q (T) in OA (M^{-1} s^{-1})	k_q (T) in acetonitrile (M^{-1} s^{-1})
6	T_1	922	[c]	$(2.3 \pm 0.1) \times 10^9$	[c]	$(1.6 \pm 0.5) \times 10^7$	[c]
1	T_1	596	77	$(1.5 \pm 0.2) \times 10^9$	17	$(2 \pm 1) \times 10^8$	2.3×10^9
2	T_1	151	63	$(1.1 \pm 0.2) \times 10^9$	10	$(4 \pm 0.8) \times 10^7$	3.5×10^9
3	T_1	65	43	$(1 \pm 0.6) \times 10^9$	8	$(7 \pm 2) \times 10^7$	[d]
4	T_1	17	29	$(2 \pm 0.5) \times 10^9$	7	$(6 \pm 2) \times 10^7$	[d]
5	T_1	4.8	13	[e]	0	-------	[d]
6	S_1	0.34	13	[e]	0	-------	1×10^{10}
7	S_1	0.05	11	[e]	0	-------	1.3×10^{10}
8	S_1	0.01	15	[e]	0	-------	1×10^{10}

[a]Determined by comparing the luminescence intensity (λ_{max}) of the capsuleplex recorded in absence and presence of 1 μM of $T^{\oplus}$.

[b]Determined by comparing the luminescence intensity (λ_{max}) of the capsuleplex recorded in absence and presence of 5 μM of T.

[c]Since **6** did not show phosphorescence at room temperature, measurements could not be made.

[d]k_q could not be determined because of self-quenching of thioketones in solution.

[e]k_q could not be determined because the lifetime of the guest molecules did not change with addition of $T^{\oplus}$.

7.2.4 Polarization transfer from the excited triplet state of an incarcerated ketone within a OA capsule to a nitroxide in the aqueous solution

The quenching of triplet states of ketones by nitroxides often generates spin-polarized nitroxides, which can be monitored by time-resolved electron paramagnetic resonance (TR-EPR) spectroscopy. Our next experiments were aimed to investigate whether spin polarization of nitroxides is also observable in the quenching processes, where the triplet ketone and the nitroxide are separated by a molecular wall (OA).

We selected 4,4′-dimethyl benzil (**1**) and the thioxanthone derivative **9** (**Scheme 7.1**) as ketones. Both the ketones have been shown to form 2:1 complexes with OA.[168,190] Efficient triplet quenching of **1**@OA_2 by $T^{\oplus}$ has been demonstrated by phosphorescence measurements (**Fig 7.10**). As **9**@OA_2 did not show only measurable phosphoresce at room temperature, laser flash photolysis experiments were performed to monitor the quenching efficiency of **9**@OA_2 triplet states by $T^{\oplus}$. Excitation of **9**@OA_2 with laser pulses (355 nm, 5 ns pulse width) generated the transient absorption spectrum shown in **Fig 7.39(i)**. The transient absorption with λ_{max} at 650 nm was assigned to the triplet state of **9** based on reported literatures.[168,191] In the presence of two equivalents of $T^{\oplus}$, the triplet state of **9** was reduced to approximately half of its original value (**Fig 7.39(ii)**) suggesting that **9**@OA_2 triplet states were quenched efficiently by $T^{\oplus}$. The titration of

9@OA_2 with $T^{\oplus}$ in flash photolysis shows the quenching of the triplet excited state of **9** with increasing amounts of $T^{\oplus}$ (**Fig 7.40**).

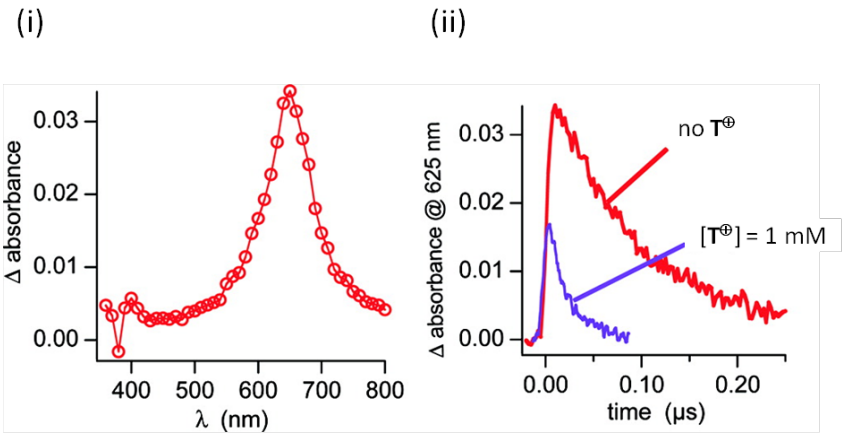

Figure 7.39 (i) Triplet–triplet absorption spectrum of **9**@OA_2 in deoxygenated aqueous buffer solution recorded at the end of the laser pulse (355 nm, 5 ns pulse width). [**9**] = 0.5 mM; [OA] = 1 mM; 10 mM borate buffer; pH = 9. (ii) Transient absorption decay traces at 625 nm in the absence and presence of $T^{\oplus}$ (1 mM).

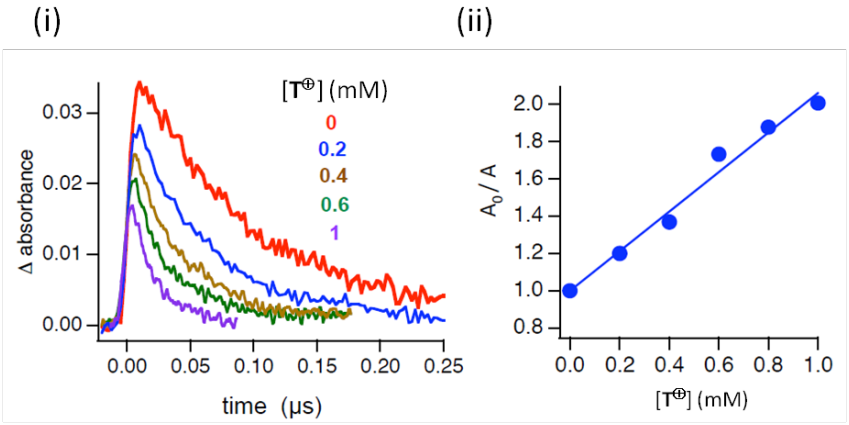

Figure 7.40 (i) Triplet-triplet absorption decay traces of **9**@OA_2 after laser pulse excitation (355 nm, 5 ns pulse width) monitored at 625 nm in the absence and presence of different concentrations of $T^{\oplus}$. Deoxygenated aqueous buffer solutions; [**9**] = 0.5 mM; [OA] = 1 mM; 10 mM borate buffer; pH = 9. (ii) Stern-Volmer plot of the triplet-triplet absorption at the end of the laser pulse in the absence (A_0) and presence of different concentrations of $T^{\oplus}$ (A).

We performed TR-EPR experiments in aqueous solutions of **9**@OA_2 complex in the presence of 20 equiv of $T^{\oplus}$ using pulsed laser excitation (355 nm). An emissive spin-polarized EPR spectrum was observed (**Figure 7.41(i)**). This observed TR-EPR spectrum is in good agreement with the steady-state EPR spectrum of the nitroxide (**Figure 7.41(i)**). As illustrated in **Fig 7.42**, with increasing concentration of $T^{\oplus}$, the TR-EPR signal increased and reached a plateau at an excess of above 20 equiv of $T^{\oplus}$. A spin polarization lifetime of 650 ns was observed at low $T^{\oplus}$ concentrations (0.2 mM), which decreased slightly at higher $T^{\oplus}$ concentrations (550 ns, 10 mM $T^{\oplus}$; **Fig 7.43(i)**). The slight decrease in spin polarization lifetime was probably caused by spin–spin interactions at higher nitroxide concentrations.

TR-EPR experiments of **9**@OA_2 in the presence of the negatively charged nitroxide ($T^{\ominus}$), in contrast to the positively charged $T^{\oplus}$, generated no detectable spin-polarized EPR signal (**Fig 7.43(ii)**). The absence of spin-polarized signals is understandable due to inefficient triplet quenching caused by electrostatic repulsion of the negatively charged nanocapsule and negatively charged nitroxide.

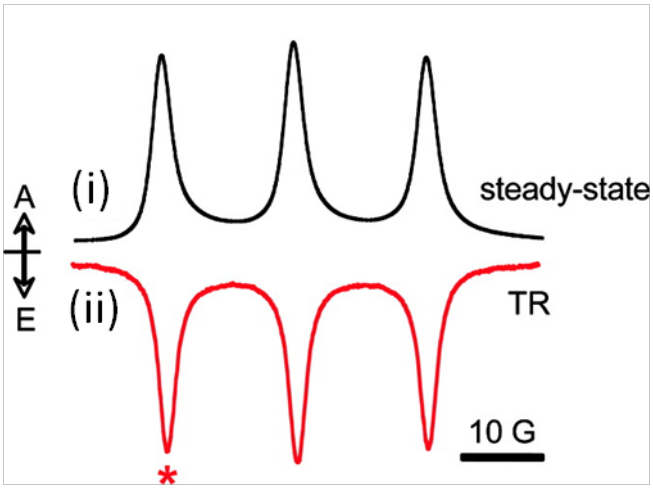

Figure 7.41 Steady-state EPR (i; integrated form) and TR-EPR (ii) spectra of **9**@$OA_2/T^{\oplus}$ solutions recorded 300–500 ns after pulsed laser excitation (355 nm, 5 ns pulse width) in deoxygenated aqueous buffer solutions at room temperature. [**9**] = 0.5 mM; [OA] = 1 mM; [$T^{\oplus}$] = 10 mM; 10 mM borate buffer; pH = 9.

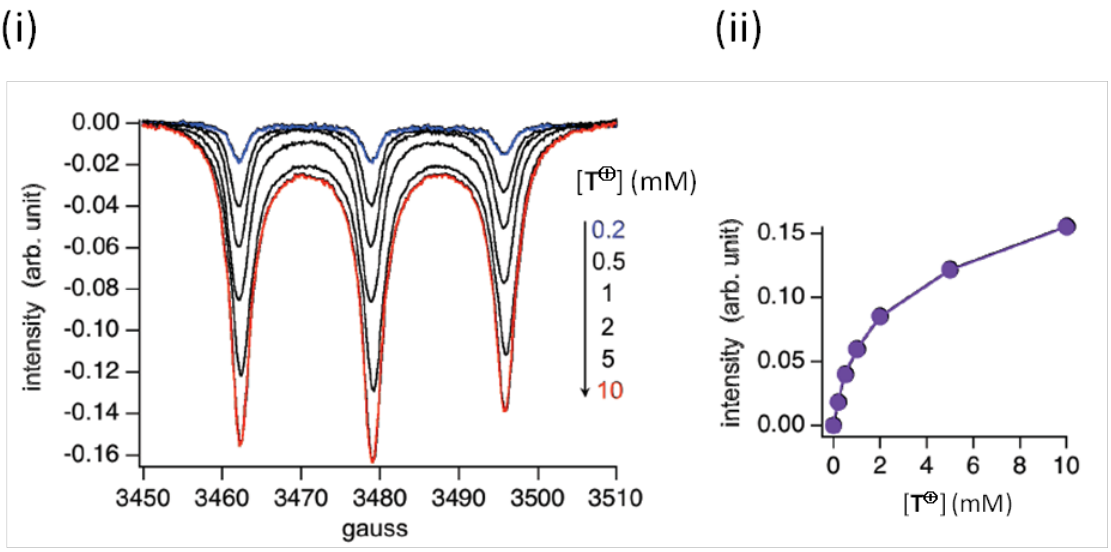

Figure 7.42 (i) TR-EPR spectra of **2**@OA2/$T^{\oplus}$ solutions recorded 100–300 ns after pulsed laser excitation (355 nm, 5 ns pulse width) in deoxygenated aqueous buffer solutions at room temperature. [**2**] = 0.5 mM; [OA] = 1 mM; [$T^{\oplus}$] 0.2 to 10 mM; 10 mM borate buffer; pH = 9. (ii) Spin polarization intensity at 3462 G at different concentrations of $T^{\oplus}$.

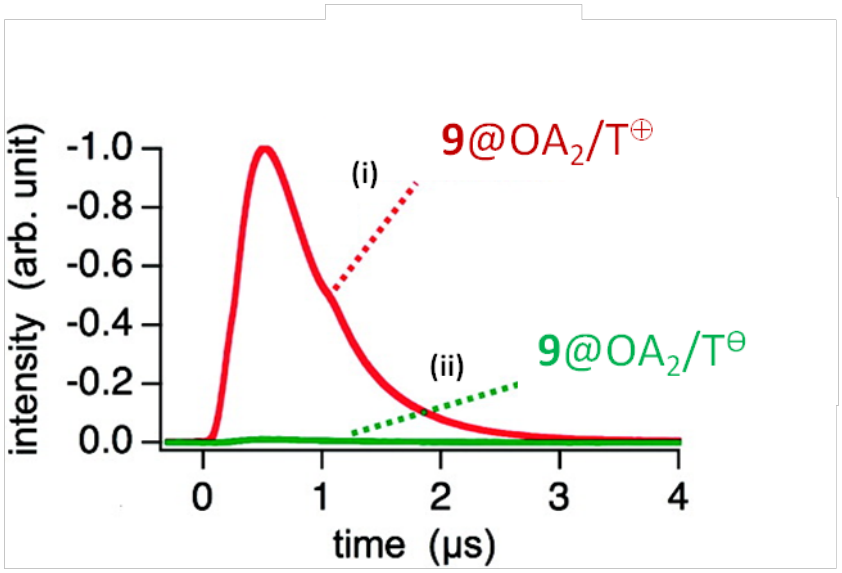

Figure 7.43 Transient EPR kinetic traces of **9**@$OA_2/T^{\oplus}$ (i, red) and **9**@$OA_2/T^{\ominus}$ (ii, green) recorded after pulsed laser excitation. [**9**] = 0.5 mM; [OA] = 1 mM; [$T^{\oplus}$] = 10 mM; [$T^{\ominus}$] = 10 mM.

The above experiments suggested that spin polarization of $T^{\oplus}$ was generated by the quenching of ketone triplet states by $T^{\oplus}$ adsorbed at the external surface of OA. A possible mechanism to generate spin polarization is the triplet spin polarization transfer mechanism[192] (**Scheme 7.4**), where triplet sublevel selective intersystem crossing from singlet excited states (S_1) produces spin-polarized ketone triplet states. This polarization of ketone triplet states is transferred to the nitroxide by electron spin exchange and electron dipole–dipole interaction between the radical and the ketone triplet during the spin interaction process. Due to short lifetime of spin polarization of triplet states (usually several nanoseconds for ketones[193]), the observed fast quenching of triplet states by positively charged $T^{\oplus}$ (observed by laser flash photolysis) and fast buildup of the spin-polarized EPR signal (**Fig 7.43(i)**) supports this mechanism. As emissive spin-polarized

triplet states were generated during intersystem crossing from singlet excited states of **9**[194] (**Scheme 7.1**), an emissive spin-polarized nitroxides was also generated in this transfer mechanism.

The other possible mechanism for generation of polarization is the radical–triplet pair mechanism. This mechanism involves interaction of nonpolarized triplets and doublets (nitroxides), involving the zero-field splitting of the triplet and the hyperfine interaction-mediated mixing of quartet and doublet states.[176] Both mechanisms would generate emissive spin-polarized nitroxides for interaction with triplet states of **9**. The triplet spin polarization transfer mechanism and the radical–triplet pair mechanism can be distinguished by measuring TR-EPR of **1**@OA_2 in presence of $T^{\oplus}$. In contrast to **9**, which generates emissive spin-polarized triplet states (T_{+1}) during intersystem crossing from singlet excited states (S_1), triplet states of **1** are absorptively polarized after photoexcitation (T_{-1}) (**Scheme 7.4**).[194] If we consider that the triplet spin polarization transfer mechanism is active during quenching of triplet states of **1**@OA_2 by $T^{\oplus}$, absorptive spin-polarized nitroxides should be observed. On the other hand, if the radical–triplet pair mechanism dominates, emissive spin polarization of nitroxides should be observed. As shown in **Fig 7.44**, the TR-EPR spectrum after laser excitation of **1**@OA_2 in the presence of $T^{\oplus}$ was absorptively polarized. This observation concluded that the triplet spin polarization transfer mechanism was responsible. The significantly lower signal-to-noise ratio for **1**@OA_2/$T^{\oplus}$ (**Fig 7.44(ii)**) compared to that of **9**@OA_2/$T^{\oplus}$ (**Fig 7.41(ii)**) was because of the poor excitation light absorption of **1** compared to that of **9**.

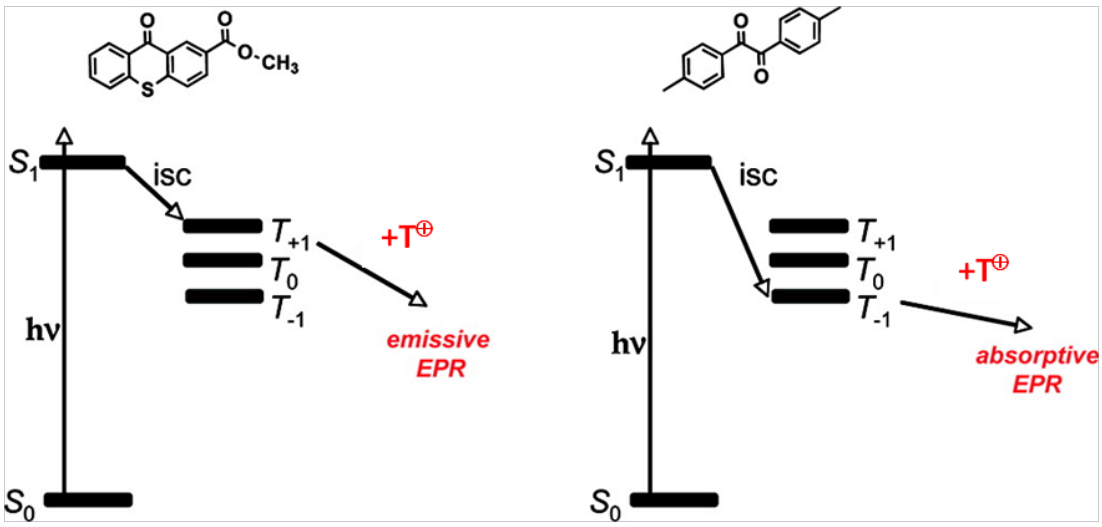

Scheme 7.4 Triplet sublevel selective intersystem crossing generating spin-polarized triplet states.

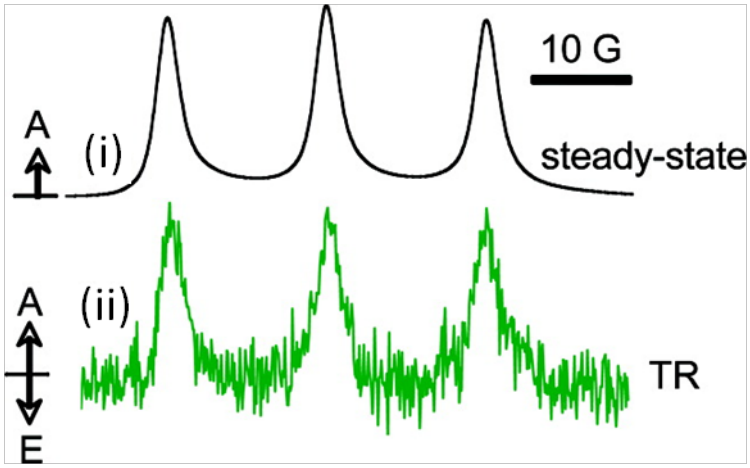

Figure 7.44 Steady-state EPR (i; integrated form) and TR-EPR (ii) spectra of **1**@$OA_2/T^{\oplus}$ solutions recorded 100–300 ns after pulsed laser excitation (308 nm, 15 ns pulse width) in deoxygenated aqueous buffer solutions at room temperature. [**1**] = 0.5 mM; [OA] = 1 mM; [$T^{\oplus}$] = 10 mM; 10 mM borate buffer; pH = 9.

7.3 Conclusion

It is reported that deactivation of electronically excited (singlet and triplet) molecules by nitroxides occurs in solution at close to diffusion limits, and the mechanism is believed to involve exchange and/or charge transfer interaction, although not clearly established. Close interaction between the excited molecule and nitroxide is required in the deactivation by both mechanisms. We have demonstrated that excited molecules encapsulated within a negatively charged (COO^-) organic container could be deactivated by a cationic nitroxide at nearly diffusion controlled rate. Clearly, the existence of a wall between the excited molecule and nitroxide inhibited neither exchange nor charge interaction between them. The rate constant of deactivation is high due to the strong complexation of the encounter complex because of Coulombic interaction between the anionic capsule and cationic nitroxide. Thus, spin–spin communication between a free radical and an excited molecule occurs even without direct overlap of their orbitals. Close interaction between these species was controlled by a second container (cucurbituril). The existence of a double wall between the excited molecule and the nitroxide totally detained the deactivation process. Among the various secondary hosts used such as cucurbituril, calixarene, and cyclodextrin, the best control was achieved with cucurbit[8]uril.

TR-EPR and transient absorption measurements demonstrated that triplet states of ketones (**1** and **9**) incarcerated in a nanocontainer (e.g. OA) were quenched efficiently by nitroxides in the bulk solution. As opposite signs of spin polarization of nitroxides were observed for thioxanthone and benzil derivatives, we concluded that the electron spin

polarization transfer mechanism of spin-polarized triplet states to nitroxides through OA wall was the major operating mechanism for generation of polarized nitroxides.

7.4 Experimental section

Materials and Methods: Guests 4,4'-dimethylbenzil (**1**), benzil (**2**), 4-carboxy-TEMPO ($T^{\ominus}$) and TEMPO (T) were used as received from Sigma-Aldrich/Acros. Camphorthione (**3**), adamantanethione (**4**), xanthione (**5**)[178], 4,4'-dimethyl stilbene (**8**) and cationic nitroxide radical ($T^{\oplus}$)[195] were synthesized following the literature procedures. Pyrene (**6**) and phenanthrene (**7**) (from Sigma-Aldrich/Acros) were recrystallized from EtOH. The hosts octa acid,[40] cucurbit[7]uril,[196] calixarene octasulfonic acid[197] were synthesized following published procedures. β-cyclodextrin and γ-cyclodextrin were purchased from Sigma-Aldrich/Acros.

General protocol for NMR study:

^{1}H NMR studies were carried out on a Bruker 500 MHz NMR spectrometer at 25 °C. 600 μL of a D_2O solution of host OA (1mM OA in 10 mM $Na_2B_4O_7$) was taken in a NMR tube and to this 0.5 equivalent increment of guest (5 μL of a 60 mM solution in DMSO-d_6) was added. The ^{1}H NMR experiments were carried out after shaking the NMR tube for 5 min after each addition. Completion of complexation was monitored by disappearance of the free host OA signals upon addition of guest. Required amount of nitroxide solution ($T^{\oplus}$, T and $T^{\ominus}$; stock solutions (30 mM) were prepared in D_2O) was added in the complex and ^{1}H NMR was recorded after shaking the NMR tube for 5 min. Spin-lattice relaxation times T_1 were determined using a standard 180-τ-90 inversion recovery pulse sequence with 10 τ values between 0.001 to 10 s. The T_1 measurements were performed on a Bruker 400 MHz NMR spectrometer at 25 °C.

General protocol for luminescence study:

Fluorescence emission spectra were recorded on a FS920CDT Edinburgh steady-state fluorimeter and the lifetime measurements on FL900CDT fluorescence lifetime spectrometer. Capsular assemblies (1 mM) were made by adding 5 μL (for 2:1; H:G complex) and 10 μL (for 2:2; H:G complex) of 60 mM solution of guest (in DMSO solution) to 0.6 mL of 1mM OA in 10 mM borate buffer in H_2O. It was diluted appropriately with 10 mM buffer solution to have the required concentration of host/guest complex. The solutions were deoxygenated by purging with nitrogen gas for 30 min prior to the emission study. 10 μL of nitroxides ($T^{\oplus}$, T and $T^{\ominus}$; stock solutions were prepared in H_2O) were added each time and further deoxygenated by purging nitrogen for 20 min and then recorded emission spectra. The quenching rate constants for nitroxide quenching were derived from the slope of the plot of nitroxide concentration vs. triplet state decay constant ($1/\tau$). Required amount of CB8 (stock solution was prepared in H_2O) was added to the solution (after quenching by nitroxide) and emission spectra were recorded after purging with nitrogen.

Triplet-triplet absorption measurements:

Transient absorption measurements were performed by laser flash photolysis employing the pulses from a Nd-YAG laser (GCR-150-30, Spectra Physics) at 355 nm (~5 ns pulse length) and a computer-controlled system that has been described elsewhere.[70]

General protocol for EPR study:

Preparation of host/guest complex: Stock solution (20 mM) of guest was prepared in $CHCl_3$. Host stock solution (5 mM) was prepared in H_2O. Required amount of guest solution in $CHCl_3$ was added in a vial and the solvent was evaporated by shaking in a

mechanical shaker. Then calculated amount of host solution and water were added and shaken by the mechanical shaker for 15 h. The required amount of nitroxide solutions were added to it and shaken for 2 h. EPR spectra were recorded at room temperature in Bruker EMX spectrometer at 9.5 GHz (X band) employing 100 KHz of field modulation frequency. Spectrometer setting: Power, 1.997 mW; amplitude modulation, 0.50 G; time constant, 163.84 ms; conversion time, 163.84 ms. Samples were loaded to quartz (CFQ) EPR tubes from Wilmad LabGlass (2 mm OD, 0.5 mm wall thickness, 10 cm height) for the EPR experiments.

EPR Simulations:

The EPR spectra of three-line signals (three hyperfine lines: 2.I.N+1 = 3) were computed by the well-established procedure of Budil and Freed.[74] The main input parameters were as follows. (a) the g_{ii} components (for the coupling between the electron spin and the magnetic field) were the ones previously used for the nitroxide (g_{xx}=2.009, g_{yy}=2.006, g_{zz}=2.0025), and were considered constant for all samples; (b) The A_{ii} principal values of the **A** tensor for the coupling between electron and nuclear spin ($<A_N> = (A_{xx}+A_{yy}+A_{zz})/3$). An increase in the environmental polarity of the NO group provokes an increase in the **A** tensor components owing to the increased electron spin density on the nitrogen nucleus. (c) The perpendicular component of the correlation time for rotational diffusion (τ_{perp}). Brownian motion was assumed in the calculation, for which the diffusion component is $D_{perp} = 1/(6\tau_{perp})$.

CHAPTER 8

High-Energy Conformer of a Piperidine Derivative within a Water-Soluble Capsuleplex

8.1 Overview

Self-assembled molecular capsules provide a unique opportunity to examine and manipulate the properties of encapsulated small molecules and reactive intermediates.[6,198] Those supramolecular assemblies have attracted considerable interest over the last couple of decades not just for their appealing complex structures and distinct interior environments but also because they can be used to perform reactions that are often problematic in aqueous solution. Gibb and co-workers have developed deep-cavity cavitand octa acid (OA, **Scheme 8.1**) that dimerize into capsules via the hydrophobic effect.[40] OA possess water-solubilizing outer coats comprising eight carboxylic groups, deep hydrophobic inner pockets, and a hydrophobic rim of the cavity that promotes self-assembly. We have described the detailed studies on microenvironment of the OA capsule and its ability to form various complexes with small molecules (**Chapters 3** and **Chapters 4)**. The alteration of the photophysical and photochemical behavior of organic molecules incarcerated within the confined space of a capsule comprised of two OA molecules has also been studied in recent years.[5,134,199,200]

Pioneering works on encapsulating a structure at the molecular level was demonstrated by Cram and coworkers in 1991.[7] They were able to isolate highly unstable, antiaromatic cylobutadiene molecule at room temperature by encapsulating it within a hemicarcerand. Based on this novel finding, there have been extensive studies on the transient species such as benzyne, cycloheptatetraene, enol, carbene, and nitrene within the inner phases of appropriate hemicarcerands.[201] However, conformational isomers of cyclohexanes trapped within the confined spaces of synthetic cavitands at room temperature remain elusive.[202,203] In this context, it must be noted that within solid

thiourea channels the axial conformers of chloro- and bromocyclohexane are largely predominant in contrast with the prevalence of the equatorial isomers in solution.[204,205]

After assessing the microenvironment of OA capsule and the different modes of complexation with small molecules, we got interested to investigate the stabilization of a high-energy conformer of a piperidine derivative within the confined space of OA capsule (**Scheme 8.1**), at room temperature in aqueous solution.[206,207] Piperidine prefers to be in a chair conformation, similar to cyclohexane. As shown in **Scheme 8.1**, each piperidine derivative (**2a-e**) would have two distinguishable chair conformations: one with the O-alkyl group at C-4 in an axial position, and the other one in an equatorial position. The equatorial conformation is expected to be more stable than the axial conformation. The axial conformation is energetically higher due to 1-3 diaxial interaction of the C-O-alkyl group at C-4 and the hydrogens at C-2 and C-6. The aim of this study was to figure out which conformer of the piperidine derivative is favored inside the OA capsule. We initiated a series of NMR experiments, such as ^{1}H NMR at room temperature as well as variable temperature, 2D DQF COSY and 2D ROESY, to examine the preferred conformation of the piperidine derivatives in OA capsule.

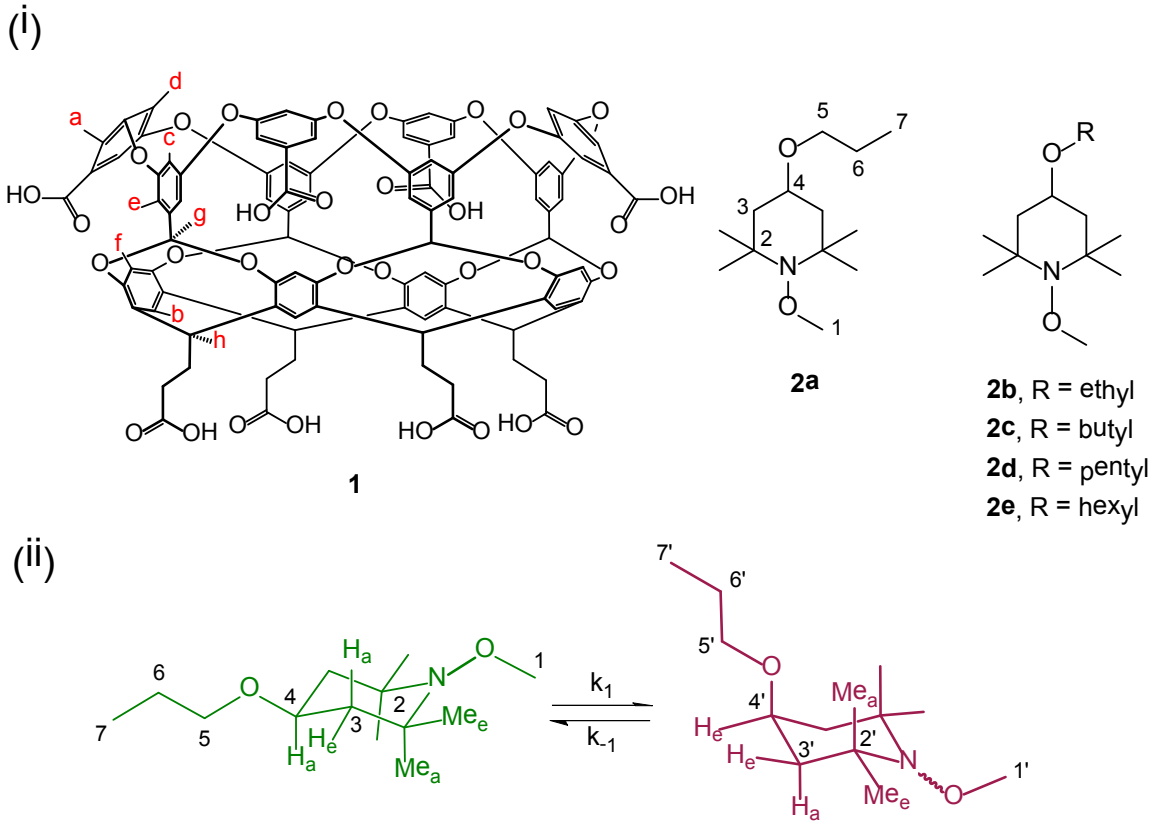

Scheme 8.1 (i) Chemical structures of octa acid (**1**) and piperidine derivatives **2a-e**. (ii) Two possible conformations of **2a** with respect to the C−O−alkyl substitution are shown. These two conformations are color coded.

8.2 Results and discussion

8.2.1 ^{1}H NMR study

We performed ^{1}H NMR study to confirm that the aforementioned piperidine derivatives (**2a-e**) form complexes with OA (**Scheme 8.1**).[127] The spectra shown in **Fig 8.1** revealed that **2a** exists in two distinctly different non-interconverting conformations (**Fig 8.1(ii)**) at room temperature within the OA capsule, while **2b−e** adopt the same conformation both in OA capsule and in solution. For clarity purpose the upfield region and the downfield region of the ^{1}H NMR spectra of the complexes are presented

individually in **Fig 8.1** and **Fig 8.2** respectively. Inclusion of the guest into the host was confirmed by the significant upfield shift of the C−O−alkyl hydrogen signals, particularly the CH_3 group of the alkyl chain (**Fig 8.1**). The assignment of the proton signals were carried out based on 2D DQF COSY that will be discussed in detail in the next section. **Fig 8.2** shows the change of OA proton signals in presence of the guest. We found that after addition of 0.5 equivalent of the guest (**2a-e**, **Scheme 8.1**), all the uncomplexed OA proton signals disappeared indicating that they form 1:2 (guest:host) complexe (**Fig 8.2**). The single set of H_d and H_f hydrogens in each of the four symmetrical panels of the OA cavitand resulted in an identical chemical shift of all these hydrogens. When OA forms a capsuleplex with a symmetrical guest, only a single signal each for all eight H_d and all eight H_f hydrogens was expected. However the host NMR signals of capsuleplexes of **2b**−**e**@OA_2 revealed the presence of independent signals for some of the identical OA hydrogens present on the top and bottom halves of the capsule (e.g., signals due to H_e in **2b** and signals due to $H_{a–f}$ for **2c**−**e** in **Fig 8.2**). This suggested that **2b**−**e** do not tumble freely within the capsule, which makes the two halves of the capsule identical, in the NMR time scale at room temperature.

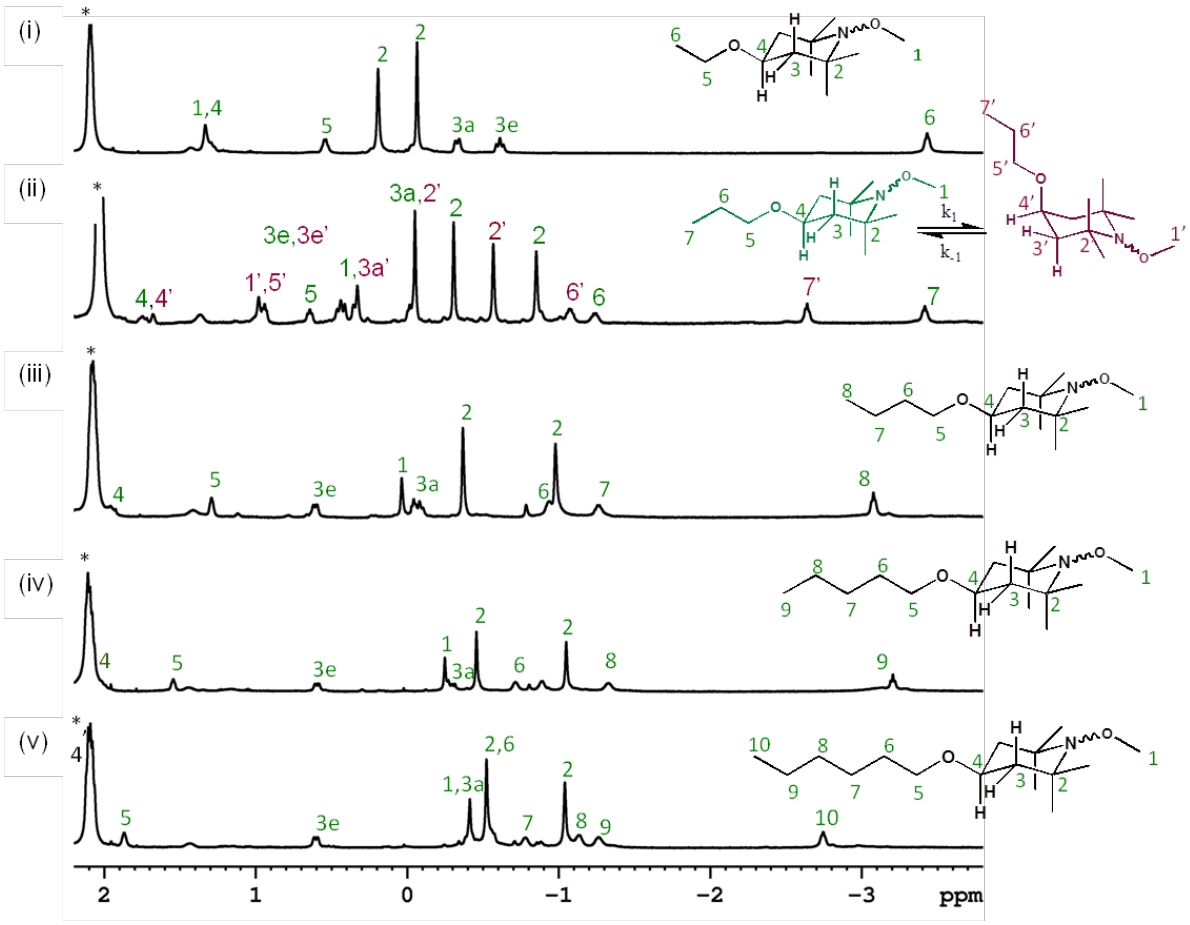

Figure 8.1 Partial ^{1}H NMR spectra highlighting the alkyl region (500 MHz, D_2O) of (i) **2b**/OA (0.5:1), (ii) **2a**/OA (0.5:1), the other isomers proton resonances can be marked with (′), (iii) **2c**/OA (0.5:1), (iv) **2d**/OA (0.5:1), (v) **2e**/OA (0.5:1). [OA] = 1 mM in 10 mM borate sodium tetraborate buffer. Numbers represent guest-proton resonances and "*" represents "j" proton of OA.

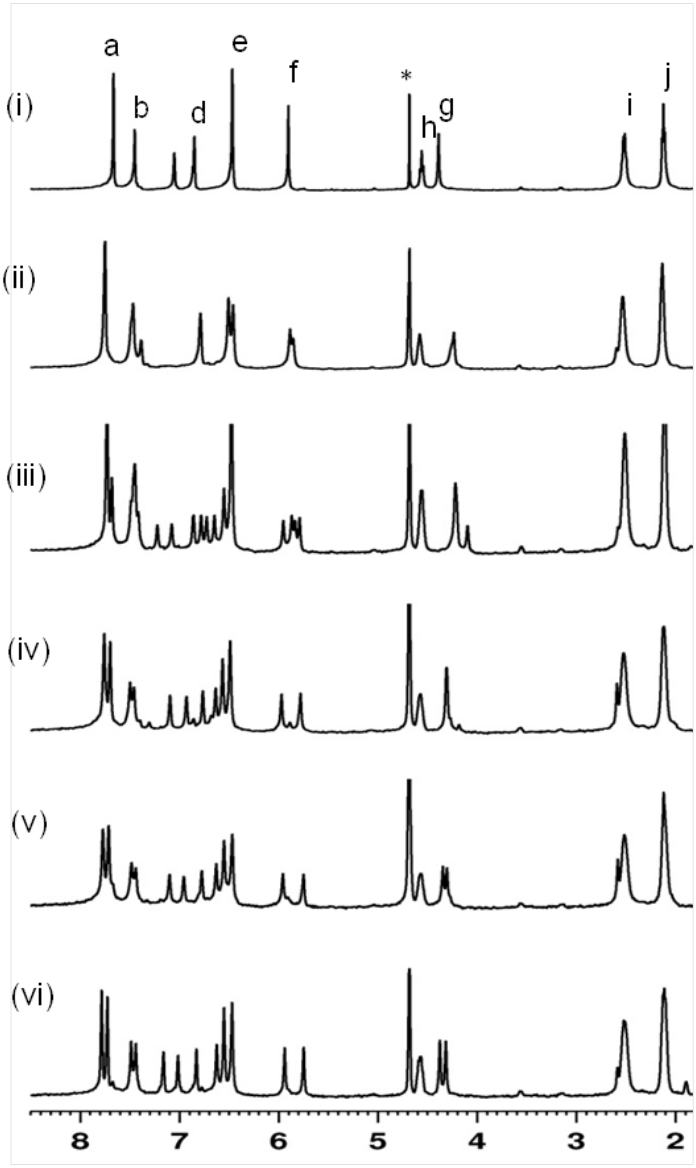

Figure 8.2 Partial ^{1}H NMR spectra highlighting the host region (500 MHz, D_2O) of (i) OA, (ii) **2b**/OA (0.5:1), (iii) **2a**/OA (0.5:1), (iv) **2c**/OA (0.5:1), (v) **2d**/OA (0.5:1), (vi) **2e**/OA (0.5:1). [OA] = 1 mM in 10 mM borate sodium tetraborate buffer. "*" represents residual H_2O resonance.

Although all the guest molecules, **2a-e** formed a 1:2 capsuleplex with OA, **2a** showed a distinctly different behavior. The ^{1}H NMR spectra of OA, **2a**, and **2a**@OA_2 are shown in **Fig 8.3**. The analysis of these spectra revealed that for the capsuleplex **2a**@OA_2 four signals for each of the H_d and H_f of OA, and two signals for each of the guest methyl groups marked 2a, 2e and CH_3-7 were present. It should be noted that for **2b-e**@OA_2 only two signals for each of H_d and H_f of OA and one signal each for 2a, 2e and terminal alkyl methyl group were found (**Fig 8.1** and **Fig 8.2**). This difference suggested that **2a** formed two types of complexes with OA. Presence of the four distinct signals for H_d and H_f of OA is consistent with the existence of "two independent unsymmetrical complexes in solution" with one set of signals, (two H_d, two H_f and one CH_3-7) belonging to one complex and the other set to the second complex.

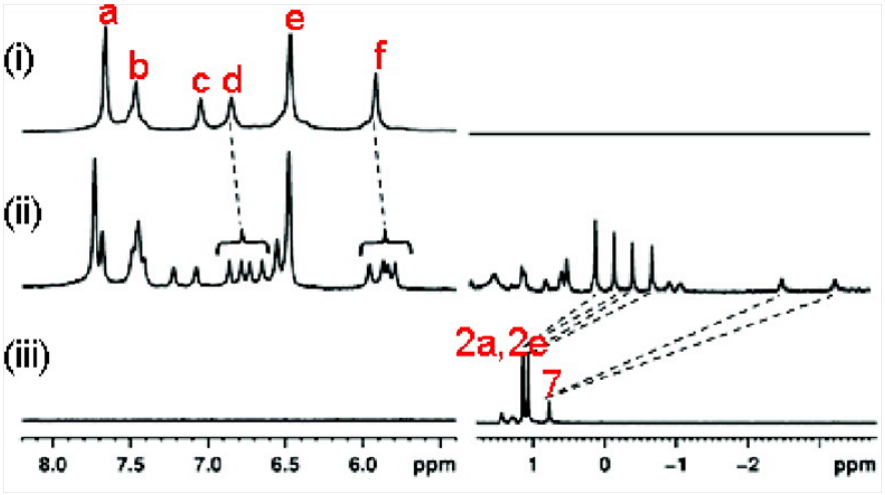

Figure 8.3 Partial ^{1}H NMR spectra (500 MHz, D_2O) of (i) OA, (ii) **2a**@OA_2 ([OA] = 1 mM; [**2a**] = 0.5 mM; 10 mM sodium tetraborate buffer), and (iii) **2a**. Host resonances are labeled in letters "a−f", and guest resonances are labeled in numbers.

8.2.2 2D DQF COSY study

One possibility for the above hypothesis of "two independent unsymmetrical complexes" is that the guest **2a** is captured in two different conformations within the capsule (**Scheme 8.1(ii)**). To gain insight into the preferred conformation of **2a** in solution and inside OA capsule, we performed 2D DQF COSY NMR experiments in D_2O. 2D COSY experiment shows the correlation between two hydrogens of the adjacent carbon atoms and allows one to determine the connectivity in a molecule by determining which protons are spin-spin coupled. 2D DQF COSY provides even more detailed information in addition of the COSY interaction peaks. Strong cross peaks between diaxial and geminal-hydrogens and weak or negligible cross peaks between axial−equatorial hydrogens are expected in 2D DQF-COSY spectra.[208,209] This served as a key experiment to assign the ^{1}H NMR signals of the guest portons and hence to ascertain its conformation. We recorded 2D DQF COSY spectrum of **2a**, **2b** and **2c** in D_2O (**Fig 8.4**, **Fig 8.5** and **Fig 8.6**, respectively) to determine the stable conformation in solution. As shown in **Scheme 8.1(ii)**, hydrogen of C-3 and C-4 are the strategic protons to identify the conformers. For the low energy conformer, C-O-alkyl group would be at equatorial position and thus hydrogen of C-4 would be at axial position. In that case hydrogen of C-4 is expected to interact strongly with the hydrogen of C-3. In all the cases of guests **2a** to **2c** in solution (**Fig 8.4**, **Fig 8.5** and **Fig 8.6**), strong cross peaks between geminal hydrogens at C-3 (marked as 3a and 3e) and between vicinal hydrogens at C-4 (marked 4) and one of the two hydrogens at C-3 (marked 3a) are observed. The absence of a cross peak between C-4 and C-3e hydrogens is also important. These data suggested that the conformation adopted by **2a**−**c** in solution had the C-O−alkyl group placed

equatorially. By examining 2D DQF COSY spectra of **2b-e**@OA_2 as shown in **Fig 8.7** to **Fig 8.10**, it was revealed that **2b-e** adopt the same conformation in OA capsule as in solution.

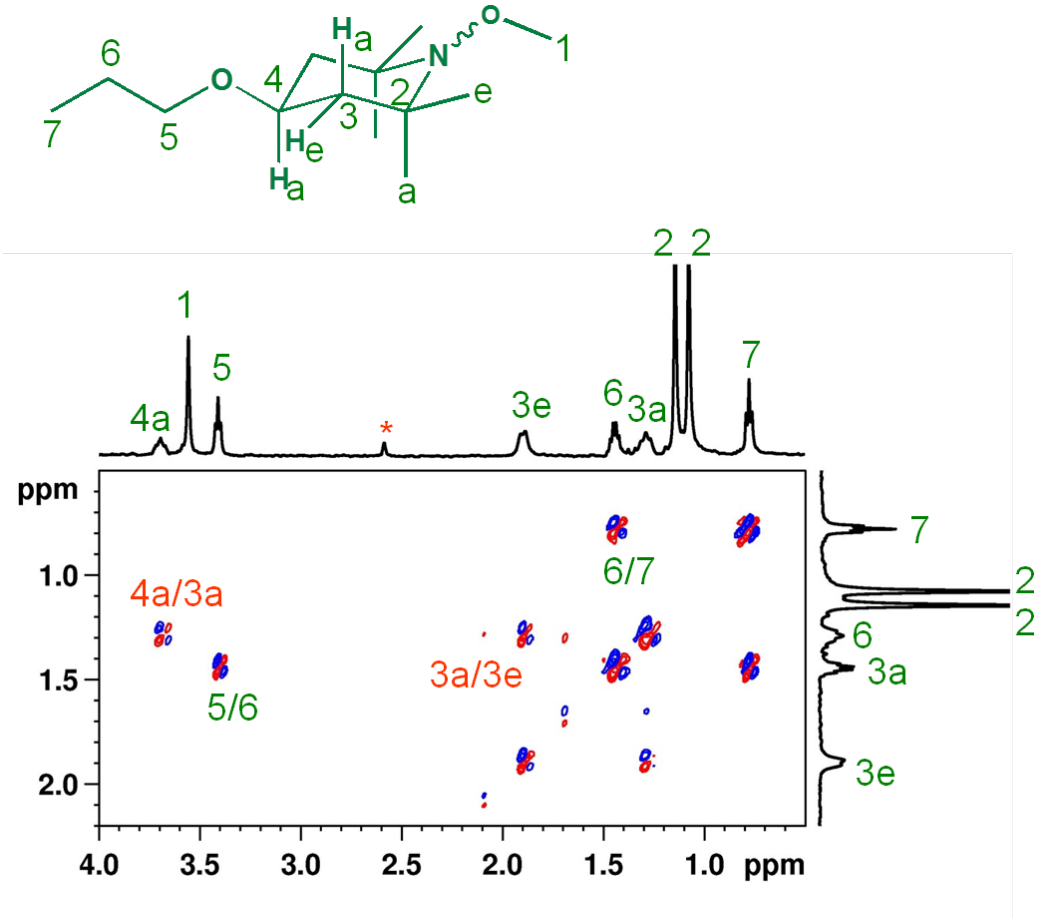

Figure 8.4 2D DQF COSY NMR spectrum (500 MHz) of **2a** in D_2O. "*" represents residual DMSO resonance.

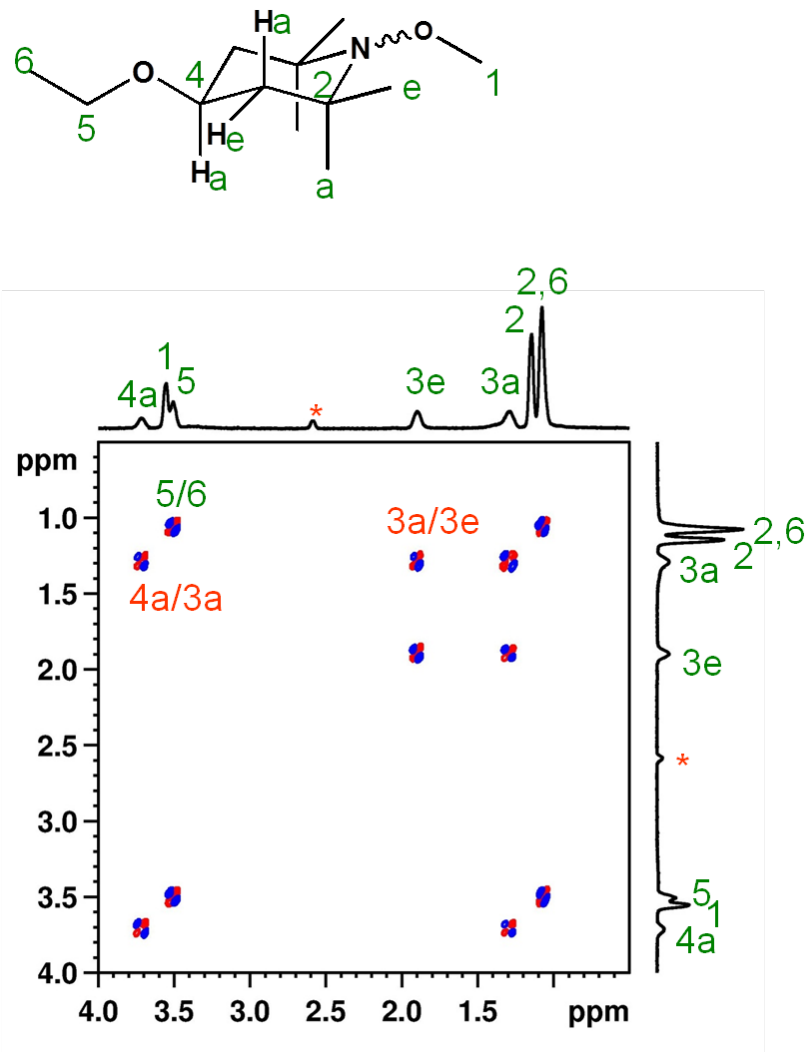

Figure 8.5 2D DQF COSY NMR spectrum (500 MHz) of **2b** in D_2O. "*" represents residual DMSO resonance

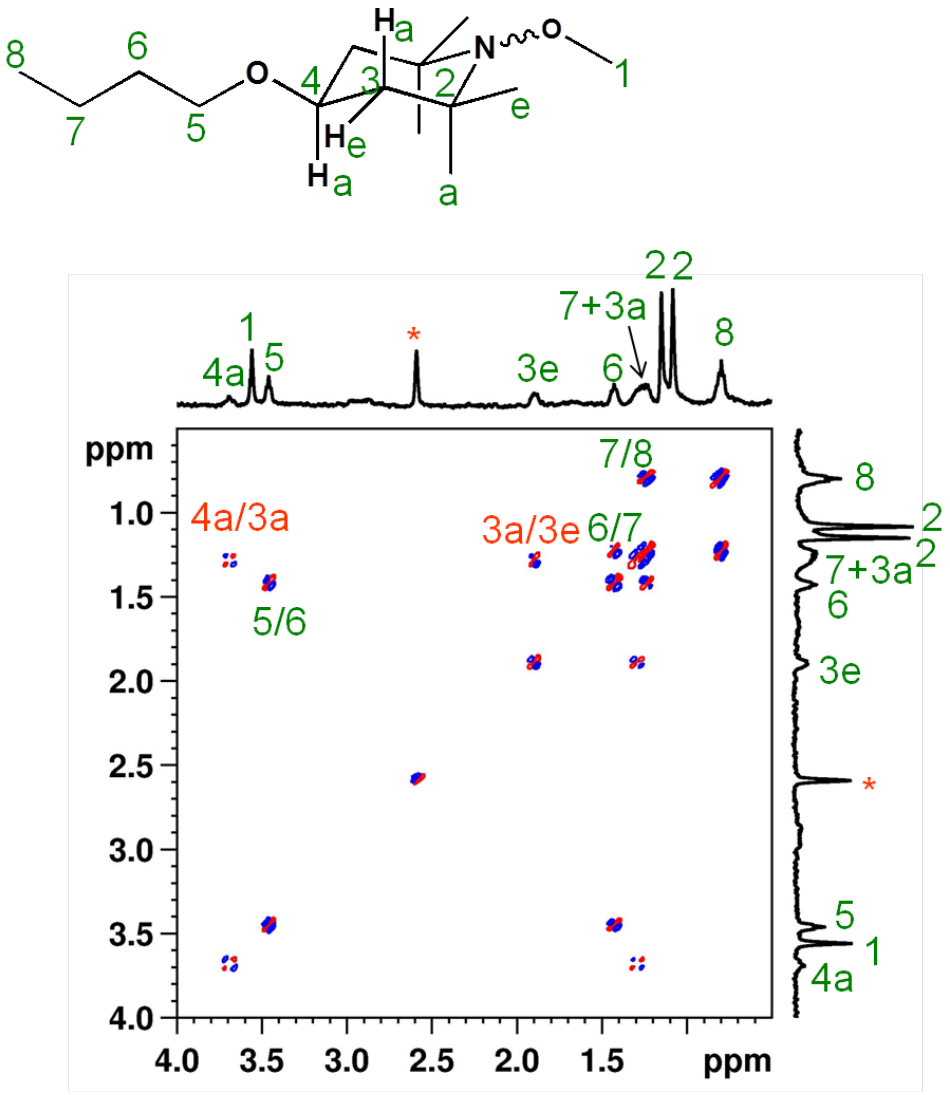

Figure 8.6 2D DQF COSY NMR spectrum (500 MHz) of **2c** in D_2O. "*" represents residual DMSO resonance

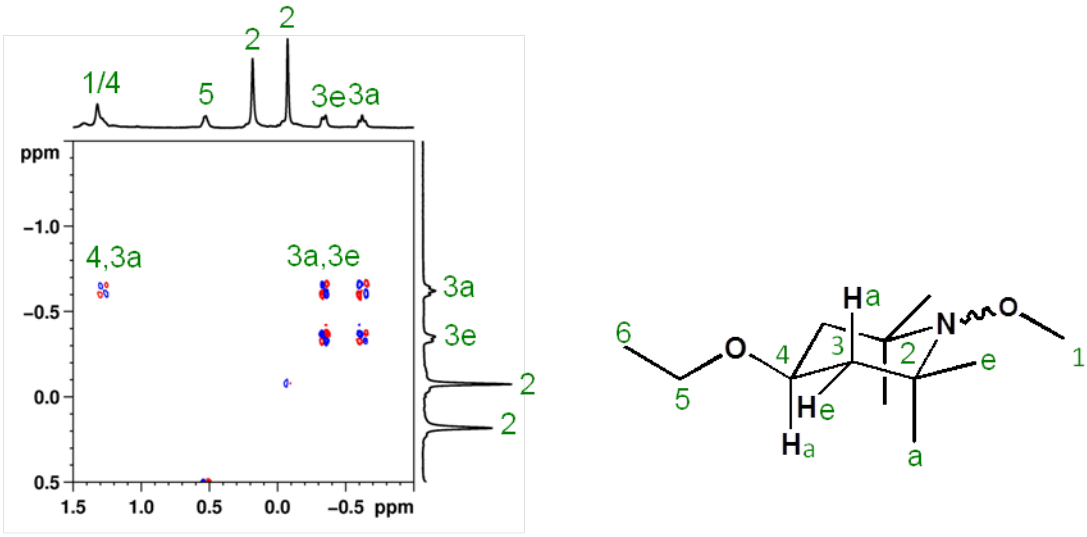

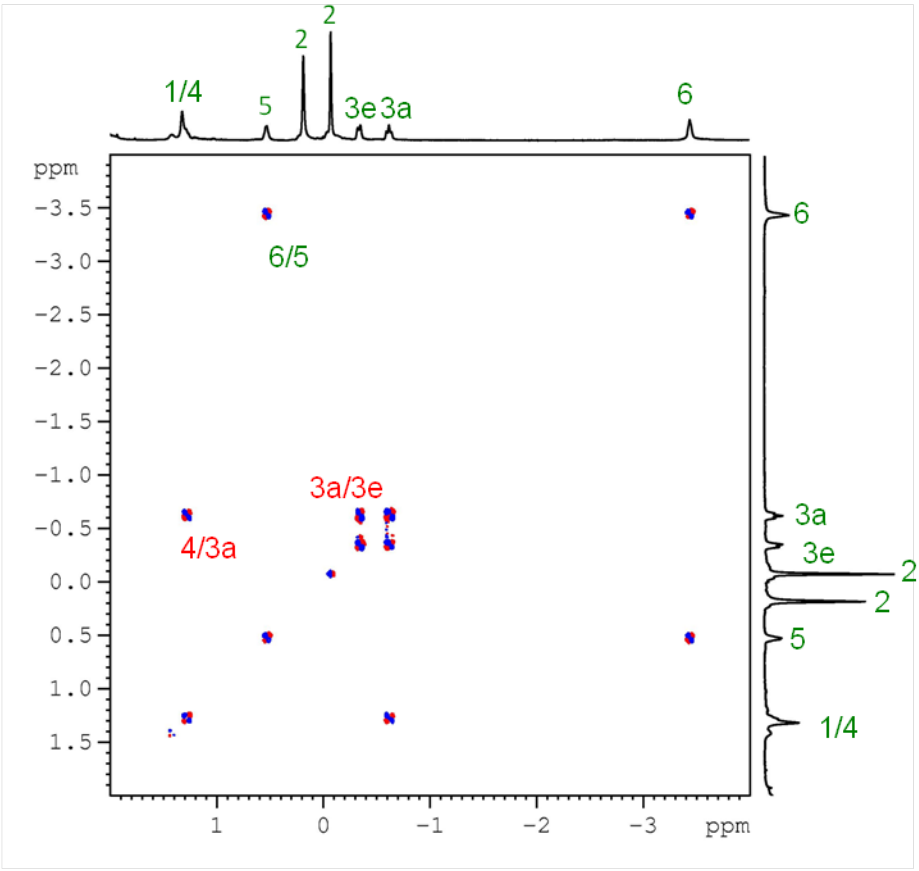

Figure 8.7 Partial 2D DQF COSY NMR spectrum (500 MHz) of **2b**@OA_2, [OA] = 5 mM in 50 mM sodium tetraborate buffer, [**2b**] = 2.5 mM.

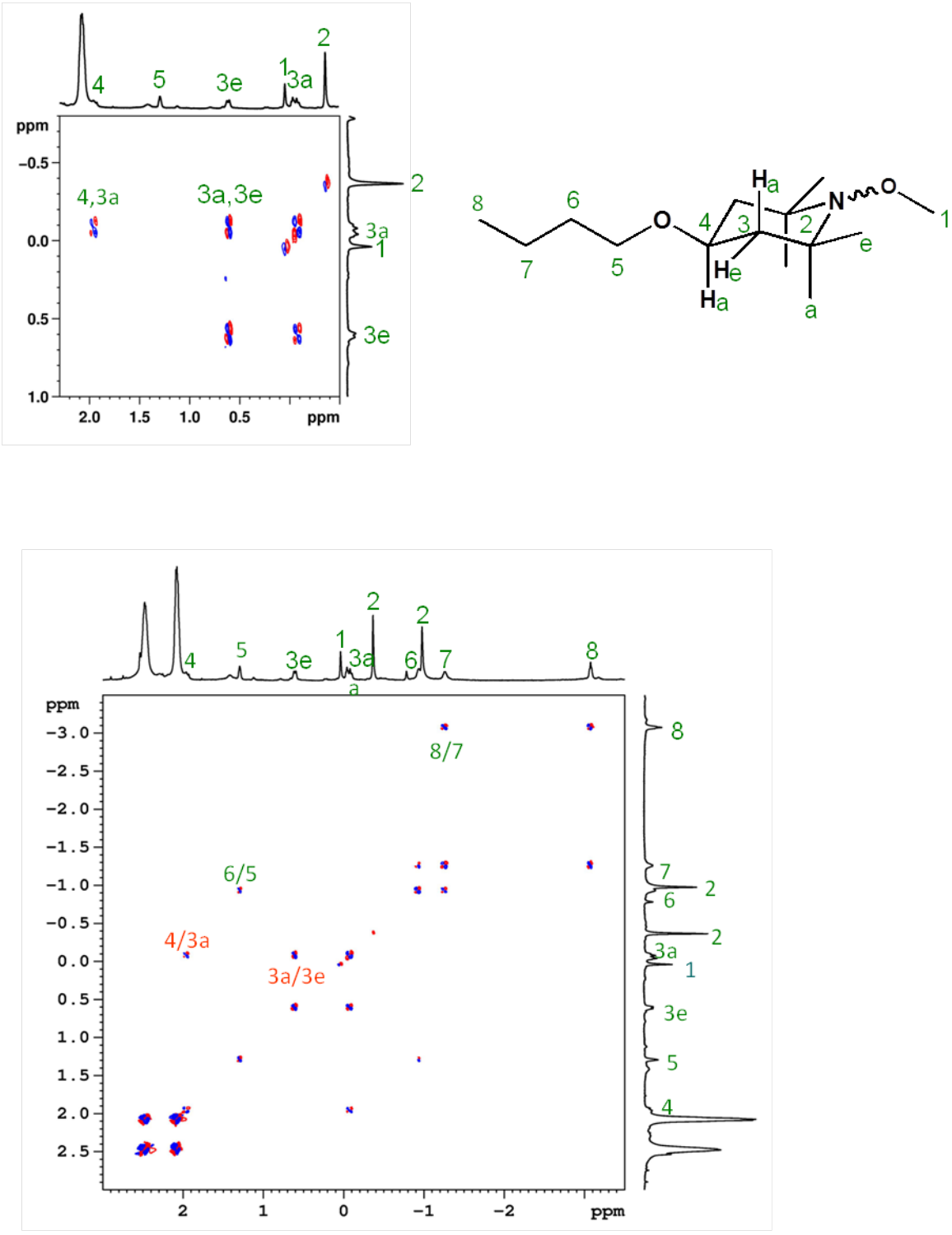

Figure 8.8 Partial 2D DQF COSY NMR spectrum (500 MHz) of **2c**@OA_2, [OA] = 5 mM in 50 mM sodium tetraborate buffer, [**2c**] = 2.5 mM.

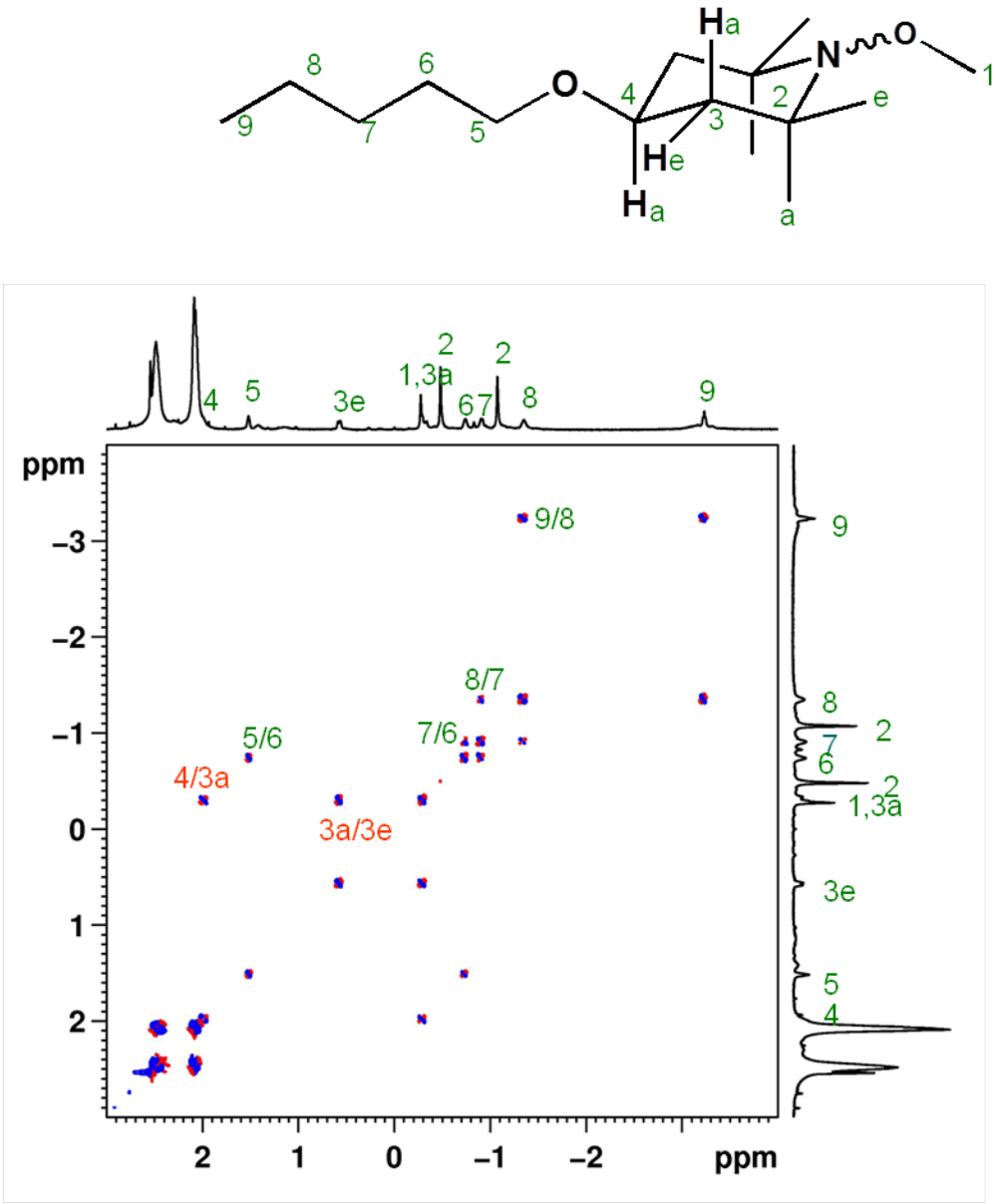

Figure 8.9 Partial 2D DQF COSY NMR spectrum (500 MHz) of **2d**@OA_2, [OA] = 5 mM in 50 mM sodium tetraborate buffer, [**2d**] = 2.5 mM.

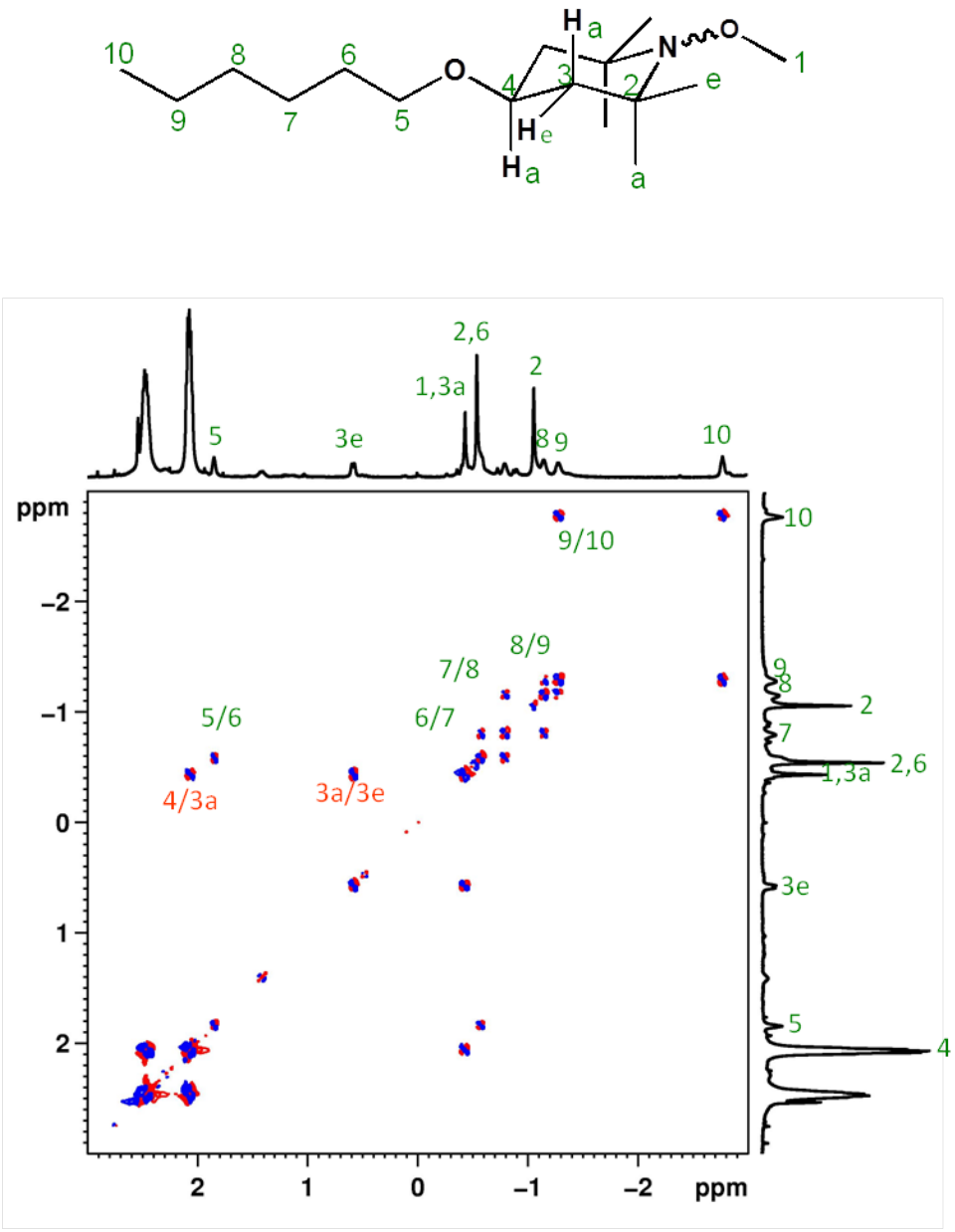

Figure 8.10 Partial 2D DQF COSY NMR spectrum (500 MHz) of **2e**@OA_2, [OA] = 5 mM in 50 mM sodium tetraborate buffer, [**2e**]=2.5 mM.

Given the existence of **2a** in a single conformation in solution (C−O−alkyl at equatorial position), the possibility of trapping an alternate conformer with the C−O−alkyl group at the axial position seemed interesting. The observed two distinct signals in ^{1}H NMR spectrum (**Fig 8.3ii**) suggested that there may indeed be two conformers trapped within the OA capsule and that they did not interconvert between the two conformers in the NMR time scale at room temperature. To test whether the above two sets of signals were indeed due to two conformers of **2a** whose C−O−alkyl groups are positioned axially (red) and equatorially (green), respectively (**Scheme 8.1**), we carried out DQF COSY NMR of **2a**@OA_2 (**Fig 8.11** and zoomed in **Fig 8.12**). Chemical structures of two conformers are represented in two different colors, green and red (**Scheme 8.1**). The color of the assigned protons in the 2D DQF COSY NMR spectrum represents the proton of the conformer with corresponding color code. Cross peaks between vicinal hydrogens H-4 and H-3 (axial) and H-3 (equatorial) of the guest in the DQF COSY NMR spectrum provided the most important information. In the green set of signals, H-4 correlates strongly with one of the two H-3 hydrogens (marked 3a) and poorly with the other H-3 (marked 3e) (**Fig 8.12**). On the other hand, in the red set of signals, H-4 correlated very weakly with both axial and equatorial H-3 (marked as 3a and 3e) (**Fig 8.12**). Such a correlation is consistent with the hypothesis that the green and red signals correspond to the guest with the C−O−alkyl group positioned equatorially and axially, respectively.

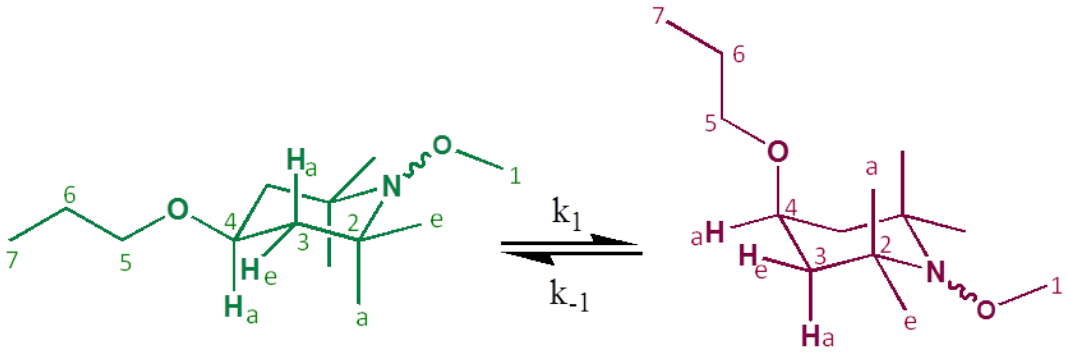

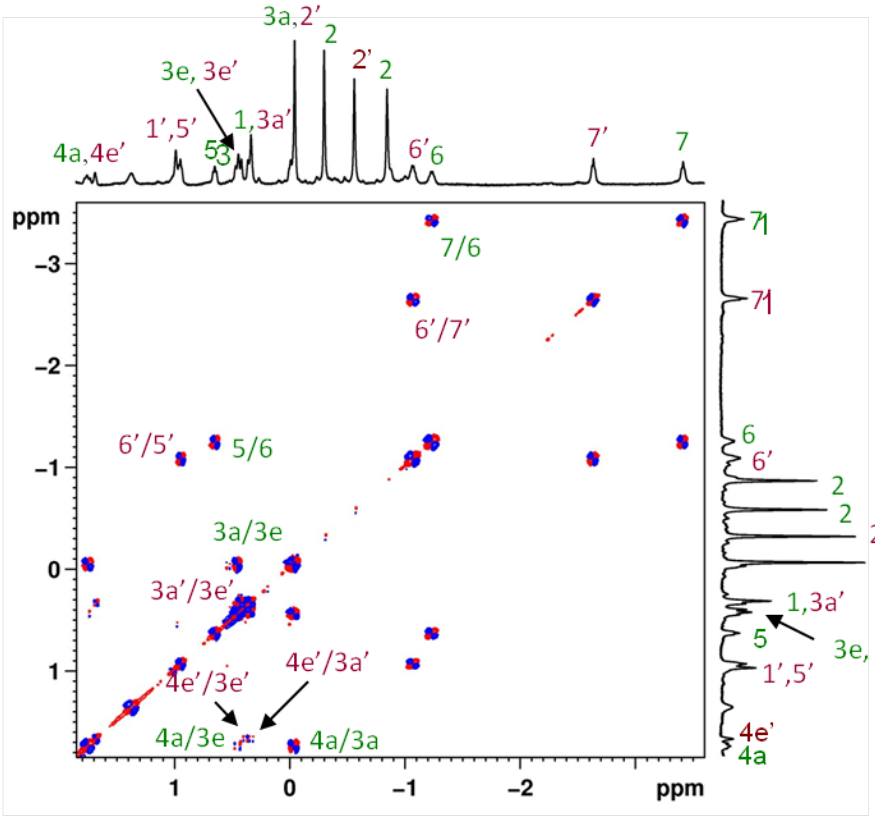

Figure 8.11 Partial 2D DQF COSY NMR spectrum (500 MHz) of **2a**@OA_2, [OA] = 5 mM in 50 mM sodium tetraborate buffer, [**2a**]=2.5 mM.

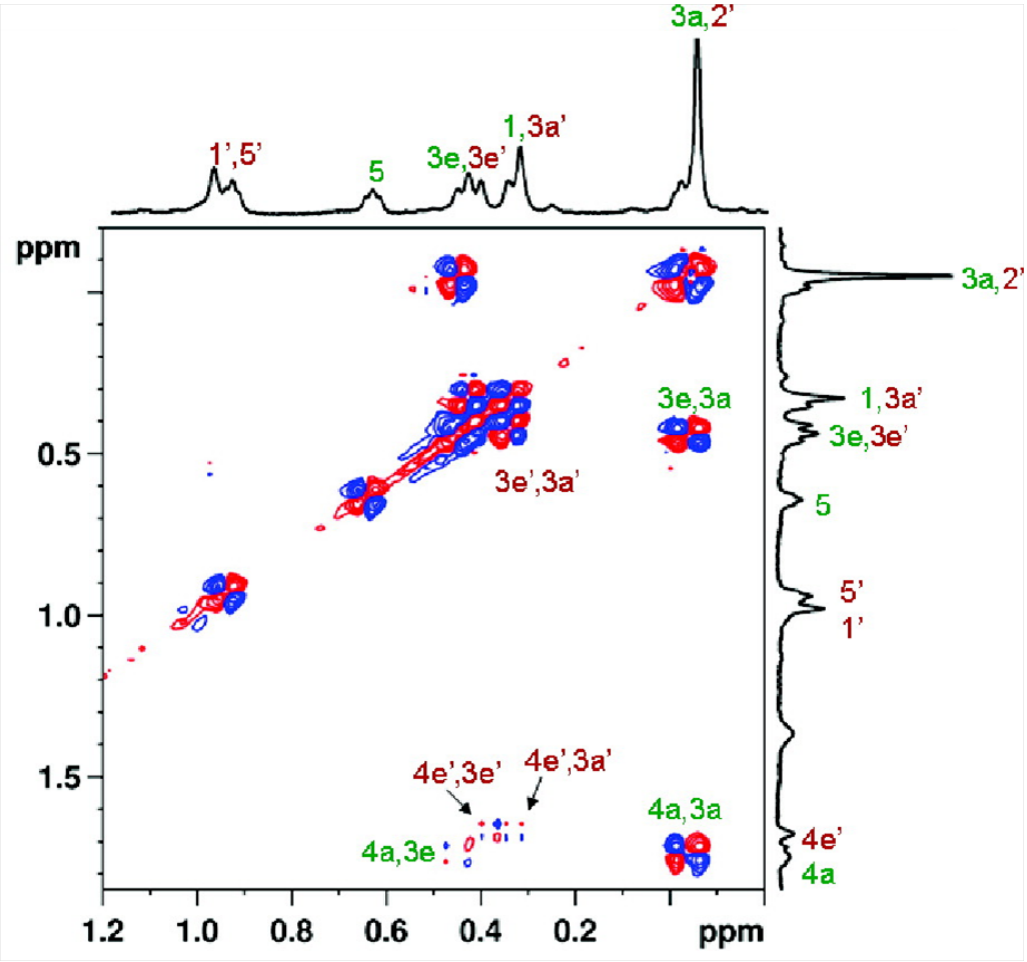

Figure 8.12 Partial 2D DQF COSY NMR spectrum (500 MHz, mixing time = 300 ms) of **2a**@OA_2 ([OA] = 5 mM, [**2a**] = 2.5 mM in 50 mM sodium tetraborate buffer). Chemical structures of two conformers are represented in two different colors. The color of the assigned protons in the 2D DQF COSY NMR spectrum represents the proton of the conformer with that particular color.

8.2.3 2D ROESY study

After revealing the existence of the two conformers of **2a** inside OA capsule, the next step was to examine if the two conformers interconverted at a longer time scale. We recorded a 2D ROESY spectrum of **2a**@OA_2 with 300 ms mixing time at room

temperature; partial spectra are displayed in **Fig 8.13** to **Fig 8.15**. The exchange peaks (EXSY) and through space interacting peaks (NOESY) are easily distinguishable in the ROESY spectrum. Importantly, the EXSY cross-peaks have the same sign as the diagonal whereas the NOESY cross-peaks have the different signs as the diagonal.[210-212] As illustrated in **Fig 8.13**, the signals due to methyl groups of the guest (marked CH_3-7, CH_3-7′, CH_3-2, and CH_3-2′) as well as others (see boxes A, B, C, D, and E) suggested that the corresponding signals exchanged in the time scale (300 ms) of the ROESY experiment. The two sets of peaks have thus been identified based on 2D ROESY cross peaks to be due to two conformers that exchange in 300 ms and accordingly are color coded in green and red in **Fig 8.13**. In these spectra, we were unable to unequivocally assign the four signals seen for the four methyl groups at 2,2′ positions to the exact conformer. As shown in **Fig 8.14**, NOESY and EXSY peaks of **2a** inside OA capsule were very distinct. Through space interacting signals between host and guest are black (NOESY signal, black rectangle **X** in the **Fig 8.14**) and exchange signals between two conformers are red (EXSY signal, red rectangle **Y** in the **Fig 8.14**) in color.

In **Fig 8.15**, a partial 2D ROESY spectrum displaying the NOESY interaction between the host and guest signals is presented. From this, it was clear that H_g signals of the two halves of the capsule interacted with the CH_3-7 and OCH_3 signals of both isomers of the guest indicating that the two ends of the two conformers were anchored at the two narrow ends of the capsule. Examination of **Fig 8.14** and **Fig 8.15** revealed that the methyl groups at the 2-positions of both isomers interact with the H_d signal of the host that is split into four, one pair for the axial and the other one for the equatorial

isomer complex. This suggested that the relative locations of the two isomers are similar within the capsule.

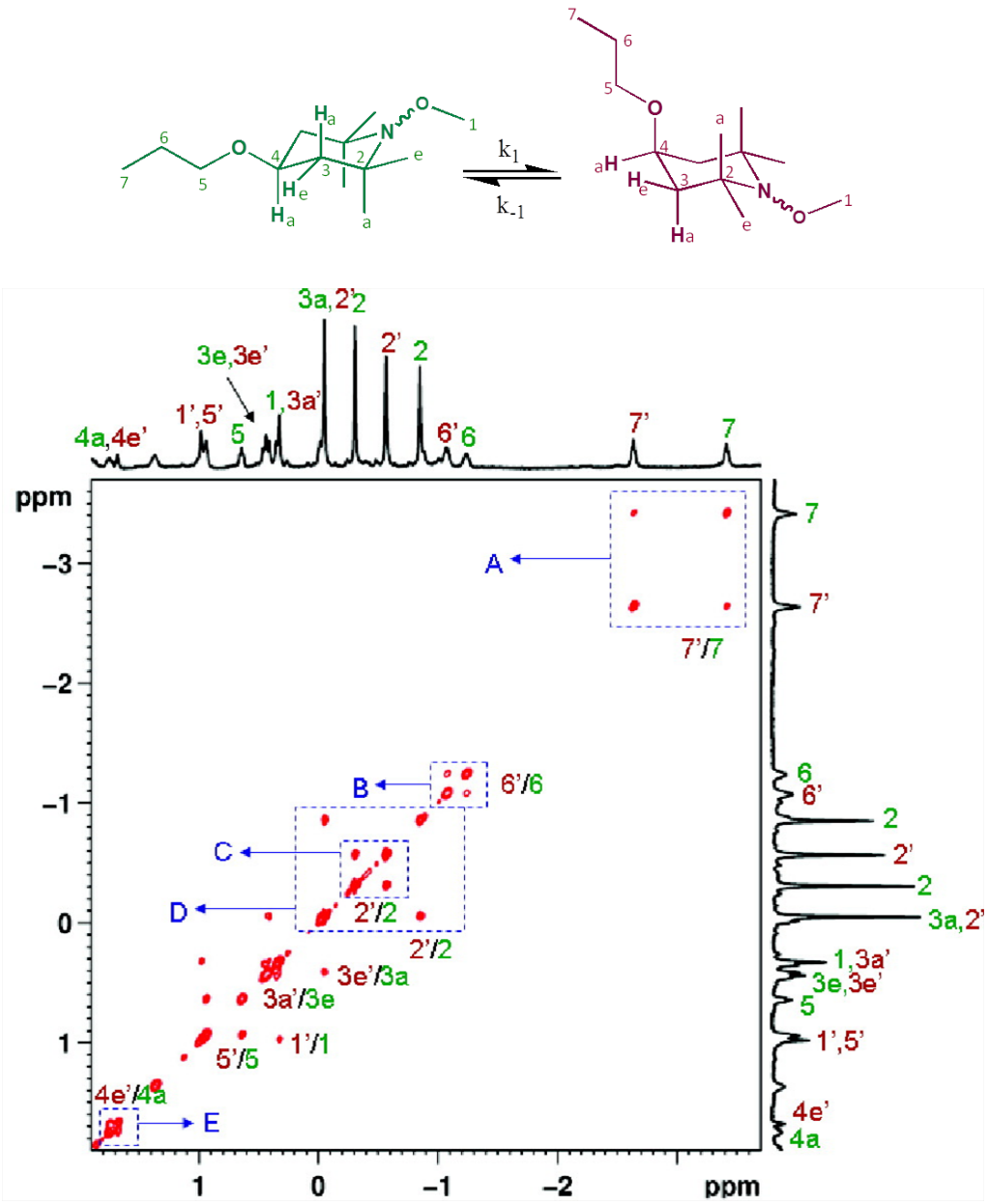

Figure 8.13 Partial 2D ROESY spectrum (500 MHz, mixing time = 300 ms) of **2a**@OA_2 ([OA] = 5 mM; [**2a**] = 2.5 mM in 50 mM sodium tetraborate buffer). The color represents the proton of the conformer of the same color in **Scheme 8.1** for **2a**.

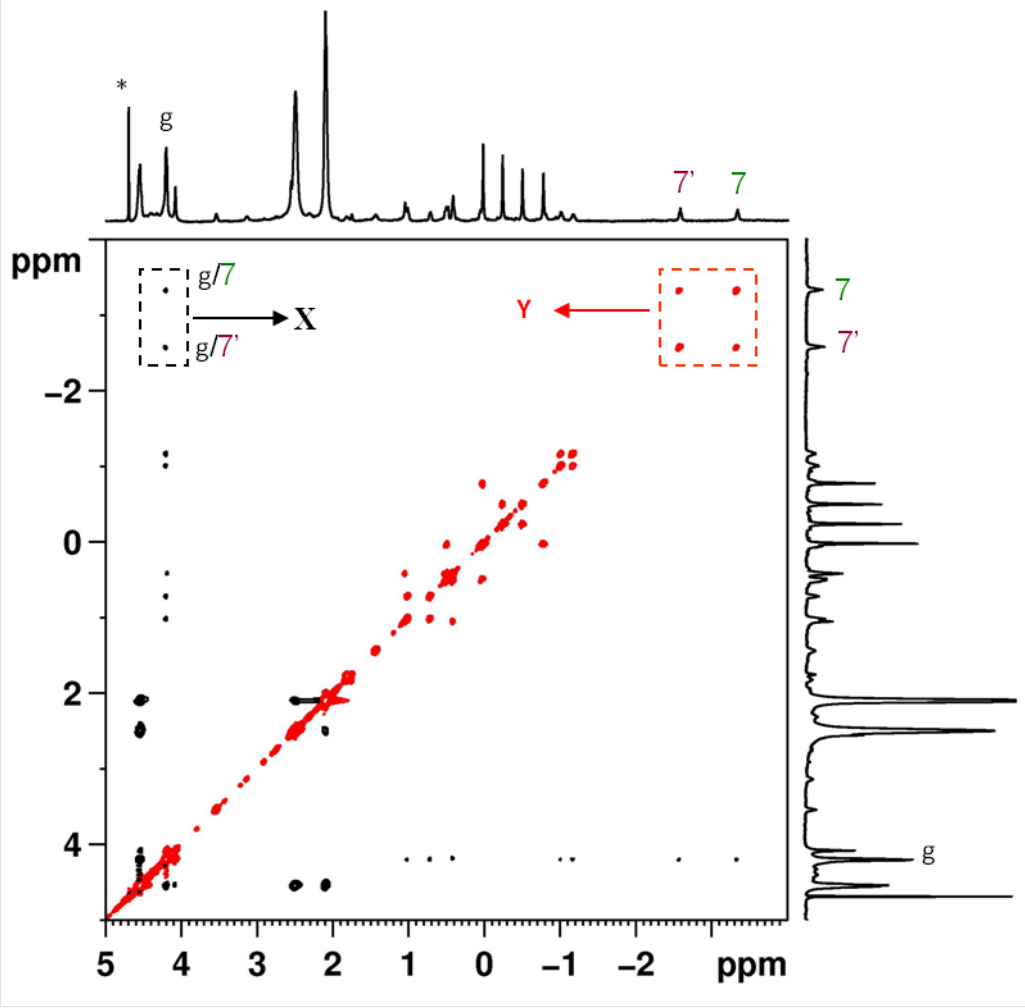

Figure 8.14 Partial 2D ROESY NMR spectrum (500 MHz, Mixing time = 300 ms) of **2a**@OA_2, [OA] = 5 mM in 50 mM sodium tetraborate buffer, [**2a**]=2.5 mM. The color represents the proton of the conformer of same color in **Scheme 8.1**. "*" represents residual H_2O resonance.

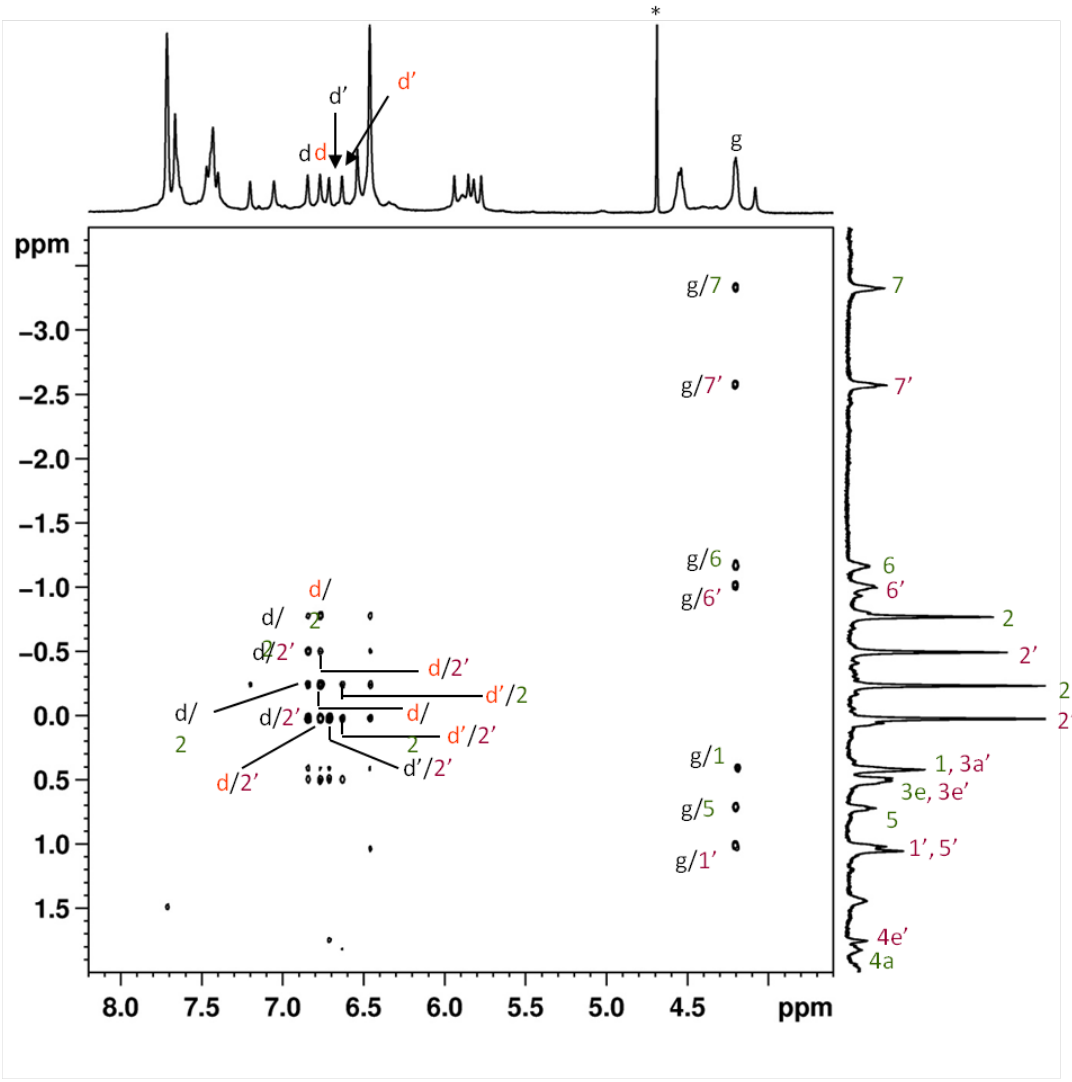

Figure 8.15 Partial 2D ROESY NMR spectrum (500 MHz, Mixing time = 300 ms) of **2a**@OA_2, [OA]=5 mM in 50 mM sodium tetraborate buffer, [**2a**]=2.5 mM. The color represents the proton of the conformer of same color in **Scheme 8.1**. "*" represents residual H_2O resonance.

The 2D ROESY experiments at 300 ms and zero mixing times at various temperatures with **2a**@OA_2 allowed us to measure the activation parameters for chair−chair interconversion of **2a**.[213] In those experiments, the areas under cross and diagonal peaks (**Fig 8.16**) were integrated for a particular set of protons that exchanged.

As shown in **Fig 8.16**, the absence of cross peaks at zero mixing time is expected due to the absence of magnetization transfer. Introduction of the integration values in the EXSY CALC program provided the magnetization exchange rate constants that are related to the conformer exchange rate constants k_1 and k_{-1} (**Scheme 8.1**). The activation parameters ($\Delta H^{\neq}$, $\Delta S^{\neq}$ and $\Delta G^{\neq}$) calculated from the Eyring plot (**Fig 8.17**) for the forward process (k_1; **Scheme 8.1**) were 17.7 kcal mol^{-1}, 1.75 eu, and 17.2 cal mol^{-1} respectively, and for the reverse process (k_{-1}; **Scheme 8.1**) were 18 kcal mol^{-1} 2.52 eu and 17.2 cal mol^{-1}, respectively.

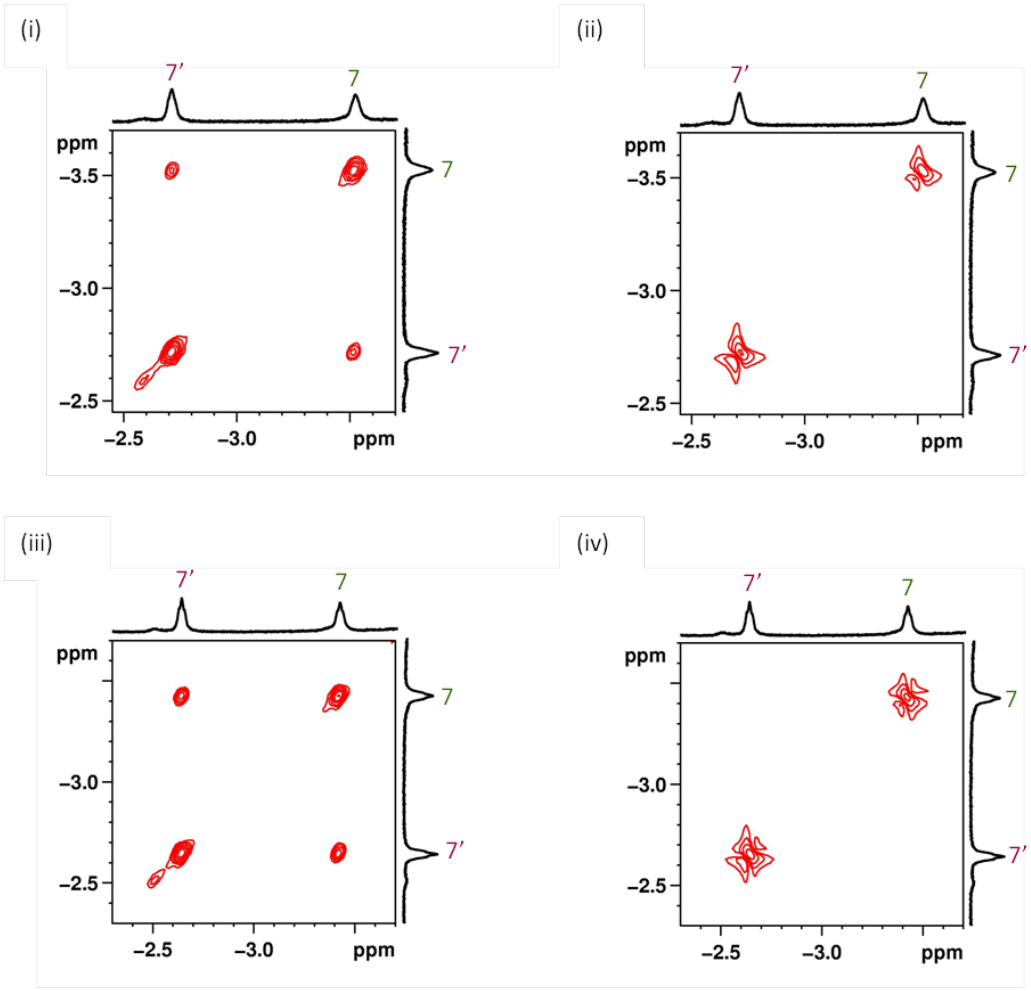

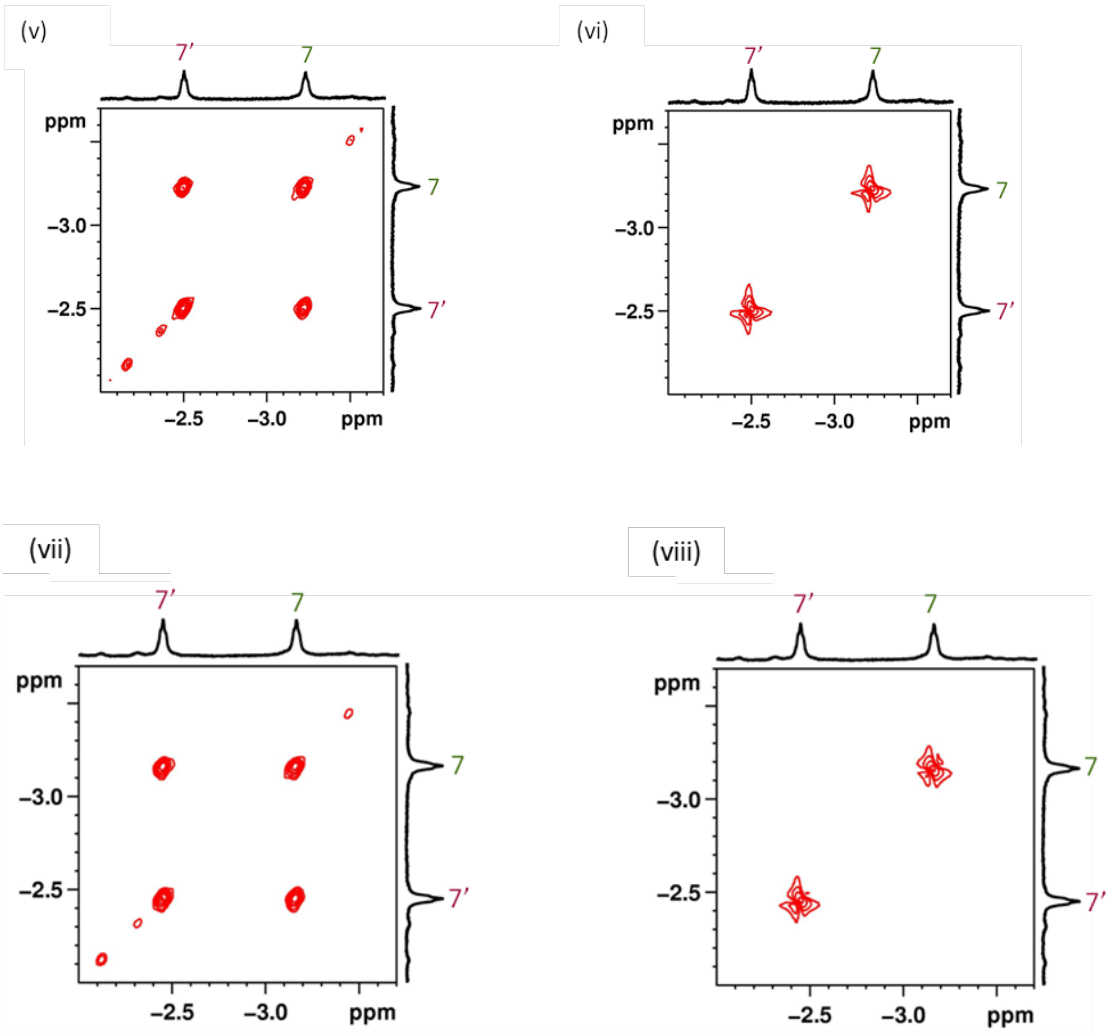

Figure 8.16 Partial 2D ROESY spectra (500 MHz, D_2O) of **2a**@ OA_2 (i) and (ii) 15 ^oC, (iii) and (iv) at 25 ^oC, (v) and (vi) at 35 ^oC and (vii) and (viii) at 40 ^oC. Spectra were recorded for (i), (iii), (v) and (vii) with 300 ms mixing time and (ii), (iv), (vi) and (viii) with 0 ms mixing time.

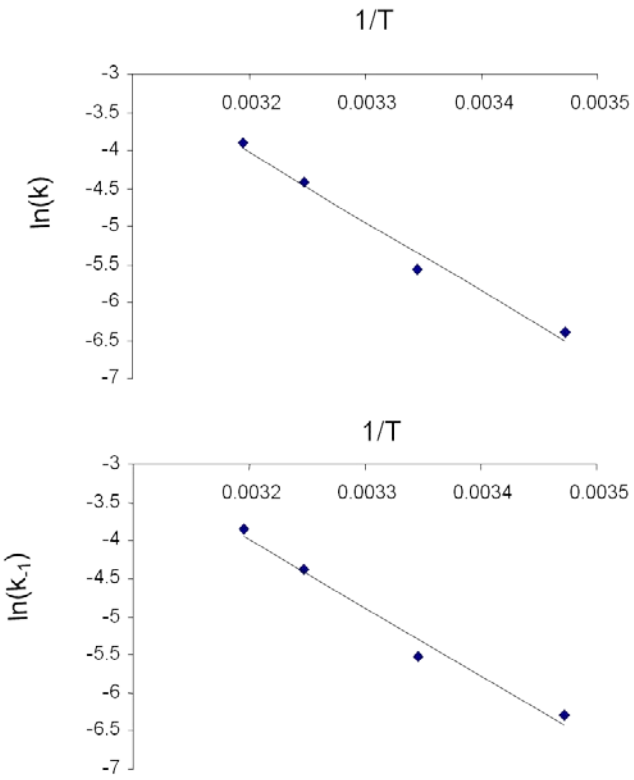

Figure 8.17 Eyring plots for exchange of two conformers of 2a in octa acid

8.2.4 Variable temperature ^{1}H NMR studies

We recorded ^{1}H NMR spectra at different temperatures to examine the possibility of interconversion between the two **2a**@OA_2 complexes. As demonstrated in **Fig 8.18** and **Fig 8.19**, the four signals due to H_d and H_f of host OA merged into two at 70 °C, while the guest methyl signals remained unaffected. The change in only the host signals suggested that the capsule was becoming symmetrical at higher temperatures.

We interpret the absence of influence of temperature on the guest signals to point out that at 70 °C it tumbles freely within the capsule without any interconversion between the two chair forms. To support this hypothesis, we recorded ^{1}H NMR spectra at various temperatures for **2b**@OA_2 (smaller than **2a**; i.e., R = ─CH_2CH_3) and **2c**@OA_2 (larger

than **2a**; i.e., ─$CH_2CH_2CH_2CH_3$). As shown in **Fig 8.20**, coalescence of signals of OA in **2b**@OA_2 occurred between 45 and 55 °C, while it was absent in the case of **2c**@OA_2 even at 70 °C (**Fig 8.21**). From these observations, we conclude that the rate constants for the tumbling motion of the guest that would make the top and bottom halves of the capsule identical vary with the size of the guest molecule (**2b**@OA_2 > **2a**@OA_2 > **2c**@OA_2).

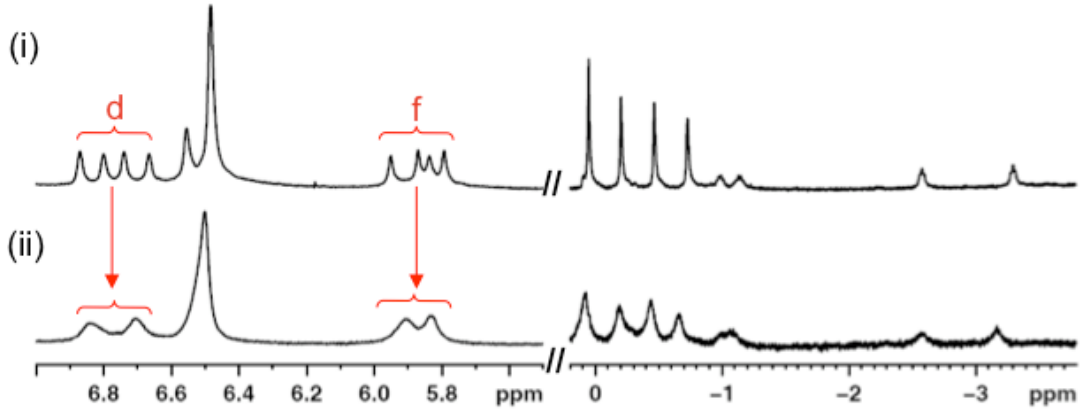

Figure 8.18 Partial ^{1}H NMR spectra (400 MHz, D_2O) of **2a**@OA_2 ([OA] = 1 mM, [**2a**] = 0.5 mM, in 10 mM sodium tetraborate buffer) at (i) 25 °C and (ii) 70 °C.

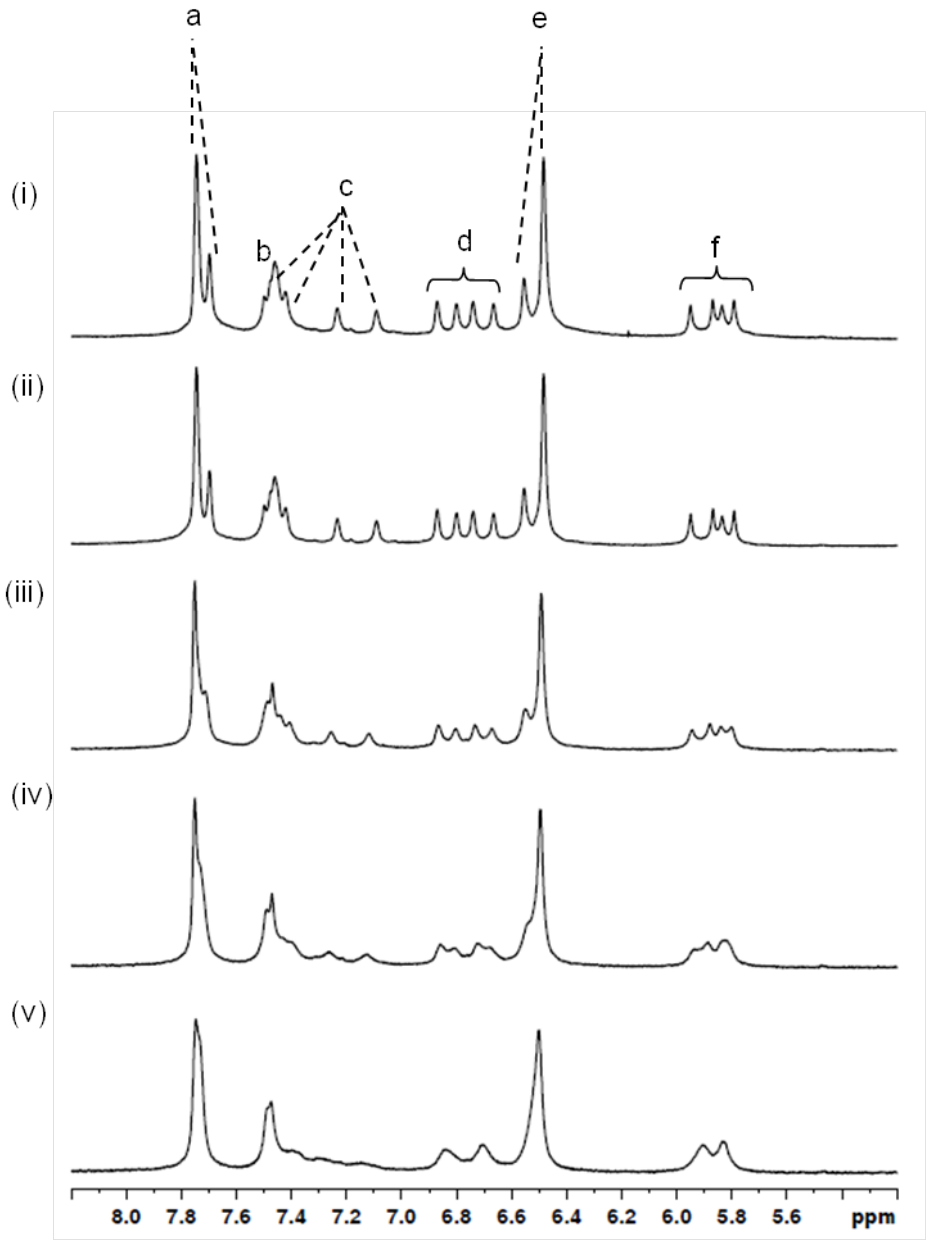

Figure 8.19 Partial ^{1}H NMR spectra (400 MHz, D_2O) of **2a**@OA_2 at (i) 25 $^{\circ}$C, (ii) 35 $^{\circ}$C, (iii) 45 $^{\circ}$C, (iv) 55 $^{\circ}$C and (v) 70 $^{\circ}$C. [OA] = 1 mM in 10 mM borate buffer.

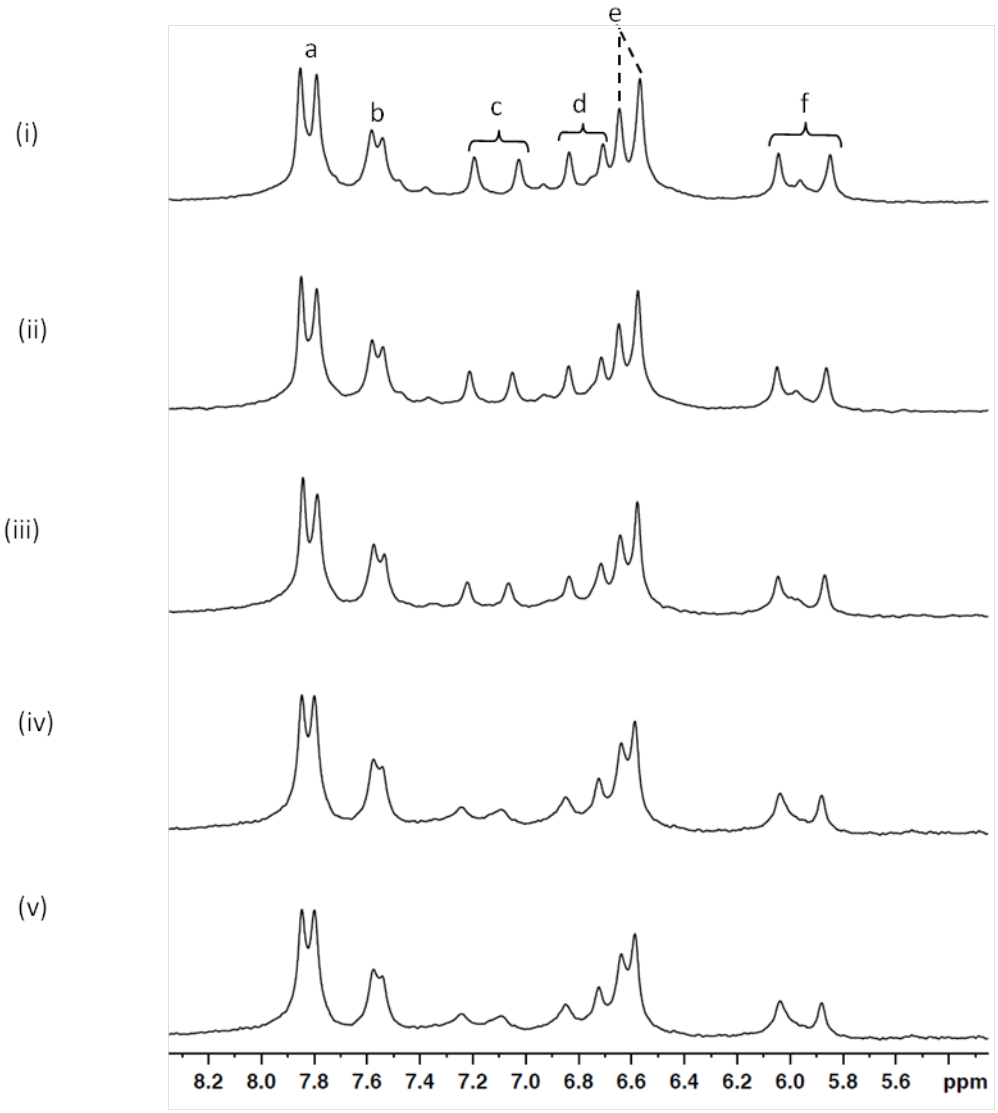

Figure 8.20 Partial ^{1}H NMR spectra (400 MHz, D_2O) of **2b**@OA_2 at (i) 25 $^{\circ}$C, (ii) 35 $^{\circ}$C, (iii) 45 $^{\circ}$C, (iv) 55 $^{\circ}$C and (v) 70 $^{\circ}$C. [OA] = 1 mM in 10 mM borate buffer.

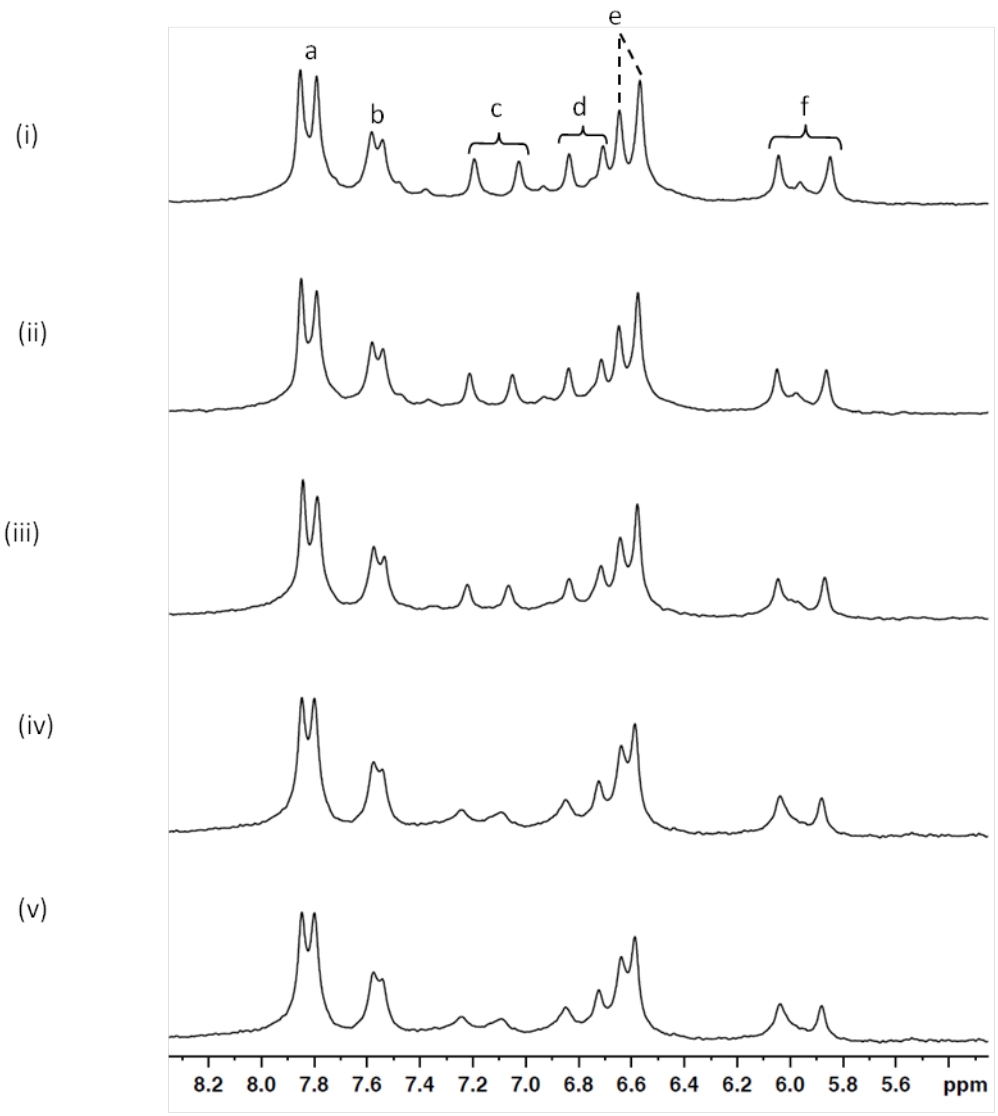

Figure 8.21 Partial ^{1}H NMR spectra (400 MHz, D_2O) of **2c**@OA_2 at (i) 25 $^{\circ}$C, (ii) 35 $^{\circ}$C, (iii) 45 $^{\circ}$C, (iv) 55 $^{\circ}$C and (v) 70 $^{\circ}$C. [OA] = 1mM in 10 mM borate buffer.

8.3 Conclusion

In this study, we have demonstrated the possibility of trapping a high-energy conformer of a piperidine derivative within a supramolecular assembly in aqueous solution. It is important to note that although only one of the five molecules we

investigated to exhibit the unusual behavior it was neither the smallest nor the largest in the series. By ^{1}H NMR study we confirmed that the piperidine derivatives (**2a** to **2e, Scheme 8.1**) formed 2:1 (host:guest) capsuleplex with OA. From 2D DQF COSY spectra, it was found that only one conformation of **2b** to **2e** with C-O-alkyl group at equatorial position exists in solution as well as inside OA capsule. Interestingly the high energy conformer of **2a** (C-O-alkyl group at axial position) was found inside OA capsule but absent in solution (**Scheme 8.2**). From 2D ROESY experiment we also established that the two conformers of **2a** exchange between each other in the longer time range (300 ms mixing time). Using EXSY CALC program we obtained magnetization exchange rate constants that are related to the conformer exchange rate constants k_1 and k_{-1} (**Scheme 8.1**). The activation parameters ($\Delta H^{\neq}$, $\Delta S^{\neq}$ and $\Delta G^{\neq}$) were calculated from the Eyring plot for both the forward and backward process. From the variable temperature ^{1}H NMR experiments, we concluded that these piperidine derivatives tumble inside OA capsule and the rate constants for the tumbling motion decreases with increasing the guest size.

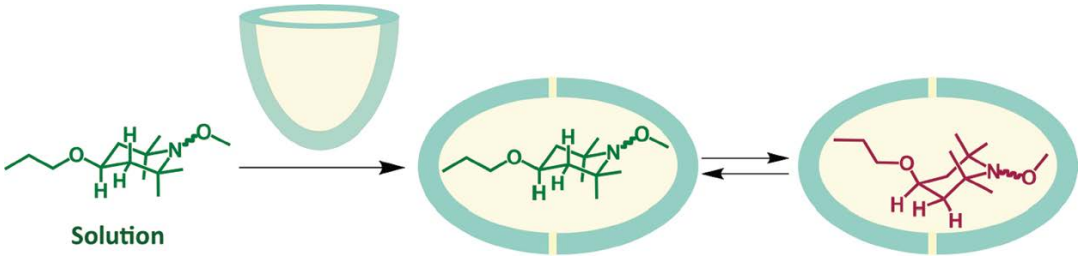

Scheme 8.2 Schematic representation of the two conformations of **2a** within OA capsule

8.4 Experimental sections

Synthesis of guests (2a to 2e)

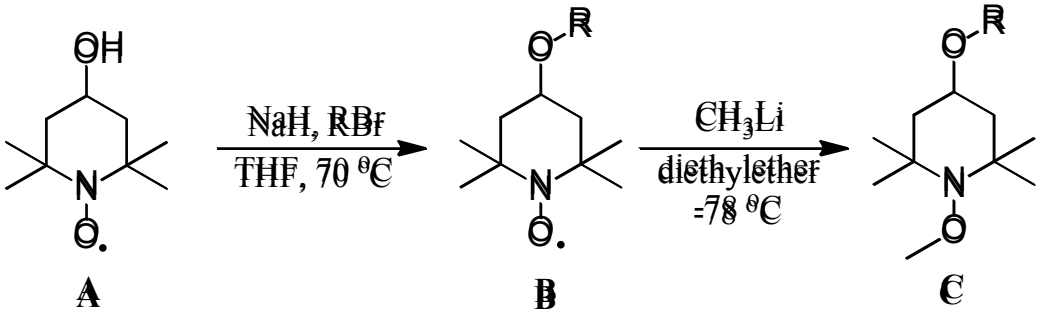

4-Hydroxy-TEMPO (**A**) (150 mg, 0.87 mmol) was dissolved in dry THF and added NaH (70 mg, 1.74 mmol, 60 % mineral oil). After refluxing for 30 min, 1.5 equivalent of corresponding alkyl bromide was added and the mixture was refluxed for two days under nitrogen atmosphere. Solvent was removed under reduced pressure. The reaction mixture was dissolved in $CHCl_3$, washed with water and dried with Na_2SO_4. The product was purified by column chromatography (SiO_2) with 10% EtOAc in hexane. The purity of the obtained products (**B**) was ascertained by comparing its EPR absolute intensity (1 mM in EtOH, deoxygenated with nitrogen) with the 1 mM solution of 4-hydroxy TEMPO.

Compound **B** (100 mg) was dissolved in dry diethyl ether and N_2 gas was passed for half an hour. The temperature of the reaction mixture was brought to –78 $^{\circ}$C using the mixture of dry ice and acetone. Then 1.5 eq. of CH_3Li was added and stirred for 4 hours at –78 ^{o}C. The temperature of the reaction mixture was brought to room temperature and washed with water. Then the solvent was removed under pressure and the product was

dried completely. Purity of the products (**C**) was ascertained by ^{1}H NMR, ^{13}C NMR, GC and GC-MS.

Compound **2a**

^{1}H NMR (300 MHz, $CDCl_3$): δ: 0.9 (t, 3H, *J* = 6 Hz), 1.1 (s, 6H), 1.2 (s, 6H), 1.41 (dd, 2H, *J* = 11 Hz), 1.57 (m, 2H), 1.83 (d, 2H, *J* = 11 Hz), 3.38 (t, 2H, *J* = 6 Hz), 3.52 (m, 1H), 3.65 (s, 3H). **^{13}C NMR (75 MHz, $CDCl_3$):** 10.7, 20.9, 23.4, 33.3, 45.1, 59.9, 65.5, 69.9, 70.3.

GC-MS (m/z, %): 229 (M+, 6%), 214 (M-15, 100%), 158 (M-17, 46%), 116 (M-113, 53%), 107 (M-122, 12%), 88 (M-141, 14%), 82 (M-147, 15%).

Compound **2b**

^{1}H NMR (300 MHz, $CDCl_3$): 1.2 (m, 15H), 1.44 (dd, 2H, *J* = 11 Hz), 1.85 (d, 2H, 11 Hz), 3.52 (m, 3H), 3.63 (s, 3H). **^{13}C NMR (75 MHz, $CDCl_3$):** 15.5, 20.6, 32.9, 44.8, 59.6, 63.1, 65.2, 69.9.

GC-MS (m/z, %): 215 (M+, 10%), 200 (M-15, 100%), 154 (M-61, 40%), 144 (M-71, 71%), 107 (M-108, 13%), 82 (M-133, 15%).

Compound **2c**

^{1}H NMR (300 MHz, $CDCl_3$): 0.96 (t, 3H, *J* = 7Hz), 1.16 (s, 6H), 1.24 (s, 6H), 1.43 (m, 4H), 1.55 (m, 2H), 1.86 (d, 2H, *J* = 11 Hz), 3.45 (t, 3H, *J* = 6Hz), 3.56 (m, 1H), 3.65 (s, 3H). **^{13}C NMR (75 MHz, $CDCl_3$):** 13.7, 19.1, 20.6, 31.9, 32.9, 44.8, 59.6, 65.1, 67.6, 69.9.

GC-MS (m/z, %): 243 (M+, 9%), 228 (M-15, 100%), 172 (M-71, 31%), 154 (M-89, 37%), 116 (M-127, 68%), 107 (M-136, 13%), 85 (M-158, 20%).

Compound **2d**

^{1}H NMR (300 MHz, $CDCl_3$): 0.96 (t, 3H, *J* = 6 Hz), 1.18 (s, 6H), 1.27 (s, 6H), 1.38 (m, H=6H), 1.61 (m, 2H), 1.88 (d, 2H, *J* = 12 Hz), 3.46 (t, 3H, *J* = 6Hz), 3.56 (m, 1H), 3.67 (s, 3H). **^{13}C NMR(75 MHz, $CDCl_3$):** 13.4, 20.2, 21.8, 27.7, 29.2, 32.5, 44.3, 59.1, 64.7, 67.5, 69.5.

GC-MS (m/z, %): 257 (M+, 5%), 242 (M-15, 100%), 186 (M-71, 18%), 154 (M-103, 30%), 116 (M-141, 63%), 107 (M-6%), 88 (M-169, 13%)

Compound **2e**

^{1}H NMR (400 MHz, $CDCl_3$) δ: 0.9 (t, 3H, *J* = 8 Hz), 1.13 (s, 6H), 1.21 (s, 6H), 1.30 (m, 6H), 1.42 (dd, 2H, *J* = 12 Hz), 1.55 (m, 2H), 1.84 (d, 2H, *J* = 12 Hz), 3.41 (t, 8 Hz), 3.49 (m, 1H), 3.61 (s, 3H). **^{13}C NMR (100 MHz, $CDCl_3$): :** 14.5, 21.3, 23, 26.3, 30.6, 32.1, 33.6, 45.5, 60.3, 65.8, 68.7, 70.6.

GC-MS (m/z, %): 271 (M+, 4%), 256 (M-15, 100%), 154 (M-117, 33%), 116 (M-155, 70%)

General protocol for NMR Study

^{1}H NMR on capsular assembly: For NMR titration experiment, a ^{1}H NMR spectrum of 600 μL of 1 mM OA in 10 mM $Na_2B_4O_7$ buffered D_2O was recorded. To this solution 0.2 equivalent increment of guest (2 μL of a 60 mM solution in DMSO) was added, the

mixture was shaken well for about 5 min, and spectra were recorded after each addition. For all 2D NMR studies 5 mM of OA and 2.5 mM of guest in 50 mM borate buffer was utilized.

For 2D ROESY experiment, water suppressed “roesyphpr’ pulse program was used to acquire the data in Bruker (500 MHz) NMR spectrometer. The data on the F1 dimension were acquired in 512 increments with 56 scans of each experiment and processed with the aid of TOPSPIN 2.1 software.

CHAPTER 9

Self Aggregation of Supramolecules of Nitroxides@Cucurbituril

9.1 Overview

Cucurbit[n]urils (CBs) are an emerging family of synthetic macrocyclic hosts that have been extensively studied in the supramolecular chemistry for their ability to incarcerate organic molecules with high association constants. The ready availability of CBs has encouraged their applications as hosts for carrying out selective reactions, vehicles for drug delivery, containers for gas storage, transporters of antibacterial agents, deaggregators of dyes, and light-driven molecular switches, sensors, and motors. A thorough knowledge on the molecular underprinting of the host−guest complexes of CBs and organic and inorganic guest molecules are fundamentally important towards developing the further applications of CBs. This prompted us to study the supramolecular assemblies between 2,2,6,6-tetramethylpiperidine-1-oxyl (TEMPO) derivatives and CBs.[214-216] The presence of a paramagnetic nitroxide group in the TEMPO radical allowed us to use electron paramagnetic resonance (EPR) spectroscopy in the investigation of the molecular dynamics of the host−guest complexation studies.

In this study, we employed three EPR-active cationic nitroxide probes 4-(N,N,N-trimethylammonium)-2,2,6,6-tetramethylpiperidinyl-N-oxybromide (CAT1), 4-(N,N-dimethyl-N-octylammonium)-2,2,6,6-tetramethylpiperidinyl-N-oxy bromide (CAT8) and 4-(N,N-dimethyl-N-dodecylammonium)-2,2,6,6-tetramethylpiperidinyl-N-oxybromide (CAT12) (**1-3**, **Scheme 9.1**) to understand in details the structure of supramolecular complexes of CB7 and CB8 with the nitroxide derivatives in aqueous media. Spin probe CAT1 was first investigated in details to establish the phenomenon and then CAT8 and CAT12 were used to support the findings. The prototypical ^{1}H NMR experiments were

unable to confirm the identity of the complex formation in aqueous solution due to the paramagnetic nature of the probes which in turn resulted in the line broadening of ^{1}H NMR signals of the host. We examined the formation of CAT1 complex with both CB7 and CB8 using ESI-MS data. We also found that the salt concentration played a key role on the above-mentioned characteristics. We further synthesized the diamagnetic analogues of CAT1 (DCAT1, **4**; **Scheme 9.1**) to study by NMR study. Finally 13 different nitroxide derivatives (**5** to **18**, **Scheme 9.1**) were examined to further validate our findings.

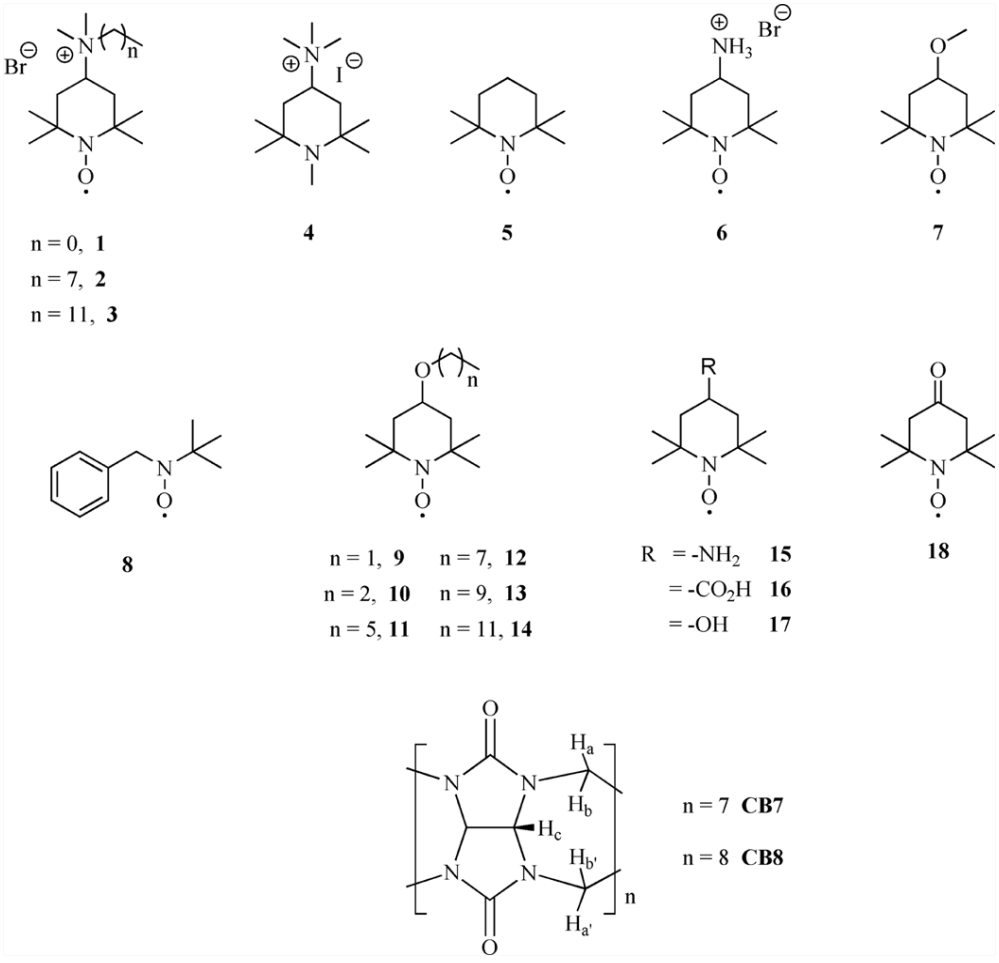

Scheme 9.1 Structures of the nitroxide derivatives and CBs

9.2 Results and discussion

9.2.1 Complexation studies on CAT1@CB7

Due of the paramagnetic nature of the guest, the direct evidence of complex formation of CAT1 and CB7 was not possible through ^{1}H NMR experiments. Stirring an aqueous solution containing equal concentration of CAT1 and CB7 readily resulted in a clear solution which was an indication of complex formation. We recorded the mass spectra of the solution to confirm the complex formation between CAT1 and CB7. For mass spectral studies, the crystal of the complex was dissolved in 10% HBr solution. Peaks at *m*/*z* 1376.4 and 688.9 in the electrospray ionization mass spectra (ESI-MS) (**Fig 9.1**) were assigned to the 1:1 complex (will be represented as CAT1@CB7) and to the protonated complex, respectively. Peaks at *m*/*z* 214.2 and 1163.2 correspond to CAT1 and protonated CB7, respectively.

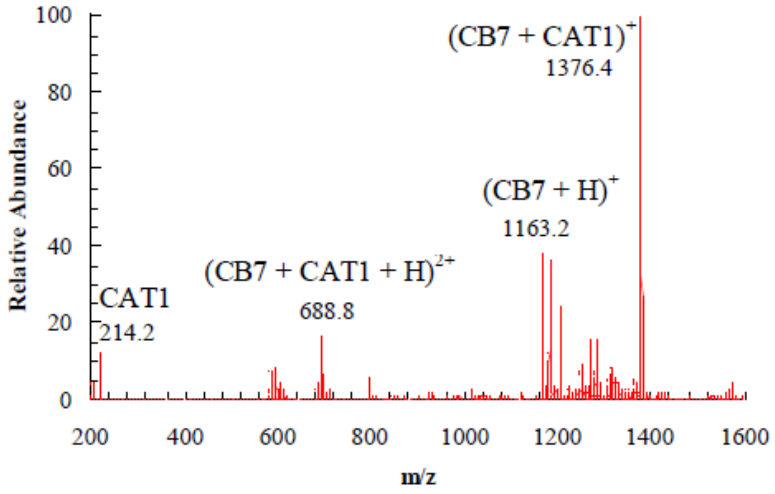

Figure 9.1 Electro-spray-ionization mass spectra of 10% HBr solutions of CAT1@CB7

9.2.1.1 NMR studies on CAT1@CB7

^{1}H NMR experiments were carried out to get information on the structure of the complex.[217] Due to the absence of ^{1}H NMR signals belonging to CAT1 due to its paramagnetic nature, its effect on the ^{1}H signals of CB7 was monitored. ^{1}H NMR spectra of CB7 solution with increasing concentration of CAT1 are shown in **Fig 9.2**. A modest broadening of NMR signals due to all three types of hydrogens at the exterior of CB7 (see **Scheme 9.1** for the identification of hydrogens) was observed upon addition of CAT1 to a solution of CB7 in water. This result suggested that the paramagnetic guest was not very close to these host hydrogens. We proposed two possibilities of the observed phenomenon: (i) a fast exchange between complexed and uncomplexed molecules and (ii) CAT1 binds to the negatively polarized portals of CB7 through its trimethyl ammonium part only (the rest being exposed to water), a scenario where the paramagnetic center would not be close to CB7 hydrogens (**Scheme 9.2**).

As CAT1 complex was not suitable for characterization through NMR, we synthesized DCAT1 (**4**; **Scheme 9.1**), the cationic diamagnetic molecule closest in structure to CAT1. The NMR information obtained with DCAT1 was used to gain insight into the structures of complexes of CAT1 with CB7. ^{1}H NMR spectra of DCAT1 were recorded in the absence and presence of CB7 (**Fig 9.3**). All experiments with DCAT1 were carried out in the presence of sodium carbonate to assure that the piperidinium nitrogen remained as N−CH_3 and was not protonated. The downfield shift of -NMe_3 group and the upfield shift of –Me group of DCAT1 supported in favor of complexation between DCAT1 and CB7. The downfield shift of –NMe_3 group indicated an interact with the carbonyl group of the portal of CB7 and hence support the structure represented

in **Scheme 9.2**. Noticeably there was no shift in the position of –NMe group of DCAT1 in presence of CB7 suggesting that this group was located in water.

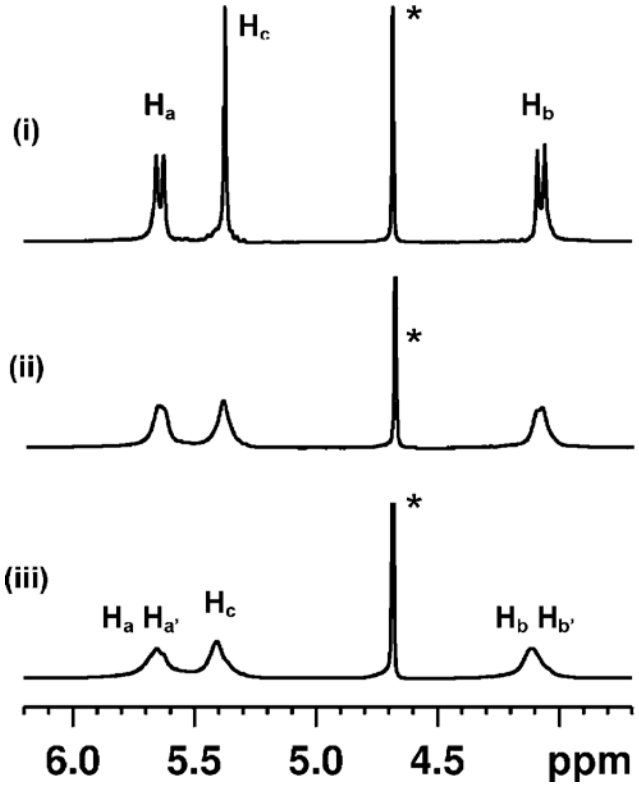

Figure 9.2 ^{1}H NMR spectra of hosts CB7 (1 mM) in the presence of CAT1 at various H/G ratios in D_2O: (i) 1:0 (H/G), (ii) 1:0.4 (H/G), and (iii) 1:1 (H/G). (*) Residual water resonances

Scheme 9.2 Proposed structures of CAT1@CB7 and DCAT1@CB7 complexes

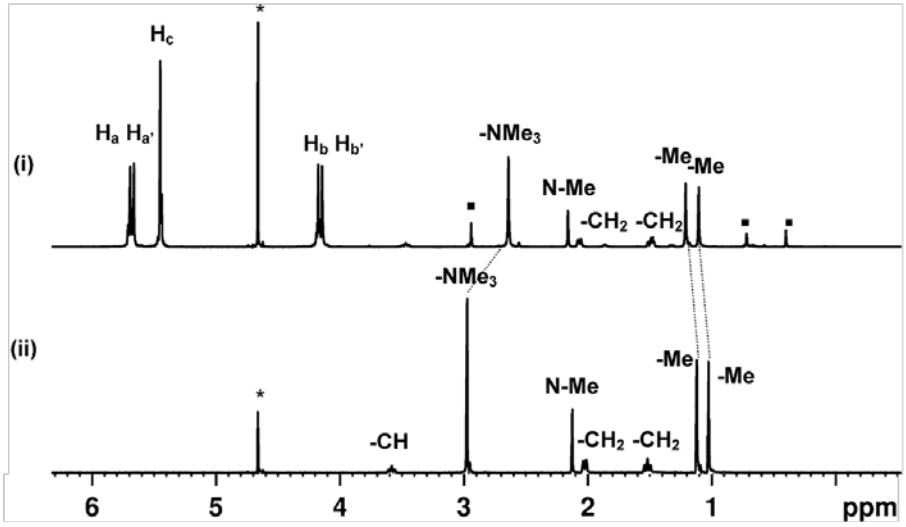

Figure 9.3 ^{1}H NMR (400 MHz, D_2O) spectra of (i) CB7/DCAT1 (1:1) [CB7] 1 mM and (ii) DCAT1. (■) represents a second type of complex in which the piperidinyl moiety is encapsulated within the CB7 cavity (about 16%). (*) Residual water resonances.

9.2.1.2 EPR studies on CAT1@CB7

As CAT1 is a paramagnetic guest, we performed EPR studies to get insight into the complex. EPR spectra of CAT1 in absence and presence of one equivalent CB7 are

provided in **Fig 9.4**. EPR spectra were simulated using a procedure due to Budil and Freed[74] and included with red lines in **Fig 9.4**. The two important parameters: (i) correlation time for motion (τ_{perp}) and (ii) the hyperfine coupling constant A_N for the micropolarity surrounding the probe were extracted from the computation. Upon addition of CB7 to a solution of CAT1 in water, a slight decrease in mobility (increase in τ_{perp} value; τ_{perp} = 0.025 ns in absence and τ_{perp} = 0.093 ns in presence of CB7, **Fig 9.4**) and no change in environmental polarity (A_N = 17 G in absence and in presence of CB7, **Fig 9.4**) of the radical was observed. The slight decrease in mobility (compared to that for uncomplexed free CAT1) was consistent with the probe being weakly bound to the host.[62,130,218] On the other hand no change in the polarity resulted from the nitroxide moiety being exposed in water.

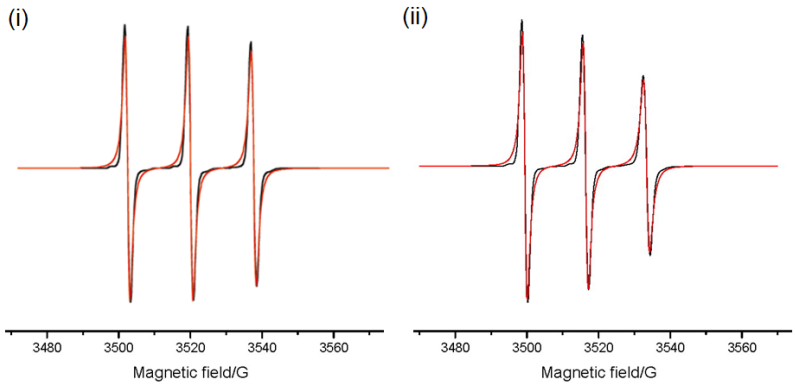

Figure 9.4 EPR spectra (black lines) and their computations (red lines) for CAT1 (i) absence and (ii) presence of CB7. The main parameters obtained from computation are A_N = 17 G; and τ_{perp}= 0.025 ns for [CB7] = 0 and A_N = 17 G, and τ_{perp}= 0. 0.093 ns for [CB7] = 1 mM. In both the cases [CAT1] = 1 mM.

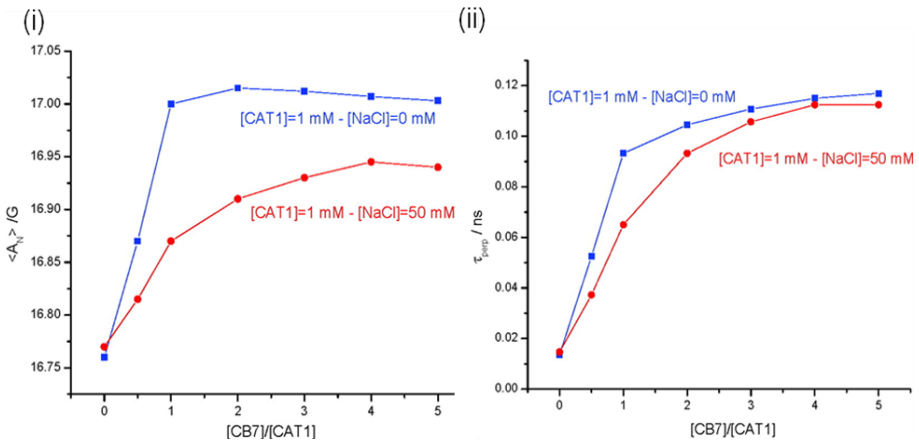

Figure 9.5 Hyperfine coupling constant (i) and rotational correlational time (ii) variations as a functions of [CB7]/[CAT1] in the absence and presence of NaCl 50 mM ([CAT1] = 10^{-3} M).

We also investigated the effect of salt (we used NaCl in this study) on CAT1@CB7 complex. As shown in **Fig 9.5,** the variation of τ_{perp} and A_N parameters for the spectra in the absence and presence of NaCl (50×10^{-3} M) as a function of the CB7/CAT1 molar ratio was obtained by using a constant CAT1 concentration (10^{-3} M). The slight increase in mobility and decrease in polarity upon addition of NaCl might be due to the change in the location of CAT1. Na^+ is known to interact strongly with portal carbonyl groups of CB7 and that could release CAT1.[219] The increase in mobility of CAT1 suggested that the probe was approaching towards water. This behavior may be well described as a competition between the Na^+ and cationic ammonium part of CAT1 for interaction with the carbonyl groups. Thus, both NMR results with DCAT1 and EPR results with CAT1 were consistent with the model that when CAT1 complexed to CB7 in water, the trimethyl ammonium group associated with the portals and the rest of the molecule was exposed to water. This structure was significantly different from the one that will be presented for CAT1@CB8 in the next section.

Overall, the ESI-MS, NMR and EPR results established that CAT1 associated with CB7 when both were present in water. The EPR spectra did not show any additional signals depending on the concentrations of CB7 and CAT1 and the presence of NaCl. In contrast, the EPR results obtained with CAT1 in CB8 were dramatically different and is discussed in the following section.

9.2.2 Complexation studies on CAT1@CB8

The sonication of a mixture of CAT1 and CB8 (concentration range 10^{-4}–10^{-3} M) resulted in a clear solution but in presence of 2×10^{-2} M NaCl. As illustrated in **Fig 9.6**, the mass spectrum of the complex, prepared from an aqueous HBr solution, confirmed the existence of a 1:1 complex between CAT1 and CB8. The peak at *m*/*z* 771.8 corresponds to the protonated doubly charged cation of the complex.

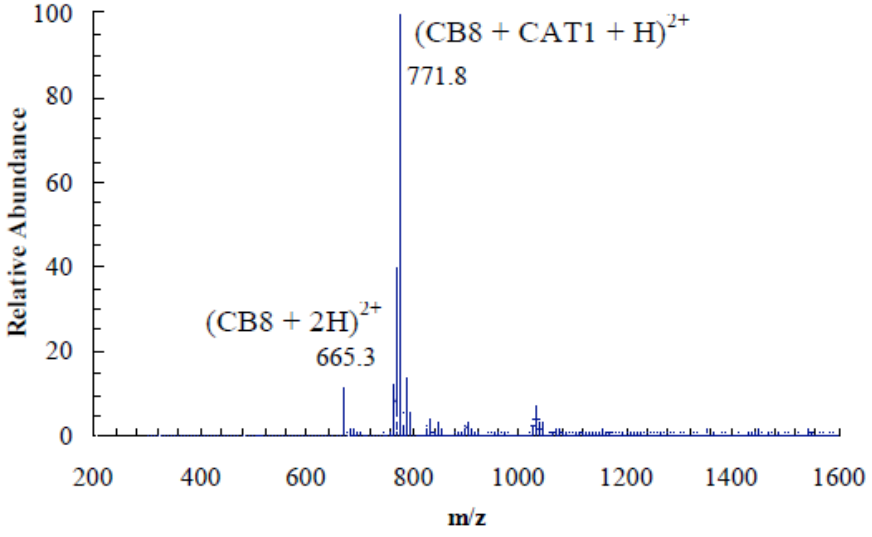

Figure 9.6 Electro-spray-ionization mass spectra of 10% HBr solutions of CAT1@CB8

9.2.2.1 NMR Study

Upon addition of CAT1 to CB8, the ^{1}H NMR signals due to all three types of hydrogens of CB8 were significantly broadened (**Fig 9.7**) suggesting that CB8, unlike CB7, associated strongly with CAT1. To gain insight into the structure of the CAT1@CB8 complex, we used DCAT1 as the model. As shown in **Fig 9.8**, the upfield shift of ^{1}H NMR signals of DCAT1 in presence of CB8 confirmed that DCAT1 formed complex with CB8. Unlike CB7, both tetramethyl hydrogens and trimethyl ammonium hydrogens of DCAT1were upfield shifted in presence of CB8. Such an upfield shift is generally attributed to the group being present within the CB cavity.[138] As illustrated in **Fig 9.8(ii)**, trimethyl ammonium hydrogens were slightly affected whereas tetramethyl hydrogens were significantly upfield-shifted. On the basis of ^{1}H chemical shifts, it was considered that the trimethyl ammonium group was near the portals and the tetramethyl piperidinyl part was deep inside the cavity (**Scheme 9.3**).

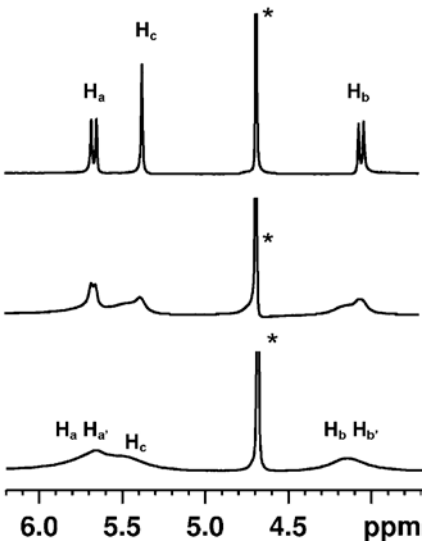

Figure 9.7 ^{1}H NMR spectra of hosts CB8 (1 mM) in the presence of CAT1 at various H/G ratios in D_2O: (i) 1:0 (H/G), (ii) 1:0.4 (H/G), and (iii) 1:1 (H/G). (*) Residual water resonances.

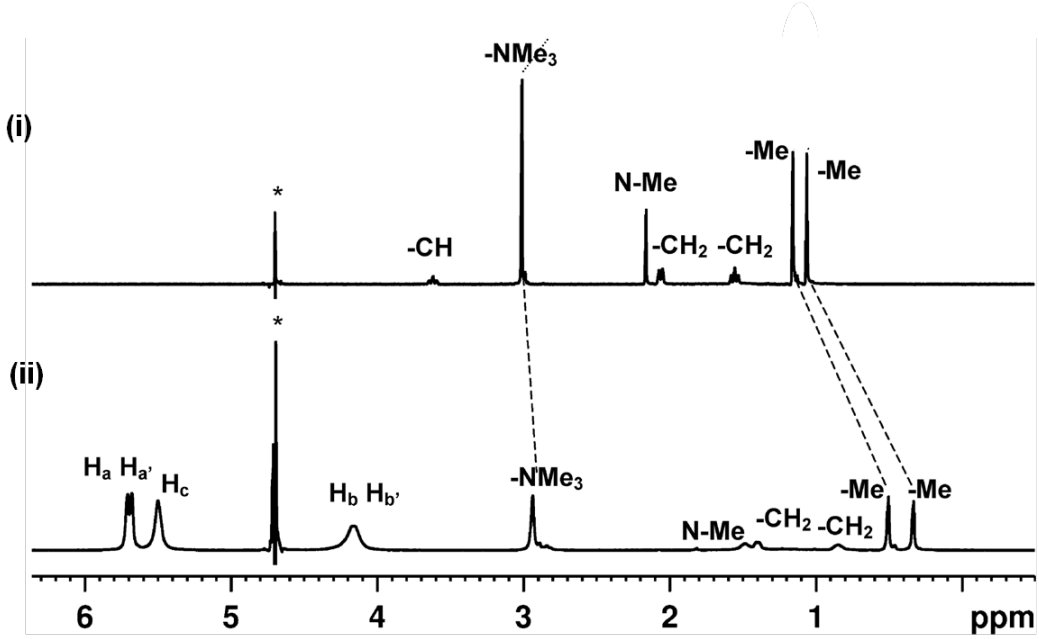

Figure 9.8 ^{1}H NMR (400 MHz, D_2O) spectra of (i) DCAT1, and (iii) CB8/DCAT1 (1:1), [CB8] = 1 mM. (*) Residual water resonances.

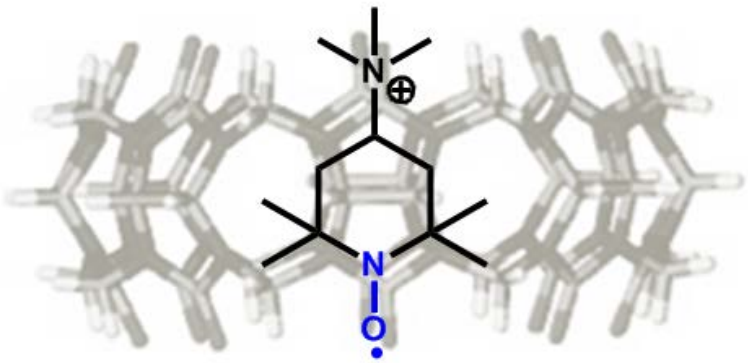

Scheme 9.3 Proposed structure of CAT1@CB8

9.2.2.2 EPR studies on CAT1@CB8

The EPR spectra of CAT1@CB8 at various concentrations of the 1:1 host/guest are shown in **Fig 9.9**. In the range of 10^{-5}–10^{-4} M CAT1@CB8, the spectra consisted of three lines characteristic of a single nitroxide radical, similar to that in the CAT1@CB7

complex (**Fig 9.4**). However, additional lines appeared in the spectrum at 10^{-3} M (**Fig 9.9(iv)**). Interestingly, the addition of NaCl to CAT1@CB8 solution showed the multiline signal even at 10^{-5} M (**Fig 9.10(i)**). Subtraction of the three-line signal observed at 10^{-5}–10^{-4} M in absence of NaCl from the signal obtained at 10^{-3} M in presence of NaCl allowed us to extract the multiline signal shown in **Fig 9.11**. The main feature of that signal was a seven-line component that was simulated (red line in **Fig 9.11**) by considering the coupling of the unpaired spin with three nitrogens at A_N = 5 G. However in presence of NaCl, the contribution of the multiline signal was also increased with the overall concentration of the CAT1@CB8 (**Fig 9.12**).

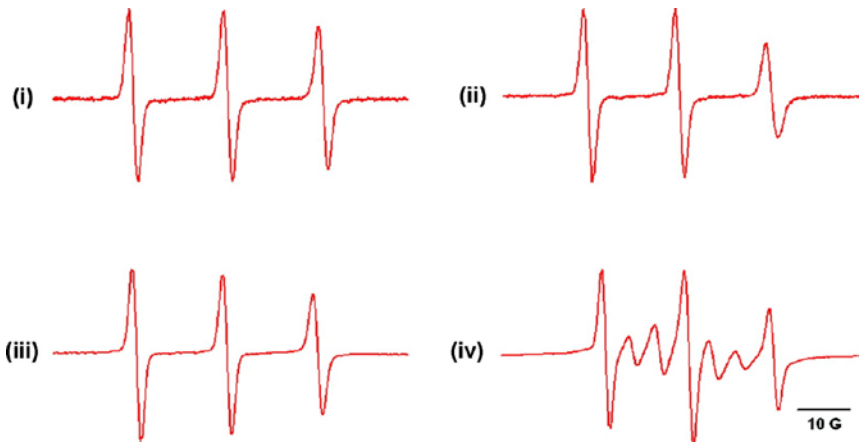

Figure 9.9 EPR spectra of the CAT1/CB8 (1:1) complex at different concentrations: (i) 1 × 10^{-5} M, (ii) 5 × 10^{-5} M, (iii) 1 × 10^{-4} M, and (iv) 1 × 10^{-3} M.

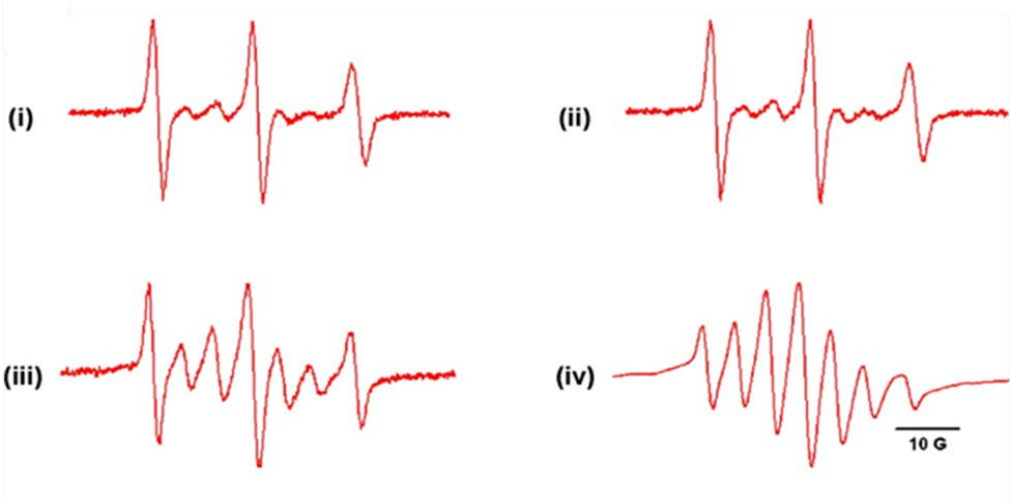

Figure 9.10 EPR spectra of the CAT1/CB8 (1:1) complex at different concentrations with 20 mM NaCl: (i) 1×10^{-5} M, (ii) 5×10^{-5} M, (iii) 1×10^{-4} M, and (iv) 1×10^{-3} M.

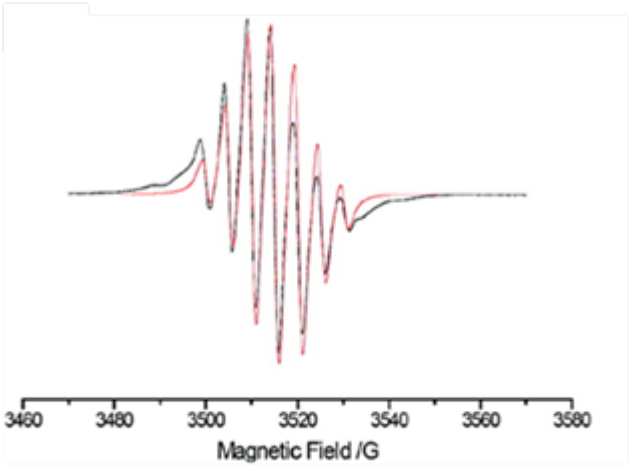

Figure 9.11 Subtracted multiline EPR signal (black line) and computed seven-line component (red line). The computation was obtained by considering the coupling of the electron spin with three nitrogens (A_N = 5 G). Computed data (jump model, red line): g_{ii} = 2.009, 2.006, 2.003; A_{ii} = 6 G, 6 G, 38 G; A_N = 16.67 G; τ_{per} = 5 ns, and dipolar line width = 10 G.

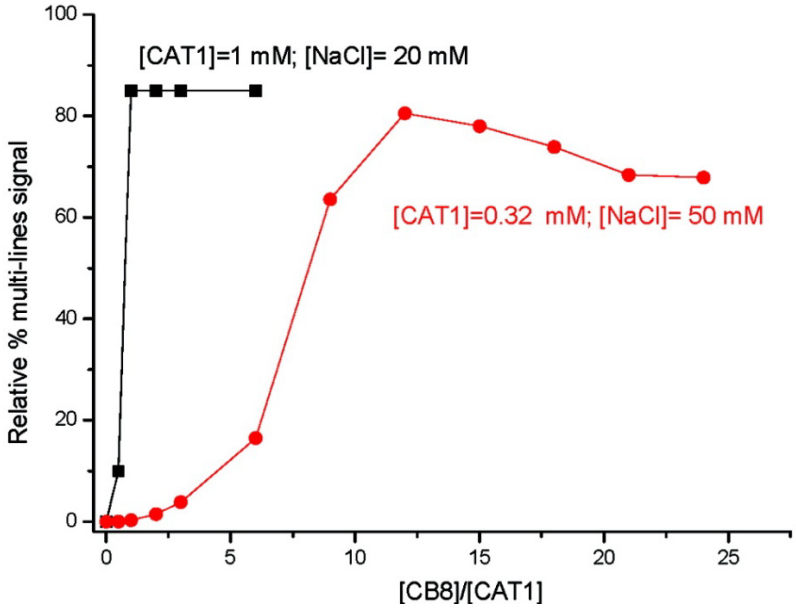

Figure 9.12 Variation of the relative percentage of the multiline signal as a function of the CB8/CAT1 molar ratio for two different CAT1−NaCl solutions selected as examples.

We were interested to explore the different features of CAT1@CB8 complex through EPR spectra. Let's consider the three-line spectrum first. The mobility ($\tau_{perp)}$ and polarity (A_N) of the three-line component decreased with increasing concentrations of the CAT1@CB8 complex. The variation of τ_{perp} and A_N respectively as a function of the CBs/CAT1 molar ratio both for CB8 and CB7 are shown in **Fig 9.13** and **Fig 9.14** ([CAT1] = 0.32 mM and [NaCl] = 50 mM). The A_N coupling constant for CAT1@CB8 (15.95 G) was significantly lower than that measured for CAT1@CB7 (17 G). The reduction in A_N value i.e. reduction in polarity was consistent with the results obtained through NMR that suggested CAT1 to be entirely within the CB8 cavity; and three-line spectrum was due to a single of CAT1 molecule located within the CB8 cavity.

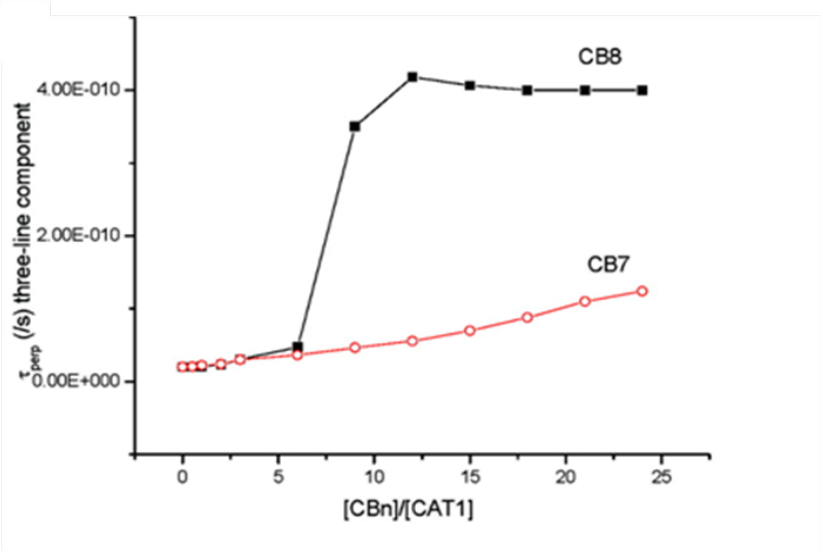

Figure 9.13 Variation of the correlation time for motion of the three-line signal as a function of the CBs/CAT1 molar ratio ([CAT1] = 0.32 mM and [NaCl] = 50 mM).

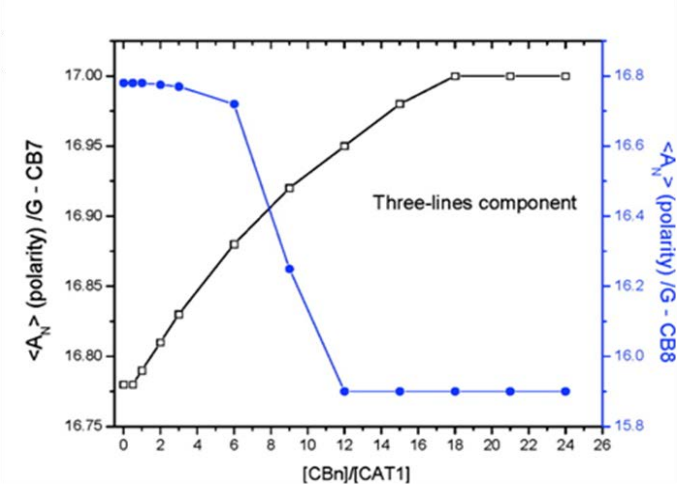

Figure 9.14 Variation the hyperfine coupling constant of the three-line signal as a function of the CBs/CAT1 molar ratio ([CAT1] = 0.32 mM and [NaCl] = 50 mM).

9.2.2.3 Investigation of the origin of the seven-line spectrum in CAT1@CB8

The next experiments were aimed at investigating the interesting origin of seven lines appearing at higher concentrations (10^{-3} M; **Fig 9.9**) and in the presence of NaCl

(**Fig 9.10**). We carried out the same EPR experiments using ^{15}N-isotope-labeled CAT1 to rule out the artifactual nature of the observed effect. As shown in **Fig 9.15**, ^{15}N-labeled CAT1 gave consistent results with the ones observed for unlabeled CAT1. In this case, the spectrum at lower concentration consisted of two lines, and an additional component with four lines appearing at higher concentrations (the same concentrations as found for ^{14}N-CAT1) and in the presence of NaCl. The subtracted signal was well reproduced as a four-line spectrum as shown in **Fig 9.16**.

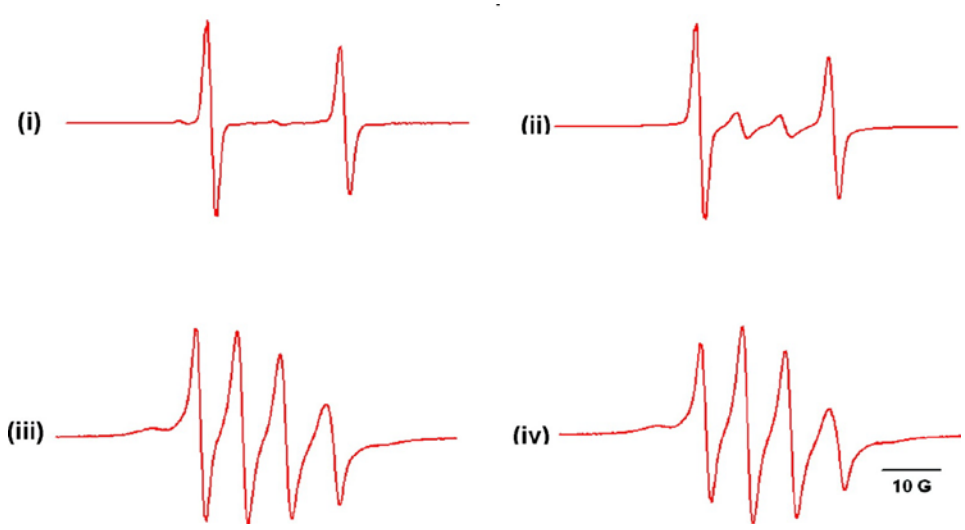

Figure 9.15 EPR spectra of the CAT1 (^{15}N-labeled)/CB8 (1:1) complex: (i) 1×10^{-4} M, (ii) 1×10^{-3} M, (iii) 1×10^{-3} M in the presence of 10 mM NaCl, and (iv) 1×10^{-3} M in the presence of 20 mM NaCl.

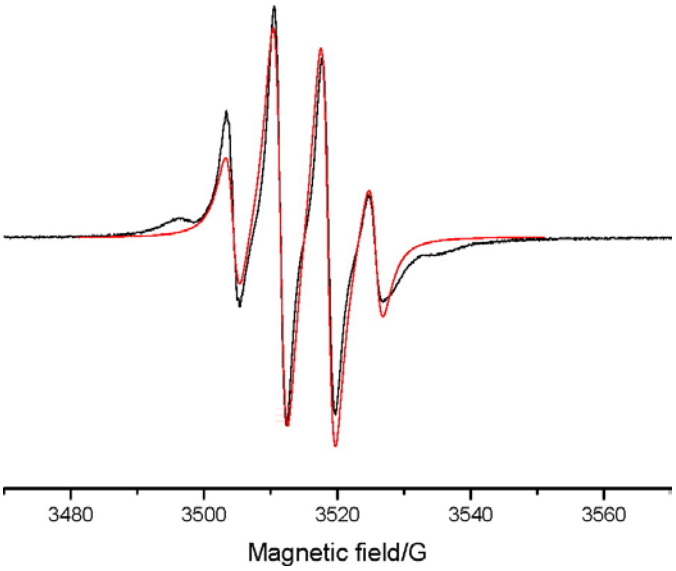

Figure 9.16 Subtracted multiline EPR signal for 1:1 ^{15}N-CAT1/CB8. Computation (red): 3-nitroxides, A_N = 7.15 G.

As shown in **Fig 9.11** and **Fig 9.16**, the coupling constant for the seven-line spectrum for ^{14}N-substituted CAT1 was 5 G, and that for the four-line spectrum of ^{15}N-substituted CAT1 was 7.15 G. Thus the results from ^{15}N-CAT1 confirmed that the seven-line component in EPR spectra of CAT1@CB8 was not an artifact. It is important to note that such a seven-line spectrum was not observed for free CAT1 or for CAT1@CB7 and was unique to CAT1@CB8. The above finding prompted us to investigate the reason behind this unique behavior. A sharp increase in the relative percentage of the multiline signal with an increase in the concentration of CB8/CAT1 complex (**Fig 9.17**) gave us an idea that the phenomenon was concentration-dependent. Hence we hypothesized that the appearance of the multiple EPR signals might be due to aggregate formation of CAT1@CB8 complex in water.

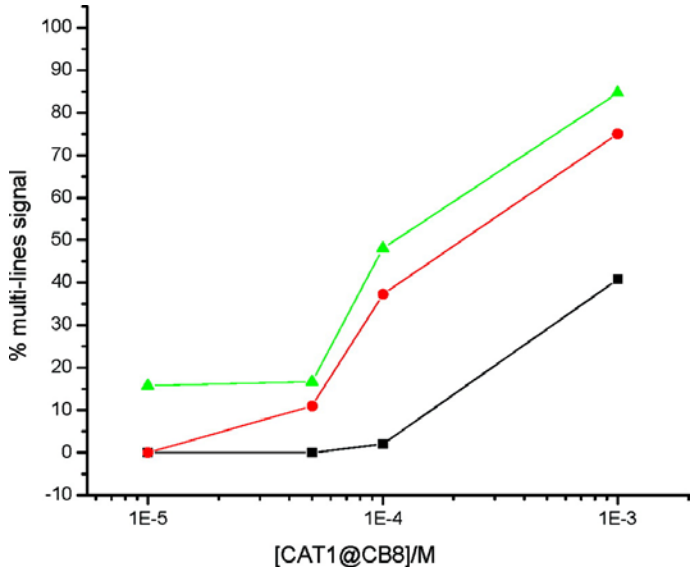

Figure 9.17 Variation of the percentage of the multiline signal as a function of the CAT1@CB8 concentration (1:1 [CAT1]/[CB8]). (Black squares) [NaCl] = 0, (red circles) [NaCl] = 10 mM, and (green triangles) [NaCl] = 20 mM.

The simulated and observed spectra in the case of both ^{14}N- and ^{15}N-substituted CAT1@CB8 were explained by assuming a spin exchange among the three nitroxide radicals. The recorded spectrum was consistent with the spectrum reported for covalently linked trinitroxide radicals where strong intramolecular spin exchange among the three radical centers was assumed.[193] On the basis of the mass spectrometry data and NMR results presented above, it was confirmed that in CAT1@CB8 only a single molecule of CAT1 was included within CB8. As neither the CAT1@CB7 complex nor free CAT1 in aqueous solution exhibited that unusual phenomenon, the role played by CB8 was evident. From the above results it was assumed that there was an association of three supramolecules of CAT1@CB8 (i.e., $[CAT1@CB8]_3$) in a specified geometry that led to spin exchange between the three radical centers. A point to note in this context is that CB8 is much less soluble than CB7 in water. Therefore, a supersaturated solution leading

to aggregation could occur in the case of CB8 complexes more readily than in CB7 complexes. A similar situation is reported in the case of cyclodextrins.[220] β-Cyclodextrin is less water-soluble than α- and γ-cyclodextrin. β-Cyclodextrin complex with a variety of organic molecules readily precipitates from water than α- and γ-cyclodextrin complexes. The aggregation of CAT1@CB8 in water, therefore, is not as fortuitous as the intuitive prediction of the aggregation of three supramolecules.

The contribution of the seven-line component increased at higher concentrations suggesting that a critical concentration of the CAT1@CB8 complex in solution was required for association to occur. For example, the % of seven-line component was ~80% at 10^{-3} M whereas it was absent at 10^{-5} M (**Fig 9.17**). It is reported that NaCl favors the aggregation of organic molecules in water.[119] The increased contribution of the multiline signal of CAT1@CB8 in presence of NaCl was consistent with the above reported fact. CsCl is known to deaggregate organic aggregates in water.[221] The addition of CsCl to a solution of CAT1@CB8 decreased the contribution of the seven-line component (**Fig 9.18**) indicating existence of aggregate in CAT1@CB8 solution. It is well established that NaCl interacts with portals of CB and thus makes the CB complex more soluble in water.[219] In that case NaCl is expected to decrease the contribution of the seven-line spectrum. The opposite phenomenon found in the current study gave a support of the above hypothesis.

Next we wanted to explore whether a mixture of CAT1@CB8 and DCAT1@CB8 could form a mixed aggregate. EPR spectra were recorded varying the composition of CAT1 and DCAT1 by keeping the overall host/guest ratio constant. In the case of mixed aggregation, there were four possibilities (i) $[CAT1@CB8]_3$, (ii)

$[CAT1@CB8]_2 \cdot [DCAT1@CB8]$, (iii) $[CAT1@CB8] \cdot [DCAT1@CB8]_2$, and (iv) $[DCAT1@CB8]_3$ (**Scheme 9.4**). If the solution contained such a mixture, then the EPR would have contributions due to three interacting radicals, two interacting radicals, and a monoradical. The recorded EPR spectra were composed of only three and seven lines (**Fig 9.19**), independent of the relative concentrations of DCAT1 and CAT1. This observation suggested that the aggregation of three supramolecular complexes did not include DCAT1@CB8.

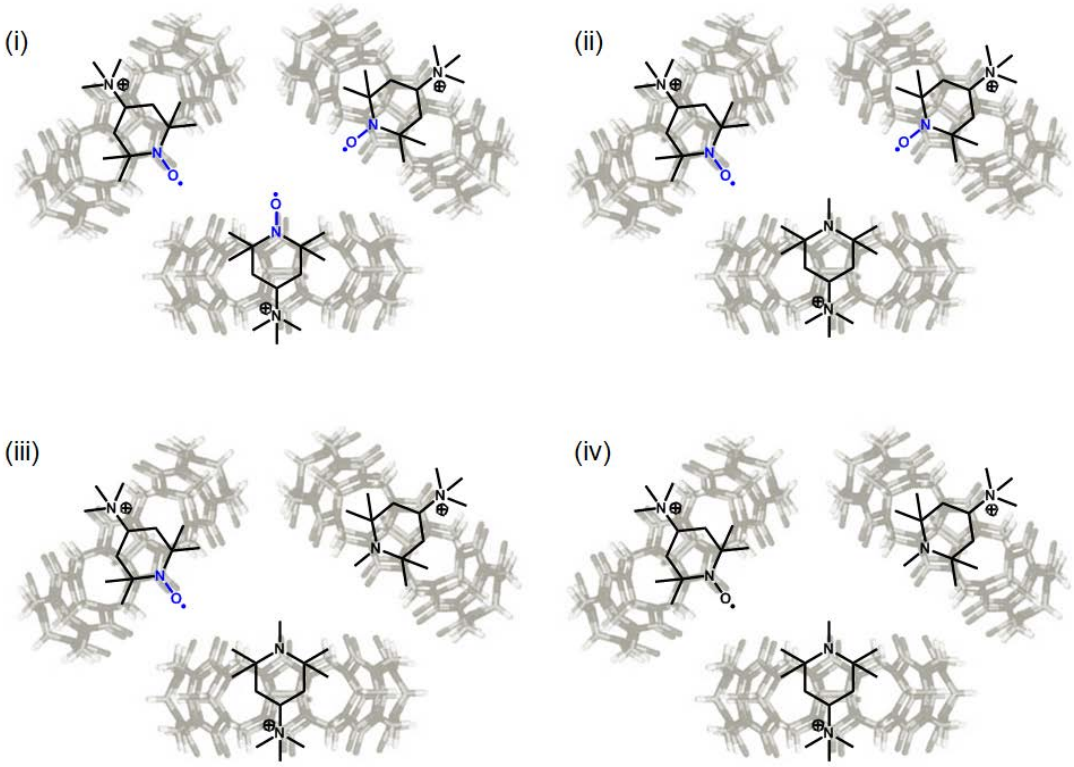

Scheme 9.4 Four possibilities of the mixed aggreagation: (i) $[CAT1@CB8]_3$, (ii) $[CAT1@CB8]_2 \cdot [DCAT1@CB8]$, (iii) $[CAT1@CB8] \cdot [DCAT1@CB8]_2$, and (iv) $[DCAT1@CB8]_3$.

To generalize the aggregation of supramolecular complexes of CB8 and spin probes, we examined two additional cationic paramagnetic probes, CAT8 (**2**) and CAT12 (**3**). Both of them showed behavior similar to that of CAT1. The experimental and simulated seven-line spectra in these two cases are shown in **Fig 9.20**. The complexes of these two molecules with CB8 exhibited both three-line and seven-line component corresponding to an interacting nitroxide molecule complexed to CB8 (**Fig 9.20**). To study whether this unusual phenomenon could be extended to other spin probes, the EPR spectra of nitroxides **5**−**18** (**Scheme 9.1**) complexed to CB8 were recorded in the absence and presence of NaCl (**Fig 9.21**). It was observed the complexes of the nitroxides **5** −**18 (Scheme 9.1)** with CB8 also exhibited the same unusual aggregation as demonstrated by the seven-line EPR spectra in presence and absence of NaCl. Thus, it became clear from the above study that a number of substituted TEMPO derivatives when complexed to CB8 undergo selective aggregation that could be detected by EPR signals.

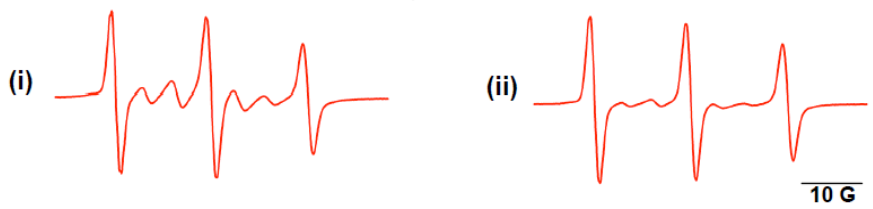

Figure 9.18 EPR spectra (X band, H_2O) of (i) CB8:CAT1 (1:1), and (ii) CB8:CAT1 (1:1) in presence of 100 mM CsCl [CB8] = 1 mM.

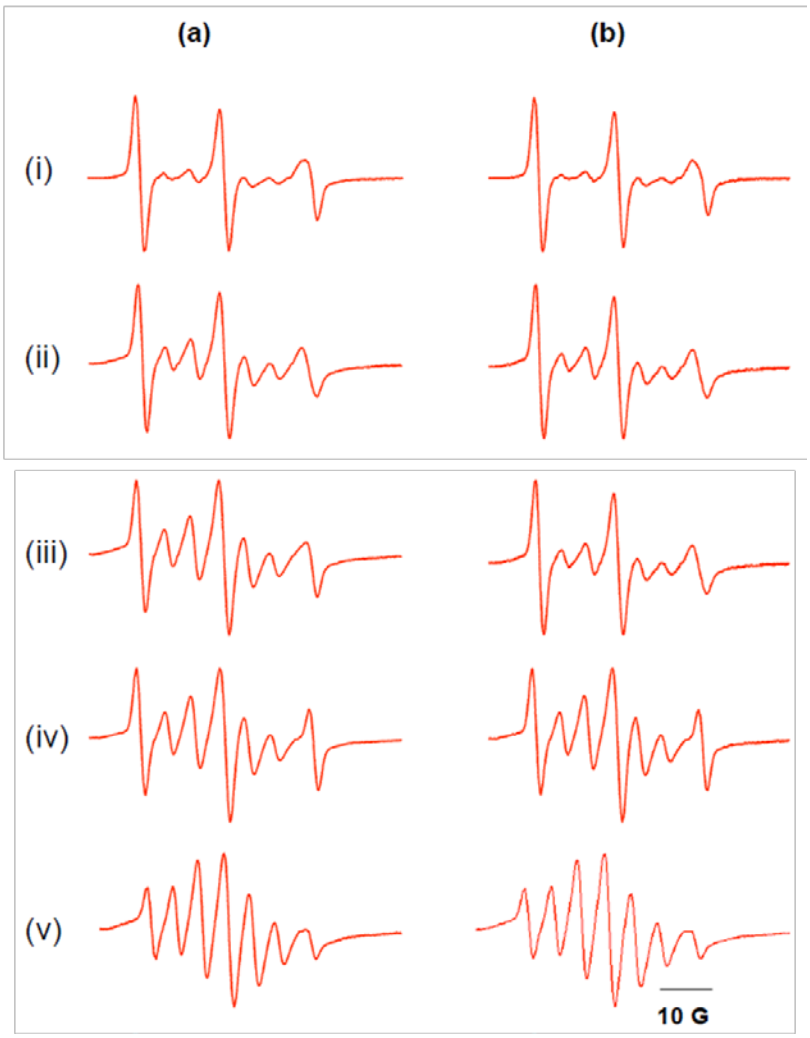

Figure 9.19 EPR spectra of a mixture of DCAT1, CAT1 and CB8 at various ratios of DCAT1and CAT1. (i) CAT1:DCAT1:CB8 (0.2:0.8:1), (ii) CAT1:DCAT1:CB8 (0.4: 0.6:1), (iii)CAT1:DCAT1:CB8 (0.6:0.4:1), (iv) CAT1:DCAT1:CB8 (0.8: 0.2:1) and (v) CAT1:DCAT1:CB8 (1:0:1); (a) in Na_2CO_3 (20 mM), and (b) in presence of Na_2CO_3 and 20 mM NaCl. In all cases [CB8]=1 mM.

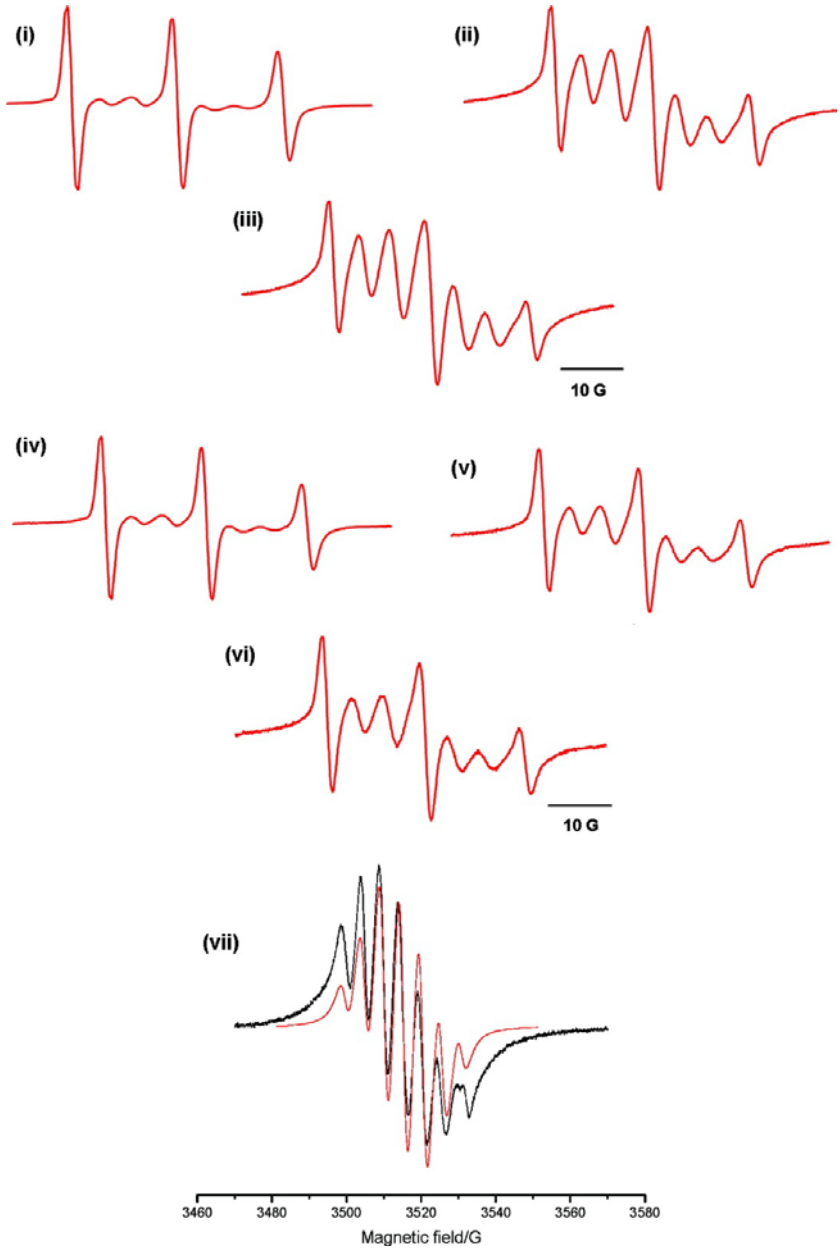

Figure 9.20 EPR spectra (X band, H_2O) of (i) CB8/CAT8 (1:1), (ii) CB8/CAT8 (1:1) in 10 mM NaCl, (iii) CB8/CAT8 (1:1) in 20 mM NaCl; (iv) CB8/CAT12 (1:1), (v) CB8/CAT12 (1:1) in 10 mM NaCl, and (vi) CB8/CAT12 (1:1) in 20 mM NaCl. (vii) Subtracted multiline signal (black line) for CAT8 or CAT12@CB8; the computation (red line) was obtained by considering 3-nitroxides with A_N = 5.15 G.

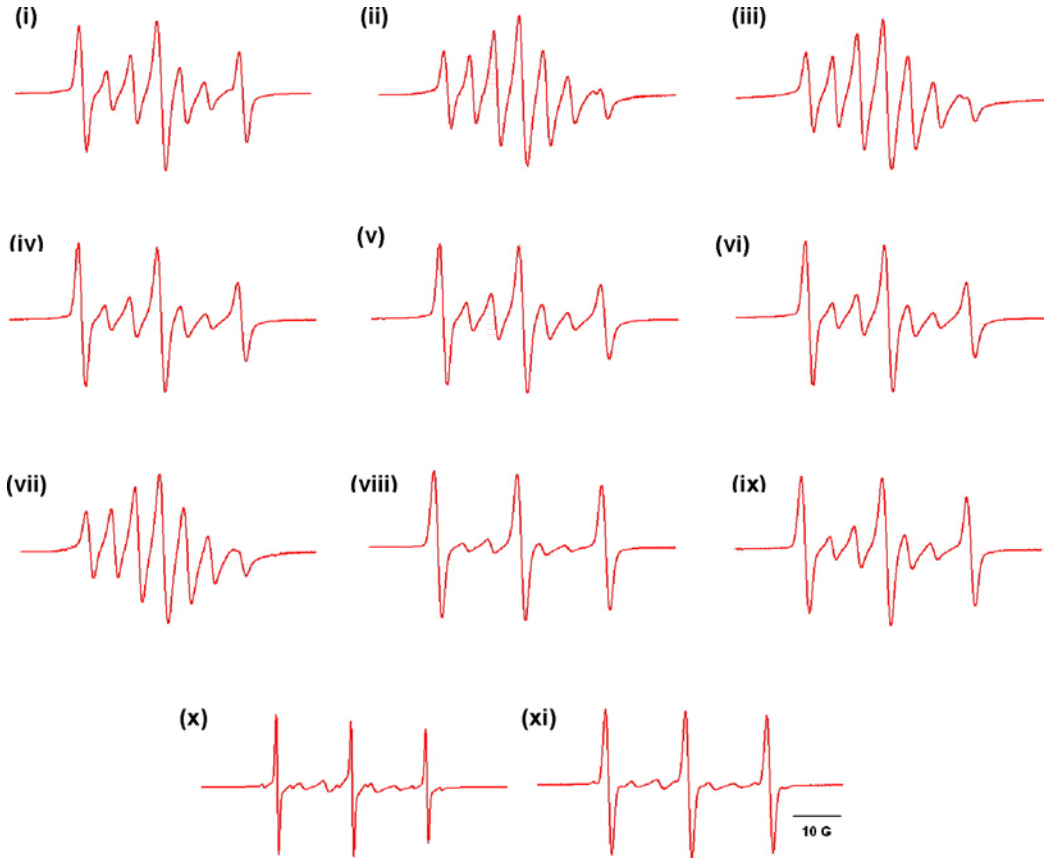

Figure 9.21 EPR spectra of (i) NET2/CB8 (1:1) in 20 mM NaCl, (ii) NET3/CB8 (1:1) in 20 mM NaCl, (iii) NET6/CB8 (1:1) in 20 mM NaCl, (iv) NET8/CB8 (1:1), (v) NET10/CB8 (1:1), (vi) NET12/CB8 (1:1), (vii) 4-amino-TEMPO/CB8 (1:1) in 20 mM NaCl, (viii) 4-carboxy-TEMPO/CB8 (1:1) in 20 mM NaCl, (ix) 4-hydroxy-TEMPO/CB8 (1:2) in 20 mM NaCl, (x) 4-oxo-TEMPO/CB8 (1:2), and (xi) TEMPO/CB8 (1:2). [TEMPO derivative] = 1 mM. See **Scheme 9.1** for the structures of the probes.

9.3 Conclusion

In summary, it was clear that a number of nitroxide molecules formed complexes with the cavities CB8 and CB7 in water. A cationic diamagnetic molecule (DCAT1, **Scheme 9.1**) closest in structure to the cationic paramagnetic guest (CAT1, **Scheme 9.1**) was synthesized to get information about the complex by NMR study. From NMR and

EPR results it was confirmed that CAT1 goes within the CB8 cavity and forms strong complex; whereas CAT1 forms a week complex with CB7.

At concentrations above 10^{-3} M, selective aggregation of three supramolecules of [nitroxide@CB8]$_3$ (**Scheme 9.5**) was detected by EPR. No such aggregation was observed in the case of CB7 complexes. The extent of aggregation enhanced with increasing the concentration of 1:1 complex of CAT1 and CB8 and also in presence of NaCl salt.

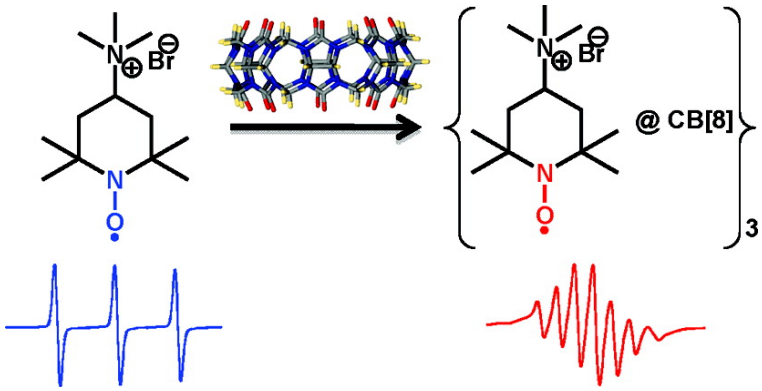

Scheme 9.5 The schematic representation of the selective aggregation of three supramolecules of [nitroxide@CB8] observed by EPR

9.4 Experimental Section

Materials and Methods: The cationic nitroxyl probes (CAT-n)[222] and neutral nitroxyl derivatives were synthesized and other probe molecules studied were purchased from Sigma-Aldrich / Acros organics. Cucurbituril-7 (CB7) and cucurbituril-8 (CB8) were synthesized by following a published procedure.[196]

Synthesis of 4-amino-2,2,6,6- tetramethyl piperidine-N-oxyl derivative (D): 2.5 g of 90 % ice cold HCOOH was added to 1.56 g 4-amino-2,2,6,6-tetramethylpiperidine (**A**) and 1.78 g of 37 % aqueous HCHO solution. The mixture was refluxed for 8 h, 1.1 g of conc. HCl was added, and the HCOOH and excess HCHO were removed under reduced pressure. The oily orange residue was dissolved in 7.5 mL of water and 3 g of solid NaOH was added. The orange layer was collected and lower aqueous layer was extracted twice with 5 mL of diethyl ether. The combined extract was added to the upper layer and dried over potassium hydroxide pellets. The ether layer was removed and distilled under reduced pressure to get a colorless liquid.

*Synthesis of 4-[N,N-Dimethyl-N-(n-alkyl)ammonium]-2,2,6,6-tetramethylpiperidinyl bromide (**C**)*: Compound **C** was prepared by refluxing the mixture of (**B**) and 1.5 equivalent of alkyl bromide at 75 °C without any solvent for one day. The product was purified by triturating the reaction mixture with hexane to afford the product as a white solid. To a mixture of $Na_2WO_4.2H_2O$ (0.15 g, 0.45 mmol) and 1 g of **C** in 15 mL of 1:1 mixture of MeOH and H_2O, 1.5 mL of 30 % ice cooled H_2O_2 was added and stirred for 10 days at rt. The final orange solution was extracted twice from CH_2Cl_2. The product was purified by triturating in petroleum ether. Purity of the product was checked by comparing absolute intensity from EPR spectra of the product (**D**) with 98% 4-hydroxy TEMPO.

*Synthesis of dicationic derivative **E***: 4-N,N-Dimethylamino-2,2,6,6-tetramethylpiperidine-N-oxyl derivative (**B**) (400 mg) was added to excess of methyl

iodide (2 mL) and refluxed for 7h under nitrogen atmosphere. Excess methyl iodide was removed under reduced pressure to afford the dicationic derivative **E** as a white solid. It was purified by recrystallization in hexane/THF).

NMR spectral data for dicationic derivative **E**: (400 MHz, D_2O) δ: 1.12 (s, 6 H), 1.22 (s, 6 H), 1.62 (dd, 2 H), 2.13 (d, 2 H), 2.23 (s, 1 H), 3.07 (s, 9 H), and 3.67 (dd, 1 H); 13C NMR (100 MHz, CDCl3) δ: 20.9, 28.5, 34.1, 40.7, 51.6, 56.2, and 68.9; FAB-MS: 213 (100 %) ($M\text{-}H^+\text{-}2I$).

*Synthesis of DCAT1(**F**)*: Neutralization of **E** with excess sodium carbonate solution gave DCAT1. In all NMR and EPR experiments DCAT1 was generated in situ by dissolving the dicationic derivative **E** in an aqueous solution containing sodium carbonate.

Synthesis of 4-alkyloxy TEMPO: 4-Hydroxy-TEMPO (150 mg, 0.87 mmol) was dissolved in dry THF and added NaH (70 mg, 1.74 mmol, 60 % mineral oil). After refluxing for 30 min, 1.5 equivalent of corresponding alkyl halide (for NET1, methyl iodide and for other compounds alkyl bromide) was added and the mixture was refluxed for two days under nitrogen atmosphere. Solvent was removed under reduced pressure. The reaction mixture was dissolved in $CHCl_3$, washed with water and dried with Na_2SO_4. The product was purified by column chromatography (SiO_2) with 10% EtOAc in hexane. Purity of the product was ascertained by GC and GC-MS. The purity of the obtained product was ascertained by comparing its EPR absolute intensity (1 mM in EtOH, deoxygenated with nitrogen gas) with 1 mM solution of 4-hydroxy TEMPO. The purity of the synthesized compounds was above 98 %.

Preparation of host/guest complex at different concentration: Stock solution of guest was prepared in water (20 mM stock solution to make the complex at 10^{-3} M, 10 mM stock solution to make the complex at 10^{-4} M and 1 mM stock solution to make the complex at 5×10^{-5} M and 10^{-5} M). Host stock solution (1 mM to make the complex at 10^{-3} M and 10^{-4} M; 0.1 mM stock solution to make the complex at 5×10^{-5} M and 10^{-5} M) was prepared in water. Required amount of water, host and guest solutions were added in order to make the H : G ratio of 1 : 1, and shacked by a mechanical shaker for 15 h. The same procedure was adopted for all guests.

Preparation of host/guest complex with different concentration of salt solution: 600 mM stock solution of salt (NaCl and CsCl) was prepared in water. Host/guest solution was prepared first following the above procedure (d). Required amount of corresponding salt solution was added, shaken for 2 h and recorded EPR spectra.

Preparation of host/guest complex with CAT1 and DCAT1 mixture: 20 mM of stock solutions of CAT1 and DCAT1 were prepared in water. Required amount of water, CB8, CAT1 and DCAT1 solutions were added according to the calculated ratios in such a way that 18 total concentration of 1 mM of guest (CAT1 + DCAT1) is maintained. The mixture was shacked for 15 h and recorded EPR spectra.

General Protocol for NMR Study: Titration Experiments

(a) NMR titration of CAT1 with CB (CB7 and CB8): A 1H NMR spectrum of 600 μL of 1 mM CB in D_2O was recorded. To this solution 0.25 equiv of guest (5 μL of a 60 mM

solution in D_2O) was added in four stages, the mixture was shaken well for about 5 min, and spectra were recorded after each addition.

(b) NMR titration of DCAT1 with CB (CB7 and CB8): A ^1H NMR spectrum of 600 μL of 1 mM DCAT1 in D_2O was recorded. To this solution 0.1 equiv of guest (4 μL of a 15 mM solution in 1 mM DCAT1 solution in D_2O) was added in 10 stages, the mixture was shaken well for about 5 min, and spectra were recorded after each addition.

Computational Studies: The calculations were carried out with the Gaussian-03 set of programs. The geometry optimizations were performed at the semiempirical MNDO level and with the density functional theory (DFT) method using Becke's three parameter hybrid functional (B3) combined with the correlation functional of Lee, Yang, and Parr (LYP),[223] with the standard 6-31G(d) basis set.

Mass Spectral Studies: ESI-MS with an Ion-Trap Mass Spectrometer. Positive-ion ESIMS spectra were obtained with a Bruker Daltonics HCT ultra mass spectrometer. The solutions containing the complexes were infused at 4 μL/min directly into the mass spectrometer. Several ionization and ion optics optimization conditions were tested. The used spray voltage was 4.0 kV and the bath gas (N_2) temperature was at 200 ºC. The spectra were obtained in the "ultrascan mode" (0.6 m/z FWHM).

NMR Study: All the ^1H NMR spectra and 2D NMR studies were carried out on a Bruker 500 or 400 MHz NMR spectrometer at 25 °C. Diffusion constant measurements were made using a Bruker 500 MHz NMR spectrometer at 25 °C. Data were collected by using

'stebpg1s' pulse sequence, Δ = 50 ms, δ = 4.0 ms, pulsed field gradients were incremented linearly from 1.06 (2 % of field gradient strength) to 50.35 G/cm (95 % of field gradient strength) in 16 steps with each step consisting of 8 scans. The collected data were processed by T1/T2 relaxation module in the TOPSIN 2.1 software. Phase sensitive 2D-ROESY was recorded in Bruker 400 MHz spectrometer at rt. ROESY spin lock time of 200 ms with the 3.5 s of relaxation delay was used to acquire the data.

EPR Study: EPR spectra were recorded at room temperature in Bruker EMX spectrometer at 9.5 GHz (X band) employing 100 KHz of field modulation frequency. Spectrometer setting: Power, 1.997 mW; amplitude modulation, 0.50 G; time constant, 163.84 ms; conversion time, 163.84 ms. Samples were loaded to quartz (CFQ) EPR tubes from Wilmad LabGlass (2 mm OD, 0.5 mm wall thickness, 10 cm height) for the EPR experiments. The ACSII files of the EPR data were imported to Igor Pro software and the spectral plots were generated.

EPR Simulations: The EPR spectra of the seven line signal were computed by using the program Simfonia by Bruker. The three-lines signals (three hyperfine lines: $2I_N+1 = 3$) were computed by the well-established procedure of Budil and Freed.[74] The main input parameters were as follows. (a) The g_{ii} components (for the coupling between the electron spin and the magnetic field) were the ones previously used for the nitroxide (g_{xx}=2.009, g_{yy}=2.006, g_{zz}=2.0025),[224] and were considered constant for all samples; (b) The A_{ii} principal values of the **A** tensor for the coupling between electron and nuclear spin ($A_N = (A_{xx}+A_{yy}+A_{zz})/3$). An increase in the environmental polarity of the NO group

provokes an increase in the **A** tensor components owing to the increased electron spin density on the nitrogen nucleus. (c) The perpendicular component of the correlation time for rotational diffusion (τ_{perp}). Brownian motion was assumed in the calculation, for which the diffusion component is $D_{perp} = 1/(6\tau_{perp})$.

CHAPTER 10

Suppression of Spin–spin Coupling in Nitroxyl Biradicals by Supramolecular Host–guest Interactions

10.1 Overview

Dynamic nuclear polarization (DNP) is a widely used approach that allows polarization enhancement by two to four orders of magnitude without an increase in the polarizing field strength. DNP has achieved a great interest among the chemists for its potential applications in magnetic resonance imaging (MRI).[225] In a typical DNP experiment, a diamagnetic sample is doped with a paramagnet and the polarization of the electron spins is transferred to the nuclei through microwave irradiation of EPR spectrum.[226] Since the DNP technique was introduced, the experiments were used to perform on monomeric paramagnetic centers such as a metal ion or nitroxide as a source of polarization.[227,228] However, the electron-electron dipole coupling is an important parameter leading to the efficiency of the three-spin processes that involves the coupling of two electrons of the polarizing agent. In this case, the system corresponds to a three-spin pool of two coupled electrons and a coupled nuclear spin. Thus, it is possible to tune the efficiency of DNP experiments by controlling the distance between the two unpaired electrons. The biradical polarizing agents attribute to a four-fold larger signal intensities over those achieved with monomeric nitroxide, such as 2,2,6,6-Tetramethylpiperidin-1-yl)oxyl (TEMPO) etc.

In recent times, biradicals have been extensively used as electron spin agents for DNP.[229,230] The efficiency of DNP in the three-spin system can be controlled by optimizing the interaction between the coupled electrons in biradicals. A significant amount of research has been put forth on the mechanistic perspective of nitroxyl biradicals.[230-237] Mostly those studies showed how the distance between the nitroxyl moieties can control the spin–spin coupling. Those findings led us to investigate the

supramolecular effect on modulation of the spin–spin coupling in biradicals. We further extended our studies with polyradicals to generalize the findings that we accomplished from the biradicals.

To explore the significance of supramolecular architectures in controlling spin communication between two close by radical centers, we studied the EPR spectra of three binitroxyls[13] namely; di-4-(2,2,6,6-tetramethyl-piperidine-1-oxyl)-terephthalate (**1**), di-4-(2,2,6,6-tetramethyl-piperidine-1-oxyl)-isophthalate (**2**), and di-4-(2,2,6,6-tetramethyl-piperidine-1-oxyl)-phthalate (**3**) in water as well as in supramolecular assembly (**Scheme 10.1**). We examined the effect of a number of hosts such as cucurbit[8]uril (CB8), cucurbit[7]uril (CB7), β-cyclodextrin (β-CD), γ-cyclodextrin (γ-CD), calixarene[8]octa sulfonic acid (CA8) and sodium dodecyl sulfate (SDS) micelle (**Scheme 10.2**)**.** It was also compared the efficiency of the different host systems to control the spin-spin exchange of the two radical centers in the above systems. Finally, the supramolecular effect was tested in the polyradicals such as a biradical **6** and a triradical **7** (**Scheme 10.2**).

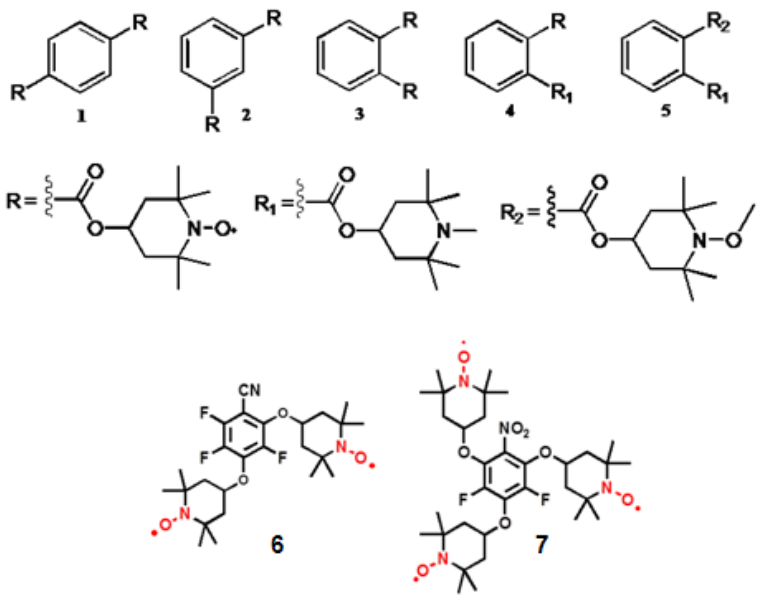

Scheme 10.1 Chemical structures of binitroxyls (**1–3, 6**), mononitroxyl (**4**) and corresponding diamagnetic derivative (**5**) and trinitroxyl (**7**).

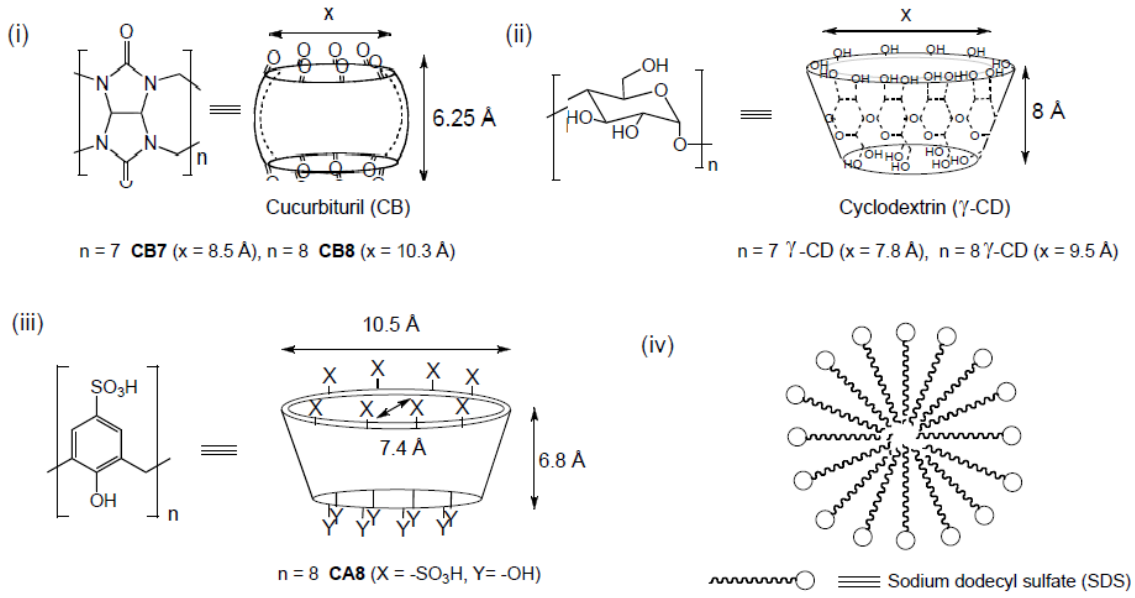

Scheme 10.2 Chemical structures of investigated hosts. Dimensions of the hosts refer to atom-to-atom distance and do not include Van der Wall's radii.

10.2 Results and discussion

10.2.1 EPR study in solution

As the probes were paramagnetic, we found EPR as an appropriate tool to gain insight into their complexes with different hosts. EPR spectra of the probes (**1–3, Scheme 10.1**) were recorded in solution to compare them in absence and presence of the various hosts. Due to low solubility in water the first two guests (**1** and **2**) were studied in DMSO–water (1 : 1); and **3** was studied in water. Experimental and computed spectra are shown in **Fig 10.1**. The spectra were simulated using the well-established procedure of Freed and co-workers.[74] The two most informative input parameters used in this simulation were: (i) the coupling constant between electron and nuclear spins $\langle A_N \rangle = (A_{xx} + A_{yy} + A_{zz})/3$ which measures the environmental polarity of the nitroxides and (ii) the correlation time (τ) for the rotational diffusion motion of the spin probe which provides information about the guest mobility.

As shown in **Fig 10.1**, binitroxyls **1** and **2** exhibited three-line EPR spectra that are typical characteristic of a mononitroxyl. This observation indicated that their radical centers were too far apart for spin–spin exchange interactions. The EPR spectrum of compound **3** was clearly different from that of **1** and **2** as shown in **Fig 10.1**. The five-line spectrum of **3** in water suggested that each electron was coupled to both the nitrogen atoms of **3** in water (**Fig 10.1**). The EPR spectrum of **3** was attributed to fast inter-conversion between conformers exhibiting weak ($J \approx 0$) and strong ($J \gg A_N$) exchange interaction. The five-line spectrum was computed as the sum of a three-line signal and a two-line signal. Both a three-line signal and a two-line signal (in between the three lines)

were simulated, and the experimental line shape was fitted by adding the two components at the proper relative percentages. We calculated the intensity (in percentage) of a five-line signal expected for very strong exchange with respect to the overall spectral intensity acquired by double integration of the experimental spectra and that enabled us to estimate the variation of the exchange interaction between two radical centers in various systems.

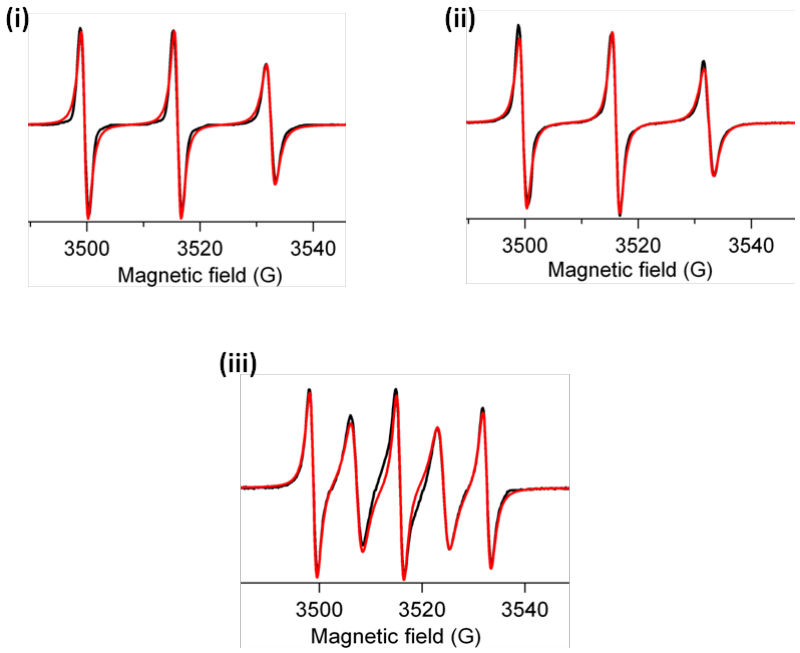

Figure 10.1 EPR spectra (black lines) and their simulations (red lines) for (i) **1** in 50% DMSO and 50% water (0.5 mM), A_N = 16.5 G, τ = 0.14 ns, (ii) **2** in 50% DMSO and 50% water (0.5 mM), A_N = 16.4 G, $\tau \approx$ 0.19 ns and (iii) **3** in water (1 mM) three-line component: A_N = 16.9 G, τ = 0.06 ns, five-line component: 88%.

From the computation of the EPR spectra of **1** and **2** in solutions (**Fig 10.1(i)** and **(ii)**), A_N values were calculated as 16.5 G and 16.4 G, respectively. The correlation times (τ) were measured to be 0.14 ns and 0.19 ns for **1** and **2**, respectively in solution. The absence of five-line component in the EPR spectra of **1** and **2** in solution (**Fig 10.1(i)** and

(ii)) suggested that the two nitroxide moieties of **1** and **2** were far enough to restrict the spin-spin interaction. The three lines (1, 3 and 5) or the two lines (**2** and **4**) in the five-line EPR spectra of **3** in water (**Fig 10.1 (iii)**) were separated by 16.9 G, slightly lower than the hyperfine splitting of TEMPO (monoradical) in water (17.1 G).[238] The correlation time (τ) was calculated as 0.06 ns which is a characteristic of fast rotating nitroxyl radicals.[239] The relative percentage of the exchange coupling (1:2:3:2:1) was estimated to be 88%. The above measurements suggested that the two nitroxyl groups in the biradical **3** dynamically approach each other in water resulting in strong spin–spin exchange. From the above study, **3** was chosen as the best candidate to further examine the influence of supramolecular hosts on spin–spin exchange between two radical centers.

10.2.2 EPR study in supramolecular systems

It is reported that mononitroxyls such as TEMPO can be incarcerated within the cavities of cyclodextrins, cucurbiturils and calixarenes and micelles.[238,240-242] We were interested to investigate whether such an inclusion would control the exchange interaction between two nearby nitroxyl centers in biradical molecules such as **3**. The EPR spectra (experimental and simulated) of **3** in the presence of one equivalent of CB8 are shown in **Fig 10.2**. The transformation of the five-line spectrum in water (**Fig 10.1(iii)**) to a three-line spectrum in the presence of CB8 (**Fig 10.2**) suggested that one equivalent of CB8 was sufficient to remove the spin–spin exchange interaction completely in **3**. From simulation of the EPR spectrum, it was measured that τ increased from 0.06 ns in pure water (**Fig 10.1(iii)**) to 0.21 ns in the presence of one equivalent CB8 (**Fig 10.2**). Addition of more than one equivalent of CB8 did not show any change

on the spectrum confirming that only one of the two nitroxyl groups could be included within CB8. The two key observations that supported our hypothesis are: (i) there was no significant change in the τ values between the addition of one and two equivalents of CB8 (0.21 ns *vs.* 0.24 ns), and (ii) estimated polarities of the nitroxyl environment based on the hyperfine splitting constant (A_N) was not reduced significantly in the presence of CB8 from that in pure water (16.9 G for **3** in water, **Fig 10.1(iii)** and 16.7 G for **3**@CB8 in water, **Fig 10.2**).[62] Similar polarity experienced by the nitroxyl radical in **3** and **3**@CB8 in water implied that one of the two nitroxyl groups in **3**@CB8 remains uncomplexed and is exposed to water. Further addition of CB8 did not result in any alteration of A_N.

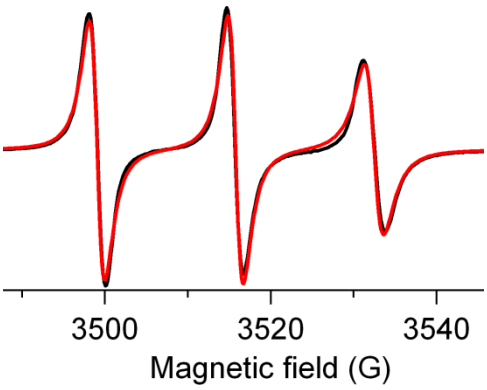

Figure 10.2 EPR spectra (black lines) and their simulations (red lines) for **3**@CB8 (1:1) A_N = 16.7 G, τ = 0.21 ns. Concentrations of host and guest: 1 mM.

Based on the above discussions, it was confirmed that the supramolecular steric effect provided by encapsulation of one paramagnetic moiety of **3** with CB8 was sufficient to eliminate the spin communication between the two nitroxyl radicals, one complexed to CB8 and other one free (**Scheme 10.3**). Three of the many possible conformations of **3** in water as well as in presence of CB8 are represented in **Scheme**

10.3. Spin communication was suppressed by adoption of a conformation where the two nitroxyl groups in **3**@CB8 were separated far enough not to exchange each other's spin and the CB8 cage wall was a barrier for spin–spin coupling.

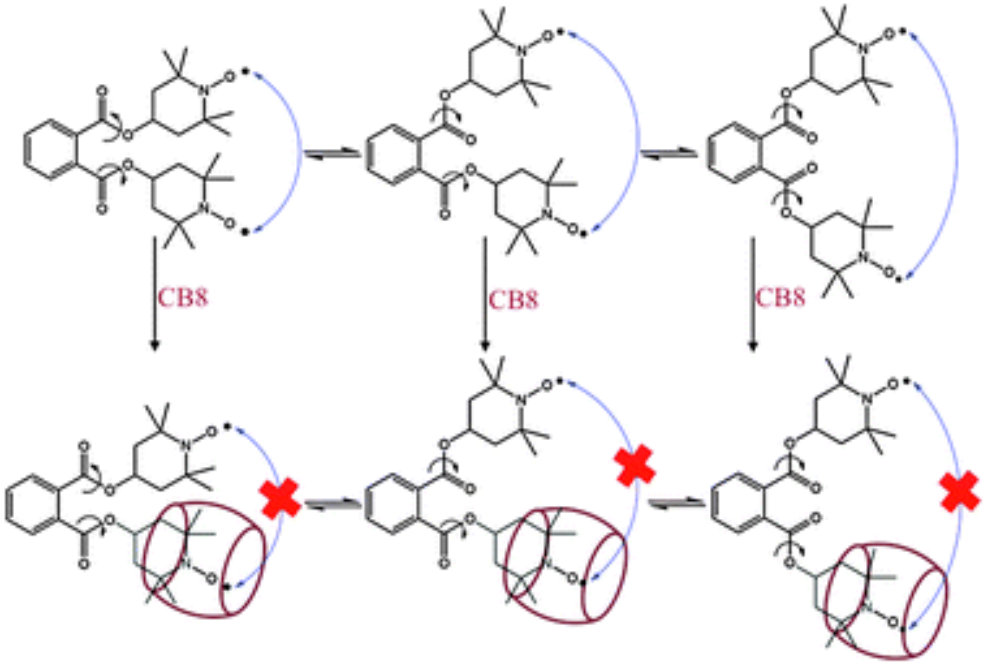

Scheme 10.3 Schematic representations of the possible conformers of **3** and **3**@CB8.

Monoradical **4**, an analogue of **3** (**Scheme 10.1**) but with one diamagnetic N–CH_3 group and one paramagnetic NO group was synthesized for further studies on the complexation process. The rationale was that the diamagnetic part could be characterized by ^{1}H NMR while the paramagnetic part with nitroxide group by EPR. ^{1}H NMR spectra of **4** in $CDCl_3$, D_2O and in presence of one equivalent of CB8 are shown in **Fig 10.3**. NMR signals of the protons of **4** in $CDCl_3$ were sharp enough to assign the signals (**Fig 10.3(i)**). In water, the paramagnetic nitroxyl group possibly broadened the ^{1}H NMR signals of the tetramethyl groups of the adjacent *N*-methylpiperidinyl indicating the

existence of electron–^{1}H spin communication between the two groups (**Fig 10.3(ii)**). An upfield shift of the signals of *N*-methylpiperidinyl group of **4** in presence of CB8 suggested its inclusion within CB8 (**Fig 10.3(iii)**). Addition of more than one equivalent of CB8 resulted in a turbid solution which did not allow us to further carry on NMR analysis. To probe whether the other part with NO group was included within CB8, we recorded the EPR spectrum of **4**@CB8 complex. The experimental and simulated spectra are shown in **Fig 10.4**. The hyperfine splitting of **4** in absence/presence of CB8 was similar (free: A_N = 16.9 G; and complexed to CB8: A_N = 17 G) indicating that the paramagnetic nitroxyl moiety was exposed in water outside the CB8 cage. However, the rotational correlation time of **4** was slightly higher in the presence of CB8 compared to **4** free in solution (complexed: 0.14 ns; free: 0.04 ns) might be due to the steric hindrance of the rotational mobility of the paramagnetic moiety by the encapsulation of the diamagnetic part with CB8. Taken together, the results indicate that the more hydrophobic piperidine moiety (with N-CH_3 group) was included within CB8 whereas less hydrophobic piperidine moiety (with NO group) was exposed in water. The ^{1}H NMR and EPR experiments with **4** proved the hypothesis that we previously made for **3** (paramagnetic analogue of **4**) stating that the inclusion of one of the two piperidine moieties inside CB8 was adequate to arrest the spin-spin interaction of the two paramagnetic centers.

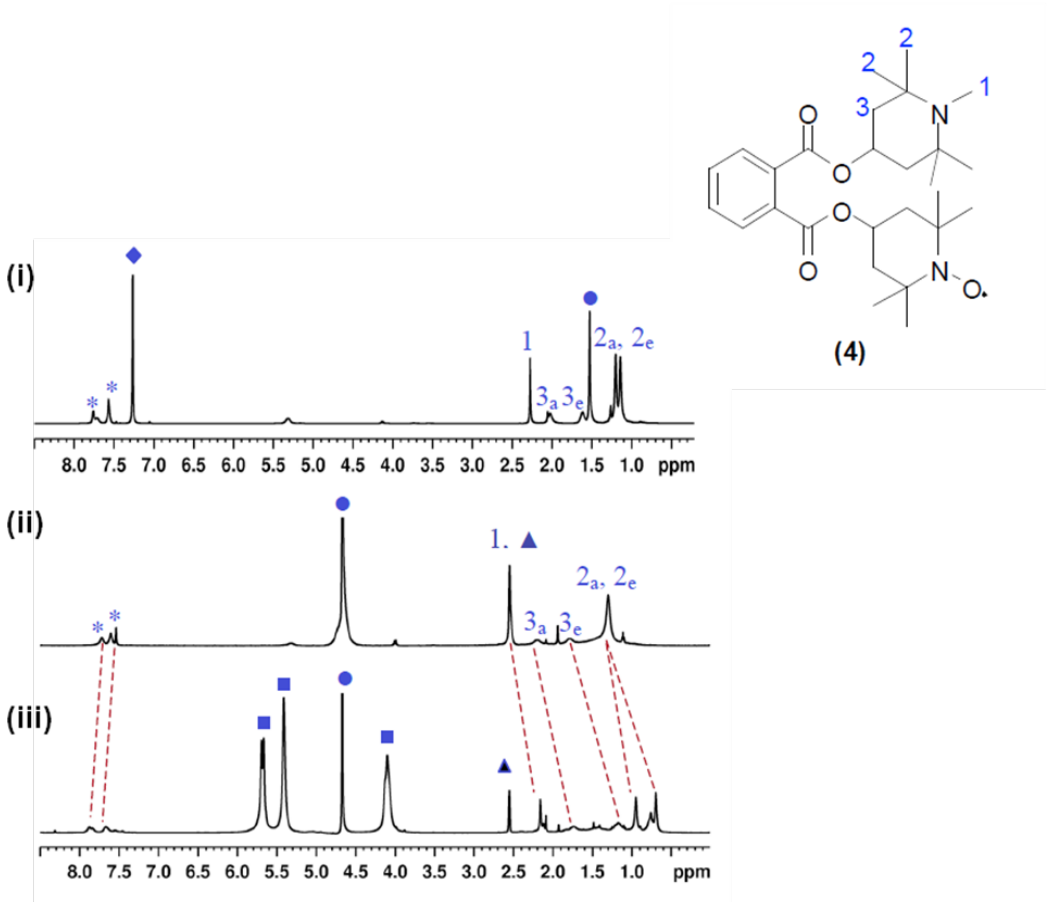

Figure 10.3 ^{1}H NMR spectra of **4** (i) in $CDCl_3$ (1 mM, 500 MHz) (ii) in D_2O (1 mM, 500 MHz) and (iii) **4**@CB8, (H:G = 1:1, [**4**] =1 mM, (500 MHz). Aliphatic guest resonances are represented with label 1-3 and aromatic guest protons are represented with label "*". The labels 'a' and 'e' represent axial and equatorial resonances. Host resonances are represented with label "■". The subscript 'a' and 'e' describes the 'axial' and 'equatorial' position in the piperidine moiety. The labels "♦", "▲" and "●"represent the residual $CHCl_3$, DMSO and H_2O resonances respectively.

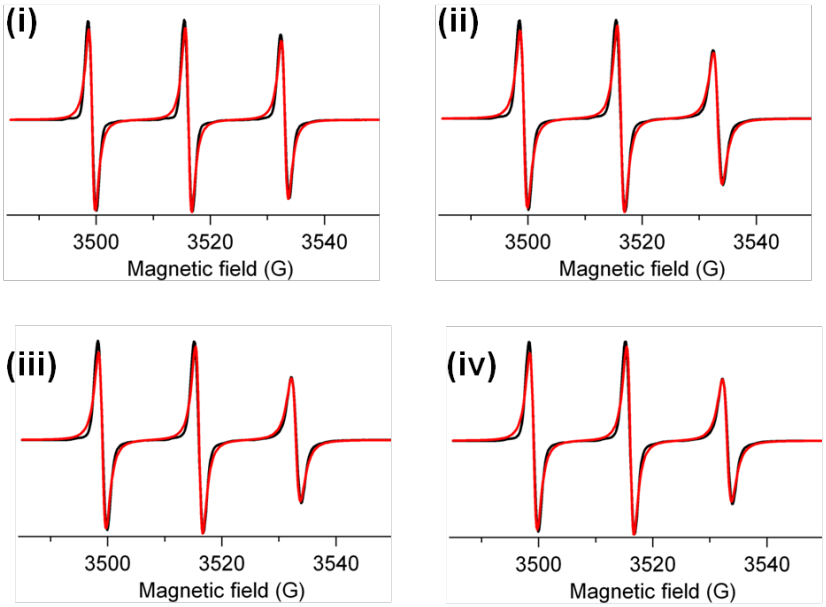

Figure 10.4 EPR spectra (black lines) and their simulations (red lines) for (i) **4** in water (1 mM), A_N = 16.9 G, τ_c = 0.042 ns (ii) **4**/CB8 (1:1), A_N = 17 G, τ_c = 0.11 ns and (iii) **4**/CB8 (1:2), AN = 16.9 G, τ_c = 0.14 ns and (iv) **4**/CB8 (1:3), A_N = 16.9 G, τ_c = 0.14 ns.

A diamagnetic equivalent compound of **3** (**5, Scheme 10.1)** was synthesized to further confirm (by ^{1}H NMR) that only one of the two groups in **3** was included within CB8. ^{1}H NMR spectra of **5** in water in the presence and absence of CB8 are shown in **Fig 10.5**. In was observed that upon addition of one equivalent of CB8, -NOMe group of **5** was not upfield shifted whereas –NMe group was upfield shifted. The upfield shift of the signals due to the four methyl groups of the *N*-methylpiperidyl ring was consistent with the above NMR data (**Fig 10.5**). This observation suggested that only piperidine moiety with N-Me group was encapsulated within CB8 whereas –NOMe located in water. Addition of more than one equivalent of CB8 resulted in no change in the spectra confirming that **5** similar to **3** and **4** forms only 1 ∶ 1 (guest ∶ host) complex with CB8. As

5 and **5**@CB8 complex had a very limited solubility in water we were unable to carry out NOESY studies to ascertain the conformation of complexed and uncomplexed **5**.

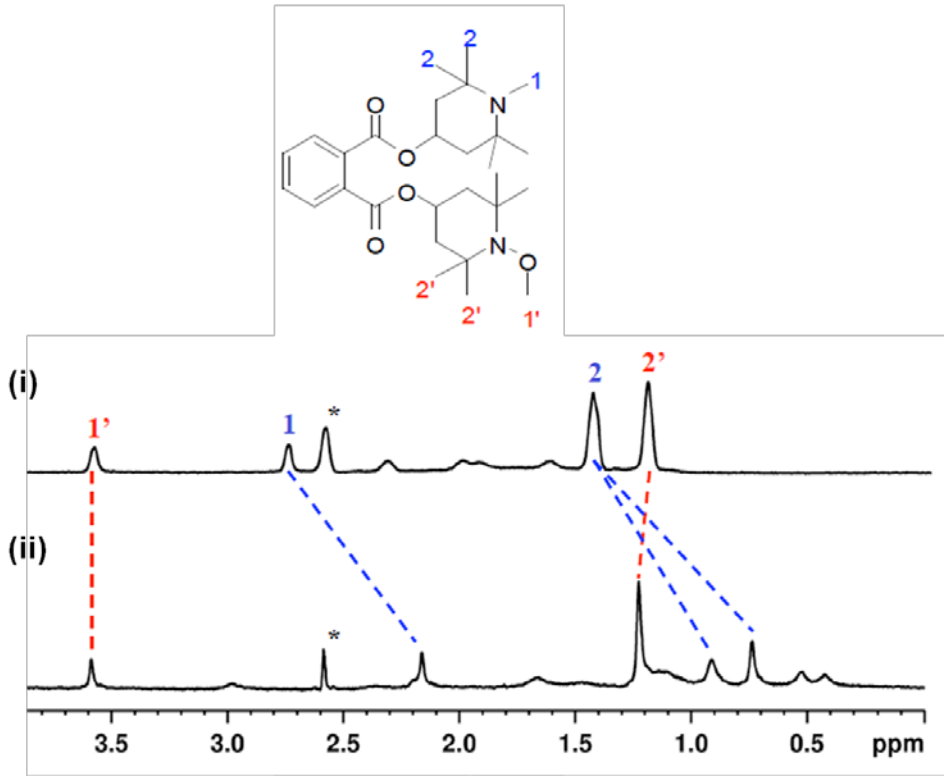

Figure 10.5 Partial 1H NMR spectra of **5** (i) in D_2O (0.5 mM, 500 MHz) and (ii) **5**@ CB8 (H:G = 1:1, [**5**] = 0.5 mM, (500 MHz). The label "*" represents residual DMSO resonance. Stock solution of guest was prepared in DMSO.

From the above study we established that CB8 was able to fully suppress the spin–spin exchange between adjacent nitroxyl groups in **3**. Our next experiments aimed to compare this feature with other hosts such as CB7, β-CD, γ-CD, CA8 and SDS micelles (**Scheme 10.2**).[243,244] The experimental and simulated EPR spectra, recorded upon addition of two equivalents (guest to host = 1 ∶ 2) of the first four hosts and in the presence of excess of SDS surfactant, are provided in **Fig 10.6**. A large excess of SDS (1 ∶ 1200) was used to avoid the presence of two or more molecules of **3** in one SDS

micelle that might cause intermolecular spin–spin interaction due to Heisenberg exchange. A 'broad' single line EPR Heisenberg component was observed even in the presence of a large excess of SDS (**Fig 10.6(vii)**, inset). The contribution of the broad component to the overall EPR signal was about 45%. This component was also present in the case of γ-CD complex to the extent of 10% (**Fig 10.6(vi)**). This broad component appeared probably due to the poor solubility of γ-CD complex.

The proportion of spin–spin exchange component (from five-line spectrum) obtained for various hosts are provided in the form of histograms in **Fig 10.7**. The exchange interaction completely disappeared in the case of CB8 whereas persisted in various degrees (28–79%) in presence of other hosts. Consistent with the above fact, the rotational correlation time was the highest in the case of CB8 indicative of the more restriction of mobility of the molecule due to formation of stronger complex with CB8 than the other host (**Fig 10.8**). The histograms of the A_N values (hyperfine splitting) in the case of various hosts are shown in **Fig 10.9**. It was surprising that though A_N value was the least in the case of micelle suggesting the formation of good complex with SDS, its spin-spin exchange interaction and the mobility was quite same as in water. This is most likely due to the soft flexible nature of the micellar interior that allows the molecule to rotate freely within its core. On the whole it was confirmed that the result with CB8 was the most exciting one and it was the best host among others to suppress the spin-spin exchange in **3**.

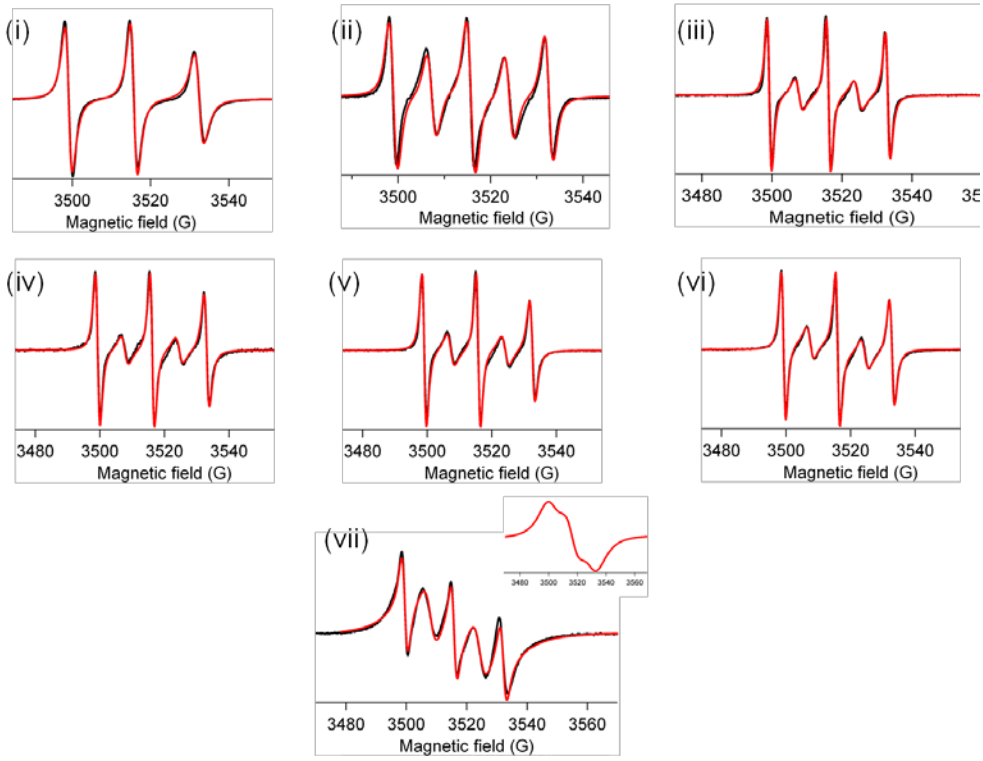

Figure 10.6 EPR spectrum (black lines) and its simulation (red lines) for (i) **3** /CB8 (1:2), A_N = 16.7 G, τ_c = 0.24 ns, (ii) **3** /CB7 (1:1), A_N = 16.9 G, τ_c = 0.07 ns, (iii) **3** /CB7 (1:2), A_N = 16.9 G, τ_c = 0.06 ns, (iv) **3** /CA8 (1:2), A_N = 16.9 G, τ_c = 0.1 ns, (v) **3** /β-CD (1:2), A_N = 16.7 G, τ_c = 0.15 ns, (vi) **3** /γ-CD (1:2), A_N = 16.8 G, τ_c = 0.12 ns, (vii) **3** @ SDS, [**3**] = 0.1 mM, [SDS] = 200 mM, A_N = 16.3 G, τ_c = 0.12 ns, in the insert (44% on the total): $\omega_{exchange}$ = 2 x 10^8 s^{-1}; line width = 3 G. From (i) to (vi), [**3**] =1 mM.

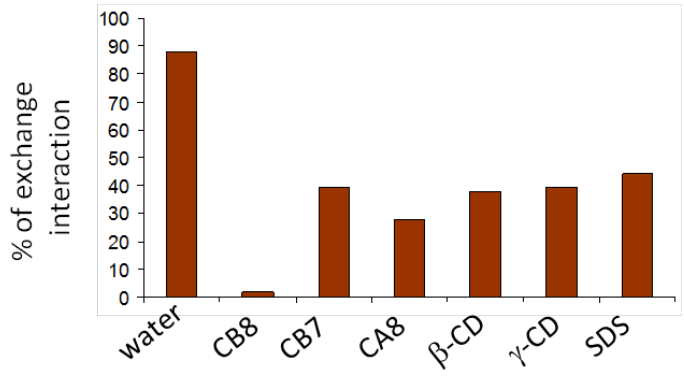

Figure 10.7 Comparison of percentage of spin–spin exchange interaction in **3**; note the exchange interaction in CB8 was 0%. For γ-CD and SDS micelles the broad Heisenberg

component was subtracted before calculation of % exchange interaction. 3 : host = 1 : 2 and in SDS (1 : 1200).

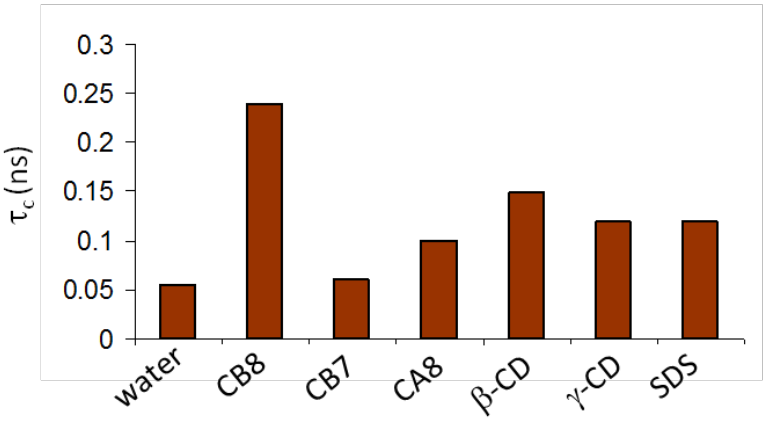

Figure 10.8 Comparison of rotational correlation time (τ_c) of **3** in absence and presence of different hosts.

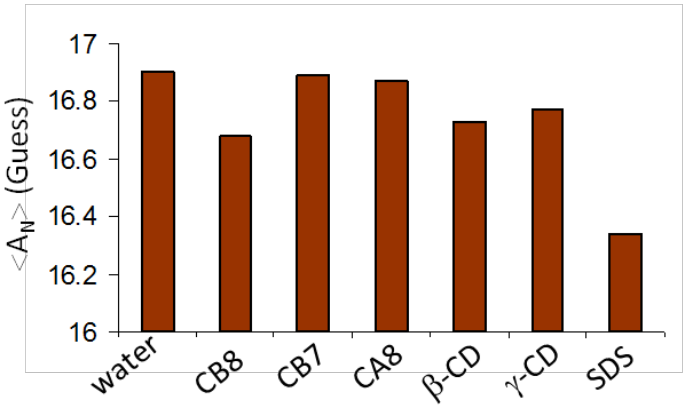

Figure 10.9 Comparison of hyperfine splitting (A_N) of **3** in absence and presence of different hosts.

10.2.3 EPR study on polyradical systems

In the previous sections, we have shown how the incarceration in supramolecular systems can modulate the spin-spin communication of a biradical. We were further interested to see whether this observation is general for other biradicals and polyradicals. Recently Ottaviani *et al.* have shown that the conformational changes in polynitroxides (di-, tri- and tetra-nitroxides), obtained from fluorinated cyano- and nitro-benzene,

promote spin communication among the nitroxide units.[245] We wanted to examine the effect of supramolecular architectures to control spin-spin communication in those polynitroxides.

We carefully screened one biradical and one triradical (**6** and **7**, **Scheme 10.1**) as the preferred guests because they have already been shown to enhance spin-spin exchange with respect to other investigated polynitroxides.[245] The probes were not soluble in pure water. We found them soluble only after addition of 50% MeOH in water. However this solvent system did not allow us to use CB8 (best host in the previous study) because of its insolubility in MeOH-water mixture. So, we tried γ-CD as it was soluble in MeOH-water solvent system.

The experimental and simulated EPR spectra of **6** and **7** in MeOH-water at 293 K are shown in **Fig 10.10**. These spectra were considered as constituted by two components: (a) a three-line component due to nitroxides in a so-called "far" conformation; in this case the spin-spin exchange coupling, J is equal to 0 (no spin-spin communication)[245]; and (b) a multiplet arising from nitroxides in a so-called "close" conformation, that is, spin-spin communicating; in this case the strong exchange interaction between the nitroxides gives $J>>A_N$, where A_N is the coupling constant between the electron spin and the nitrogen nuclear spin. As described earlier, the spectra were computed by adding Lorentzian lines at the proper fields, line widths and relative intensities, but the three-line component attributed to "far" nitroxides was computed using the well-established procedure of Freed and co-workers.[74]

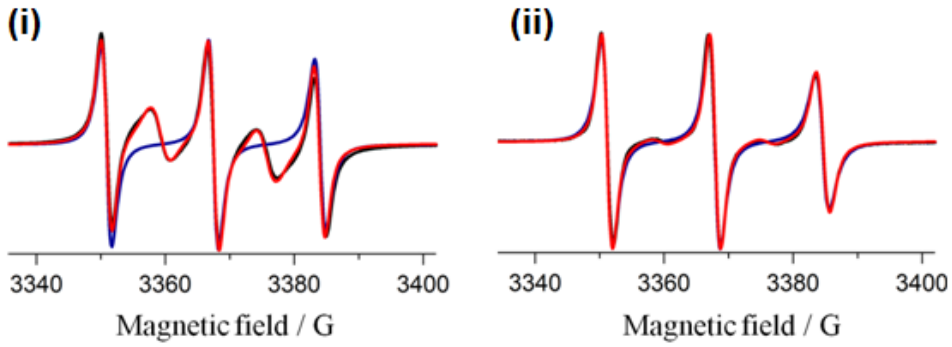

Figure 10.10 Experimental EPR spectra (black line) and their simulations (red line: addition of Lorentzian lines; blue line: computation of the three-line component) for (i) **6** in 1:1 MeOH/water, A_N = 16.5 G , τ_c = 0.08 ns, five-line component = 40 % and (ii) **6**: γ-CD = 1:20, A_N = 16.55 G , τ_c = 0.23 ns, five-line component = 7.5 %; [guest] = 0.1 mM; T = 293 K.

Fig 10.10(i) represents the experimental and computed spectra of **6** in 1:1 MeOH/water mixture. A multiplet of five lines with relative intensities of 1:2:3:2:1 (each electron was strongly coupled to both nitrogens of **6**) were superimposed to the three-line component and the inter-conversion between the two conformers result in a weak ($J \approx 0$) and strong ($J >> A_N$) exchange interaction. In the earlier report[245], the dinitroxide EPR spectrum was simulated by adding the three-line computed component and a two-line signal component (two Lorentzian lines in-between the three lines) at the proper relative intensities. The later two-line signal was considered to belong to the five-line signal (at 1:2:3:2:1 relative intensities of the five lines) expected for very strong exchange interaction. The percentage of the five-line signal was calculated with respect to the overall spectral intensity obtained by double integration of the experimental spectra. The proportion of the five-line exchange component of **6** in 1:1 MeOH/water mixture was 40%, indicating that there was an exchange between the two conformers. Hyperfine

splitting of **6** in MeOH/water mixture (16.5 G) was slightly lower than that in water (17 G). The correlation time (τ) of 0.08 ns was characteristic of fast rotating nitroxide radicals.

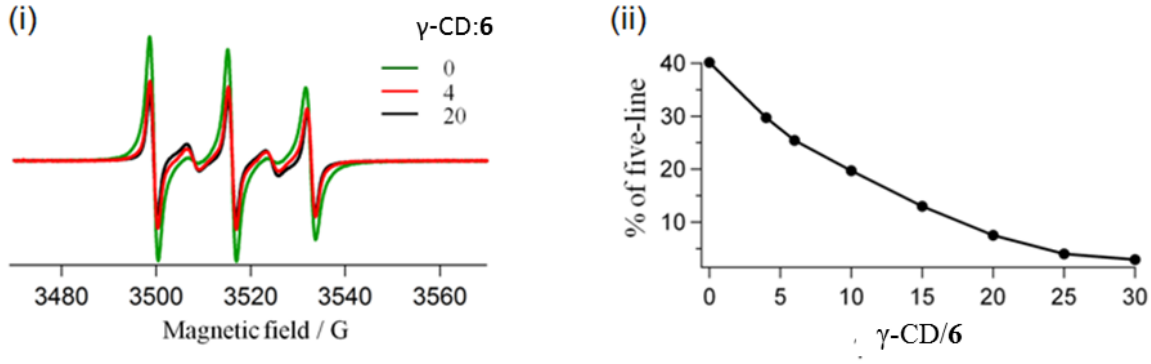

Figure 10.11 (i) EPR titration of **6** with γ-CD and (ii) plot of % of five-line component of **6** *vs* molar ratio of γ-CD: **6**; [**6**] = 0.1 mM.

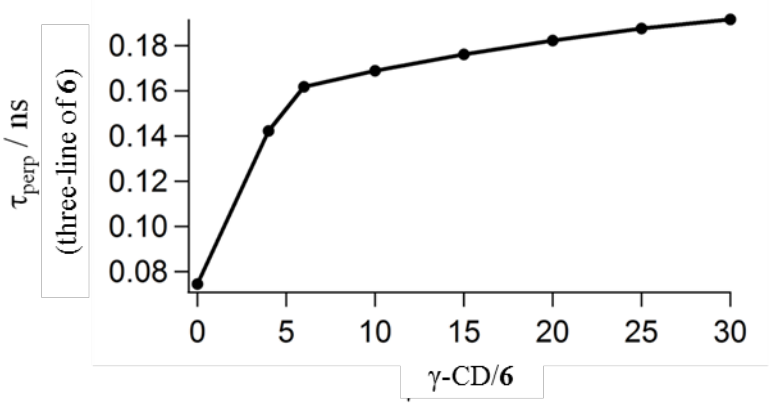

Figure 10.12 Plot of τ_{perp} of three-line component of **6** *vs* molar ratio of γ-CD: **6**, [**6**] = 0.1 mM.

Upon addition of γ-CD to a solution of **6** with increasing molar ratios between the cage and **6**, the five-line component progressively reduced and the relative intensity of the three-line signal increased (**Fig 10.11(i)**). This effect indicates that internalization of nitroxyl moiety of **6** within γ-CD cage eliminates the spin-spin exchange interaction. The

experimental and simulated EPR spectrum of **6** at a molar ratio host: guest = 1:20 (T=293 K) is shown in **Fig 10.10(ii)**. The spin-spin exchange interaction decreased from 40% to 7.5% upon addition of 20 equivalent of host (**Fig 10.11ii**). The necessity of excess host might be due to the equilibrium between an internalized within γ-CD cage and a free nitroxyl component. The decrease in mobility (τ_c) of the nitroxide (from 0.08 ns in MeOH/water to 0.18 ns in 20 equivalents γ-CD, **Fig 10.12**) also confirmed the internalization of nitroxyl part of **6** within γ-CD cage. No considerable change in A_N was observed in the absence (16.5 G) and presence (16.6 G) of the host. At this point we were unable to investigate whether the both or only one nitroxyl moiety of **6** was internalized within the cage to switch off spin-spin interaction.

In the absence of γ-CD, the experimental spectrum of **7** in water-methanol (**Fig 10.13(i)**) was constituted by the superimposing the three-line component and a seven-line component, arising from the strong exchange coupling among the three nitroxides. In that case the computation of the seven-lines component in **Fig 10.13i** was performed by adding Lorentzian lines, otherwise, as described by Ottaviani *et al.* [245] the relative intensities of the lines could not be reproduced by considering the coupling of the electron spin with three equivalent nitrogens. The relative percentage of seven-line component ($J>>A_N$) with respect to the three line component ($J\approx0$) of **7** in solution (50% MeOH in water) was 57%. It should be noted that the presence of the third nitroxide promotes the exchange interaction (57% for **7**, **Fig 10.13i** *vs* 40% for **6**, **Fig 10.10i**). The rotational correlation time (τ_c = 0.08 ns) and polarity (A_N = 16.54 G) of **7**, calculated for the three-line component, was the same as **6** in solution. However we have to consider

that the computation of the spectra of **6** and **7** (**Fig 10.10(i)** and **Fig 10.13(i)** respectively) also needed an additional broad signal (computed as a single Lorentzian line with width of 18 G). This was due to a fraction (15% for **6** and 45% for **7**) of undissolved probes, arising from self-aggregation of the polynitroxyls in polar solvent.[245]

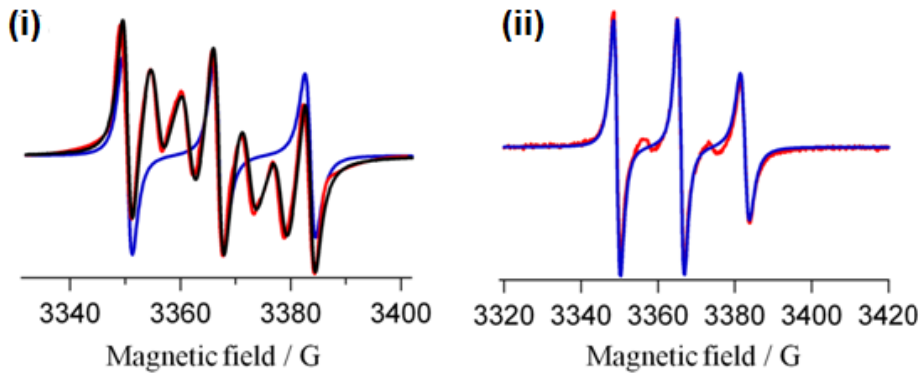

Figure 10.13 Experimental EPR spectra (black line) and their simulations (red line: addition of Lorentzian lines; blue line: computation of the three-line component) for (a) **7** in 1:1 MeOH/water, A_N = 16.5 G , τ_c = 0.08 ns, seven-line component = 57 %; (b) **7**: γ-CD = 1:20, A_N = 16.65 G, τ_c = 0.25 ns, five-line component = 5 % [guest] = 0.1 mM; T=293 K.

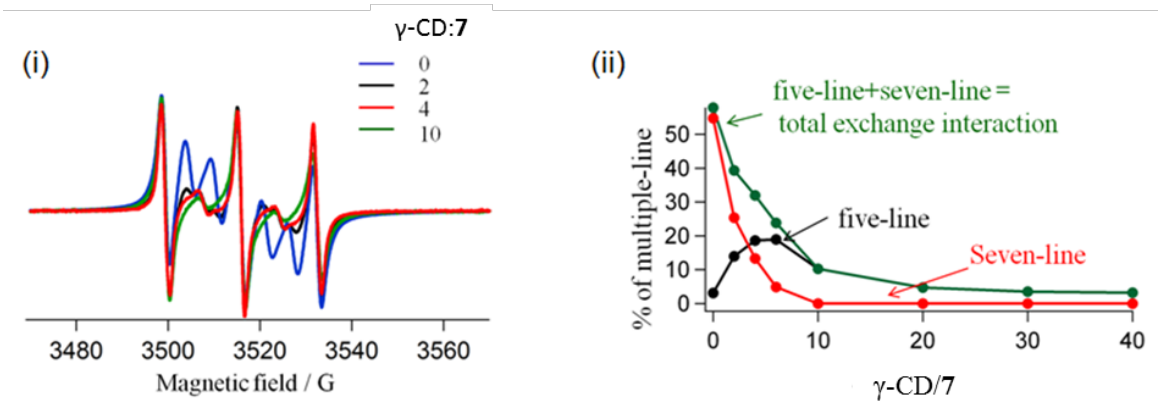

Figure 10.14 (i) EPR titration of **7** with γ-CD and (ii) % of multiple-line component of **7** *vs* molar ratio of γ-CD: **7**; [**7**] = 0.1 mM.

The experimental and computed EPR spectra of **7** in the presence of γ-CD at ratio 1:20 are provided in **Fig 10.13(ii)**. We observed that upon addition of γ-CD to a solution of **7** in 1:1 MeOH/water mixture, broad component of EPR spectrum disappeared suggesting that the solubility of **7** enhanced in presence of γ-CD. With increasing the concentration of γ-CD to **7**, the relative amount of seven-line component decreases while the three-line component enhanced indicating that the internalization of nitroxide within γ-CD cage suppresses spin-spin communication among the nitroxides (**Fig 10.14(i)**). As shown in **Fig 10.14(ii)**, host to guest molar ratio up to five, a five-line component appeared and gained intensity with the disappearance of seven-line signal. The maximum relative amount of five-line component reached 20% at γ-CD: **7** ~ 1:5. At molar ratio higher than five, the seven-line component almost disappeared (it was zero at host:guest = 10:1) and the intensity of five-line signal started decreasing (**Fig 10.14(ii)**). After addition of 20 equivalent of γ-CD to a solution of **7**, the amount of five-line component reached 5% and slowly disappeared with further increasing the concentration of γ-CD. Based on the above results we concluded that γ-CD to **7** ratio up to five, a fraction of the probes behaved like dinitroxide, because only one of the three nitroxides was internalized into the γ-CD cage and other two are free to communicate each other. Further increasing the concentration of γ-CD, second nitroxide also was internalized within the cage and hence the spin-spin communication was suppressed completely (**Scheme 10.4**). Thus we were able to distinguish three distinct behaviors of **7** as triradical, biradical and monoradical, by varying the amount of γ-CD in **7** solution.

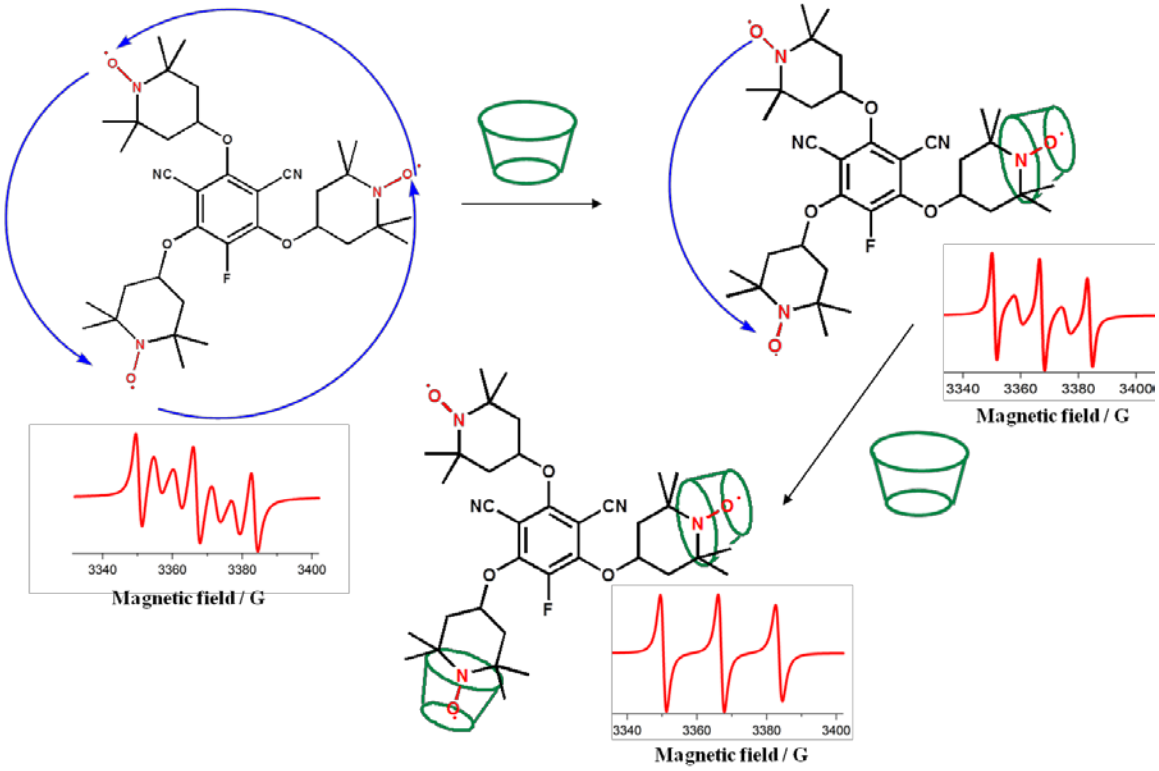

Scheme 10.4 Schematic representation of step wise encapsulation of **7** with γ-CD

10.2.4 Calculation of thermodynamic parameters for the spin-spin exchange in polynitroxide

Our next experiments aimed to measure the thermodynamic parameters (ΔH and ΔS) for the exchange between the two conformers of polynitroxides, termed as "far" and "close" on the basis of the relative distances among the nitroxides, ($\tau_{J\sim0}$ / $\tau_{J>>AN}$), in absence and presence of γ-CD. It is reported[245] that the logarithmic (Arrhenius) plot of the life time ratio of the two conformers *vs* the inverse of temperature leads to measure the above thermodynamic parameters. Therefore, EPR spectra of the polynitroxides were recorded in absence and presence of γ-CD at various temperatures. Upon increasing

temperature from 293K to 343K, it was observed that (**Fig 10.15** and **Fig 10.18**) the EPR spectra of both **6** and **7** in 1:1 MeOH/water mixture became well resolved and the amount of broad component needed for the computation decreased suggesting the reduction of self-aggregation of the polyradicals with temperature. In addition, the decrease in line width by increasing temperature resolved in-between lines for **6**, as shown in **Fig. 9.15**. In this conditions, the EPR spectrum of the nitroxide biradical consisted of the three-lines, corresponding to the nuclear configurations I(1)=I(2)=-1,0,+1, and in-between six lines, corresponding to the nuclear configurations I(1)=/I(2) (0,1; 1,0; 1,-1; -1,1; -1,0; 0,-1). The averaged *J* coupling coefficient can be calculated from the theoretical predictions using $J=a^2/(2g\beta\Delta B-2a)$, where ΔB is the distance between the 2nd (0,1) and the 8th (0,-1) lines (**Fig 10.15**).[6,7] We obtained *J*=120 MHz which corresponds to about *J*/a=2.5. However, the positions of the lines did not change by increasing the temperature (**Fig 10.15**) and this is in line with a slow exchange between the "far" and the "close" conformers which is a necessary condition to calculate the thermodynamic parameters.

From the Arrhenius plot, (**Fig 10.16** and **Fig 10.19**), we calculated ΔH and ΔS for **6** as 15 kJ mol^{-1} and 48 J mol^{-1} respectively and for **7** these values were 19.3 kJ mol^{-1} and 68.6 J mol^{-1} respectively in 1:1 MeOH/water. ΔH and ΔS for **6**:γ-CD = 1:20 were 44.7 kJ mol^{-1} and 121 J mol^{-1} respectively and for **7**:γ-CD = 1:20 were 14 kJ mol^{-1} and 42 J mol^{-1} respectively (**Fig 10.17** and **Fig 10.20**). On a thermodynamic point of view, an increase in ΔH reflects the increased energy needed to approach the nitroxides to each other, whereas an increase in ΔS reflects the increased complexity of the system. The thermodynamic parameters of **6** reflect that both the enthalpy and entropy of the transition process

increased in presence of γ-CD. The rationale behind that is at room temperature internalization within γ-CD strongly slowed down the exchange between the two conformations. At high temperature the percentages of the close conformation for the two systems, **6** as free and as internalized in γ-CD, poorly differ. **6**@γ-CD behave similar to free **6** as the nitroxide group internalized at room temperature becomes free at high temperature. At higher temperature, one nitroxide group of **7** was completely internalized into the γ-CD cage, while the second one was exchanging from inside to outside the cage and may approach the third (the non-internalized) one. Further the similarity between the thermodynamic parameters of **7**@γ-CD and free **6** in solution supports this hypothesis.

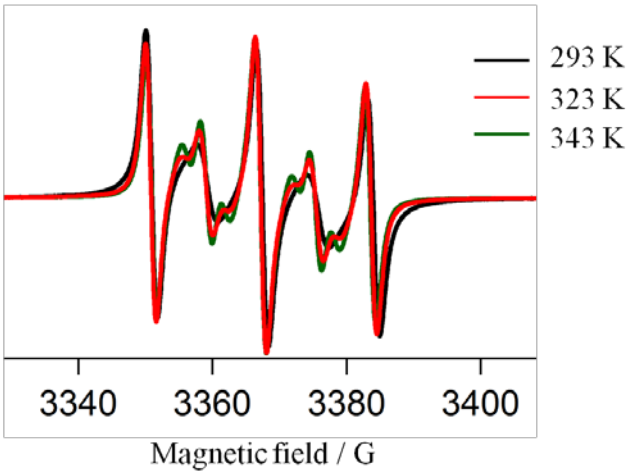

Figure 10.15 EPR spectra of **6** in 1:1 MeOH/water at various temperatures; [**6**] = 0.1 mM.

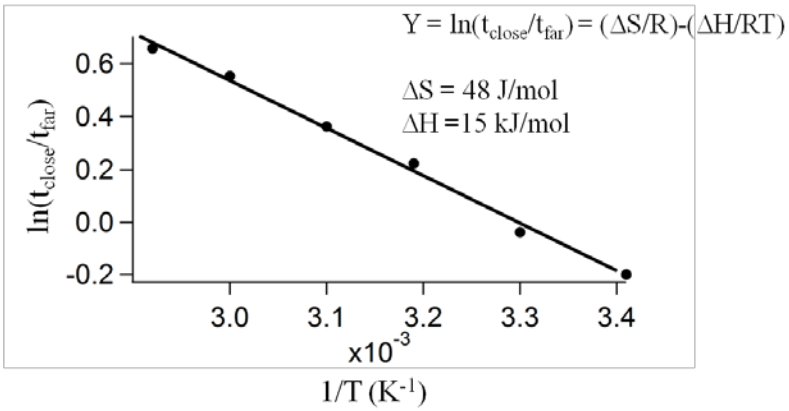

Figure 10.16 Arrhenius plot for **6** in 1:1 MeOH/water

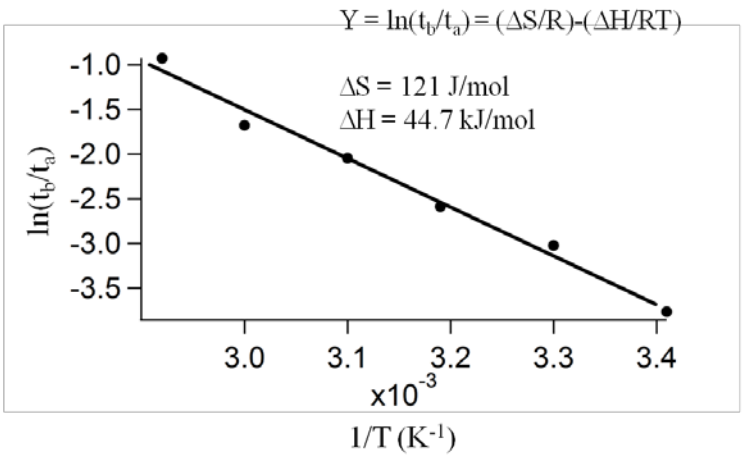

Figure 10.17 Arrhenius plot for **6**: γ-CD = 1: 20 in 1:1 MeOH/water

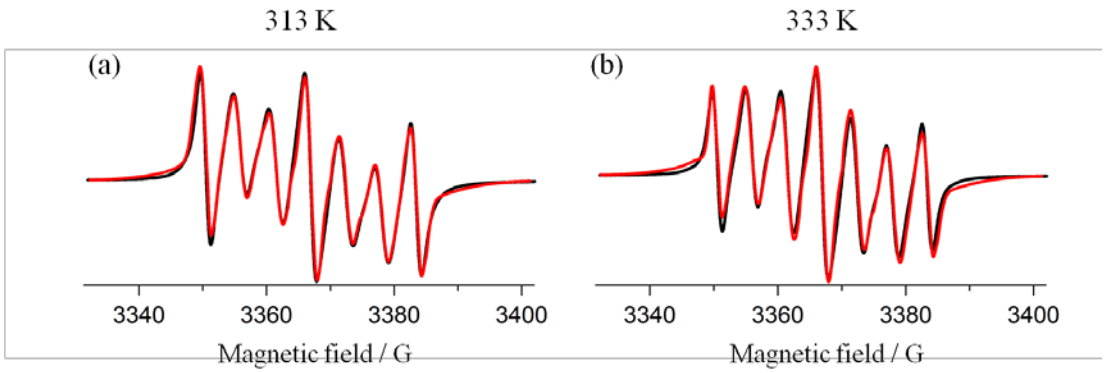

Figure 10.18 EPR spectra of **7** in 1:1 MeOH/water at different temperatures.

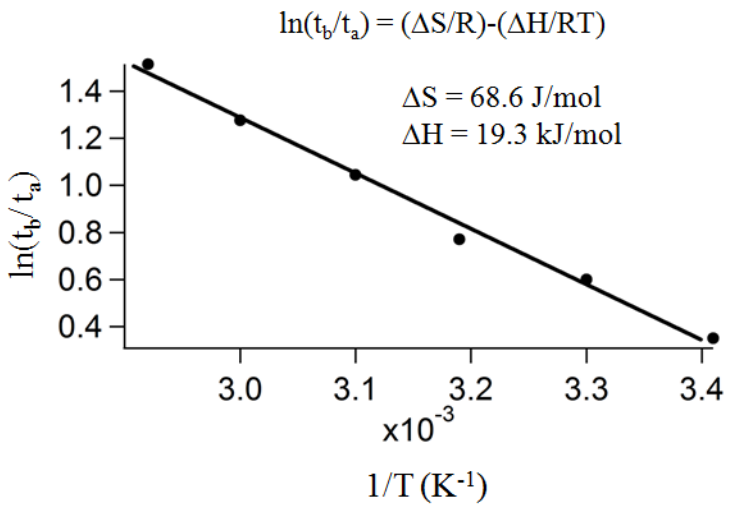

Figure 10.19 Arrhenius plot for **7** in 1:1 MeOH/water

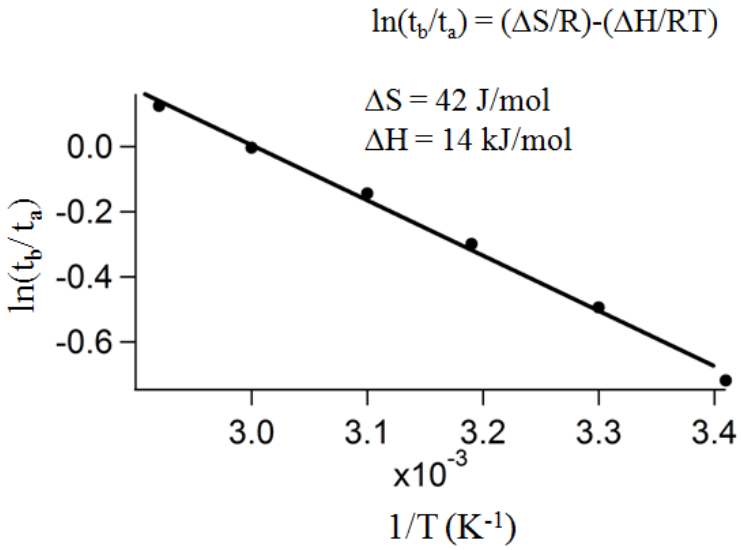

Figure 10.20 Arrhenius plot for **7**: γ-CD = 1: 20 in 1:1 MeOH/water

10.3 Conclusion

In summary, we established that the spin communication of polyradicals was quenched due to internalization of nitroxyl radical into a cage. There are two possible reasons: (i) the cage wall creates a barrier to spin exchange; (ii) conformational

modifications due to complexation keep the nitroxyls apart. It was shown that CB8 was the best among all the studied hosts to suppress the spin-spin communication between the two nitroxyls in **3** and encapsulation of only one nitroxyl moiety was sufficient for complete suppression. The 'supramolecular steric effect' to control the spin–spin exchange in biradicals was extended to other polyradicals. It has also been shown that variation of host/guest ratio can tune the nature of a trinitroxide from triradical to biradical to monoradical. Given the role of nitroxyl polyradicals for use in dynamic nuclear polarization (DNP) by controlling their spin–spin interaction, supramolecular assemblies as described here could play a significant role in the development of a more sensitive and tunable DNP.

10.4 Experimental section

Materials and Methods

CB7 and CB8 were synthesized by following a published procedure[1]. β-CD and γ-CD were purchased from Sigma-Aldrich. CA8 was synthesized using the published procedure.[2,3,4]

Synthesis of the nitroxide probes used in the study

Compound 1-3:

The corresponding dicarboxylic acid (300 mg) was mixed with 4-hydroxy-2,2-6,6-tetramethyl piperidine-N-oxyl (0.8 g) and DMAP (cat.) in dry dichloromethane (20 mL) at 0 $^{\circ}$C. A suspension of 1-ethyl-3-(3-dimethylaminopropyl) carbodiimide (EDCI) (0.83g) in dichloromethane was added to the above reaction mixture at 0 $^{\circ}$C, it was

allowed to warm up to room temperature and stirred for 15 h, washed with water and dried over Na_2SO_4. The crude reaction mixture was purified by column chromatography to afford the corresponding biradical. FAB-MS (m/z): 475 $(M+H)^+$ The purity was further ascertained by comparing the absolute intensity of 4-hydroxy TEMPO.

Compound 4:

The synthetic route for Compound **4** is shown in **Scheme 10.5**.

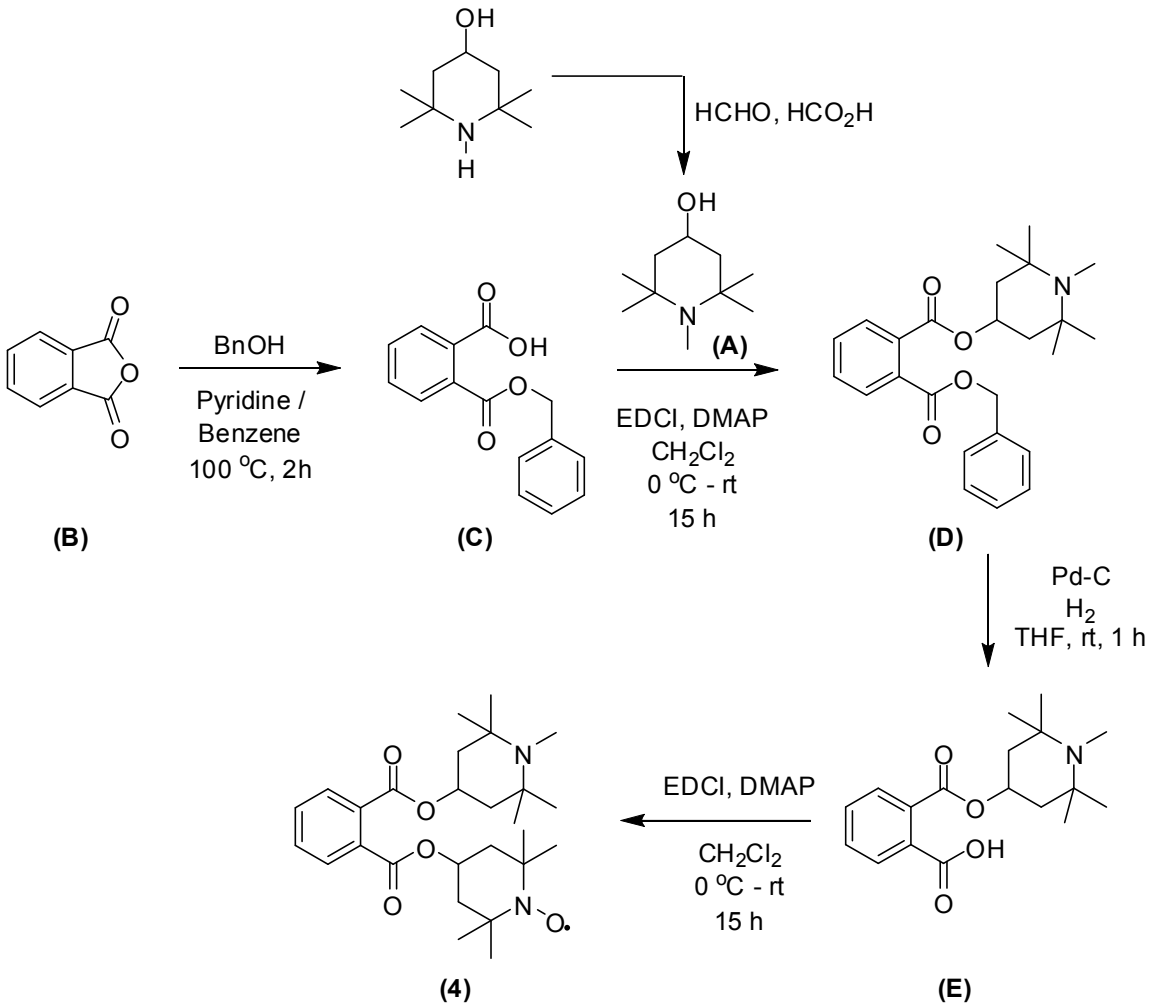

Scheme 10.5 Synthetic route for compound **4**.

Compound C:

A solution containing 10 mmol of benzylalcohol and phthalicanhydride in 10 mL of pyridine and 50 mL of benzene was heated at 100 $^{\circ}$C for 2 h. The reaction mixture was cooled and poured in to ice-water mixture, acidified with conc. HCl and extracted with $CHCl_3$ and washed with 5% aqueous sodium carbonate solution. The aqueous solution was further acidified with conc. HCl and extracted with $CHCl_3$ to afford the required *o*-(benzyloxycarbonyl)benzoic acid in quantitative yield.

^{1}H NMR (500 MHz, $CDCl_3$) d: 5.37 (2 H, s), 7.29–7.9 (9 H, m); ^{13}C NMR (125 MHz, $CDCl_3$) d: 67.9, 128.45, 128.56, 128.63, 128.87, 129.9, 129.97, 130.94, 132.36, 133.24, 135.24, 167.95, 172.32.

Compound A:

4-Hydroxy-2,2-6,6-tetramethylpiperidine (1.5 g) was mixed with 2 mL of formalin (37 % formaldehyde) solution and 0.5 mL of formic acid and refluxed for 7 h. The solution was poured in to ice and the solution was made basic with KOH and extracted with diethyl ether to afford the required 4-Hydroxy-2,2-6,6-tetramethyl-N-methylpiperidine in 85 % yield.

^{1}H NMR (500 MHz, $CDCl_3$) d: 1.01 (6 H, s), 1.15 (6 H, s), 1.36 (dd, 2 H), 1.83 (d, 2 H), 2.22 (3 H, s) 3.91 (1 H, m); ^{13}C NMR (125 MHz, $CDCl_3$) d: 20.54, 28.04, 33.28, 50.06, 55.34, 63.91. GC-MS (m/z): 171 (M^+, 10 %), 156 (M-15, 100 %).

Compound D:

O-(benzyloxycarbonyl)benzoic acid (0.68g) was admixed with 4-hydroxy-2,2-6,6-tetramethyl-N-methylpiperidine (0.35 g) and DMAP (cat.) in dry dichloromethane (20 mL) at 0 $^{\circ}$C. A suspension of EDCI (0.55 g) in dichloromethane was added to the above reaction mixture at 0 $^{\circ}$C, it was allowed to warm up to rt and stirred for 15 h, washed with water and dried over Na_2SO_4. The crude reaction mixture was purified by column chromatography to afford the product **D** in 60 % yield.

^{1}H NMR (500 MHz, $CDCl_3$) d: 1.03 (6 H, s), 1.17 (6 H, s), 1.58 (dd, 2 H), 1.95 (m, 2 H), 2.26 (3 H, s), 5.28 (1 H, m), 7.36-7.73 (9 H, m); ^{13}C NMR (125 MHz, $CDCl_3$) d: 20.71, 28.02, 33.25, 45.58, 55.34, 67.43, 69.38.

Compound E:

The compound **D** was dissolved in THF and degassed with nitrogen for 15 min, charged with Pd-C (5 % on carbon, 10 % by weight) cautiously and purged with hydrogen gas for 1 h, Pd-C was removed by filtration over celite pad and the solution was concentrated to give the product in quantitative yield.

^{1}H NMR (500 MHz, $CDCl_3$) d: 1.35 (6 H, s), 1.52 (6 H, s), 2.26 (dd, 2 H), 2.46 (dd, 2 H), 2.68 (3 H, s), 5.32 (1 H, m), 7.35-7.77 (4 H, m); ^{13}C NMR (125 MHz, $CDCl_3$) d: 22.72, 28.96, 41.99, 46.27, 63.59, 65.95, 129.06, 129.18, 131.53, 133.52, 134.04, 139.08, 169.14, 171.12.

Compound 4:

O-(benzyloxycarbonyl)benzoic acid (0.22 g) was admixed with 4-hydroxy TEMPO (0.16 g) and DMAP (cat.) in dry dichloromethane (15 mL) at 0 $^{\circ}$C. A suspension of EDCI (0.19 g) in dichloromethane was added to the above reaction mixture at 0 $^{\circ}$C and stirred at room temperature for 15 h, washed with water and dried over Na_2SO_4. The crude reaction mixture was purified by column chromatography to afford the product **4** in 50 % yield. FAB-MS (m/z): 473 $(M+H)^+$

The purity was further ascertained by comparing the absolute intensity of 4-hydroxy TEMPO.

Preparation of host/guest complex: Stock solution (20 mM) of guest was prepared in $CHCl_3$. Host stock solution (5 mM) was prepared in H_2O. Required amount of guest solution in $CHCl_3$ was added in a vial and solvent was evaporated by shaking in a mechanical shaker. Then calculated amount of host solution and water were added and shacked by the mechanical shaker for 15 h. The same procedure was adopted for all guests.

EPR study: EPR spectra were recorded at room temperature in Bruker EMX spectrometer at 9.5 GHz (X band) employing 100 KHz of field modulation frequency. Spectrometer setting: Power, 1.997 mW; amplitude modulation, 0.50 G; time constant, 163.84 ms; conversion time, 163.84 ms. Samples were loaded to quartz (CFQ) EPR tubes from Wilmad LabGlass (2 mm OD, 0.5 mm wall thickness, 10 cm height) for the EPR

experiments. The ASCII files of the EPR data were imported to Igor Pro software and the spectral plots were generated.

Protocol for NMR study: A ^{1}H NMR spectrum of 600 μL of 1 mM CB8 in D_2O was recorded. To this solution 1 equivalent of guest (10 μL of 60 mM solution of **4** in DMSO) was added. The mixture was shaken well for about 5 min and the spectra were recorded.

REFERENCES

1. Lehn, J.-M. *Supramolecular chemistry: Concepts and perspectives*, (Wiley-VCH, Weinheim, 1995).

2. Schalley, C.A., Lützen, A. & Albrecht, M. Approaching supramolecular functionality. *Chem.-Eur. J* **10**, 1072-1080 (2004).

3. Dodziuk, H. *Introduction to supramolecular chemistry*, (Kluwer Academic Publishers Norwell, 2002).

4. Cram, D.J. Preorganization-from solvents to spherands. *Angew. Chem., Int. Ed.* **25**, 1039-1057 (1986).

5. Porel, M., Jayaraj, N., Kaanumalle, L.S., Maddipatla, M.V.S.N., Parthasarathy, A. & Ramamurthy, V. Cavitand octa acid forms a nonpolar capsuleplex dependent on the molecular size and hydrophobicity of the guest. *Langmuir* **25**, 3473-3481 (2009).

6. Turro, N.J., Ramamurthy, V. & Scaiano, J.C. *Modern Molecular Photochemistry of Organic Molecules*, (2010).

7. Cram, D.J., Tanner, M.E. & Thomas, R. The taming of cyclobutadiene. *Angew. Chem., Int. Ed.* **30**, 1024-1027 (1991).

8. Warmuth, R. & Yoon, J. Recent highlights in hemicarcerand chemistry. *Acc. Chem. Res.* **34**, 95-105 (2001).

9. Fieser, L.F. & Fieser, M. *Steroids*, (Reinhold Publishing Corporation, New York, 1959).

10. Pedersen, C.J. The discovery of crown ethers (noble lecture). *Angew. Chem., Int. Ed.* **27**, 1021-1027 (1988).

11. Pedersen, C.J. Cyclic polyethers and their complexes with metal salts. *J. Am. Chem. Soc.* **89**, 2495-6 (1967).

12. Szejtli, J. & Osa, T. *Comprehensive Supramolecular Chemistry, Vol 3*, (Pergamon, Oxford, 1996).

13. Murakami, Y. & Hayashida, O. Large water-soluble cavities. *Compr. Supramol. Chem.* **2**, 419-438 (1996).

14. Casnati, A., Sciotto, D. & Arena, G. Water-soluble calixarenes: Calixarenes 2001. in *Calixarenes 2001* 440-456 (2002).

15. Lagona, J., Mukhopadhyay, P., Chakrabarti, S. & Isaacs, L. The cucurbit[n]uril family. *Angew. Chem., Int. Ed.* **44**, 4844-4870 (2005).

16. Moran, J.R., Karbach, S. & Cram, D.J. Cavitands: synthetic molecular vessels. *J. Am. Chem. Soc.* **104**, 5826-5828 (1982).

17. Boerrigter, H., Verboom, W. & Reinhoudt, D.N. Ligands for Eu(III), Fe(III), Sr(II), and UO2(II) based on carbamoylmethylphosphine oxide-functionalized resorcin-arene cavitands. Synthesis and extraction. *Liebigs Ann./Recl.*, 2247-2254 (1997).

18. Irwin, J.L. & Sherburn, M.S. Practical synthesis of selectively functionalized cavitands. *J. Org. Chem.* **65**, 602-605 (2000).

19. Ahn, D.-R., Kim, T.W. & Hong, J.-I. Water-soluble resorcin[4]arene: complexation of anionic aromatic guests by cooperativity of electrostatic and hydrophobic interactions. *Tetrahedron Lett.* **40**, 6045-6048 (1999).

20. Fraser, J.R., Borecka, B., Trotter, J. & Sherman, J.C. An asymmetric carceplex and new crystal structure yield information regarding a 1 million-fold template effect. *J. Org. Chem.* **60**, 1207-13 (1995).

21. Gansey, M.H.B.G., Bakker, F.K.G., Feiters, M.C., Geurts, H.P.M., Verboom, W. & Reinhoudt, D.N. Water-soluble resorcin[4]arene based cavitands. *Tetrahedron Lett.* **39**, 5447-5450 (1998).

22. Kim, K. & Paek, K. Facile synthesis and functionalizations of a tetrakis(bromomethyl)cavitand. *Bull. Korean Chem. Soc.* **14**, 658-60 (1993).

23. Lim, C.W. & Hong, J.-I. Intramolecular binding site organization by Pd(II) complexation with a resorcin[4]arene derivative. *Tetrahedron Lett.* **41**, 3113-3117 (2000).

24. Middel, O., Verboom, W. & Reinhoudt, D.N. Water-soluble cavitands - synthesis, solubilities and binding properties. *Eur. J. Org. Chem.*, 2587-2597 (2002).

25. Park, S.J. & Hong, J.-I. The cooperative effect of electrostatic and hydrophobic forces in the complexation of cationic molecules by a water-soluble resorcin[4]arene derivative. *Tetrahedron Lett.* **41**, 8311-8315 (2000).

26. Pellet-Rostaing, S., Nicod, L., Chitry, F. & Lemaire, M. Synthesis and cesium-complexing properties of water-soluble cavitands. *Tetrahedron Lett.* **40**, 8793-8796 (1999).

27. Sebo, L., Diederich, F. & Gramlich, V. Tetrakis(phenylamidinium)-substituted resorcin[4]arene receptors for the complexation of dicarboxylates and phosphates in protic solvents. *Helv. Chim. Acta* **83**, 93-113 (2000).

28. Sorrell, T.N. & Pigge, F.C. A convenient synthesis of functionalized cavitands via free-radical bromination. *J. Org. Chem.* **58**, 784-785 (1993).

29. Trembleau, L. & Rebek, J., Jr. Helical conformation of alkanes in a hydrophobic cavitand. *Science* **301**, 1219-1221 (2003).

30. Mezo, A.R. & Sherman, J.C. Water-soluble cavitands: synthesis of methylene-bridged resorcin[4]arenes containing hydroxyls and phosphates at their feet and bromomethyls and thiomethyls at their rims. *J. Org. Chem.* **63**, 6824-6829 (1998).

31. Hof, F., Trembleau, L., Ullrich, E.C. & Rebek, J., Jr. Acetylcholine recognition by a deep, biomimetic pocket. *Angew. Chem., Int. Ed.* **42**, 3150-3153 (2003).

32. Haino, T., Rudkevich, D.M., Shivanyuk, A., Rissanen, K. & Rebek, J., Jr. Induced-fit molecular recognition with water-soluble cavitands. *Chem.-Eur. J.* **6**, 3797-3805 (2000).

33. Haino, T., Rudkevich, D.M. & Rebek, J., Jr. Kinetically stable caviplexes in water. *J. Am. Chem. Soc.* **121**, 11253-11254 (1999).

34. Gui, X. & Sherman, J.C. Host-guest binding of simple cavitands in water. *Chem. Commun.* , 2680-2681 (2001).

35. Cram, D.J., Choi, H.J., Bryant, J.A. & Knobler, C.B. Host-guest complexation. 62. Solvophobic and entropic driving forces for forming velcraplexes, which are 4-fold, lock-key dimers in organic media. *J. Am. Chem. Soc.* **114**, 7748-65 (1992).

36. Hof, F., Craig, S.L., Nuckolls, C. & Rebek, J., Jr. Molecular encapsulation. *Angew. Chem., Int. Ed.* **41**, 1488-1508 (2002).

37. Corbellini, F., Fiammengo, R., Timmerman, P., Crego-Calama, M., Versluis, K., Heck, A.J.R., Luyten, I. & Reinhoudt, D.N. Guest encapsulation and self-assembly of molecular capsules in polar solvents via multiple ionic interactions. *J. Am. Chem. Soc.* **124**, 6569-6575 (2002).

38. Zadmard, R., Schrader, T., Grawe, T. & Kraft, A. Self-assembly of molecular capsules in polar solvents. *Org. Lett.* **4**, 1687-1690 (2002).

39. Zadmard, R., Junkers, M., Schrader, T., Grawe, T. & Kraft, A. Capsule-like assemblies in polar solvents. *J. Org. Chem.* **68**, 6511-6521 (2003).

40. Gibb, C.L.D. & Gibb, B.C. Well-defined, organic nanoenvironments in water: the hydrophobic effect drives a capsular assembly. *J. Am. Chem. Soc.* **126**, 11408-11409 (2004).

41. Maverick, E. & Cram, D.J. Carcerands and hemicarcerands: host that imprison molecular guests. *Compr. Supramol. Chem.* **2**, 367-418 (1996).

42. Yoon, J. & Cram, D.J. The first water-soluble hemicarceplexes. *Chem. Commun.* , 497-498 (1997).

43. Piatnitski, E.L., Flowers, R.A., II & Deshayes, K. Highly organized spherical hosts that bind organic guests in aqueous solution with micromolar affinity: microcalorimetry studies. *Chem.-Eur. J.* **6**, 999-1006 (2000).

44. Whitesides, G., Mathias, J. & Seto, C. Molecular self-assembly and nanochemistry: a chemical strategy for the synthesis of nanostructures. *Science* **254**, 1312-1319 (1991).

45. Steed, J.W., Turner, D.R. & Wallace, K.J. *Core Concepts in Supramolecular Chemisty and Nanochemistry*, (2007).

46. Van Leeuwen, P.W.N.M. & Freixa, Z. Supramolecular catalysis: refocusing catalysis. in *Supramolecular Catalysis* 255-299 (Wiley-VCH Verlag GmbH & Co. KGaA, 2008).

47. Koblenz, T.S., Wassenaar, J. & Reek, J.N.H. Reactivity within a confined self-assembled nanospace. *Chem. Soc. Rev.* **37**, 247-262 (2008).

48. Pluth, M.D., Bergman, R.G. & Raymond, K.N. Acid catalysis in basic solution: a supramolecular host promotes orthoformate hydrolysis. *Science* **316**, 85-88 (2007).

49. Bertrand, N., Gauthier, M.A., Bouvet, C., Moreau, P., Petitjean, A., Leroux, J.-C. & Leblond, J. New pharmaceutical applications for macromolecular binders. *J. Controlled Release* **155**, 200-210 (2011).

50. Day, A.I. & Collins, J.G. Cucurbituril receptors and drug delivery. in *Supramol. Chem.* (John Wiley & Sons, Ltd, 2012).

51. Saleh, N.i., Koner, A.L. & Nau, W.M. Activation and stabilization of drugs by supramolecular pKa shifts: drug-delivery applications tailored for cucurbiturils. *Angew. Chem., Int. Ed.* **47**, 5398-5401 (2008).

52. Becuwe, M., Cazier, F., Bria, M., Woisel, P. & Delattre, F. Tuneable fluorescent marker appended to β-cyclodextrin: a pH-driven molecular switch. *Tetrahedron Lett.* **48**, 6186-6188 (2007).

53. Kyba, E.B., Koga, K., Sousa, L.R., Siegel, M.G. & Cram, D.J. Chiral recognition in molecular complexing. *J. Am. Chem. Soc.* **95**, 2692-2693 (1973).

54. Ward, M.D. Photo-induced electron and energy transfer in non-covalently bonded supramolecular assemblies. *Chem. Soc. Rev.* **26**, 365-375 (1997).

55. Sessler, J.L., Johnson, M.R., Creager, S.E., Fettinger, J.C. & Ibers, J.A. Synthesis and characterization of quinone-substituted octaalkyl porphyrin monomers and dimers. *J. Am. Chem. Soc.* **112**, 9310-9329 (1990).

56. Sessler, J.L., Johnson, M.R. & Lin, T.-Y. Absorption and static emission properties of monometalated quinone-substituted porphyrin dimers: evidence for "superexchange" mediated electron transfer in multicomponent photosynthetic model systems. *Tetrahedron* **45**, 4767-4784 (1989).

57. Wasielewski, M.R. Photoinduced electron transfer in supramolecular systems for artificial photosynthesis. *Chem. Rev.* **92**, 435-461 (1992).

58. Borden, W.T. *Diradicals*, (John Wiley, New York, 1982).

59. Forrester, A.R. *Organic chemistry of stable free radicals*, (Academic Press, London, 1968).

60. Ionita, G., Sahini, V.E., Semenescu, G. & Ionita, P. Kinetics of oxidation of amino acids by some free stable hydrazyl radicals. *Acta Chim. Slov.* **47**, 111-119 (2000).

61. Ionita, P., Gilbert, B.C. & Chechik, V. Radical mechanism of a place-exchange reaction of au nanoparticles. *Angew. Chem., Int. Ed.* **44**, 3720-3722 (2005).

62. Ottaviani, M.F., Martini, G. & Nuti, L. Nitrogen hyperfine splitting of nitroxide solutions: Differently structured and charged nitroxides as probes of environmental properties. *Magn. Reson. Chem.* **25**, 897-904 (1987).

63. Lee, C., Yang, W. & Parr, R.G. Development of the Colle-Salvetti correlation-energy formula into a functional of the electron density. *Phys. Rev. B* **37**, 785-789 (1988).

64. Natarajan, A., Kaanumalle, L.S., Jockusch, S., Gibb, C.L.D., Gibb, B.C., Turro, N.J. & Ramamurthy, V. Controlling photoreactions with restricted spaces and weak intermolecular forces: exquisite selectivity during oxidation of olefins by singlet oxygen. *J. Am. Chem. Soc.* **129**, 4132-4133 (2007).

65. Sundaresan, A.K. & Ramamurthy, V. Making a difference on excited-state chemistry by controlling free space within a nanocapsule: photochemistry of 1-(4-alkylphenyl)-3-phenylpropan-2-ones. *Org. Lett.* **9**, 3575-3578 (2007).

66. Sundaresan, A.K. & Ramamurthy, V. Consequences of controlling free space within a reaction cavity with a remote alkyl group: photochemistry of para-alkyl dibenzyl ketones within an organic capsule in water. *Photochem. Photobiol. Sci.* **7**, 1555-1564 (2008).

67. Basilio, N., García-Río, L. & Martín-Pastor, M. NMR Evidence of slow monomer−micelle exchange in a calixarene-based surfactant. *J. Phy. Chem. B* **114**, 4816-4820 (2010).

68. Perrin, C.L. & Dwyer, T.J. Application of two-dimensional NMR to kinetics of chemical exchange. *Chem. Rev.* **90**, 935-967 (1990).

69. Yamanaka, M., Shivanyuk, A. & Rebek, J. Kinetics and thermodynamics of hexameric capsule formation. *J. Am. Chem. Soc.* **126**, 2939-2943 (2004).

70. Yagci, Y., Jockusch, S. & Turro, N.J. Mechanism of photoinduced step polymerization of thiophene by onium salts: reactions of phenyliodinium and diphenylsulfinium radical cations with thiophene. *Macromolecules* **40**, 4481-4485 (2007).

71. Chuang, C.-H., Doane, T.L., Lo, S.S., Scholes, G.D. & Burda, C. Measuring electron and hole transfer in core/shell nanoheterostructures. *ACS Nano* **5**, 6016-6024 (2011).

72. Chuang, C.-H., Lo, S.S., Scholes, G.D. & Burda, C. Charge separation and recombination in CdTe/CdSe core/shell nanocrystals as a function of shell coverage: probing the onset of the quasi type-II regime. *J. Phy. Chem. Lett.* **1**, 2530-2535 (2010).

73. Mao, B., Chuang, C.-H., Wang, J. & Burda, C. Synthesis and photophysical properties of ternary I–III–VI $AgInS_2$ nanocrystals: intrinsic versus surface states. *J. Phy. Chem. C* **115**, 8945-8954 (2011).

74. Budil, D.E., Lee, S., Saxena, S. & Freed, J.H. Nonlinear-least-squares analysis of slow-motion EPR spectra in one and two dimensions using a modified Levenberg-Marquardt algorithm. *J. Magn. Reson. A* **120**, 155-189 (1996).

75. Klajnert, B., Cangiotti, M., Calici, S., Majoral, J.P., Caminade, A.M., Cladera, J., Bryszewska, M. & Ottaviani, M.F. EPR study of the interactions between dendrimers and peptides involved in Alzheimer's and prion diseases. *Macromolecular Bioscience* **7**, 1065-1074 (2007).

76. Karplus, M. & Fraenkel, G.K. Theoretical interpretation of carbon-13 hyperfine interactions in electron spin resonance spectra. *J. Chem. Phys.* **35**, 1312-1323 (1961).

77. Jenks, W.S. & Turro, N.J. Exchange effects and CIDEP. *Res. Chem. Inrermed.* **13**, 237-300 (1990).

78. Obi, K. & Imamura, T. Time resolved ESR of intersystem crossing and energy tansfer processes. *Rev. Chem. Inrermed.* **7**, 225-242 (1986).

79. Adrian, F.J. Theoretical aspects of chemically induced magnetic polarization. *Res. Chem. Inrermed.* **16**, 99-125 (1991).

80. Trifunac, A.D., Lawler, R.G., Bartels, D.M. & Thurnauer, M.C. Magnetic resonance studies of paramagnetic transients in liquids. *Prog. Reacr. Kinet.* **14**, 43-156 (1986).

81. Imamura, T., Onitsuka & Obi, K. Memory of spin polarization in triplet-doublet systems *J . Phys. Chem.* **90**, 6741 (1986).

82. Jenks, W.S. & Turro, N.J. Indirect observation of spin polarization in triplet fluorenylidene at room temperature. *Tetrahedron Lett.* **30**, 4469 (1989).

83. Whitten, D.G., Russell, J.C. & Schmehl, R.H. Photochemical reactions in organized assemblies: environmental effects on reactions occurring in micelles, vesicles, films and mutilayer assemblies and at interfaces *Tetrahedron* **38**, 2455-2487 (1982).

84. Whitten, D.G. Photochemistry and photophysics of trans-stilbene and related alkenes in surfactant assemblies. *Acc. Chem. Res.* **26**, 502-509 (1993).

85. Turro, N.J. From boiling stones to smart crystals: supramolecular and magnetic isotope control of radical−radical reactions in zeolites. *Acc. Chem. Res.* **33**, 637-646 (2000).

86. Ramamurthy, V. *Photochemistry in Organized and Constrained Media*, (1991).

87. Ramamurthy, V. Organic photochemistry in organized media. *Tetrahedron* **42**, 5753-5839 (1986).

88. Gibb, C.L.D., Sundaresan, A.K., Ramamurthy, V. & Gibb, B.C. Templation of the excited-state chemistry of α-(n-Alkyl) dibenzyl ketones: how guest packing within a nanoscale supramolecular capsule influences photochemistry. *J. Am. Chem. Soc.* **130**, 4069-4080 (2008).

89. Kaanumalle, L.S., Gibb, C.L.D., Gibb, B.C. & Ramamurthy, V. Controlling photochemistry with distinct hydrophobic nanoenvironments. *J. Am. Chem. Soc.* **126**, 14366-14367 (2004).

90. Kaliappan, R., Kaanumalle, L.S., Natarajan, A. & Ramamurthy, V. Templating photodimerization of stilbazoles with water-soluble calixarenes. *Photochem. Photobiol. Sci.* **5**, 925-930 (2006).

91. Kaliappan, R., Maddipatla, M.V.S.N., Kaanumalle, L.S. & Ramamurthy, V. Crystal engineering principles applied to solution photochemistry: controlling the photodimerization of stilbazolium salts within γ-cyclodextrin and cucurbit[8]uril in water. *Photochem. Photobiol. Sci.* **6**, 737-740 (2007).

92. Karthikeyan, S. & Ramamurthy, V. Templating photodimerization of coumarins within a water-soluble nano reaction vessel. *J. Org. Chem.* **71**, 6409-6413 (2006).

93. Karthikeyan, S. & Ramamurthy, V. Templating photodimerization of trans-cinnamic acid esters with a water-soluble Pd nanocage. *J. Org. Chem.* **72**, 452-458 (2007).

94. Natarajan, A., Mague, J.T. & Ramamurthy, V. Viability of a covalent chiral auxiliary method to induce asymmetric induction in solid-state photoreactions explored. *Cryst. Growth Des.* **5**, 2348-2355 (2005).

95. Natarajan, A., Mague, J.T. & Ramamurthy, V. Asymmetric induction during yang cyclization of α-oxoamides: the power of a covalently linked chiral auxiliary is enhanced in the crystalline state. *J. Am. Chem. Soc.* **127**, 3568-3576 (2005).

96. Pattabiraman, M., Kaanumalle, L.S., Natarajan, A. & Ramamurthy, V. Regioselective photodimerization of cinnamic acids in water: templation with cucurbiturils. *Langmuir* **22**, 7605-7609 (2006).

97. Pattabiraman, M., Kaanumalle, L.S. & Ramamurthy, V. Photoproduct selectivity in reactions involving singlet and triplet excited states within bile salt micelles. *Langmuir* **22**, 2185-2192 (2006).

98. Pattabiraman, M., Natarajan, A., Kaanumalle, L.S. & Ramamurthy, V. Templating photodimerization of trans-cinnamic acids with cucurbit[8]uril and γ-cyclodextrin. *Org. Lett.* **7**, 529-532 (2005).

99. Liu, S. & Gibb, B.C. High-definition self-assemblies driven by the hydrophobic effect: synthesis and properties of a supramolecular nanocapsule. *Chem. Commun.*, 3709-3716 (2008).

100. Kaanumalle, L.S., Nithyanandhan, J., Pattabiraman, M., Jayaraman, N. & Ramamurthy, V. Water-soluble dendrimers as photochemical reaction media: chemical behavior of singlet and triplet radical pairs inside dendritic reaction cavities. *J. Am. Chem. Soc.* **126**, 8999-9006 (2004).

101. Kaanumalle, L.S. & Ramamurthy, V. Photodimerization of acenaphthylene within a nanocapsule: excited state lifetime dependent dimer selectivity. *Chem. Commun.*, 1062-1064 (2007).

102. Sundaresan, A.K. & Ramamurthy, V. Making a difference on excited-state chemistry by controlling free space within a nanocapsule: photochemistry of 1-(4-alkylphenyl)-3-phenylpropan-2-ones. *Org. Lett.* **9**, 3575-3578 (2007).

103. Dong, D.C. & Winnik, M.A. The py scale of solvent polarities. Solvent effects on the vibronic fine structure of pyrene fluorescence and empirical correlations with ET and Y values. *Photochem. Photobiol.* **35**, 17-21 (1982).

104. Kalyanasundaram, K. & Thomas, J.K. Environmental effects on vibronic band intensities in pyrene monomer fluorescence and their application in studies of micellar systems. *J. Am. Chem. Soc.* **99**, 2039-2044 (1977).

105. Nakajima, A. Solvent effect on the vibrational structures of the fluorescence and absorption spectra of pyrene. *Bull. Chem. Soc. Jpn.* **44**, 3272-3277 (1971).

106. Kalyanasundaram, K. & Thomas, J.K. Solvent-dependent fluorescence of pyrene-3-carboxaldehyde and its applications in the estimation of polarity at micelle-water interfaces. *J. Phys. Chem.* **81**, 2176-2180 (1977).

107. Kroning, P. Long-wave length fluorescence of 3-pyrenecarbaldehyde *Z. Naturforsch.* **28a**, 109-116 (1973).

108. Kroning, P. Dependence of the fluorescence quantum yield on the excitation wavelength for carbonyl derivatives of pyrene. *Z. Naturforsch.* **29a**, 804-804 (1974).

109. Kumar, C.V., Chattopadhyay, S.K. & Das, P.K. A laser flash photolysis study of pyrene-1-aldehyde. Intersystem crossing efficiency, photoreactivity and triplet state properties in various solvents. *Photochem. Photobiol.* **38**, 141-152 (1983).

110. Lianos, P. & Cremel, G. Environmental effects on the electronic spectral properties of 1-pyrenecarboxaldehyde and their application in probing biological structures. *Photochem. Photobiol.* **31**, 429-434 (1980).

111. Tamaki, T. The photoassociation of 1- and 2-acetylanthracenes with methanol. *Bull. Chem. Soc. Jpn.* **55**, 1761-1767 (1982).

112. Tamaki, T. Solvent effects on the fluorescence quantum yields and lifetimes of 1- and 2-acetyl- or benzoylanthracenes. *Bull. Chem. Soc. Jpn.* **55**, 1756-1760 (1982).

113. Nag, A., Chakrabarty, T. & Bhattacharya, K. Effect of .gamma-cyclodextrin on the intramolecular charge transfer processes in aminocoumarin laser dyes. *J. Phys. Chem.* **94**, 4203-4206 (1990).

114. Van Gompel, J.A. & Schuster, G.B. Photophysical behavior of ester-substituted aminocoumarins: a new twist. *J. Phys. Chem.* **93**, 1292-1295 (1989).

115. Muthuramu, K. & Ramamurthy, V. Photodimerization of coumarin in aqueous and micellar media. *J. Org. Chem.* **47**, 3976-3979 (1982).

116. Muthuramu, K. & Ramamurthy, V. 7-Alkoxy coumarins as fluorescence probes for microenvironments. *J. Photochem.* **26**, 57-64 (1984).

117. Seixas de Melo, J.S., Becker, R.S. & Macanita, A.L. Photophysical behavior of coumarins as a function of substitution and solvent: experimental evidence for the existence of a lowest lying 1(n,.pi.*) state. *J. Phys. Chem.* **98**, 6054-6058 (1994).

118. Wagner, B.D., Fitzpatrick, S.J. & McManus, G.J. Fluorescence suppression of 7-methoxycoumarin upon inclusion into cyclodextrins. *J. Inclusion Phenom. Macrocycl. Chem.* **47**, 187-192 (2003).

119. Breslow, R. Hydrophobic effects on simple organic reactions in water. *Acc. Chem. Res.* **24**, 159-164 (1991).

120. Breslow, R., Maitra, U. & Rideout, D. Selective diels-alder reactions in aqueous solutions and suspensions. *Tetrahedron Lett.* **24**, 1901-1904 (1983).

121. Catalán, J., Zimányi, L. & Saltiel, J. Medium-controlled aggregation of trans-stilbene. *J. Am. Chem. Soc.* **122**, 2377-2378 (2000).

122. Li, G. & McGown, L.B. Model for bile salt micellization and solubilization from studies of a "polydisperse" array of fluorescent probes and molecular modeling. *J. Phys. Chem.* **98**, 13711-13719 (1994).

123. Kaanumalle, L.S., Gibb, C.L.D., Gibb, B.C. & Ramamurthy, V. A Hydrophobic nanocapsule controls the photophysics of aromatic molecules by suppressing their favored solution pathways. *J. Am. Chem. Soc.* **127**, 3674-3675 (2005).

124. Sundaresan, A.K. & Ramamurthy, V. Consequences of controlling free space within a reaction cavity with a remote alkyl group: photochemistry of para-alkyl dibenzyl ketones within an organic capsule in water. *Photochem. Photobiol. Sci.* **7**, 1555-1564 (2008).

125. Jayaraj, N., Zhao, Y., Parthasarathy, A., Porel, M., Liu, R.S.H. & Ramamurthy, V. Nature of supramolecular complexes controlled by the structure of the guest molecules: formation of octa acid based capsuleplex and cavitandplex. *Langmuir* **25**, 10575-10586 (2009).

126. Kulasekharan, R., Jayaraj, N., Porel, M., Choudhury, R., Sundaresan, A.K., Parthasarathy, A., Ottaviani, M.F., Jockusch, S., Turro, N.J. & Ramamurthy, V. Guest rotations within a capsuleplex probed by NMR and EPR techniques. *Langmuir* **26**, 6943-6953 (2010).

127. Jayaraj, N., Zhao, Y., Parthasarathy, A., Porel, M., Liu, R.S.H. & Ramamurthy, V. Nature of supramolecular complexes controlled by the structure of the guest molecules: formation of octa acid based capsuleplex and cavitandplex. *Langmuir* **25**, 10575-10586 (2009).

128. Earle, K.A., Budil, D.E. & Freed, J.H. Millimeter wave electron resonance using quasioptical techniques. *Adv. Magn. Opt. Reson.* **19**, 253-323 (1996).

129. Ottaviani, M.F., Martini, G. & Nuti, L. Nitrogen hyperfine splitting of nitroxide solutions: Differently structured and charged nitroxides as probes of environmental properties. *Magn. Reson. Chem.* **25**, 897-904 (1987).

130. Knauer, B.R. & Napier, J.J. The nitrogen hyperfine splitting constant of the nitroxide functional group as a solvent polarity parameter. The relative importance for a solvent polarity parameter of its being a cybotactic probe vs. its being a model process. *J. Am. Chem. Soc.* **98**, 4395-4400 (1976).

131. Chen, J.Y.C., Jayaraj, N., Jockusch, S., Ottavianai, M.F., Ramamurthy, V. & Turro, N.J. An EPR and NMR study of supramolecular effects on paramagnetic interaction between a nitroxide incarcerated within a nanocapsule with a nitroxide in bulk aqueous media. *J. Am. Chem. Soc.* **130**, 7206-7207 (2008).

132. Lewis, F.D., Bedell, A.M., Dykstra, R.E., Elbert, J.E., Gould, I.R. & Farid, S. Photochemical generation, isomerization, and oxygenation of stilbene cation radicals. *J. Am. Chem. Soc.* **112**, 8055-64 (1990).

133. Samori, S., Hara, M., Tojo, S., Fujitsuka, M. & Majima, T. Important factors for the formation of radical cation of stilbene and substituted stilbenes during resonant two-photon ionization with a 266- or 355-nm laser. *J. Photochem. Photobiol., A* **179**, 115-124 (2006).

134. Parthasarathy, A., Kaanumalle, L.S. & Ramamurthy, V. Controlling photochemical geometric isomerization of a stilbene and dimerization of a styrene using a confined reaction cavity in water. *Org. Lett.* **9**, 5059-5062 (2007).

135. Gaudiello, J.G., Larkin, D., Rawn, J.D., Sosnowski, J.J., Bancroft, E.E. & Blount, H.N. On the mechanism of the electrochemical reduction of N-methylpyridinium ion. *J. Electroanal. Chem. Interfacial Electrochem.* **131**, 203-14 (1982).

136. Green, B.S., Rejto, M., Johnson, D.E., Hoyle, C.E., Simpson, J.T., Correa, P.E., Ho, T.I., McCoy, F. & Lewis, F.D. Cycloaddition reactions of stilbene-electron-poor-alkene exciplexes. *J. Am. Chem. Soc.* **101**, 3325-31 (1979).

137. Jones, G.I., Griffin, S.F., Choi, C.Y. & Bergmark, W.R. Electron donor-acceptor quenching and photoinduced electron transfer for coumarin dyes. *J. Org. Chem* **49**, 2705-2708 (1984).

138. Ling, Y., Mague, J.T. & Kaifer, A.E. Inclusion complexation of diquat and paraquat by the hosts cucurbit[7]uril and cucurbit[8]uril. *Chem.-Eur. J.* **13**, 7908-7914 (2007).

139. Park, Y.-T., Hwang, C.-G., Kim, K.-W., Song, N.W. & Kim, D. Photocyclization mechanism of halopyridinium salt tethered to arene: flash photolysis observation of a pyridinium σ, cyclohexadienyl radicals, and a dihalide radical anion in aqueous solution. *J. Am. Chem. Soc.* **119**, 10677-10683 (1997).

140. Peon, J., Tan, X., Hoerner, J.D., Xia, C., Luk, Y.F. & Kohler, B. Excited state dynamics of methyl viologen. ultrafast photoreduction in methanol and fluorescence in acetonitrile. *J. Phys. Chem. A* **105**, 5768-5777 (2001).

141. Day, A., Arnold, A.P., Blanch, R.J. & Snushall, B. Controlling factors in the synthesis of cucurbituril and its homologues. *J. Org. Chem.* **66**, 8094-8100 (2001).

142. Parthasarathy, A. & Ramamurthy, V. Role of free space and weak interactions on geometric isomerization of stilbenes held in a molecular container. *Photochem. Photobiol. Sci.* **10**, 1455-1462 (2011).

143. Yagci, Y., Jockusch, S. & Turro, N.J. Mechanism of photoinduced step polymerization of thiophene by onium salts: reactions of phenyliodinium and diphenylsulfinium radical cations with thiophene. *Macromolecules* **40**, 4481-4485 (2007).

144. Ardo, S. & Meyer, G.J. Photodriven heterogeneous charge transfer with transition-metal compounds anchored to TiO2 semiconductor surfaces. *Chem. Soc. Rev.* **38**, 115-164 (2009).

145. Gray, H.B. & Winkler, J.R. *Electron Transfer in Chemistry Vol. 3: Biological Systems, Artificial Supramolecular Systems*, (2001).

146. Hagfeldt, A., Boschloo, G., Sun, L., Kloo, L. & Pettersson, H. Dye-sensitized solar cells. *Chem. Rev.* **110**, 6595-6663 (2010).

147. Peter, L.M. The Grätzel cell: where next? *J. Phys. Chem. Lett.* **2**, 1861-1867 (2011).

148. Choi, H., Kang, S.O., Ko, J., Gao, G., Kang, H.S., Kang, M.S., Nazeeruddin, M.K. & Grätzel, M. An efficient dye-sensitized solar cell with an organic sensitizer encapsulated in a cyclodextrin cavity. *Angew. Chem., Int. Ed.* **48**, 5938-5941 (2009).

149. Freitag, M. & Galoppini, E. Cucurbituril complexes of viologens bound to TiO_2 films. *Langmuir* **26**, 8262-8269 (2010).

150. Haque, S.A., Park, J.S., Srinivasarao, M. & Durrant, J.R. Molecular-level insulation: an approach to controlling interfacial charge transfer. *Adv. Mater.* **16**, 1177-1181 (2004).

151. Pagba, C., Zordan, G., Galoppini, E., Piatnitski, E.L., Hore, S., Deshayes, K. & Piotrowiak, P. Hybrid photoactive assemblies: electron injection from host−guest complexes into semiconductor nanoparticles. *J. Am. Chem. Soc.* **126**, 9888-9889 (2004).

152. Kavarnos, G.J. *Fundamentals of Photoinduced Electron Transfer*, (VCH Publishers, New London, CT, 1993).

153. Jones, G., Griffin, S.F., Choi, C.Y. & Bergmark, W.R. Electron donor-acceptor quenching and photoinduced electron transfer for coumarin dyes. *J. Org. Chem.* **49**, 2705-2708 (1984).

154. Gupta, S., Adhikari, A., Mandal, A.K., Bhattacharyya, K. & Ramamurthy, V. Ultrafast singlet–singlet energy transfer between an acceptor electrostatically attached to the walls of an organic capsule and the enclosed donor. *J. Phys. Chem. C* **115**, 9593-9600 (2011).

155. Freitag, M. & Galoppini, E. Molecular host–guest complexes: Shielding of guests on semiconductor surfaces. *Energy Environ. Sci.* **4**, 2482-2494 (2011).

156. Porel, M., Jockusch, S., Parthasarathy, A., Rao, V.J., Turro, N.J. & Ramamurthy, V. Photoinduced electron transfer between a donor and an acceptor separated by a capsular wall. *Chem. Commun.* **48**, 2710-2712 (2012).

157. Agrawal, S., Dev, P., English, N.J., Thampi, K.R. & MacElroy, J.M.D. First-principles study of the excited-state properties of coumarin-derived dyes in dye-sensitized solar cells. *J. Mater. Chem.* **21**, 11101-11108 (2011).

158. Kilså, K., Mayo, E.I., Katz, J., Brunschwig, B.S., Gray, H.B., Lewis, N.S. & Winkler, J.R. Anchoring group and auxiliary ligand effects on the binding of ruthenium complexes to nanocrystalline TiO_2 photoelectrodes. *J. Phys. Chem. B* **108**, 15640-15651 (2004).

159. Rochford, J. & Galoppini, E. Zinc(II) tetraarylporphyrins anchored to TiO_2, ZnO, and ZrO2 nanoparticle films through rigid-rod linkers. *Langmuir* **24**, 5366-5374 (2008).

160. Thyagarajan, S., Galoppini, E., Persson, P., Giaimuccio, J.M. & Meyer, G.J. Large footprint pyrene chromophores anchored to planar and colloidal metal oxide thin films. *Langmuir* **25**, 9219-9226 (2009).

161. Qu, P. & Meyer, G.J. Proton-controlled electron injection from molecular excited states to the empty states in nanocrystalline TiO_2. *Langmuir* **17**, 6720-6728 (2001).

162. Rothenberger, G., Fitzmaurice, D. & Graetzel, M. Spectroscopy of conduction band electrons in transparent metal oxide semiconductor films: optical determination of the flatband potential of colloidal titanium dioxide films. *J. Phys. Chem.* **96**, 5983-5986 (1992).

163. Horng, M.L., Gardecki, J.A., Papazyan, A. & Maroncelli, M. Subpicosecond measurements of polar solvation dynamics: Coumarin 153 revisited. *J . Phys. Chem.* **99**, 17311-17337 (1995).

164. Porel, M., Jayaraj, N., Kaanumalle, L.S., Maddipatla, M.V.S.N., Parthasarathy, A. & Ramamurthy, V. Cavitand octa acid forms a nonpolar capsuleplex dependent on the molecular size and hydrophobicity of the guest. *Langmuir* **25**, 3473-3481 (2009).

165. Rochford, J., Chu, D., Hagfeldt, A. & Galoppini, E. Tetrachelate porphyrin chromophores for metal oxide semiconductor sensitization: effect of the spacer length and anchoring group position. *J. Am. Chem. Soc.* **129**, 4655-4665 (2007).

166. Taratula, O., Rochford, J., Piotrowiak, P., Galoppini, E., Carlisle, R.A. & Meyer, G.J. Pyrene-terminated phenylenethynylene rigid linkers anchored to metal oxide nanoparticles. *J. Phys. Chem. B* **110**, 15734-15741 (2006).

167. Chen, J.Y.C., Jayaraj, N., Jockusch, S., Ottaviani, M.F., Ramamurthy, V. & Turro, N.J. An EPR and NMR study of supramolecular effects on paramagnetic interaction between a nitroxide incarcerated within a nanocapsule with a nitroxide in bulk aqueous media. *J. Am. Chem. Soc.* **130**, 7206-7207 (2008).

168. Jockusch, S., Zeika, O., Jayaraj, N., Ramamurthy, V. & Turro, N.J. Electron spin polarization transfer from a nitroxide incarcerated within a nanocapsule to a nitroxide in the bulk aqueous solution. *J. Phys. Chem. Lett.* **1**, 2628-2632 (2010).

169. Gijzeman, O.L.J., Kaufman, F. & Porter, G. Quenching of aromatic triplet states in solution by nitric oxide and other free radicals. *J. Chem. Soc., Faraday Trans. 2* **69**, 727-737 (1973).

170. Hoijtink, G.J. The influence of paramagnetic molecules on singlet-triplet transitions. *Mol. Phys.* **3**, 67-70 (1960).

171. Hoytink, G.J. Intermolecular electron exchange. *Acc. Chem. Res.* **2**, 114-120 (1969).

172. Kobori, Y., Takeda, K., Tsuji, K., Kawai, A. & Obi, K. Exchange interaction in radical−triplet pairs: evidences for CIDEP generation by level crossings in triplet−doublet interactions. *J. Phys. Chem. A* **102**, 5160-5170 (1998).

173. Mitsui, M., Kobori, Y., Kawai, A. & Obi, K. Quenching mechanism of excited coronene by a nitroxide radical studied by probing dynamic electron polarization. *J. Phys. Chem. A* **108**, 524-531 (2004).

174. Murrell, J.N. The effect of paramagnetic molecules on the intensity of spin-forbidden absorption bands of aromatic molecules. *Mol. Phys.* **3**, 319-329 (1960).

175. Watkins, A.R. Solvent effects on triplet state quenching by tetramethylpiperidcme-N-oxide. *Chem. Phys. Lett.* **70**, 262-265 (1980).

176. Kawai, A. & Shibuya, K. Electron spin dynamics in a pair interaction between radical and electronically-excited molecule as studied by a time-resolved ESR method. *J. Photochem. Photobiol., C* **7**, 89-103 (2006).

177. Jenks, W.S. & Turro, N.J. Exchange effects and CIDEP. *Res. Chem. Intermed.* **13**, 237-300 (1990).

178. Jayaraj, N., Jockusch, S., Kaanumalle, L.S., Turro, N.J. & Ramamurthy, V. Dynamics of capsuleplex formed between octaacid and organic guest molecules — Photophysical techniques reveal the opening and closing of capsuleplex. *Can. J. Chem.* **89**, 203-213 (2011).

179. Kosen, P.A. [5] Spin labeling of proteins. *Methods Enzymol.* **177**, 86-121 (1989).

180. Lagona, J., Mukhopadhyay, P., Chakrabarti, S. & Isaacs, L. The cucurbit[n]uril family. *Angew. Chem., Int. Ed.* **44**, 4844-4870 (2005).

181. Lee, J.W., Samal, S., Selvapalam, N., Kim, H.J. & Kim, K. Cucurbituril homologues and derivatives: new opportunities in supramolecular chemistry. *Acc. Chem. Res.* **36**, 621-630 (2003).

182. Li, Y., Lei, X., Lawler, R.G., Murata, Y., Komatsu, K. & Turro, N.J. Distance-dependent paramagnet-enhanced nuclear spin relaxation of $H_2@C_{60}$ derivatives covalently linked to a nitroxide radical. *J. Phys. Chem. Lett.* **1**, 2135-2138 (2010).

183. Solomon, I. & Bloembergen, N. Nuclear magnetic interactions in the HF molecule *J. Chem. Phys.* **25**, 261-266 (1956).

184. Sundaresan, A.K. & Ramamurthy, V. Consequences of controlling free space within a reaction cavity with a remote alkyl group: photochemistry of para-alkyl dibenzyl ketones within an organic capsule in water. *Photochem. Photobiol. Sci.* **7**, 1555-1564 (2008).

185. Green, J.A. & Singer, L.A. Di-tert-butyl nitroxide as a convenient probe for excited singlet states. pyrene luminescence. *J. Am. Chem. Soc.* **96**, 2730-2733 (1974).

186. Green, J.A., Singer, L.A. & Parks, J.H. Fluorescence quenching by the stable free radical di-t-butylnitroxide *J. Chem. Phys.* **58**, 2690-2695 (1973).

187. Schwerzel, R.E. & Caldwell, R.A. Quenching of excited states by stable free radicals. II. Mechanism of triplet quenching by di-tert-butyl nitroxide. *J. Am. Chem. Soc.* **95**, 1382-1389 (1973).

188. Evans, T.R. Singlet quenching mechanisms. *J. Am. Chem. Soc.* **93**, 2081-2082 (1971).

189. Turro, N.J., Lehr, G.F., Butcher, J.A., Moss, R.A. & Guo, W. Temperature dependence of the cycloaddition of phenylchlorocarbene to alkenes. Observation of negative activation energies. *J. Am. Chem. Soc.* **104**, 1754-1756 (1982).

190. Porel, M., Jockusch, S., Ottaviani, M.F., Turro, N.J. & Ramamurthy, V. Interaction between encapsulated excited organic molecules and free nitroxides: communication across a molecular wall. *Langmuir* **27**, 10548-10555 (2011).

191. Ferreira, G.C., Schmitt, C.C. & Neumann, M.G. Dependence of the thioxanthone triplet-triplet absorption spectrum with solvent polarity and aromatic ring substitution. *J. Braz. Chem. Soc.* **17**, 905-909 (2006).

192. Obi, K. & Imamura, T. Time-resolved ESR of intersystem crossing and energy transfer processes. *Rev. Chem. Intermed.* **7**, 225-242 (1986).

193. Turro, N.J., Khudyakov, I.V., Bossmann, S.H. & Dwyer, D.W. An electron spin polarization study of the interaction of photoexcited triplet molecules with mono- and polynitroxyl stable free radicals. *J. Phys. Chem.* **97**, 1138-1146 (1993).

194. Kawai, A., Okutsu, T. & Obi, K. Spin polarization generated in the triplet-doublet interaction: hyperfine-dependent chemically induced dynamic electron polarization. *J. Phys. Chem.* **95**, 9130-9134 (1991).

195. Jayaraj, N., Porel, M., Ottaviani, M.F., Maddipatla, M.V.S.N., Modelli, A., Da Silva, J.P., Bhogala, B.R., Captain, B., Jockusch, S., Turro, N.J. & Ramamurthy, V. Self aggregation of supramolecules of nitroxides@cucurbit[8]uril revealed by EPR spectra. *Langmuir* **25**, 13820-13832 (2009).

196. Day, A., Arnold, A.P., Blanch, R.J. & Snushall, B. Controlling factors in the synthesis of cucurbituril and its homologues. *J. Org. Chem.* **66**, 8094-8100 (2001).

197. Gutsche, C.D., Dhawan, B., No, K.H. & Muthukrishnan, R. Calixarenes. 4. The synthesis, characterization, and properties of the calixarenes from p-tert-butylphenol. *J. Am. Chem. Soc.* **103**, 3782-3792 (1981).

198. Brinker, U.H. & Mieusset, J.L. *Molecular Encapsulation*, (2010).

199. Gibb, C.L.D., Sundaresan, A.K., Ramamurthy, V. & Gibb, B.C. Templation of the excited-state chemistry of α-(n-alkyl) dibenzyl ketones: how guest packing within a nanoscale supramolecular capsule influences photochemistry. *J. Am. Chem. Soc.* **130**, 4069-4080 (.2008).

200. Sundaresan, A.K. & Ramamurthy, V. Making a difference on excited-state chemistry by controlling free space within a nanocapsule: photochemistry of 1-(4-alkylphenyl)-3-phenylpropan-2-ones. *Org. Lett.* **9**, 3575-3578 (2007).

201. Warmuth, R., Brinker, U.H. & Mieusset, J.L. *Molecular Encapsulation*, (2010).

202. Bao, X., Reith, S., Stojanovic, S., Hadad, C.M. & Badjic, J.D. Molecular recognition of a transition state. *Angew. Chem., Int. Ed.* **49**, 4816-4819 (2010).

203. O'Leary, B.M., Grotzfeld, R.M. & Rebek, J. Ring inversion dynamics of encapsulated cyclohexane. *J. Am. Chem. Soc.* **119**, 11701-11702 (1997).

204. Aliev, A.E. & Harris, K.D.M. Conformational properties of monosubstituted cyclohexanes in their thiourea inclusion compounds and in solution: variable-temperature one-dimensional and two-dimensional carbon-13 NMR investigations. *J. Am. Chem. Soc.* **115**, 6369-6377 (1993).

205. Muller, K. ^{13}C magic angle spinning NMR investigations of thiourea inclusion compounds. *Magn. Reson. Chem.* **30**, 228-234 (1992).

206. Lambert, J.B., Bailey, D.S. & Michel, B.F. Steric effects on the configuration at nitrogen in piperidines. *J. Am. Chem. Soc.* **94**, 3812-3816 (1972).

207. Yousif, G.A. & Roberts, J.D. Nuclear magnetic resonance spectroscopy. Conformational equilibria and equilibration of 4,4-difluoropiperidine. Measurement of the N-H inversion rate in a six-membered ring. *J. Am. Chem. Soc.* **90**, 6428-6432 (1968).

208. Columbus, I. & Biali, S.E. Cyclohexyl rings in spatial proximity: stereochemistry of tricyclohexylmethane. *J. Org. Chem.* **58**, 7029-7035 (1993).

209. Keeler, J. *Understanding NMR Spectroscopy*, (2005).

210. Basilio, N., Rio, L.G. & Pastor, M.M. NMR Evidence of slow monomer−micelle exchange in a calixarene-based surfactant. *J. Phys. Chem. B* **114**, 4816-4820 (2010).

211. Perrin, C.L. & Dwyer, T.J. Application of two-dimensional NMR to kinetics of chemical exchange. *Chem. Rev.* **90**, 935-967 (1990).

212. Yamanaka, M., Shivanyuk, A. & Rebek, J.J. Kinetics and thermodynamics of hexameric capsule formation. *J. Am. Chem. Soc.* **126**, 2939-2943 (2004).

213. Abel, E.W., Coston, T.P.J., Orrell, K.G., Sik, V. & Stephenson, D. Two-dimensional NMR exchange spectroscopy. Quantitative treatment of multisite exchanging systems. *J. Magn. Reson.* **70**, 34-53 (1986).

214. Bardelang, D., Banaszak, K., Karoui, H., Rockenbauer, A., Waite, M.l., Udachin, K., Ripmeester, J.A., Ratcliffe, C.I., Ouari, O. & Tordo, P. Probing cucurbituril assemblies in water with TEMPO-like nitroxides: a trinitroxide supraradical with spin−spin interactions. *J. Am. Chem. Soc.* **131**, 5402-5404 (2009).

215. Kirilyuk, I., Polovyanenko, D., Semenov, S., Grigor'ev, I., Gerasko, O., Fedin, V. & Bagryanskaya, E. Inclusion complexes of nitroxides of pyrrolidine and imidazoline series with cucurbit[7]uril. *J. Phys. Chem. B* **114**, 1719-1728 (2010).

216. Mezzina, E., Cruciani, F., Pedulli, G.F. & Lucarini, M. Nitroxide radicals as probes for exploring the binding properties of the cucurbit[7]uril host. *Chem.-Eur. J.* **13**, 7223-7233 (2007).

217. Gunther, H. *NMR Spectroscopy*, (1992).

218. Improta, R. & Barone, V. Interplay of electronic, environmental, and vibrational effects in determining the hyperfine coupling constants of organic free radicals. *Chem. Rev.* **104**, 1231-1254 (2004).

219. Ong, W. & Kaifer, A.E. Salt effects on the apparent stability of the cucurbit[7]uril−methyl viologen inclusion complex. *J. Org. Chem* **69**, 1383-1385 (2004).

220. Szejtli, J. & Osa, T. *Comprehensive Supramolecular Chemistry*, 13 (1996).

221. Sein, A. & Engberts, J.B.F.N. Micelle to lamellar aggregate transition of an anionic surfactant in dilute aqueous solution induced by alkali metal chloride and tetraalkylammonium chloride salts. *Langmuir* **11**, 455-465 (1995).

222. Kwan, C.L., Atik, S. & Singer, L.A. An electron spin resonance study of the association of a surfactant nitroxyl radical with a cationic micelle using spin-intensity measurements and hyperfine structure analyses. *J. Am. Chem. Soc.* **100**, 4783-4786 (1978).

223. Lee, C., Yang, W. & Parr, R.G. Development of the Colle-Salvetti correlation-energy formula into a functional of the electron density. *Physical Review B* **37**, 785-789 (1988).

224. Klajnert, B., Cangiotti, M., Calici, S., Majoral, J.P., Caminade, A.M., Cladera, J., Bryszewska, M. & Ottaviani, M.F. EPR Study of the interactions between dendrimers and peptides involved in alzheimer's and prion diseases. *Macromol. Biosci.* **7**, 1065-1074 (2007).

225. Griffin, R.G. & Prisner, T.F. High field dynamic nuclear polarization-the renaissance. *Phys. Chem. Chem. Phys.* **12**, 5737-5740 (2010).

226. Wind, R.A., Duijvestijn, M.J., van der Lugt, C., Manenschijn, A. & Vriend, J. Applications of dynamic nuclear polarization in ^{13}C NMR in solids *Prog. Nucl. Magn. Reson. Spectrosc.* **17**, 33-67 (1985).

227. Carver, T.R. & Slichter, C.P. Polarization of nuclear spins in metals. *Phys. Rev.* **92**, 212-213 (1953).

228. Overhauser, A.W. Polarization of nuclei in metals. *Phys. Rev.* **92**, 411-415 (1953).

229. Matsuki, Y., Maly, T., Ouari, O., Karoui, H., Le Moigne, F., Rizzato, E., Lyubenova, S., Herzfeld, J., Prisner, T., Tordo, P. & Griffin, R.G. Dynamic nuclear polarization with a rigid biradical. *Angew. Chem., Int. Ed.* **48**, 4996-5000 (2009).

230. Song, C., Hu, K.-N., Joo, C.-G., Swager, T.M. & Griffin, R.G. TOTAPOL: A biradical polarizing agent for dynamic nuclear polarization experiments in aqueous media. *J. Am. Chem. Soc.* **128**, 11385-11390 (2006).

231. Closs, G.L., Forbes, M.D.E. & Piotrowiak, P. Spin and reaction dynamics in flexible polymethylene biradicals as studied by EPR, NMR, optical spectroscopy, and magnetic field effects. Measurements and mechanisms of scalar electron spin-spin coupling. *J. Am. Chem. Soc.* **114**, 3285-3294 (1992).

232. Ferruti, P., Gill, D., Klein, M.P., Wang, H.H., Entine, G. & Calvin, M. Synthesis of mono-, di-, and polynitroxides. Classification of electron spin resonance spectra of flexible dinitroxides dissolved in liquids and glasses. *J. Am. Chem. Soc.* **92**, 3704-13 (1970).

233. Forbes, M.D.E., McCaffrey, V.P. & Harbron, E.J. Structure and dynamics of macromolecular free radicals. *Spectrum (Bowling Green, OH, U. S.)* **18**, 12-17 (2005).

234. Smith, C.D., Bott, R.C., Bottle, S.E., Micallef, A.S. & Smith, G. New isoindoline aminoxyl based polyradicals for spin probes and molecular magnetic materials. *J. Chem. Soc., Perkin Trans. 2*, 533-537 (2002).

235. Szydlowska, J., Pietrasik, K., Glaz, L. & Kaim, A. An ESR study of biradicals formed from two 4-amino-TEMPOs linked by -(CH_2)n-, (n =2, 3, 4, 6). *Chem. Phys. Lett.* **460**, 245-252 (2008).

236. Tran, V.A., Kokorin, A.I., Grampp, G. & Rasmussen, K. Features of spin exchange in nitroxide biradicals in the ionic liquid bmimPF_6. *Appl. Magn. Reson.* **35**, 389-398 (2009).

237. Turro, N.J., Khudyakov, I.V., Bossmann, S.H. & Dwyer, D.W. An electron spin polarization study of the interaction of photoexcited triplet molecules with mono- and polynitroxyl stable free radicals. *J. Phys. Chem.* **97**, 1138-1146 (1993).

238. Jayaraj, N., Porel, M., Ottaviani, M.F., Maddipatla, M.V.S.N., Modelli, A., Da Silva, J.P., Bhogala, B.R., Captain, B., Jockusch, S., Turro, N.J. & Ramamurthy, V. Self Aggregation of supramolecules of nitroxides@cucurbit[8]uril revealed by EPR spectra. *Langmuir* **25**, 13820-13832 (2009).

239. Ottaviani, M.F. Analysis of resolved ESR spectra of neutral nitroxide radicals in ethanol and pyridine: the dynamic behavior in fast motion conditions. *J. Phys. Chem.* **91**, 779-84 (1987).

240. Jose, B.J., Bales, B.L. & Peric, M. Electron paramagnetic resonance study of the surface hydration of triton X-100 micelles in water with added monovalent alkali salts. *J. Phys. Chem. B* **113**, 13257-13262 (2009).

241. Ionita, G., Caragheorgheopol, A., Caldararu, H., Jones, L. & Chechik, V. Inclusion complexes of cyclodextrins with nitroxide-based spin probes in aqueous solutions. *Org. Biomol. Chem.* **7**, 598-602 (2009).

242. Ananchenko, G.S., Udachin, K.A., Coleman, A.W., Polovyanenko, D.N., Bagryanskaya, E.G. & Ripmeester, J.A. Crystalline inclusion complex of a calixarene with a nitroxide. *Chem. Commun.*, 223-225 (2008).

243. Franchi, P., Lucarini, M. & Pedulli, G.F. Use of nitroxide radicals to investigate supramolecular entities. *Curr. Org. Chem.* **8**, 1831-1849 (2004).

244. Ionita, G., Meltzer, V., Pincu, E. & Chechik, V. Inclusion complexes of cyclodextrins with biradicals linked by a polyether chain-an EPR study. *Org. Biomol. Chem.* **5**, 1910-1914 (2007).

245. Ottaviani, M.F., Modelli, A., Zeika, O., Jockusch, S., Moscatelli, A. & Turro, N.J. EPR Analysis and DFT Computations of a Series of Polynitroxides. *J. Phys. Chem. A* **116**, 174-184 (2011).